PALEOLANDSCAPE RECONSTRUCTION USING GEOPROXY EVIDENCE AT ERFKROON, SOUTH AFRICA

by

Sarah E. Morris, B.S.

A thesis submitted to the Graduate Council of
Texas State University in partial fulfillment
of the requirements for the degree of
Master of Arts
with a Major in Anthropology
December 2019

Committee Members:

Britt Bousman, Chair

David Kilby

Michael Toffolo

FAIR USE AND AUTHOR'S PERMISSION STATEMENT

Fair Use

Duplication Permission

ACKNOWLEDGEMENTS

I would like to take this opportunity to sincerely thank my thesis committee, Drs. Britt Bousman, David Kilby, and Michael Toffolo for their support and encouragement over the course of my degree program. I would also like to acknowledge Dr. Charles Frederick for generously accommodating my research needs by enabling access to his geological laboratory. I also extend my thanks to the National Museum of Bloemfontein and former director of the Florisbad Quaternary Research Station, Dr. James Brink, for housing, laboratory space, and access to unique fossil and archaeological collections during my stays at the Florisbad Quaternary Research Station. I must also thank the community of friends and family who continue to provide unwavering support as I carry on my academic journey, namely my parents, Paul and Lorri Himes, and dear friends Taylor Morey and Dr. Chris Lintz. Finally, my deepest gratitude is reserved for my husband, Brice Morris, whose unwavering belief in my abilities and constant emotional and financial support has seen me through to the successful completion of my degree. Realization of this goal would not have been possible without him.

TABLE OF CONTENTS

Page

LIST OF TABLES

Table **Page**

LIST OF FIGURES

Figure **Page**

ABSTRACT

The site of Erfkroon, located in the Western Free State Province, South Africa, is characterized by a complex alluvial system in which paleoenvironmental, fossil, microbotanical and archaeological materials from the Late Quaternary period are preserved in abundance. Multi-disciplinary investigations have demonstrated the presence of Middle and Later Stone Age human occupations in the site's overbank deposits in which sedimentation and phases of pedogenic development span ~120 ka. Better defining periods of sedimentation, erosion, geomorphic stability and pedogenesis within these deposits is fundamental to understanding Erfkroon's geological, paleoclimatical and archaeological records. There are currently two competing models describing the genesis of these strata: The Single-Terrace Accretionary Hypothesis (Tooth et al. 2013; Lyons et al. 2014) and the Multiple Terrace Allostratigraphy Hypothesis (Bousman & Brink 2014). This study evaluates the validity of both models using multiple theoretical and methodological approaches. Systematic field description of multiple profile exposures across the study area, coupled with magnetic susceptibility, particle size, and micromorphological analytical techniques provides one of the highest resolution geological studies of the terrace system to-date, and further clarifies the nature of these deposits within the context of human occupation and paleoclimatic change in the continental interior at the Pleistocene-Holocene transition.

1. INTRODUCTION

A long history of aridity and erosion characterizing Quaternary landscapes of southern Africa makes it difficult to contrive paleoenvironmental models of the past. This is especially true for central southern Africa and the South African interior, where glacial-interglacial cycling at the terminus of the Pleistocene perpetuated phases of moisture and aridity in geographically varied ways (Mitchell 2016). The onset of the Holocene, marked by increasing aridity and warming temperatures, was also unconducive for the preservation of organic signatures (Chase & Meadows 2007). However, geological landforms such as dunes, paleolake shorelines, spring mounds, and alluvial architecture comprising dryland floodplains are being recognized for their potential to contain relict, geoproxy evidence telling of ecosystem dynamics during the late Quaternary (e.g. Butzer 1971; Nanson & Tooth 1999; Verster & van Rooyen 1999; Tooth 2007; Reid 2009; Tooth et al. 2013; Lyons et al. 2014).

The central interior is known for its rolling grassy plains accentuated by eroded stair-stepped dolerite-capped koppies and hill swarms punctuated by river systems that perpetuate bedrock erosion, and the aggradation, incision, and alteration of alluvial landforms. Alluvial terraces, formed by alluvial sedimentation between cyclic phases of erosion, are common features among the interior's dryland flood plains. Alteration of such landforms is perpetuated by external pressures such as climate change and eustatic sea level fluctuation (Leopold et al. 1964; Born & Ritter 1970; Merritts et al. 1994; Bridgeland & Westaway 2008) which can obscure or remove the history of genesis. Geochronological gaps within and between alluvial sedimentation sequences are a common result (Lewin & Macklin 2003), as are episodes of bank incision and the erosion

of deep gullies known as "*dongas*." Despite these factors, alluvial landscapes are becoming better recognized as productive sources for archaeological and paleoenvironmental information because their visibility is often aided by erosional processes. This is the case at sites such as Erfkroon in the Western Free State, where erosion and fluvial incision works in favor of paleoenvironmental and archaeological research (Tooth et al. 2013; Lyons et al. 2014; Bousman & Brink 2014). A long history of bank incision and erosion exposes its primary, archaeology-bearing terrace in three-dimensions, offering a unique opportunity to piece together landscape formation processes while examining contents within (Bousman & Brink 2014).

The Erfkroon study area, situated in the active floodplain of the Modder River in the Western Free State Province, epitomizes alluvial landscapes of the interior. The region is characterized by a well-stratified, complex alluvial system in which paleoenvironmental and archaeological data is preserved in abundance. Though erosion continuously alters its sediments, heavily weathered deposits are both accessible and visible (Figure 1.1). Ongoing research since the late 1990's demonstrates the prevalence of well-preserved late Quaternary fauna in several strata dating to the Late Pleistocene, some of which represent an extinction event concurrent with the onset of the Holocene. An abundance of these fauna has since marked the region as one of the largest (~400,000 m^2) open-air Quaternary fossil localities in southern Africa (Churchill et al. 2000; Brink et al. 2015). Archaeological investigations have also demonstrated the presence of Middle and Later Stone Age human occupations within alluvial overbank deposition heavily altered by pedogenesis and comprising ~120 ka of sedimentation (Bousman & Brink 2014; Tooth et al. 2013; Lyons et al. 2014). The geological relationship between

these strata and the paleoenvironmental implications responsible for their expression on the landscape are the focus of this study.

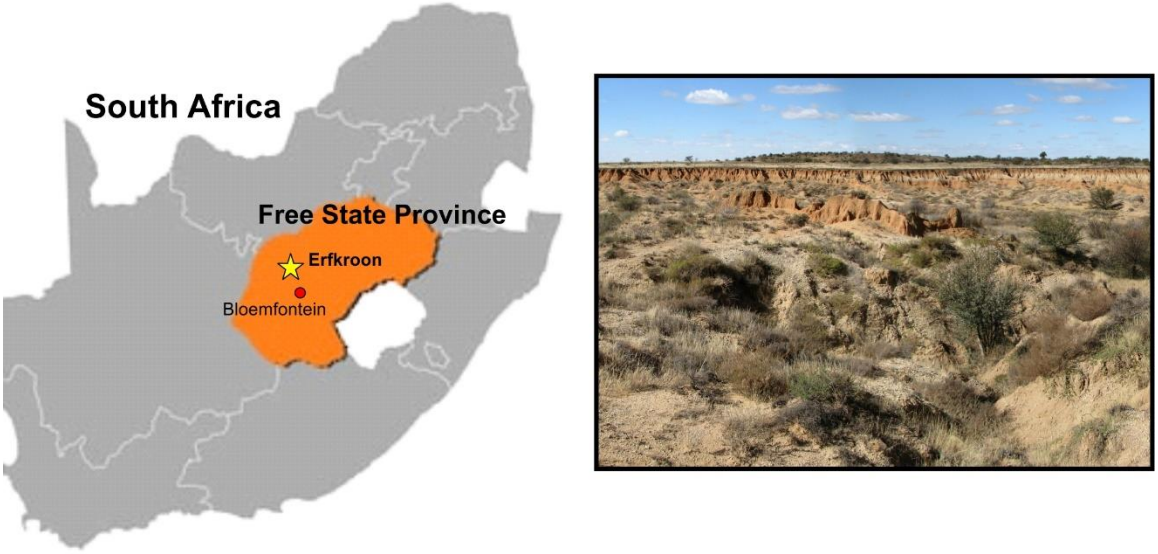

Fig. 1.1. Location of the Erfkroon study area, Western Free State Province, South Africa.

Overbank alluvial sequences altered by pedogenesis comprise the upper strata of Erfkroon's archaeology-bearing terrace, and better defining periods of landscape stability within these deposits is fundamental to understanding the area's geological, paleoclimatical, and occupational history (Figure 1.2). Two models describing the genesis of these strata have been proposed since 2013. This study represents an attempt to evaluate the validity of both models using multiple theoretical and methodological approaches, including methodologies previously untried in the study area.

Fig. 1.2. Landscape overview of stratified dongas & alluvial architecture at Erfkroon.

Theoretical Review

Unraveling the genesis and development of Erfkroon's alluvial terrace system is complicated by time, erosion, and weathering. But characterizing these sediments to account for such impacts is inextricably tied to understanding the paleoenvironmental conditions under which they formed. To-date, two geological models explaining the formation of the primary, archaeology-bearing alluvium at Erfkroon have been proposed: (1) the Single-Terrace Accretionary Hypothesis (Tooth et al. 2013; Lyons et al. 2014) and (2) the Multiple-Terrace Allostratigraphy Hypothesis (Bousman & Brink 2014).

The Single Terrace Accretionary Hypothesis was published by Tooth et al. (2013) and Lyons et al. (2014). They use a lithostratigraphic framework, incorporating stratigraphic terminology deriving from *Quaternary Sediments: Methods for the Study of Unlithified Rocks* (Gale & Hoare 1992), to interpret depositional succession. The Multiple-Terrace Allostratigraphy Hypothesis was developed around the same time by

Britt Bousman and James Brink (Bousman & Brink 2014; Bousman et al. *in prep*). This model incorporates the use of soil horizon concepts and nomenclature from the *Soil Survey Manual* (Soil Survey Staff 1993) combined with the concepts and terminology of allostratigraphy as defined in the North American Commission on Stratigraphic Nomenclature's *North American Stratigraphic Code* (NACSN 2005) (Bousman & Brink 2014; Bousman et al. *in prep*). The Single-Terrace Accretionary Hypothesis identifies one terrace and a "*paleodonga* fill" or gulley deposit at Erfkroon, while the Allostratigraphy Hypothesis identifies three separate terraces, each containing sedimentary gaps as a product of non-sedimentation and in some cases, erosion.

The Accretionary Hypothesis identifies two landforms. The first is a paired terrace containing 8 sedimentary units, where the upper four units characterized as paleosols contain most of the MSA and LSA archaeological materials previously recorded at Erfkroon (see Bousman & Brink 2014 and Palmison 2014). The Accretionary model assumes that paleosol (ancient soil) formation occurred within four separate, sedimentary, overbank deposits where brief periods of slow or non-sedimentation allowed for intermittent soil development. The implications are that periods of landscape stability were relatively short-lived because accretionary sedimentation was constant. This also infers that the Erfkroon landscape saw no dynamic changes in climate or fluvial action capable of disrupting the cyclic pattern of slow sedimentation and pedogenic development. The second landform refers to a channel fill, described as a separate, younger sequence resting unconformably on top of the paleosols comprising the upper reaches of the terrace (Tooth et al. 2013; Lyons et al. 2014).

The Multiple Terrace Allostratigraphy Hypothesis fundamentally differs in that episodes of pedogenesis are treated as temporally distinct events, not necessarily in tandem or sequential with sedimentation (Bousman & Brink 2014). From this perspective, Bousman and Brink separate strata according to pedogenic features and sedimentary units (Bousman et al *in prep*). The Allostratigraphy Hypothesis identifies three distinct terrace formations, where the Accretionary Hypothesis only identifies one and another limited to donga fill. The landform containing the most productive archaeology-bearing paleosols described in the Accretionary Hypothesis comprise what Bousman and Brink (2014) name the Orangia Terrace where they define three allostratigraphic units. Each allostratigraphic unit is described from a lithological/pedological perspective, in which soil formation is considered "time transgressive" (Bousman et al. *in prep*). From this perspective, soil formation events are thought to occur within sedimentary deposits of differing ages, indicating sediments themselves cannot be used as consistent, geochronological and stratigraphic markers. Ultimately, this hypothesis argues that allostratigraphic boundaries make better temporal markers because they represent spatially traceable temporal gaps in the sequence (Bousman et al. *in prep*).

Evaluating the legitimacy of each hypothesis as they concern interpretations of Erfkroon's archaeology-bearing strata comes down to identifying, if any, unconformable boundaries within the overbank sequence. Allostratigraphy, which subdivides sediments according to bounding discontinuities, is one way to achieve this goal, but must be used in tandem with other perspectives. This study combines the theoretical framework of five geological perspectives: (1) Lithostratigraphy, (2) Allostratigraphy, (3) Pedology & soil

geomorphology, (4) Paleopedology, and (5) Micromorphology, to holistically describe and characterize the combined expression of pedogenesis and sedimentation. As it pertains to Erfkroon, this study is the first of its kind to combine all five modes of interpretation into a single, cohesive analytical framework.

Lithostratigraphy. Lithostratigraphy refers to the classification of rock units by observable lithological properties of strata and their relative stratigraphic positions (Salvador 1994; Weerts & Westerhoff 2007). Lithostratigraphic units are defined by sediment color, texture, grain size, and composition, conforming to the Law of Superposition, and may contain pedological horizons referred to as "pedostratigraphical units" (NACSN 2005). Pedostratigraphical units refer to soils developing in parent materials that change sequentially along a gradient. Differences in parent material from this perspective are related to many factors including changes in texture, coarse fraction content, and mineralogy over time (Schaetzl 1991; Graham & O'Green 2010; Werts & Milligan 2012; Schaetzl & Thompson 2015). Lithostratigraphic nomenclature used in this and previous geological studies at Erfkroon (see Bousman & Brink 2014; Bousman et al. *in prep*) derive from those published in the *North American Stratigraphic Code* (NACSN 2005).

Allostratigraphy. Allostratigraphy refers to mapping rock units by the timing of their accumulation and is the only geological perspective that allows for stratigraphy to be characterized according to observed discontinuities (NACSN 1983:865-867; Hughes 2007). The application of this perspective is common when dealing with (1) successions of discontinuously bounded, lithologically similar deposits, (2) adjoining, genetically related deposits bounded by discontinuities, and (3) geographically separated units that

are further separated by discontinuities (NACSN 1983; Hughes 2010). Discontinuous boundaries of a unit may also be called unconformities or disconformities, or referred to as a land surface. A land surface may represent a modern, stable geomorphic (land) surface, or a buried surface that manifests in profile as a paleosol or episode of pedogenic development (Autin 1992). Allostratigraphic nomenclature used in this study derive from those published in the *North American Stratigraphic Code* (NACSN 2005).

Pedology & Soil Geomorphology. Soil studied in its natural setting, as it is altered by time, climatic conditions, parent material, topography, and biological activity, refers to the science of Pedology and 'pedogenesis' refers the process of soil formation (Birkeland 1999). Birkeland (1999:2) defines a soil as "a natural body consisting of layers (horizons) of mineral and/or organic constituents of variable thicknesses, which differ from the parent materials in their morphological, physical, chemical, and mineralogical properties and their biological characteristics." Conceptually, pedology complements other soil sciences, particularly soil geomorphology which refers to the study of soil distribution, properties, and behavior across a landscape— characteristics typically ignored in formal geological and pedological investigations because of a difference in scale. What makes soil geomorphology a fundamental component of pedology is that it places soil science within a greater landscape perspective, allowing for relationships between lithology, hydrology, stratigraphy, geomorphology, and climate to be examined (Soil Science Division Staff 2017).

Soil units of varying size (soil profiles and pedons) are characterized from both pedological and soil geomorphological perspectives in this study. A soil profile refers to a two-dimensional body of soil, the expression of which is created by removing the outer

layer of weathered surface materials to expose the unaltered sediments within (Birkeland 1999). Such exposures are typically called a soil profile, and depending on its size, a profile can reveal boundaries between soil horizons or sedimentary units from which morphological characterizations can be made. A smaller unit of study is the pedon which refers to a three-dimensional body of soil that typically reflects the nature of pedogenic development within a stratum. The pedon is the smallest unit of a complete soil profile that can be examined in the field and contains features used to designate soil horizons (Birkeland 1999; Soil Science Division Staff 2017).

Paleopedology & Paleosols. A paleosol refers to an ancient/fossilized soil (Birkeland 1999) preserved in sedimentary deposits, and the study of paleosol genesis, morphology, stratigraphy, and classification is referred to as the science of Paleopedology. Paleosols can be characterized as (1) a buried soil, (2) an exhumed soil, or (3) a relict soil (Ruhe 1956, 1965, 1970; Catt 1998). Buried soils refer to those formed at the surface of the earth, but that become buried by younger sediments often interrupting or ceasing active pedogenic processes (Catt 1998). In Quaternary stratigraphy, buried paleosols are used as stratigraphic markers as they are indicative of geomorphically stable periods of little or no erosion or sediment deposition (a land surface) (Ruhe et al. 1971). Exhumed soils refer to those that were once buried but become re-exposed to the earth's surface (exhumed). Paleosols are once again subjected to contemporary pedogenic and geomorphic processes when exhumed (Bushue et al. 1974). Relict soils refer to those that remain on the surface today, but that formed under preexisting conditions (i.e. past climatic conditions), and that have never been subject to burial (Ruellan 1971; Hall & Goble 2012; Heinz 2002).

Alluvial and colluvial movement of surface materials and sediment commonly result in the burial and preservation of soils (Catt 1998). In these circumstances, buried paleosols become reliable proxies for reconstructing paleoenvironmental and paleoclimatic conditions pervasive during a soil's active pedogenic interval. However, the burial process often coincides with erosion and post-burial modification caused by pedodiagenesis, the combined effects of pedogenesis (surficial weathering processes altering soils from the top down) and diagenesis (processes associated with compaction, heat buildup, and fluid circulation post-burial) (Ruhe & Olson 1980; Olson & Nettleton 1998). Such processes can limit a paleosol's preservation potential or alter its pre-burial pedogenic character. A common result is the poor preservation, obscuration, and/or modification of a buried paleosol's surface horizons (O and A-horizons) (Mack 1993; Retallack 1994). Diagenetic processes including the precipitation of minerals via groundwater penetration, clay diagenesis propagated by chemical exchange, and compression caused by overlying sediments over time are all post-burial factors capable of altering original pedogenic characteristics (Ruellan 1971). Sub-surface B-horizons are, therefore, commonly associated with the top of a paleosol profile.

Micromorphology. Micromorphology refers to the branch of soil science interested in the description, interpretation, and measurement of microscopic features and fabrics within a soil (Bullock et al. 1985; Stoops 2003). The examination of soil features is traditionally done via optical microscopy with cross-polarized light. Increasingly, micromorphology is being paired with other geological analyses such as magnetic susceptibility, radiometric dating, and stable isotope analysis to better interpret soil environments prone to pedogenic overprinting and disruption caused by erosional

agencies. This study, concerned with the presence or absence of erosional unconformities and disruption in pedogenic development, relies heavily on this method in conjunction with other above-mentioned techniques to extrapolate pedogenic and sedimentary relationships. Two references guide the methodological approach and interpretations of micromorphological constituents observed in thin section: (1) *Interpretations of Micromorphological Features of Soils and Regoliths* (Stoops et al. 2010), and (2) *Guidelines for Analysis and Description of Soils and Regolith Thin Sections* (Stoops 2003).

Stoops et al. (2010:623) differentiate between paleosols ("paleosoils") and relict soils. They define a paleosol as a buried soil of any age, where pedogenesis becomes completely or partially inhibited by burial. Alternatively, a relict soil refers to those belonging to the present-day surface but that contain characteristics inherited from past environmental conditions, different from those occurring today. The implementation of micromorphology in this research is meant to accomplish three goals: (1) verify the presence of buried or relict soils at Erfkroon, (2) identify, if any, the presence of *in situ* soil characteristics that can help interpret relationships between vertically bounded horizons suggested to share unconformable boundaries, and (3) to identify, if any, the presence of pedogenic features indicative of a specific horizon or post-depositional process associated with a particular paleoclimate. A list of terminologies from which interpretations are based are summarized in Table 1.1.

Table 1.1. Micromorphology terminology & definitions (content modified from Stoops 2003).

Micromorph Observations	**Definition**
c/f related distribution	Distribution of individual fabric units in relation to smaller fabric units and associated pores (Stoops 2003:42).
Structure & voids	Size, shape & arrangement of primary particles and voids in aggregated and non-aggregated materials, including arrangement, size and shape of aggregates (see Stoops 2003:68-69).
Coarse fraction	Characteristics of silt, sand, and gravel-sized particles, their degree of sphericity, size, sorting, mineral identification, etc. (see Stoops 2003:37-56).
Fine fraction (b-fabric)	Characteristics of the b-fabric (very fine particles; clays) including limpidity, color, distribution/orientation and patterns.
Pedofeatures	Discrete fabric units recognizable (different) from adjacent material by a difference in concentration of a component(s) (Stoops 2003:91).

Pedogenic Models & Concepts

Pedogenic development of soil profiles, the development of soil horizons, and factors contributing to and affecting these processes are complex. As such, several conceptual pedogenic models have been proposed (Runge 1973; Huggett 1975, 1976; Simonson 1978; Johnson 1993, 2000). The characterization and interpretation of pedogenic features presented in this study are based on the methods, descriptions, and interpretations presented in the United States Department of Agriculture's *Soil Survey Manual* (Soil Science Division Staff 2017) and the *Field Book for Describing and Sampling Soils* (Schoeneberger et al. 2012). Both references facilitate mapping, describing, classifying, and interpreting three-dimensional bodies of soil on the landscape (Soil Science Division Staff 2017:xxiii). It bears mentioning that the underlying conceptual framework for soil description derive from two primary models: (1) the Functional-Factorial Model and (2) the Soil Evolution Model.

Conceptual understanding of soil expressions across a landscape are adapted from Dokuchaev (1883) and Jenny's (1941) Functional-factorial Model. Specifically implemented is the concept of horizonation which conforms to the idea that soil bodies contain a sequence of identifiable horizons (zones) that occur in repeating patterns on a landscape as a result of pedogenic factors (e.g. climate, biota, relief, parent material, and time) (Jenny 1941; Soil Science Division Staff 2017). The horizonation concept is employed in this study, within an understanding that the presence or absence of a horizon may be telling of unconformable boundaries. Nomenclature for soil horizons published in this document conscribe to definitions printed in *The Soil Survey Manual* (Soil Science Division Staff 2017).

The Soil Evolution Model was developed by Johnson and Watson-Stegner (1987) to acknowledge pathways (mechanisms) by which pedogenesis can be limited or propagated over time, and how these conditions manifest on a landscape. They describe three main pedogenic pathways: (1) progressive, (2) regressive, and (3) static. Progressive pedogenesis refers to soil formation and organization, and includes processes leading up to horizon differentiation. This type of pedogenesis typically corresponds with thicker, well-expressed genetic horizons and anistropic profiles (Johnson & Watson-Stegner 1987; Schaetzl & Thompson 2015). Anistropic is a term denoting preferential flow direction in soils and other geologic materials due to the shape of grains comprising a soil matrix (Todd 1980; Freeland 2013). Regressive pedogenesis refers to the slowing, reversing or ceasing of soil development. When a pedogenic horizon is undergoing regression, it might appear thinner, blurred, mixed, or eroded on the landscape. Static pedogenesis occurs when forces of regressive and progressive pedogenic development

are equalized, resulting in non-development or stasis in a horizon (Johnson & Watson-Stegner 1987; Schaetzl & Thompson 2015). Acknowledging that pedogenesis occurs on a spectrum brings attention to the presence or absence of pedogenic permutations, or changes, in the relative thickness and expression of soil over time. Such factors are considered in the interpretations of Erfkroon's alluvial sequence.

Concluding Remarks

The theoretical underpinnings for this study derive from multiple perspectives including pedology and soil geomorphology, lithostratigraphy, allostratigraphy, and micromorphology. Implementation of a multi-conceptual approach coincides with the desired goal of presenting a holistic interpretation of Erfkroon's archaeology-bearing alluvial sequence. This goal is further realized by utilizing standardized reference texts including the *Soil Survey Manual* (Soil Science Division Staff 2017), *Field Book for Describing and Sampling Soils* (Schoeneberger et al. 2012), *Guidelines for Analysis and Description of Soils and Regolith Thin Sections* (Stoops 2003), and the *North American Stratigraphic Code* (NACSN 2005).

2. REGIONAL SETTING

Erfkroon is situated in central southern Africa, within South Africa's continental Interior Plateau in the Gariep-Vaal River basin. The site is near where the Kalahari, Karoo, and Grassveld regions meet (Wellington 1944, 1955; King 1963; Tooth et al. 2004). Rivers, the Vaal, Modder and Riet, coursing through the region, occur on or close to bedrock and are variably controlled by the relative resistivity of underlying lithologies. Reaches with increased gradients occur on more resistant bedrock varieties (i.e. andesite and dolerite intrusions) and produce limited quantities of alluvial sedimentation. Lower gradient reaches typically occur over less resistive bedrock (i.e. Ecca group shales) and tend to create wider floodplains where alluvial terracing, channel incision, and donga (gully) formation is common (Tooth et al. 2004; Tooth et al. 2013).

The Erfkroon site sits on the right (north) bank of the Modder River within the Modder River catchment (17,360 km^2), approximately 1,480 km inland from the Atlantic Ocean (Barker 2011; Tooth et al. 2013) and ~115 km from the Modder's confluence with the Riet River to the west. The Modder River catchment occupies a small portion of a much larger drainage known as the Gariep (prev.: Orange) River and its catchment (~953,000 km^2) consists of other westward-coursing rivers including the Vaal (Figure 2.1) (Holmes 2017). The section of the Modder where Erfkroon is located is best described as a low-gradient reach where channel incision, alluvial sedimentation, and donga formation is pervasive.

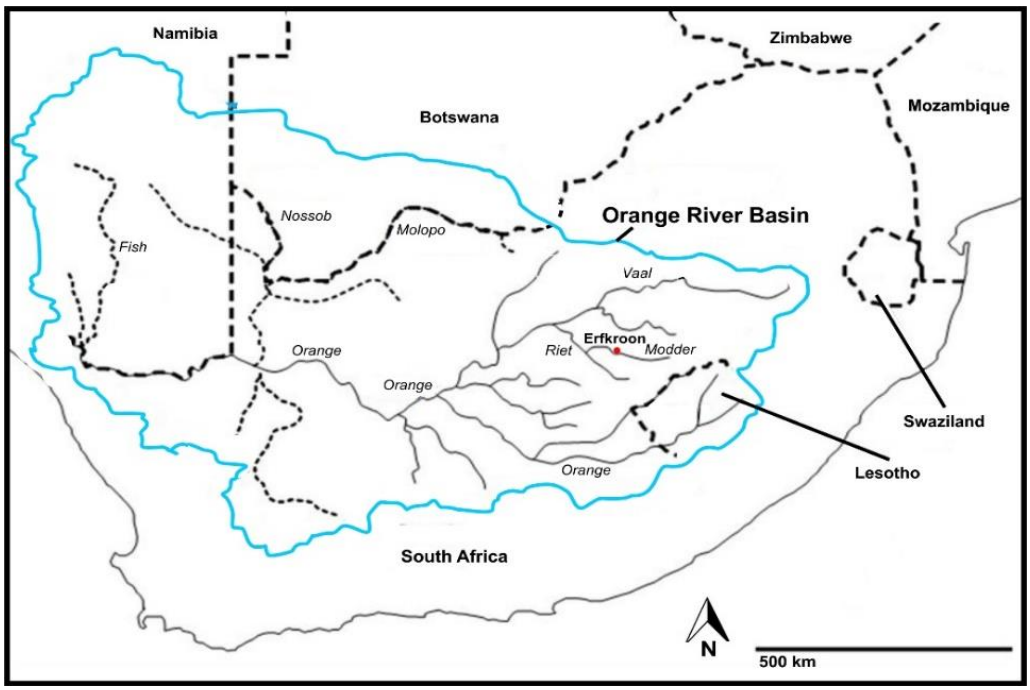

Fig. 2.1. Erfkroon's location within the Orange River Basin catchment. Erfkroon is marked by a red dot, and the catchment is outlined in blue (modified from Kistin & Ashton 2008).

Modern Climate & Vegetation

The terrestrial landscape of central southern Africa is characterized by dry-adapted Highveld Grassland and Kalahari Hardveld and Bushveld communities typical of the summer rainfall zone (SRZ) (Holmes 2017). These communities comprise three of nine prevailing biomes found in and near the Erfkroon study area: (1) Grassland, (2) Savanna, and (3) Nama Karoo (Figure 2.2). Erfkroon rests within the western reaches of the Grassland Biome and is bounded to the northwest by Savanna, and to the southwest by the Nama Karoo. The area's proximity to the Savanna and Nama Karoo boundaries mark this region as a transitional zone. Mucina and Rutherford (2006) define this as the

Western Free State Clay Grassland, a vegetation sub-region of the Dry Highveld Grassland.

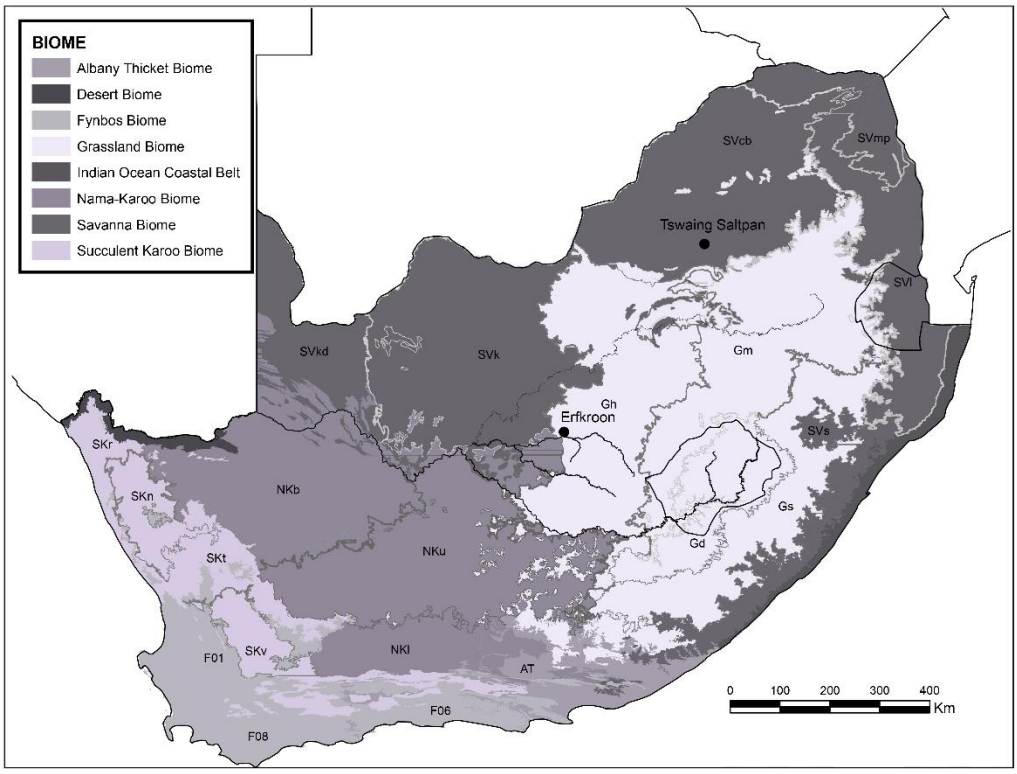

Fig. 2.2. Biomes of South Africa. Erfkroon indicated by black dot.

The Grassland biome comprises the central interior, including the Western Free State Province, and is characterized by grass species from the *Aristida* genus, intermixed with genus such as *Cynaodon, Eragrostis, Panicum*, and *Themeda.* Shrubs and bushes from the *Pentzia globose* and *Lycium cinereum* genus are also typical of the area. Microenvironments include copious small (up to 3000 hectares) deflation basins containing fresh to brackish seasonal lakes known locally as "*pans*." These salt-enriched areas support grass communities from several genus including *Cyperus, Diplachne, Eragrostis, Hemarthria, Juncus, Panicum, Setaria,* and *Andropogon,* and shrub species such as *Salsola glabrescens* (Mucina & Rutherford 2006).

Vegetation of the central interior primarily consists of arid-adapted C_4 grass- and bush species. These proliferate among the central and western reaches of the summer rainfall zone (SRZ). The SRZ refers to climates that are controlled by the seasonal interplay between easterly flows of the Intertropical Convergence Zone (ICZ) and subtropical high-pressure systems forming over the Indian Ocean (Nash 2017). Regions within the SRZ receive the most rainfall between the months of October and March (Figure 2.3) (Crétat et al. 2012; Roffe et al. 2019; Nash 2017).

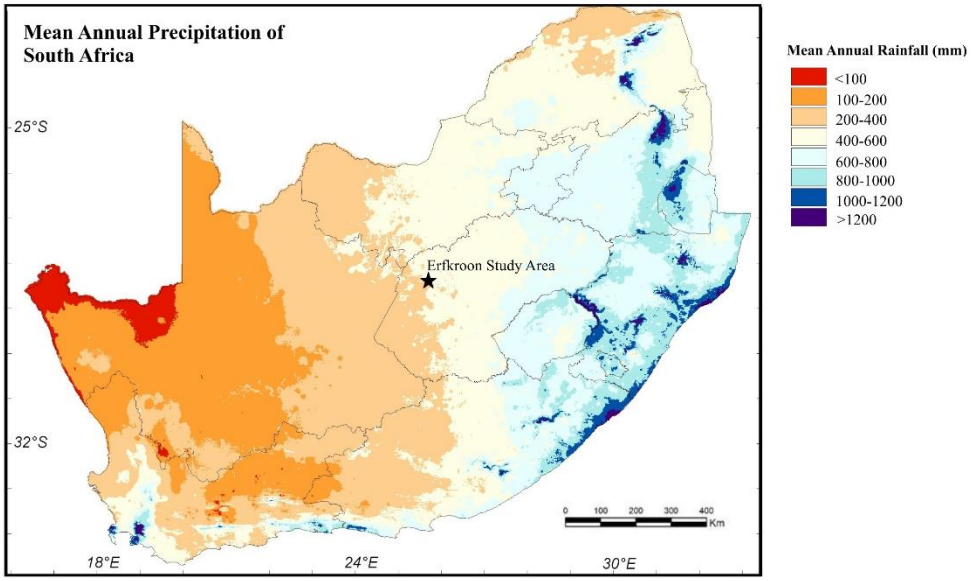

Fig. 2.3. Mean annual precipitation in South Africa (modified from Lynch & Schulze 2007).

Rainfall in the central interior varies east to west, where the extreme east can receive up to ~800 mm of rain annually, while the extreme west may receive ~200 mm or less (Holmes 2017). The Western Free State Province and Erfkroon receive around 400 to 500 mm of rain annually (Goddard & Graham 1999). Gradational, east to west vegetation trends also characterize inland areas of the eastern coastline, mountainous regions of the KwaZulu Natal, and central portions of the Eastern Cape (Rutherford et al. 2006).

The northwest border of the Nama-Karoo (Upper Karoo) occurs about 10 km southwest of Erfkroon. The entire biome encompasses the central plateau region of the Cape Province, extending past the Orange River into Namibia. Its position, overlapping the higher elevations of the Great Escarpment, separates the Karoo into Upper and Lower ecoregions according to elevation. The Upper Karoo refers to areas ~900-1,300 m above sea level and the Lower Karoo refers to areas ~550-900 m above sea level. Northern reaches of the Upper Karoo occur nearest to Erfkroon where a range of tall and low-lying C_3 shrub species, known as *bossies*, and arid-adapted C_4 grasses proliferate. Low bossie species such as *Chrysocoma ciliate*, *Gnidia polycephala*, and *Pentzia calcarean* are common, as are taller bossies from the *Lycium* genus. Dominant grass species in the region include *Aristida adscensionis, A.* (Mucina & Rutherford 2006).

The Savannah biome occurs in the Northern Cape Province to the north, extending south and east into the Western Free State and northern regions of the Gauteng Province. Vegetation is largely comprised of woody C_3 shrubs and trees commonly called the bushveld. A sub-vegetation zone called the Kimberley thornveld comprises northwestern portions of the Orange Free State and the Northern Cape approximately 30 km to the west of Erfkroon.

Local vegetation types at Erfkroon include various drought-adapted tree species, shrubs, and grasses. It being a transitional zone, tree species of varying heights are more common than in the Grassland Biome proper. Taller tree species include *Acacia erioloba* and shorter species such as *Acacia karroo, A. tortillis* subsp. *Heteracantha*, and *Rhuslancia* are common. Shrubs, including taller species such as *Asparagus laricinus, Diospyros lycioides* subsp. *lycioides, Diospyros pallens,* and *Gymnosporia buxifolia* are

also found in the area. Smaller shrubs typical of the Kimberley thornveld also proliferate, including species such as *Acacia hebeclada* subsp. *hebeclada, Aptosimum decumbens, Chrysocoma ciliate, Gnidia polycephala*, and *Pentzia viridis*. Dominant C_4 grass communities primarily consist of *Eragrostis lehmanniana* (Rutherford et al. 2006).

Regional Geology & Geomorphology

South Africa's continental interior is underlain by sedimentary and volcanic bedrock which comprise the depositional sequence of the Main Karoo Basin (~700,000 km^2) (Figure 2.4). The Basin's strata are collectively known as the Karoo Supergroup (Hawthorne 1975; Partridge & Maud 1987; Gilchrist et al. 1994) which are dominated by sandstones, mudstones, and siltstones (Holmes & Barker 2006). Collectively, the Karoo Supergroup reflects major depositional events spanning roughly 120 million years, from 300 Ma to 180 Ma (Johnson et al. 2006). Much of the strata is heavily eroded though areas near the Cape Fold Belt contain isolated thicknesses surpassing 6 km in depth (Smith 1990). Dolerite intrusions are common across the landscape and promote the insurgence of lithologically-controlled mesa and butte landforms (Holmes 2017).

The Karoo supergroup underlies around two-thirds of central southern Africa and is subdivided into five groups differentiated by lithology and chronology. These include the (1) Dwyka (Late Carboniferous), (2) Ecca (Early Permian), (3) Beaufort (Late Permian to Middle Triassic), (4) Stormberg (Late Triassic to Early Jurassic), and (5) Drakensberg (Middle Jurassic) (Johnson 1991; Baiyegunhi et al. 2017) (Figure 2.5). The diverse terrain corresponding with each formation is an expression of the area's dynamic history of sedimentation (Smith 1990). The Dwyka group, corresponding with the Late-Carboniferous (Pennsylvanian) to Early Permian, reflects glacial sedimentation. Marine

and lacustrine depositional environments characterize Ecca Group deposits during the Early Permian, followed by fluvial sedimentation referred to as the Beaufort Group spanning the Late Permian to Middle Triassic. The youngest member of the Karoo supergroup refers to the Stormberg, which largely derived from Late Triassic and Early Jurassic aeolian deposition (Johnson 1991; Baiyegunhi et al. 2017).

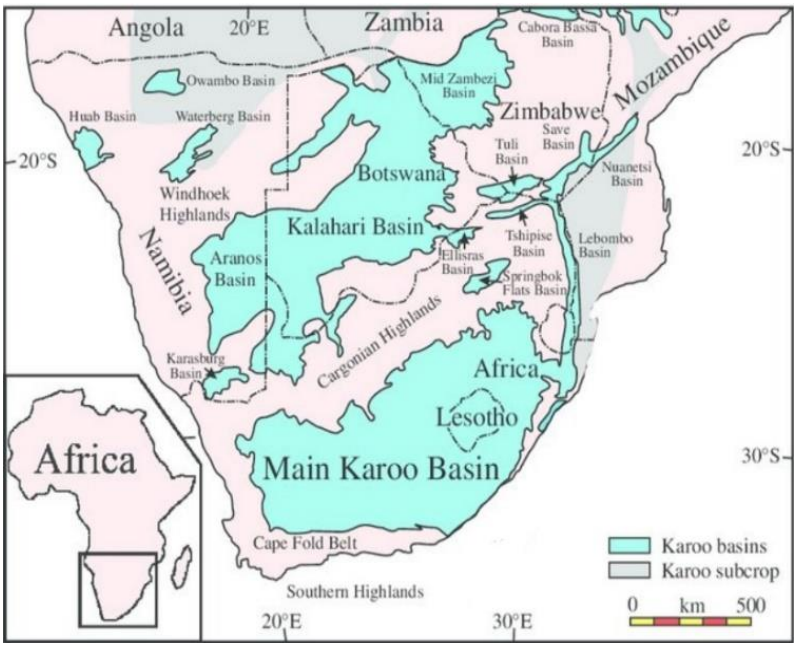

Fig. 2.4. Extent of the Main Karoo Basin (modified from Isbell et al. 2008 and Catuneanu et al. 2005).

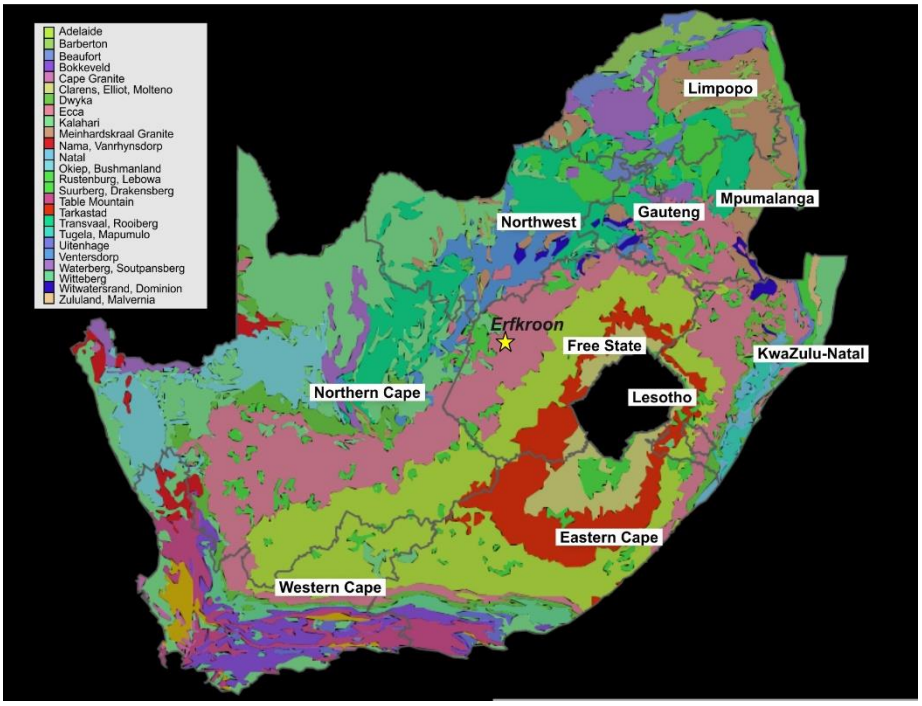

Fig. 2.5. Bedrock geological map of South Africa. The Erfkroon study area occurs on the Ecca Group formation.

Ecca group formations underly the northern aspect of the Free State Province and consist of the Vryheid Formation, the lower Pietermaritzburg Formation, and the upper Volksrust formation (Figure 2.6). Erfkroon is positioned on the Volksrust Formation which represents the youngest, northeastern facies of the Ecca Group and is comprised of fine-grained, dark grey shales and sandstones consistent with late-Permian (upper Ecca) lacustrine deposition (Baiyegunhi et al. 2017). Its lithology is a relic of shallow marine sedimentation that occurred when the area was inundated by the inland Ecca Sea (Catuneanu et al. 2005). The main channel of the Modder River down-cuts into the less resistant Volksrust formation, carrying bed-loads containing poorly sorted gravels, sands, silts, and clays. Though the Modder is perennial, highly seasonal rainfall typical of the

summer months in the SRZ cause faster flows and periodic flooding. These factors encourage incision and erosion of modern embankments and relict landforms, as well as deposition. The landscape topography is now characterized by deeply incised dongas that expose several meters of stratified alluvium from the past and present.

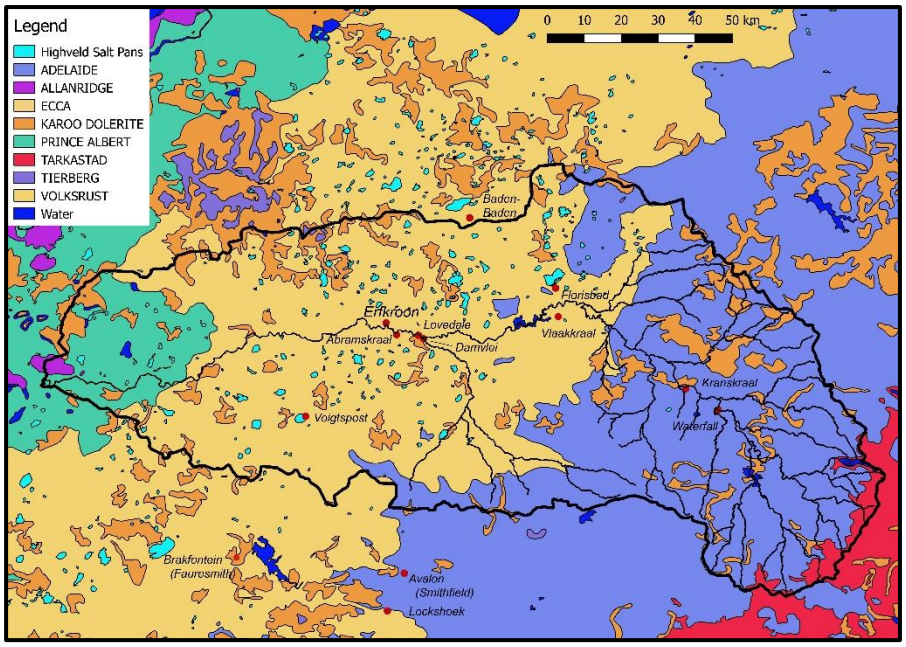

Fig. 2.6. Bedrock geological map of the Modder River Catchment. The Erfkroon study area and a selection of major archaeological locales marked by red dots.

Paleoenvironmental background of the Continental Interior from the terminal Pleistocene to the Holocene

Erfkroon is situated in South Africa's northern continental interior. Historically, the region was referred to as the Basutolian Ecozone which encompassed the area between the Drakensberg Escarpment in Lesotho, the plateau regions of the Orange Free State Province, the southern aspect of the Transvaal, and the northern reaches of the Bushveld (Deacon & Lancaster 1988). Paleoclimate reconstructions of the Highveld Ecoregion at the terminal Pleistocene (40-12 ka) indicate areas to the east were primarily sub-humid, while those to the west were predominantly semi-arid. Highly variable moisture regimes and relatively cooler temperatures coincided with this interval and more

generally, epitomizes the climatic patterns at the Pleistocene-Holocene boundary. Paleoenvironmental proxies including fossilized faunal remains, palynological data, stable carbon and oxygen isotopes, and mineral magnetic signatures helps to illustrate temperature and precipitation trends characterizing the interior from 128 ka to the present.

Established geochronology at Erfkroon derives from an alluvial terrace formation containing archaeology spanning the Middle Stone Age to historic times, where aggradation of its deposits began as early as ~120 ka (Tooth et al. 2013; Lyons et al. 2014; Bousman & Brink 2014). This time interval is referred to as the Late Quaternary period and is characterized by major paleoclimatic shifts corresponding with the Late Pleistocene and Pleistocene-Holocene transition. Intervals of climate change correlate with Marine Isotope Stages (MIS) 5 through 1 (Table 2.1).

Table 2.1. Approximate start and end dates for Marine Isotope Stages 1-5 (modified from Scott & Neumann 2018 and Railsback et al. 2015; based on ice-core data published in Rasmussen et al. 2014).

MIS	Approx. Start Date (cal ka/ka BP)	Approx. End Date (cal ka/ka BP)	Major Climate Event
1	11.7	0	End of Younger Dryas & start of the Holocene
2	32	11.7	Last Glacial Maximum (LGM)
3	57	32	Weichselian High Glacial
4	73	57	Transition into Last Glacial
5a	85	73	Peak of interglacial sub-stage
5b	87	85	Peak of glacial sub-stage
5c	105	87	Peak of interglacial sub-stage
5d	115	105	Peak of glacial sub-stage
5e	130	115	Peak of interglacial sub-stage

The paleoenvironmental record for the Western Free State and South Africa's continental interior spanning the Late Pleistocene (~126 ka to 11.7 ka) through early Holocene derives from geological, faunal, and palynological proxies recovered from

archaeological and paleontological sites, and in some cases, geological landforms. Archaeological sites that are major providers of these data include Wonderwerk Cave, Equus Cave, Florisbad, Wonderkrater, Tswaing Crater, Kathu Pan, Cave of Hearths, Baden-Baden, Bundu Farm, Blydefontein, and Erfkroon to name a few (Figure 2.7).

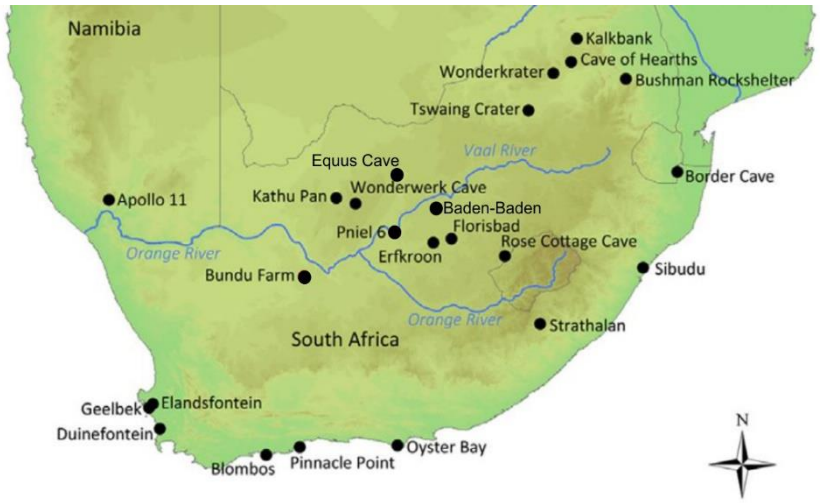

Fig. 2.7. Distribution of interior sites containing paleoenvironmental data from the Late Pleistocene and Early Holocene (modified from Hutson 2018).

The Late Pleistocene (MIS 5-1) coincides with relatively rapid glacial-interglacial cycling that stimulated sudden precipitation and vegetation shifts across southern Africa. Within the continental interior, these cycles typically corresponded with increased aridity (Stokes et al. 1998) and were coupled with vegetation shifts from C_3 to C_4 grasslands (Mucina & Rutherford 2006). The site at Erfkroon is no exception (Bousman & Brink 2014; Bousman et al. *in prep*).

The Tswaing Crater (a.k.a. Pretoria Saltpan) in addition to other nearby sites such as Wonderkrater, provide some of the longest paleoenvironmental records for central southern Africa and the continental interior (Scott 1999). At Tswaing, rainfall estimates span the last 200,000 years and provide the framework for which other climate indices

are compared. Those associated with the Last Glacial Maximum (~24 cal BP) complement other terrestrial paleoclimatic records and characterize the LGM as markedly cool (a temperature difference of 4-5ºC) and dry (Partridge et al. 1999; Heaton et al. 1986; Partridge et al.1990; Talma & Vogel 1992). A cooling trend is also supported by pollen evidence recorded at Wonderkrater, though interpretations of a more arid interval is contradicted by the presence of pollen from moisture/humidity-loving Ericaceous species at MIS 2 (Scott 2016).

Evidence in support of dry and moist conditions at the MIS 3-MIS 2 transition in the continental interior likely have been recovered at sites in the western central portion such as Baden-Baden and Erfkroon. At Erfkroon, general climatic trends reflecting the environment at the MIS 3-2 boundary have been extracted from stable carbon isotopes (Bousman & Brink 2014). These data illustrate a shift from arid-adapted C_4 species to cool-adapted C_3 species at and around the LGM, and into MIS 2. While it is not explicitly known if the C_3-adapted plants are members of the grass or shrub family, nearby sites such as Baden-Baden contain pollen evidence from similar time periods that clarify. Baden-Baden is a spring mound site located approximately 40 km northeast of Erfkroon. Recovered pollen samples dating to 25.8 ka reflect high percentages of grass taxa but also include cold-adapted genus such as *Stoebe* and *Passerina*. Today, both taxa are only found in cool, high-altitude environments conducive to C_3 vegetation growth (Mucina & Rutherford 2006).

An abundance of palynological data specific to the Karoo and western regions of the interior are also good proxies for estimating temperature. Palynological data from Baden-Baden generally suggests widespread, productive grasslands carpeted areas near

Erfkroon at ~25 ka (van Aardt 2015). Such grasslands would have proliferated in cool, moist environments. The presence of these conditions is further supported by pollen spectra from Aliwal North, where a transition from cool and wet conditions coincided with a date of 12,600 BP (Coetzee 1967). But evidence also suggests that the area became warmer and drier at 9,650, near the end of the Younger Dryas and onset of the Holocene (Scott et al. 1995). The terminus of the LGM and transition from MIS 2 (24.11-12.05 ka) to MIS 1 (12.01-0 ka) coincided with a general increase in temperature from ~15 ka (Scott et al. 2012). Geomagnetic proxies extracted from paleosol samples by Lyons et al. (2014) validate this find, further suggesting that precipitation regimes became increasingly seasonal as temperatures gradually increased at the MIS 2-1 transition (15-7 ka).

Global, inter-glacial cycling leading up to the Last Glacial Maximum (24 cal BP) is associated with significant eustatic sea level change, where levels dropped to create habitats conducive for grazing species (Fisher et al. 2010). Continental shelves exposed along the coastal regions of South Africa provided additional, “plains-like” habitats for less specialized grazers, while lacustrine environments formed in the continental interior. These interior lake-systems supplied unique habitats for a range of extinct fauna. Reconstructions of the interior’s late Pleistocene landscape are made possible by the recovery of these taxa, which collectively represent species of the Florisian Land Mammal Age (700-10 ka). Their fossilized presence at locales such as Florisbad illustrates a humid, cooler landscape in the interior up until the Pleistocene-Holocene transition and terminus of the Younger Dryas. Ancient lakes now manifest as modern salt pans (Marshall 1987) and the presence of fossils from locally extirpated, aquatic-adapted

taxa such as lechwe and hippopotamus allude to presence of ancient shorelines (Brink 2005:85-88).

Perennial water sources within the continental interior also supported highly productive grassland ecosystems at the Pleistocene-Holocene boundary. These indulged a variety of grazers, including now-extinct bovid and equid species (Brink et al. 2015). Such species have been recovered from Erfkroon, including the large-bodied wildebeest *Megalotragus priscus,* and giant zebra, *Equus capensis* (Bousman & Brink 2014; Brink et al. 2015). The conspicuous absence of such grazers in the early Holocene fossil record coincides with a reduction in soil moisture and less productive grasslands. These are said to be an effect of warming temperatures and decreased rainfall in the central interior during the Pleistocene-Holocene transition (Brink & Lee-Thorp 1992; Lyons et al. 2014).

Erfkroon's Late Pleistocene-early Holocene paleoenvironmental record mirrors the general patterns described above. More specific interpretations derive from geoproxy evidence reported by Lyons et al. (2014) and Bousman and Brink (2014), and are presented in detail in Chapter 4, "Previous Research at Erfkroon."

3. REVIEW OF MIDDLE & LATER STONE AGE ARCHAEOLOGY IN SOUTH AFRICA

The Middle and Later Stone Age sequences collectively span ~300,000 years, beginning with the mid-Pleistocene Early Middle Stone Age (300-130 ka), and ending with the final Later Stone Age (<2 ka) at the onset of the Holocene (Lombard et al. 2012) (Table 3.1). Archaeological investigations at Erfkroon reveal the existence of both MSA and LSA occupations as well as post-European contact, historic-era sites. Of interest in this study is the contextual integrity, geochronological association, and paleoenvironmental context associated with archaeological components found within the alluvial sequence of Erfkroon's primary terrace system. These occupations have been assigned to the middle MSA, later MSA, Early LSA, and later LSA, and demonstrate the persistence of human occupation in the area for ~100,000 years (Bousman & Brink 2014; Tooth et al. 2013; Lyons et al. 2014).

The technological characteristics of South Africa's MSA and LSA sequences vary with geography and time, and in most cases, coincide with changing paleoenvironmental conditions. These relationships, including a brief historical review of the Stone Age concept, are explored in the following subsections to contextualize archaeology at Erfkroon.

Table 3.1. Timeline of the Stone Age sequences in South Africa and Lesotho (modified from Lombard et al. 2012).

Period	South African Lithic Technocomplex	Also known as (Including regional variants)	Broadly Associated MISs
Later Stone Age	*ceramic Final Later Stone Age (<2 ka)*	Ceramic post-classic Wilton, Late Holocene with pottery (Doornfontein, Swartkop)	MIS 1
<40 ka	*final Later Stone Age (0.1-4 ka)*	post-classic Wilton, Holocene microlithic (Smithfield, Kabeljous, Wilton)	MIS 1
	Wilton (4-8 ka)	Holocene microlithic (Springbokoog)	MIS 1
	Oakhurst (7-12 ka)	Terminal Pleistocene/early Holocene non-microlithic (Albany, Lockshoek, Kuruman)	MIS 1
	Robberg (12-18 ka)	Late Pleistocene microlithic	MIS 2
	early Later Stone Age (18-40 ka)	(informal designation); Late Pleistocene microlithic	MIS 2-MIS 3
Middle Stone Age	*final Middle Stone Age (20-40 ka)*	(informal designation) MSA IV at Klasies River, MSA 4 generally	MIS 2-MIS 3
>20 to <300 ka	*Sibudu (45-58 ka)*	late MSA/post-Howieson's Poort or MSA III at Klasies and MSA 3 generally (all informal designations)	MIS 3
	Howiesons Poort (58-66 ka)		MIS 3-MIS 4
	Still Bay (70-77 ka)		MIS 4-MIS 5a
	pre-Still Bay (72-96 ka)	(informal designation)	MIS 4-MIS 5
	Mossel Bay (77-105 ka)	MSA II at Klasies River, MSA 2b generally (Pietersburg, Orangian)	MIS 5a-c

Brief Conceptual Review of the Stone Age

John Goodwin and Clarence Van Riet Lowe (1929) are credited with developing the archaeological culture history of South Africa in the 1920s. Their contribution was the development of the three-age system collectively termed the Stone Age. Since the late 20th century it has been established that the Earlier, Middle, and Later Stone Age sequences are chronologically synonymous with the European Lower, Middle, and Upper Paleolithic, and correspond with major cognitive, technological, and cultural shifts

among early and anatomically modern humans occupying Africa during the Pleistocene and early Holocene.

The presence of archaeological materials alluding to the antiquity of humans in Africa had been acknowledged since the 1850's (see Malan 1970), however, it was not until the 1880's and later that scholars and geologists systematically prospected South Africa's Cape Coastal Belt and colonial territories (Underhill 2011). By 1900, South African lithic assemblages were the foci of study. Paper and article publications from 1910 and later predominately focused on regionally specific lithic assemblages, many of which illuminated the inadequacies of implementing a Eurocentric, Paleolithic-based typological scheme in their description and contextualization (Underhill 2011). Louis Péringuey (1911), entomologist and director of the South African Museum in Cape Town, was the first to divide South African tools into types deviating from Paleolithic classifications. He employed names such as "Stellenbosch" or "Orange River" to describe assemblages failing to meet Paleolithic type-standards (Shepherd 2002:131).

Paleontological findings also inspired a non-Eurocentric reexamination of the South African archaeological record. Raymond Dart published his description of *Australopithecus africanus* (1925), a hominin fossil excavated at Taung, four years before Goodwin and Van Riet Lowe introduced their Stone Age cultural scheme. Dart's discovery drew international attention and called for more scrutiny of local artifact assemblages— particularly their context within the chronological trajectory of human evolution in Africa (see Le Gros Clark 1946; Richmond 2012).

A research assistantship undertaken by Goodwin in 1923 set the stage for the development of the Stone Age concept. Under directorship of A. Radcliff-Brown at the

University of Cape Town, Goodwin was tasked with cataloguing unprovenanced stone tool collections at the South African Museum. His organizational strategy, based on tool form and geochronological context, gradually took the shape of an archaeological system for typology that deviated from the Paleolithic type system. Successful demonstration of these differences perpetuated Goodwin's desire to create a new typological framework for characterizing archaeological assemblages in Africa (Goodwin 1958; Underhill 2011).

Goodwin's call for a new culture historic framework tailored to African antiquity gained momentum among the scientific community only after he was able to present palpable evidence. This was made possible by his partnership with Clarence Van Riet Lowe. Van Riet Lowe worked as a bridge engineer in the Orange Free State Province prior to pursuing a career in archaeology. His friendship with Goodwin developed into a scientific partnership after agreeing to provide Goodwin with field access and financial support to substantiate his Museum observations (Shepherd 2002). Together, Goodwin and Van Riet Lowe conducted field research and accumulated considerable evidence to argue for an Africa-specific culture history they would coin the "Stone Age" (Klein 2009).

The Stone Age cultural sequence was formally published in *The Stone Age Cultures of South Africa* in a volume of the South African Museum's annual journal in 1929 (Shepherd 2002; Underhill 2011). Its contents differentiated and characterized chronologically unique assemblages based on prevalence or absence of prominent lithic typologies, regional locations, and associated geological contexts (Goodwin & Van Riet Lowe 1929). The Early Stone Age was characterized by the production of maintainable tools, proto-levallois cores and hand-axe technologies (Acheulian) (Goodwin & Van Riet

Lowe 1929), the Middle Stone Age was distinguished by the production of prepared core-tools (Levallois) and other flexible tool-types such as unifaces and hafted projectiles (Goodwin 1927), and the LSA was characterized by the marked increase in the production of microlithic technologies and the use of groundstone implements (Goodwin & Van Riet Lowe 1929).

New archaeological and paleontological discoveries, the recovery of new paleoenvironmental data, and advancements in chronometric dating techniques continue to augment the Stone Age sequence, but the Goodwin-Van Riet Lowe culture historic framework remains intact. In addition, the Stone Age concept, coupled with these combined data, further elucidates the interplay between regional and chronologically unique technological innovations in the archaeological record, adaptative pressures enforced by climate change, and the evolutionary trajectory of modern cognition among *H. sapiens*. These relationships, nested within the Stone Age framework, guide interpretations pertaining to Erfkroon's archaeological record.

Archaeology of the MSA

The South African MSA persisted from ~300,000 to ~20,000 years ago (Lombard 2012; Lombard et al. 2012; Dusseldorp et al. 2013, Wurz 2013) and coincided with the earliest appearances of anatomically modern humans (Clark et al. 2003; McDougall et al. 2005; Grün 2006; Grün et al. 1996). Recent research in the Northern Cape indicates several MSA technological elements had their origins in the Fauresmith as early as ~500 ka (Wilkins and Chazan 2012; Wilkins et al. 2012; Wilkins and Schoville 2016). Occupations of the Middle and later phases of the MSA are summarized in the following subsections.

The Middle Stone Age (MSA) in South Africa is characterized by a broadening of regional tool adaptations paralleling behavioral and cognitive advancements among anatomically modern humans. The regular manufacture of sophisticated flakes and blades from prepared cores, particularly through specific reduction processes such as Levallois, was a hallmark of the MSA. The production of bifacial and unifacial flakes and blades, triangular points, and the implementation of hafting and pyrotechnologies were also popularized during this time (Lombard & Phillipson 2010; Wurz 2013; Wadley et al. 2009).

Archaeology of the Middle MSA. The Middle MSA spans ~100 to ~45 ka and is proceeded by the late MSA and Early LSA (~45 to ~20 ka) (Lombard et al. 2012; Bousman & Brink 2018). Highly variable tool traits and overlapping ages between regionally unique assemblages makes the use of index-based artifact chronologies difficult, therefore, the temporal framework generated by marine isotope stages are more commonly employed to discuss chronological relationships among MSA archaeological traditions (Wurz 2013; Barham & Mitchell 2008; Lombard et al. 2012). The MSA proper roughly corresponds with MIS 5, MIS 4, and the MIS 4-MIS 3 boundary. Climatic instability over the course of these intervals is considered one of the controlling forces behind behavioral innovations characterizing MSA technologies (Lombard et al. 2012). The following summary of the MSA will rely on MIS phases as chronological markers, rather than artifact type chronologies (Table 3.1).

MIS 5 (ca. 130-73 ka BP) corresponds with the Early to Middle Stone Age transition and the MIS 5-4 boundary (ca. 73 ka BP) and coincides with the earliest known occurrences of formal MSA toolkits (Railsback et al. 2015; Lombard et al. 2012). Sites

with long and consistent occupations such as Klasies River Mouth, Blombos Cave, Diepkloof Rock Shelter, Border Cave and Pinnacle Point have well-documented records of this shift in the coastal archaeological record. Sites of the continental interior such as Florisbad, Erfkroon, Kathu Pan, Rose Cottage Cave, Elandsfontein, and Cave of Hearths also contain temporally similar assemblages, though, interior MSA lithics are often described as variants of coastal assemblages. Such differences demonstrate that toolkit variability was just as much a function of geography and climate as it was of time (Lombard et al. 2012).

Acute climatic fluctuations throughout the MIS 5, 4, and 3 (ca. 73 ka BP) (Railsback et al. 2015) intervals contributed to the proliferation of geographically unique paleoenvironments across South Africa's landscape. During MIS 5, the eastern and western coasts of South Africa were characterized by warm temperatures and moist conditions associated with higher sea levels. These conditions slowly receded at the MIS 4 boundary, corresponding with gradual vegetation shifts from C_4 to C_3 adapted species, and the onset of slightly cooler and drier conditions along the southern coast (Scott & Neumann 2018). Increasing aridity and cooler temperatures characterized the boundary at MIS 4 (ca. 73-57 ka BP) and MIS 3 (ca. 57-32 ka BP), which was followed by a warming trend through MIS 3 and MIS 2 (32-11.7 ka BP) (Railsback et al. 2015; Scott & Neumann 2018).

The South African coastal landscape is known for its well-stratified and intact MSA occupations. The best preserved of these are found in coastal rockshelters at sites such as Klasies River, Pinnacle Point, Border Cave, Klipdrift Shelter, Blombos Cave, Diepkloof Rock Shelter, and Sibudu Cave. While regionally variant MSA technologies

are documented, MSA assemblages found in these contexts are dominated by the Still Bay industry (ca. 77-73 ka), with some expressions of the Howieson's Poort industry (ca. 65-59 ka) (Figure 3.1) (Henshilwood & Marean 2003; Jacobs et al. 2008; Henshilwood 2012a). Both industries are also found in the continental interior, however, Howieson's Poort is more prevalent. Interior sites with Howieson's Poort occupations include Wonderwerk Cave, Rose Cottage Cave, Elandsfontein, Cave of Hearths, and Kathu Pan. Continental sites containing both Still Bay and Howieson's Poort assemblages are less common and have only been documented at Rose Cottage Cave, Cave of Hearths, and Apollo 11 (Wurz 2013).

The Still Bay complex refers to multifunctional, bifacially retouched foliate points (Lombard 2006; Wadley 2007). Still Bay materials were typically manufactured from locally sourced raw materials using hard and soft hammer percussion, pressure flaking, and heat treatment techniques; this being the first occurrence of purposeful heat treatment on lithics anywhere in the world (Porraz et al. 2013; Schmidt et al. 2013; Villa et al. 2009), and one of the first examples of pressure flaking (Mourre et al. 2010). Residue and microwear analyses also suggest some Still Bay tools were hafted and used for cutting. This technology spans MIS 5a (~85 ka BP) through MIS 4 (~57 ka BP) and has been identified at sites throughout the Western Cape including Dale Rose Parlour, Hollow Rock Shelter, Diepkloof Rock Shelter, and Blombos Cave. Other sites include Umhlatuzana and Sibudu Cave in KwaZulu Natal, and Apollo 11 in Namibia (Minichillo 2005; Steele et al. 2012; Wadley 2007; Wurz 2013).

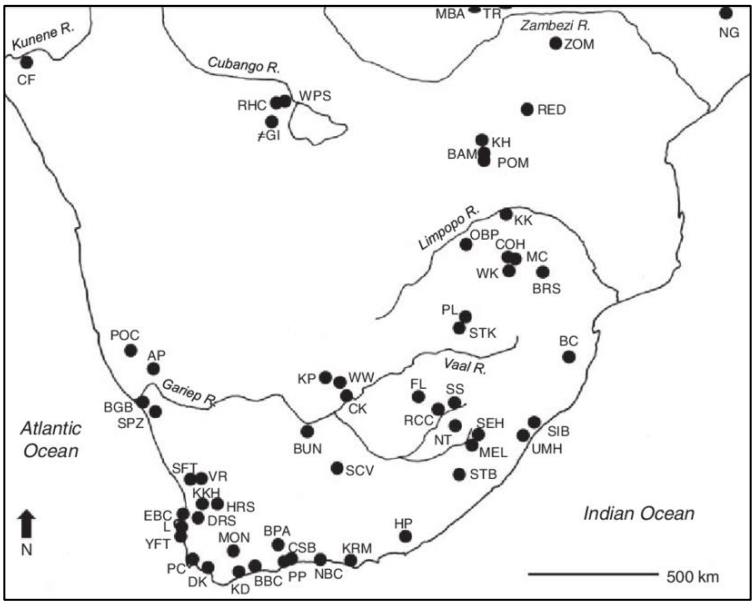

Fig. 3.1. L. Wadley's (2015) mapped distribution of major southern African MSA sites. Abbreviations: AP Apollo 11; BAM Bambata; BBC Blombos Cave; BC Border Cave; BGB Boegoeberg; BPA Boomplaas; BRS Bushman Rock Shelter; BUN Bundu Farm; CF Cufema Reach; CK Canteen Kopje; COH Cave of Hearths; CSB Cape St Blaize; DK Die Kelders Cave 1; DRS Diepkloof Rock Shelter; EBC Elands Bay Cave; FL Florisbad; ≠GI ≠Gi; HP Howiesons Poort;HRS Hollow Rock Shelter; KD Klipdrift; KKH Klein Kliphuis; KH Khami; KK Kudu Koppie; KP Kathu Pan; KRM Klasies River Main Site; L Langebaan; MBA Mumbwa Caves; MC Mwulu's Cave; MEL Melikane; MON Montagu Cave; NBC Nelson Bay Cave; NG Ngalue; NT Ntloana Tšoana; OBP Olieboomspoort; PC Peers Cave; POC Pockenbank; PL Plover's Lake; POM Pomongwe; PP Pinnacle Point; RCC Rose Cottage Cave; RED Redcliff; RHC Rhino Cave; SCV Seacow Valley; SFT Soutfontein; SEH Sehonghong; SIB Sibudu Cave; SPZ Spitzkloof Rock Shelter; SS Sunnyside 1; STB Strathalan Cave B; STK Sterkfontein; TR Twin Rivers; UMH Umhlatuzana; VR Varsche Rivier 003; WPS White Paintings Shelter; WK Wonderkrater; WW Wonderwerk; YFT Ysterfontein 1; ZOM Zombepata Cave.

The production of Still Bay tools paralleled several behavioral and cognitive innovations unique to the MSA including ochre use in the production of compound tools, and the use of decorative elements indicative of symbolic behavior. The earliest direct evidence for the use of ground ochre was as an additive to hafting compounds, the earliest use of which was identified in Sibudu Cave (~70 ka). Evidence of ochre being used in similar fashions has since been found in increasingly later occupations, dating as

late as ~35 ka (into the Early LSA) (Wadley et al. 2004; Lombard 2005; Lombard 2006). Other hafting compounds have been identified on backed tools at Umhlatuzana and Rose Cottage Cave with dates ranging from ~65 to 69 ka (Gibson et al. 2004; Lombard 2005; Lombard 2006). Decorative elements and art alluding to symbolic behavior have been recovered from Blombos and Sibudu Caves. At Blombos Cave, a date of ~77 ka coincides with the recovery of an engraved stone, followed by 'tick shell' (*Nassarius kraussianus*) beads recovered from a slightly younger depositional context (~72 ka) (Henshilwood et al. 2004). African Periwinkle (*Afrolittorina africana*) beads dating to ~71 ka have also been recovered from Sibudu Cave (d'Errico et al. 2008; Lombard 2012).

Howieson's Poort assemblages appear in the record shortly after the abandonment of Still Bay technologies. These are characterized by the increased production of small blades (Deacon 1995; Goodwin & van Riet Lowe 1929) and backed pieces with prepared platforms (Wilkins & Chazan 2012; Wurz 2001). The Howieson's Poort industry occurs in concert with the onset MIS 4 (~73 ka BP) and persists through the MIS 4-3 boundary (~57 ka BP) (Henshilwood et al. 2003; Jacobs et al. 2008; Henshilwood 2012b; Railsback et al. 2015). Radiocarbon dates excluded, dates associated with Howieson's Poort occupations occur tightly between ~65-60 ka, making the tools themselves a reliable MSA marker horizon (Wadley 2015; Jacobs et al. 2008).

Well-dated evidence of Howieson's Poort replacing the production of Still Bay in South Africa occurs at several sites including Sibudu Cave, Umhlatuzana, Diepkloof Rock Shelter, and Rose Cottage Cave (Jacobs & Roberts 2008; Lombard et al. 2012). The best evidence for the transition is found at Rose Cottage Cave which contains an MSA

sequence spanning ~100,000 years. Dates recovered from a well-stratified component of the site containing both complexes demonstrated that pre-Howieson's Poort industries occurred from ~96-72 ka, and post- Howieson's Poort industries after ~63 ka (Jacobs & Roberts 2008; Lombard et al. 2012).

Use-wear and residue analysis on Howieson's Poort materials indicate small, backed blades were inserted into projectile-type implements. Like Still Bay occupations, direct evidence shows that red ochre and plant materials were mixed as adhesive agents for hafting backed blades to compound weaponry (Wadley 2013). Fracturing from impact has also been described on these tools, implying their use as spears or projectiles (Villa & Soriano 2010). The recovery of bone points in Howieson's Poort occupations at Sibudu share similarities with poison-tipped arrows used in later, Holocene contexts (Backwell et al. 2008; d'Errico et al. 2012).

The production of Still Bay and Howieson's Poort industries with other cognitive and behavioral innovations are jointly discussed as strategic adaptations during a period of climatic uncertainty at MIS 5a (~73 ka) and the MIS 5-4 boundary (Railsback et al. 2015; Thackeray 2009; Ziegler et al. 2013). The Still Bay industry entered the archaeological record at the MIS 5-MIS 4 boundary, but was replaced by the Howieson's Poort industry at the boundary between MIS 4 and MIS 3. Punctuated production of Howieson's Poort is thought to represent a behavioral adaptation and strategy for survival during acute intervals of climate fluctuation (Roberts et al. 2016; Bar-Matthews et al. 2010; Ziegler et al. 2013).

This climate change adaptation hypothesis is supported by the recovery of pollen data illustrating dramatically changing vegetation regimes at the time. The introduction of

the Still Bay industry coincides with the return of glaciation at the MIS 5-4 boundary. Reduced proportions of pollen associated with woodland taxa during the terminal phases of MIS 5 and at the MIS 5-MIS 4 boundary suggests increased aridity during this phase encouraged the proliferation of grasslands, especially among coastal environments (Scott & Neumann 2018). Such evidence suggests Howieson's Poort materials replaced Still Bay technologies during MIS 4 with the onset of a stable, mesic interlude (Railsback et al. 2015; Thackeray 2009; Ziegler et al. 2013; Scott & Neumann 2018).

Archaeology of the Late MSA. Highly variable and unconstrained tool varieties collectively named "post-Howeison's Poort" replace Howieson's Poort industries around ~58 ka, then persists until ~25 ka (Wurz 2013). The Post-Howieson's Poort industry is an ill-defined category within the broader spectrum of later MSA technocomplexes because it fails to meet Howieson's Poort morphological constraints (Lombard et al. 2012). Its variability has since become a defining characteristic of later MSA toolkits, and variations in style, raw materials, and tool classifications are thought to coincide with the expansion of exploitable environments, as well as regional adaptations to acute climate change events associated with the onset of MIS 3 (Wurz 2013).

MIS 3 (57-32 ka BP) is associated with significant climatic shifts around ~57 ka (Railsback et al. 2015) and coincides with the Later MSA-LSA transition (Cochrane 2008; Wurz 2013). The nature of this period and its impact on human occupation in South Africa remains largely unknown due to poorly preserved climatic proxies and by a general lack of archaeological data available for the period (Deacon & Thackeray 1984; Steele & Klein 2009). Available proxies (e.g. pollen and stable carbon and oxygen isotopic data) suggest that MIS 3 was affected by eustatic sea level fluctuations and

intense periods of rainfall followed by aridification (Fisher et al. 2010; Scott & Neumann 2018; Deacon & Thackeray 1984). Geographically disparate fluctuations in pollen ratios associated with the western, eastern, and southern coastlines, as well as the continental interior suggest regionally specific, and highly variable climates could be found across South Africa at this time (see Scott & Neumann 2018).

Broadly speaking, climate change events during MIS 3 perpetuated regionally disparate paleoclimates throughout southern Africa and corresponded with the production of diverse lithic technologies ranging from post-Howieson's Poort industries of the Middle MSA, to industries of the Later and terminal MSA. These assemblages are best represented at sites such as Rose Cottage Cave and Sibudu Cave. At Rose Cottage Cave, a well-stratified post-Howieson's Poort occupation was dated to ~63 ka (Jacobs & Roberts 2008; Lombard et al. 2012) and consisted of convex scrapers, points, and a few backed tools (Wadley 1997; Mohapi 2007). A similar assemblage was identified at Sibudu Cave in Kwatzulu Natal, but with the addition of later and final MSA components. Post-Howieson's Poort occupations at Sibudu occurred from ~58 to ~57 ka, later MSA occupations from ~50-40 ka, and final MSA occupations dating to ~38 ka (Jacobs et al. 2008; Wadley 2013). Sibudu's Later MSA occupation consisted of unifacial points with evidence of retouch, Levallois flakes, and unifacially and bifacially retouched points (Lombard 2004; Wadley 2013). The final MSA occupation (~37 ka) at Sibudu was characterized by scrapers, segmented and notched pieces, and bifacially and unifacially retouched points (Wadley 2013).

Archaeology of the MSA-LSA transition. The transitional phase between the MSA and LSA occurred sometime around ~40 to ~30 ka (Mitchell 1994; Mitchell 2008; Clark

1997; Lombard et al. 2012), though more recent studies conducted by Bousman and Brink (2018) suggest the transitional bracket is broader, with significant overlaps between the terminus of the later MSA (~20 ka BP) and the onset of the Early LSA (ELSA). Bousman and Brink argue the MSA-ELSA transition occurred rapidly within sites, but was geographically time transgressive from east (~45 ka) to west (~23 ka) across southern Africa. The technological character of this transitional is associated with the production of bifacial, unifacial and hollow-based points, including flakes manufactured through bipolar reduction. Specific chronologies for the MSA-LSA transition remain ambiguous but bipolar reduction techniques were more readily seen during this time and became increasingly visible with the onset of the ELSA (Beaumont 1978; Lombard 2012). The MSA-LSA transition also coincides with a rise in microlithic "bladelet" production (Villa et al. 2012) and other prominent LSA trends including the production and use of ground-stone technologies, bone arrowheads, awls, and digging sticks (d'Errico et al. 2012).

Archaeology of the Later Stone Age

The Later Stone Age (LSA) in southern Africa was first described by Beaumont and Vogel (1972) and characterized based on assemblages recovered from Border Cave dating to ~45 ka and later. Microlithic technologies produced via bipolar core reduction was a common attribute of this phase and has become one of the defining characteristics of LSA industries. Other implements, including scrapers, bone points, awls, digging sticks, and ground-stone technologies have also been noted, sometimes without the presence of microlithic artifacts (Beaumont et al. 1978; d'Errico et al. 2012; Bousman, personal communications 2019).

Assemblages characterizing the LSA appear in the South African archaeological record during MIS 3 (58-32 ka BP), where production of LSA technologies persisted through the MIS 3-2 boundary. Early LSA occupations occur around 45 ka cal BP. This period was characterized by an interglacial when the continental interior was dominated by savanna biomes and warm temperatures, and coastal areas by cool, moist conditions capable of hosting more ericaceous species (Bousman & Brink 2018; Scott & Neumann 2018). Later LSA occupations coincide with the MIS 3-2 boundary which incurred rapid fluctuations in moisture regimes. In the 1970's, Deacon (1984a) suggested the production of microlithic technologies associated with Robberg (~22-12 ka) and later industries were adaptive responses to changing availability of floral and faunal resources as a result of climate change, where such tools were manufactured to complete specialized tasks. Others, such as Bousman (2005), suggest subtler environmental shifts at the regional level were catalysts for technological change. Both scenarios are plausible given the variety of regionally unique paleoenvironments characterizing the terrestrial landscape of southern Africa during the Pleistocene-Holocene transition.

Archaeology of the LSA [proper]. Industries defining the LSA [proper] include the Robberg (~22-12 ka), Oakhurst (~12-7 ka), Wilton and Smithfield (~8-4 ka) (Sampson 1974; Deacon & Deacon 1999). The Robberg industry occurs stratigraphically above transitional and Early LSA assemblages and is characterized by the systematic production of microlithic "bladelets" (Deacon 1984a, 1984b). These were first described at sites such as Nelson's Bay Cave and Melkhoutboom (Klein 1974; H. Deacon 1976, J. Deacon 1978), and have been found elsewhere along the coast and continental interior at Kangara, Blydefontein, Erfkroon, Equus, Umhlatuzana, Sehonghong, Shongweni,

Faraoskop, and Ravenscraig among others (Bousman & Brink 2018). Recent models (see Bousman & Brink 2018) suggest the appearance and use of Robberg industries occurred rapidly, then persisted over a period of about 20 ka starting as early as ~25 ka (Carter & Vogel 1974; Mitchell & Vogel 1994) and as late as ~9180 ka BP (Kaplan 1989).

The Oakhurst complex refers to flake technologies produced during the MIS 2-1 transition, from ~12 to 8 ka (Deacon 1976; Deacon & Deacon 1999; Humphreys & Thackeray 1983; Mitchell 1997, 2002; Parkington 1984; Sampson 1974). The industry was formally characterized by Garth Sampson in 1974 after a reexamination of a lithic assemblage recovered from Oakhurst Cave in the Southern Cape. Typical lithic technologies of the Oakhurst complex include broad flakes, many with unfaceted platforms, and large, single-platform cores (Sampson 1974:259). However, Sampson's continued investigations of Oakhurst-like assemblages revealed significant geographic variation. This resulted in the subdivision of Oakhurst into three sub-industries meant to reflect the geographic region in which they proliferate: (1) the Oakhurst Industry (originally termed Smithfield A), (2) Lockshoek Industry, and (3) the Pomongwan Industry (Sampson 1974). Lockshoek refers to the regional variant of Oakhurst that was produced in the continental interior and has been identified at sites including Florisbad, Rose Cottage Cave, Blydefontein, Uitzigt, Wonderwerk, and Dikbosh 1 (Wadley 2000; Bousman 2005).

The Wilton complex broadly refers to a microlithic industry proceeding Oakhurst at around ~8 ka (Deacon & Deacon 1999) and consists of a range of tool forms including segments (crescents), backed bladelets, and a variety of micro-scraper technologies. The Wilton complex has, however, undergone several revisions since Goodwin and Van Riet

Lowe's initial codification of the phase. Wilton was initially defined by Hewitt (1921) and accepted by Goodwin and Van Riet Lowe (1929) as a 'culture' of the Later Stone Age that broadly included scrapers, backed blades, ornaments, bone tools, and segmented (crescent-shaped) pieces. This description derived from Hewitt's initial analysis of an assemblage recovered from the Wilton Rock Shelter and type-site located along the Cape coast. The Smithfield industry referred to the interior counterpart of coastal Wilton assemblages and was first classified by Van Riet Lowe in the 1920's from a contextually mixed surface collection sourced to the Free State province. It was originally suggested that Wilton was a predecessor of Smithfield (Goodwin & Van Riet Lowe 1929:149). Various surveys conducted by van Riet Lowe and others further attributed surface finds to Smithfield occupations, where differences in patination and form led to the designation of three primary Smithfield phases: A, B, and C. Smithfield A represented the earliest phase and Smithfield C was the youngest, where all three phases shared a similar chronology with coastal Wilton assemblages. The absence of backed tools and segmented pieces, along with the presence of large scrapers, primarily differentiated interior Smithfield assemblages from their coastal Wilton counterparts (Goodwin & Van Riet Lowe 1929).

An absolute chronology for Wilton/Smithfield complexes was not established until 1974, when Sampson published results from an exhaustive archaeological investigation of the Orange River. His project was effectively a mitigation effort to collect archaeological data within the boundaries of the Orange River Scheme, a government-mandated project that would result in the construction of two hydroelectric dams and subsequent flooding of a ~740 sq km tract of land (Sampson 1974). Sampson's

investigation resulted in the identification of 942 Stone Age sites, 11 of which were excavated (Sampson 1974:3, 180). Six of the 11 excavated sites contained LSA assemblages and were subsequently radiocarbon dated.

Sampson (1974) grouped the Orange River LSA assemblages by respective radiometric time scales and created a new LSA classification scheme reduced to three complexes: (1) Oakhurst, (2) Wilton, and (3) Smithfield. Revisions were suggested as follows: (1) "Oakhurst" was proposed as a replacement of the former Smithfield A industry, (2) "Wilton," formerly subdivided into Wilton and Smithfield's A-C, was proposed to collectively accommodate Sampson's Interior Wilton, Smithfield C, and coastal Wilton assemblages, and (3) "Smithfield" was proposed for all Holocene-age Smithfield B assemblages (Sampson 1974). Sampson's Interior Wilton complex, a component of his Wilton designation, was divided into four phases: (1) Early, (2) Classic, (3) Developed, and (4) Ceramic.

Early and Classic Wilton assemblages span ~8 to ~4 ka, while Developed and Ceramic Wilton assemblages appear after ~4 ka. Few Early Wilton assemblages have been documented. Tloutle Rock Shelter in western Lesotho represents one of the few well-documented sites containing evidence for the phase which is characterized by various microlithics and large flakes and scrapers showing evidence for steep lateral retouch (Mitchell 1993). Classic Wilton assemblages are far more abundant and are characterized by small, formal tool types with evidence of standardized retouch such as scrapers and backed elements manufactured from fine-grained materials. Such assemblages were first identified at the type site, Wilton Large Cave, in the Eastern Cape, but have since been recovered along the coast and to some extent, as far inland as the

Cape Fold Belt. Assemblages have also been identified in the central and western interior at sites such as Rose Cottage Cave (Wadley 1997) and Jubilee Shelter (Wadley 1986). Wilton materials have also been recovered [less frequently] in the Northern Cape (Humphreys and Thackeray 1983; Bousman 2005). Non-lithic technologies associated with the Wilton type-industry include bone points, awls, linkshafts, and decorative items produced from bone, marine shell and ostrich eggshell (Sealy 2016).

Archaeology of the Terminal LSA. The terminal LSA in South Africa is characterized by Post (Developed) Wilton and Ceramic Wilton industries (~4-2 ka), and Smithfield (~2 ka and later) industries (Sampson 1974; Deacon & Deacon 1999) that collectively replace Classic Wilton at ~4 ka. Forms of each industry vary geographically but mutually display a reduction in standard manufacturing techniques; movement away from the production of more formal scraper technologies and segmented pieces characteristic of Classic Wilton assemblages.

Sampson's (1974) Developed Wilton (also referred to as Post-Wilton) refers to a range of informal and microlithic tools. Coastal, Post-Wilton (Developed Wilton) assemblages are largely characterized by informal flakes and chunks often manufactured from crude raw materials such as quartzite. A reduced presence of formal microlithics among coastal assemblages coincides with greater quantities of bone-tools and other organics, alluding to a declining reliance on stone tool technologies. However, Post-Wilton/Developed Wilton assemblages among interior sites demonstrate a continuance of more formal microlithic manufacturing practices observed at sites such as Blydefontein (Bousman 2005).

The archaeological visibility of the post-Wilton toolkit is generally greater than earlier Wilton assemblages, and is thought to reflect expanding population densities. This is implied by the "sudden" appearance of post-Wilton tools in the interior, where no previous record of Wilton occupations existed. This is also the case for reaches of the interior Karoo where Developed Wilton materials provide the only evidence for human occupation after ~4 ka (Deacon 1974; Deacon 1984a). Population growth during the Developed Wilton phase is also suggested by the presence of large middens identified among coastal sites, some containing meters of debris. The sheer size and diverse contents of middens at sites such as Elands Bay Cave alludes to intensification of marine resources and evolving hunting strategies geared towards the exploitation of smaller game (Parkington et al. 1988; Jerardino 2010).

The Smithfield complex coincides with occupations dating to ~2 ka and later and refers to a geographically unique technology found in the central interior. The industry is primarily characterized by the production of flakes with evidence for formal retouch, the production of end-scrapers, and less frequently, the manufacture of backed microlithics from hornfels and quartz among other crypto-crystalline materials. This industry overlaps with the onset of the Iron Age at ~1000 AD, where evidence for lithic production coincides with the manipulation of iron, and in some cases, the production of ceramic materials. This is demonstrated at interior sites such as Canteen Kopje in the Northern Cape, where Smithfield scrapers occur in the same depositional context as ceramic and iron materials (Mitchell 2002).

It bears mentioning that the first evidence for pastoralism and ceramic production occurs sometime after Post-Wilton and during the Smithfield industrial phase. Ceramics

enter the archaeological record as early as ~2000 BP, either closely followed by or coinciding with pastoralism around 2000-1600 BP (Sampson 1974; Klein 1986; Sadr & Smith 1991; Sealy & Yates 1994). As with lithic technologies, ceramic types vary with time and geography where notable differences in form, function, and manufacturing techniques have been noted between coastal and interior assemblages (Sampson 1974). The earliest documentation for ceramic production in the continental interior occurs at sites in the Upper Karoo, while early coastal ceramic production has been noted among sites on the Cape coast. In the Upper Karoo, sites such as Boundary Shelter contain relatively thin-walled, fiber-tempered ceramics dating to 2160 BP (Sadr & Sampson 2006). Those identified along the Cape coast occur at sites such as Kasteelberg and contain evidence of mineral-tempered ceramics dating to ~1860±60 BP (Sadr & Smith 1991).

4. PREVIOUS RESEARCH AT ERFKROON

Erfkroon has been the focus of paleontological, archaeological, and geological investigations since its discovery in the late 1990's. Here, previous archaeological and paleontological research is summarized, followed by a comprehensive review of previous geological research.

Previous Archaeological & Paleontological Research at Erfkroon

The Erfkroon study area was discovered in 1996 by James Brink during a paleontological survey of the Modder River valley. Brink was drawn to the Modder's highly visible, well-stratified and heavily eroded alluvial architecture— a landscape thought to be promising for well-preserved archaeological and fossil materials as several such sites had been previously recorded in the valley by van Hoepen in the 1920s and 1930s (van Hoepen 1928, 1932). Along the Modder, Brink found that overbank sequences were well-exposed as a product of lateral bank incision, and fossil and archaeological materials once completely buried within, were visible due to erosion. These observations were enough to prompt a series of archaeological, paleontological, and geological investigations in later years. The first formal archaeological and paleontological investigations to occur followed shortly after Brink's discovery. This manifested as the 1997 Duke University field school collaboratively directed by Steven Churchill, James Brink, and Lee Berger.

The Duke University field school investigations at Erfkroon resulted in the identification of 17 locales (EFK-1 through EFK-17) containing archaeological and/or paleontological materials observed within or eroding out of incised alluvial exposures. Artifact assemblages spanning the Middle and Later Stone Age were observed, some of

which occurred in context with well-preserved faunal remains. Other areas, particularly older channel deposits, contained fossilized fauna from the late Pleistocene Florisian Land Mammal Age (Hendey 1974) all together illustrating Erfkroon's potential to contain important paleoenvironmental information spanning the Quaternary (Churchill et al. 2000).

Five of the 17 localities were excavated: EFK-1, EFK-2, EFK-4, EFK-5, & EFK-7, and Optically Stimulated Luminescence (OSL) samples were collected from EFK-1 and EFK-2. EFK-1 yielded an OSL date of 25±1.2 ka. This was recovered from a deposit containing in situ faunal remains of grassland-adapted mammals typical of South Africa's central interior during the Middle and Late Pleistocene, i.e., Florisian Land Mammal Age (Henley 1974). The corresponding deposit was described in later research as the Upper Grey Paleosol (see Tooth et al. 2013; Bousman & Brink 2014). EFK-2 yielded an OSL date of 113±6 ka and was taken from a context associated with an extinct species of hippo morphologically like *Hippopotamus gorgops*, suggesting the persistence of an aquatic ecosystem during this interval. The sample was extracted from a stratum later described as the "Upper sandy gravels with bivalves" in more formalized geological investigations (see Tooth et al. 2013).

EFK-4 contained a fossil assemblage dominated by grassland-adapted mammals, while EFK-5 yielded a well-preserved, partial cranium of *Megalotragus priscus*, a form of extinct giant wildebeest. Fossilized remains from an extinct wetland adapted bovid, *Kobus ellipsiprymnus,* was identified in a similar geological context, as were other fossil materials from EFK-7. These were dominated by the remains of grassland-adapted micromammals (Churchill et al. 2000). The presence of ecologically disparate taxa in

similar geological contexts alludes to a highly variable ecosystem at Erfkroon during the Late Quaternary. Results from the Duke University Field School excavations were later published as a preliminary study highlighting Erfkroon's archaeological and paleontological potential by Churchill et al. (2000).

University of Witwatersrand student, Aaron Hutchison, conducted an independent excavation at Erfkroon from 1998 to 1999. He excavated an 8-x-8 m unit informally called "Hutchison's Pit" in later literature (see Palmison 2014; Bousman & Brink 2014). The unit was positioned between Bousman and Brink's Area E and Area G excavation localities and reached a maximum depth of about 90 cm. The unit, exposing the Brown and the top aspect of the Upper Grey alluvial units of the main terrace, produced 49 artifacts associated with the Later Stone Age Robberg Industry. Though Hutchison would never formally publish his data, photographs, descriptions, and analyses of the collection were published in a 2014 master's thesis by Molly Palmison (2014) through Texas State University.

Archaeological and paleontological excavations resumed at Erfkroon in 2006 and continued into 2014. These were supervised by Britt Bousman and James Brink and include Molly Palmison's MA Thesis research. Bousman and Brink collectively excavated 57 units from 15 locales referred to as areas A, B, C, D, E, Upper F, Lower F, G, H, I, J, K, L, the Equid Site, and the New Meg Site (Figure 4.1) (Bousman & Brink 2014). Palmison's excavations occurred in Areas K, G, and L in 2013, as a component of Bousman and Brink's long-term study. Her excavations revealed the first recorded, open-air Robberg assemblage within the continental interior. Their collective efforts provide documentation of a long history of human occupation spanning the MSA (~100 ka to ~50

ka) into the final MSA/Early LSA around ~20 ka (Bousman & Brink 2014) within Erfkroon's main terrace formation. OSL dates produced from samples associated with in situ archaeological or paleontological materials are presented in Table 4.1.

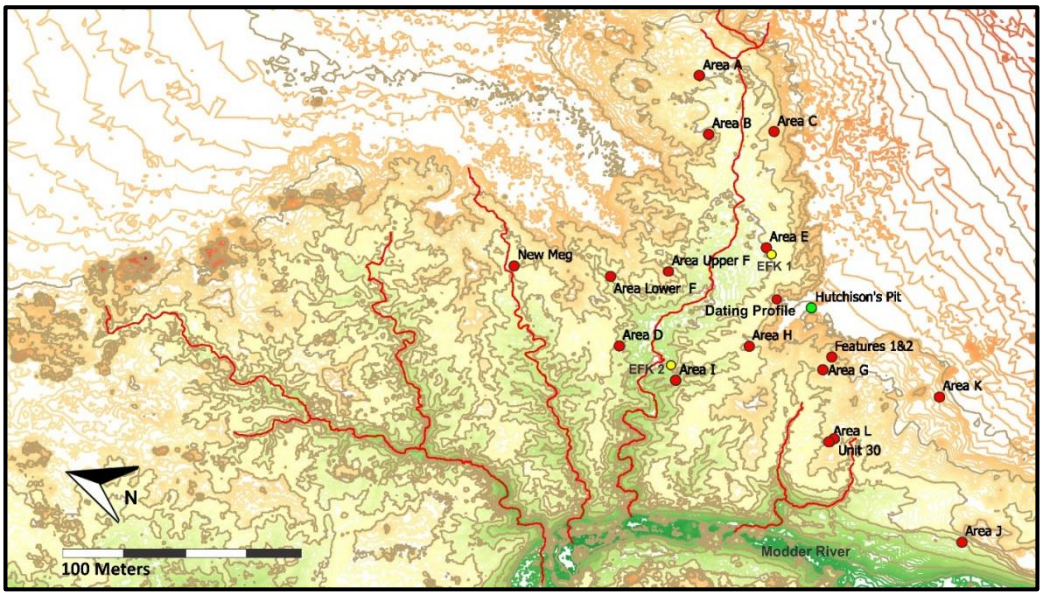

Fig. 4.1. Topographic map with locations of previously tested archaeological and paleontological locales at Erfkroon. Bousman & Brink (2014) excavation areas are labeled with red dots, the Churchill et al. (2000) excavation areas are labeled with yellow dots (only areas EFK-1 and EFK-2 portrayed), and the location of Hutchison's Pit is labeled in green.

Table 4.1. Bousman & Brink (2014) OSL results for samples collected at archaeological & paleontological locales. Dates represent best age estimates for samples collected in units containing in situ archaeological materials. OSL dates were produced by Mark Bateman using single-grain and single-aliquot methods. Abbreviations: mbs= meters below surface.

Excavation Area	Associated Strata	mbs	Archaeology	OSL Date	±
Upper F	Upper Grey	2.82	Late MSA	27.2	1.6
Upper F	Upper Grey	2.95	Late MSA	34.1	2
Area B	Red	1.88	Late MSA	32.1	3.1
Area B	Lower Grey	2.11	Late MSA	25.9	1.7
Area C	Lower Grey	4.13	Late MSA	38.82	2.28
Area C	Lower Grey	4.28	Late MSA	38.52	2.37
Area C	Lower Grey	4.38	Late MSA	31.79	3.09
Lower F	Lower Grey	4.34	Middle MSA	99.4	6.6
New Meg	Lower Grey	3.43	*Megalotragus priscus*	60.88	4.18

The most productive excavation units were dated by collecting OSL samples. These were used to corroborate the contextual integrity of recovered MSA and LSA

artifacts, and for later comparisons with Tooth & Lyon's geochronology as a component of Bousman and Brink's geology-specific research (see Tooth et al. 2013; Lyons et al. 2014). Area F produced the oldest in situ component which corresponded with the earlier portion of the Late MSA (~88 ka). Recovered archaeological materials included alternately beveled and unifacially-re-sharpened flake-blades. Later MSA materials were collected from Area B where sediments produced an OSL date of 25.9±1.7 (Bousman & Brink 2014). Area C also produced later MSA components, two OSL dates, and a radiocarbon date. Two OSL samples produced a date range from 38.52±2.37 ka to 38.82±2.28 ka and a single radiocarbon date produced an age of >50 ka, though Bousman and Brink report that archaeology in Area C is likely out of context due to redeposition as suggested by artifact size sorting. If this is the case, then the 50 ka radiocarbon date most likely applies.

An artifact assemblage consisting of broken grinding stones and bipolar pieces (e.g., *pièces esquillées*) constructed from flakes characteristic of LSA technologies were found in the Upper Grey in Area F. No dateable samples were collected from this locale, but the stratigraphic context of the artifacts laterally correlated with OSL age estimates (~20 and 19 ka) produced by the Lyons et al. (2014) geological study at the nearby Dating Profile (see Figure 4.7). However, two OSL dates of 34.1±2 ka and 27.2±1.6 ka were collected stratigraphically below the archaeological finds (Bousman & Brink 2014). In addition to archaeology, Bousman and Brink also identified seven faunal classes and thirty species. Four classes and 18 species were identified within the Brown, Upper Grey, Red, and Lower Grey sediments of the main terrace (later named Orangia Terrace) alone (see Table 4.2) (Bousman & Brink 2014).

Table 4.2. Summary of faunal classes, species, and species counts recovered by Bousman & Brink (2014) in the Orangia Terrace at Erfkroon. Primary strata in which fauna were found are described according to the original naming system published in Tooth et al. (2013) and modified by Lyons et al. (2014).

Fauna		**Stratigraphic Association in Overbank Alluvium**			
Class	Species	Brown	Upper Grey	Red	Lower Grey
Mollusca	*Unio caffer*				19
	Corbicula fluminalis				2
Rodenitia	*Otomys sp.*		1		
Perissodactyla	*E. lylei*		2		
	E. quagga		2		
	Equus capensis				1
	Equus sp. `				1
Artiodactyla	*Phacochoerus aethiopicus*				1
	Syncerus antiquus		1		
	cf. Oryx gazella		1		
	Megalotragus priscus			1	1
	Connochaetes taurinus		1		
	C. gnou		1	1	1
	Connochaetes sp.				1
	Antidorcas marsupialis		1		
	A. bondi				1
	Bovidae indet. (Large-Medium)				2
	Bovidae indet. (Small)				1
Totals by Stratigraphic Association		0	10	2	31

Previous Geological Research at Erfkroon

Churchill's publication highlighting Erfkroon's potential for containing well-preserved archaeology and paleoenvironmental data catalyzed efforts to better understand the region's alluvial geology. Stephen Tooth (Tooth et al. 2013) was the first to investigate the region from a geomorphological perspective in the early 2000's. His efforts produced the first interpretation and geochronological sequence for the region where he identified a single, paired terrace containing channel deposits superimposed by four accretionary paleosol sequences. The use of IRSL and OSL dating methods demonstrated these sediments collectively spanned the late Pleistocene through the early Holocene. Tooth's description of the single terrace and his accretionary hypothesis

concerning the overbank paleosol sequence provided the foundation for geological investigations conducted in later years by Richard Lyons, Britt Bousman, and James Brink (Tooth et al. 2000; Tooth et al. 2013; Lyons et al. 2014; Bousman & Brink 2014).

Richard Lyons, a former graduate student under Tooth at the University of the Witwatersrand, expanded Tooth's investigation by conducting a detailed paleoenvironmental study of the overbank sequence comprising the upper reaches of Tooth's paired terrace. He investigated the validity of Tooth's accretionary interpretation by analyzing sediments using magnetic susceptibility and diffuse reflectance spectroscopy analysis (DRS), an analytical method that measures infrared radiation (IR) interactions with fine particles in the IR spectrum. DRS helps to obtain information about the molecular structure of organic and inorganic (amorphous, disordered, crystalline etc.) materials (Dalal & Henry 1986; Janik & Skjemstad 1995; Viscarra Rossel et al. 2006), and in this context, was used to identify and characterize iron oxides in paleosols. With these combined methods, Lyons created a rainfall and sedimentation model for the terrace's formation, ultimately concluding that Tooth's accretionary hypothesis was correct. His study provided the first paleoenvironmental reconstruction of Erfkroon's alluvial geology (Lyons et al. 2014). Lyons also re-dated the sequence using single-grain and small aliquot OSL techniques which offers the most detailed and reliable chronology for the sequence to-date.

Tooth and Lyons' geological research occurred simultaneously with archaeological investigations led by Britt Bousman and James Brink from 2006-2014. In excavating several archaeological locales at Erfkroon, Bousman and Brink invariably exposed the same alluvial strata previously described by Tooth and Lyons as accretionary

paleosols. These excavations provided a unique opportunity to observe Erfkroon's alluvial geology from a variety of finer-grained depositional contexts, empowering Bousman and Brink to contrive their own interpretations of the alluvial setting. The outcome of their investigation was the construction of a multi-terrace model for Erfkroon in which three separate terraces were identified. These were named by Bousman and Brink, then published for the first time in a 2015 paleontological paper. In descending order of age, terraces are named: the Erfkroon Terrace, Orangia Terrace, and Soetdoring Terrace (Bousman & Brink 2014; Brink et al. 2015). Bousman and Brink (personal communications, 2013) also identified a fourth terrace sandwiched chronologically between the Erfkroon and Orangia Terraces at the site of Lovedale, an archaeological location upstream from Erfkroon and on the opposite bank on the Modder River.

The Tooth et. al. (2013) Study

In the early 2000's, Stephen Tooth and his team selected Erfkroon as a case study to characterize dry-land river systems in South Africa's continental interior. The Modder River, with its deeply incised riverbanks exposing meters of alluvial sedimentation, provided a unique opportunity to characterize formation processes and explore paleoenvironmental trends in a sequence known to contain Quaternary fossils and archaeology (Churchill et al. 2000). Their study employed topographic survey, sediment sampling, description of various sediment exposures at 23 locales across the landscape, and the implementation of IRSL and OSL dating methods (refer to Figure 4.2).

Tooth's survey and description of exposed strata resulted in the characterization of two depositional sequences: (1) a single, paired terrace bisected by the modern Modder river channel, and (2) a series of limited cut-and-fill sequences collectively referred to as

"Paleodonga Fill." Both landforms were divided into lithostratigraphic "facies" or "litho-facies." The single, paired terrace was subdivided into eight litho-facies. The stratigraphically lowest and oldest components were described as channel deposits named as follows: (1) Sandy Gravel, (2) Cross-stratified Sandy Gravel, (3) Upper Sandy Gravel with Bivalves, and (4) Silty Sand. Tooth et al. (2013) then identified four overbank facies superimposed on the channel deposits. These were collectively described as an accretionary paleosol sequence. In descending order of age/stratigraphic position, individual paleosols were named the (5) Lower Grey Paleosol, (6) Red Paleosol, (7) Upper Grey Paleosol, and (8) Brown Paleosol (refer to Figure 4.3).

The second sedimentation episode identified by Tooth et al. (2013) was named the Paleodonga Fill. This referred to a collection of younger, intrusive sediments comprising cut-and-fill sequences altering the main terrace landform. Two facies of the fill were identified: (1) Cross-stratified silts and sands, and (2) the Sandy Cap, a fine, silty sand lag deposit "capping" the paleodonga fill and comprising the uneroded, modern surface superimposing the main terrace. Both facies were described as resting unconformably above the terrace's overbank alluvium and in some cases, inset within recent erosional incisions (Tooth et al. 2013:549).

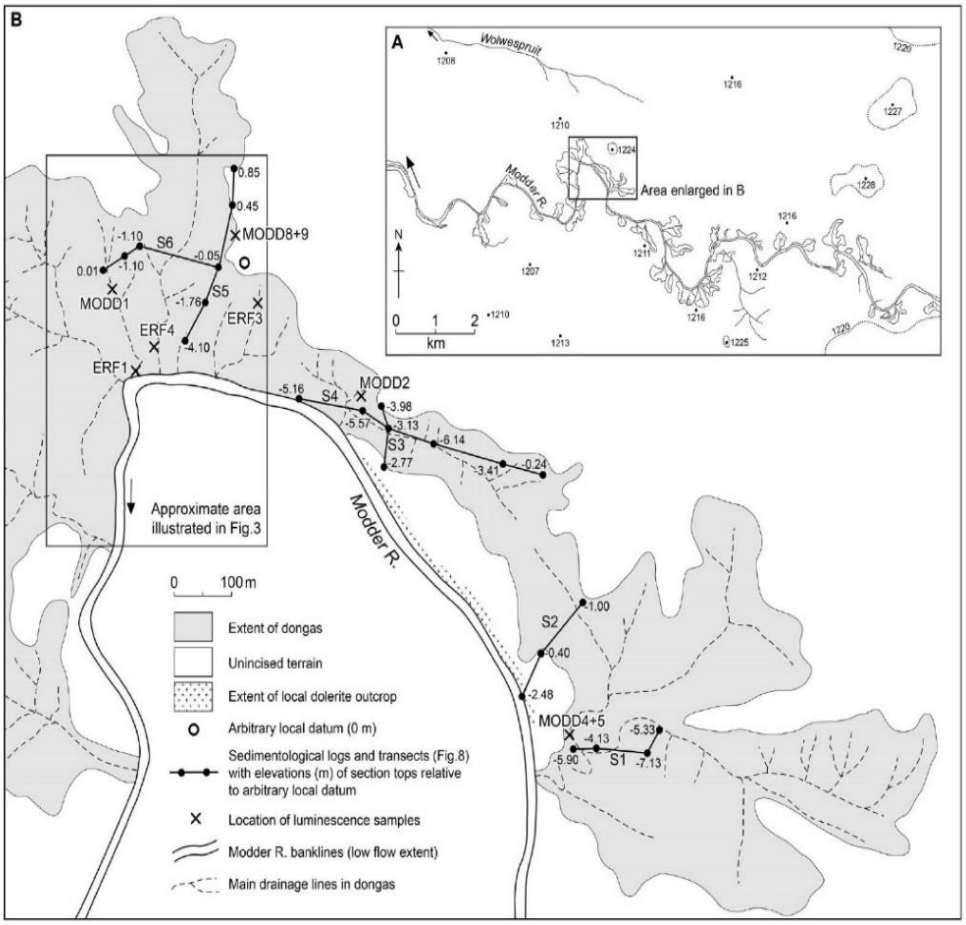

Fig. 4.2. Tooth et al. (2013) geological survey area. Image A: Overview of study area within the greater Modder River Valley. Image B: Tooth et al. (2013) survey transects and associated profile locations. Sample locales for dating marked with an "x"; those labeled MODD refer to samples collected by Tooth et al. (2013), those labeled ERF refer to samples collected by Churchill et al. (2000) (image from Tooth et al. 2013:544).

Tooth et al. (2013) channel facies description. Channel facies comprising the paired terrace were described as sand- and gravel-rich lithostratigraphic units: The Lower Sandy Gravels, Cross-Stratified Sandy Gravels, and Upper Sandy Gravels with Bivalves. The Lower Sandy Gravels referred to clast- and matrix-supported gravels ranging in size from pebbles to cobbles in horizontal stratigraphy of varied depths. Corresponding OSL and IRSL dates were not recovered from this unit during Tooth's study but a previous IRSL (ERF1) date of 163±7 ka was provided by Churchill et al. (2000). The Cross-

Stratified Sandy Gravels referred to granule and pebble-sized clasts supported by a sandy matrix in cross-stratified layers held together laterally by extensive calcrete formation. An OSL date (MODD2) of > 70-45 ka was recovered at 4.5 m below the surface, providing a loose age estimate for the deposit despite evidence of soil mixing. The Upper Sandy Gravel with Bivalves referred to pebble and cobble sized gravels containing shale, carbonate concretions, shell, and buried in situ bivalves. The unit also contained sandy interbeds ranging in thicknesses as great as 1.5 meters. Tooth interpreted this as fluvial deposition from the paleo-Modder river, where high flow regimes supported abundant bivalve populations. Paired IRSL and OSL ages placed the facies at 118±35 ka and ~71 ka respectively. The 71 ka age estimate associated with the MODD1 OSL sample is considered a minimum age for the facies' burial due to aliquot dose saturation (refer to Tooth et al. 2013:551). This sample was extracted near Bousman and Brink's Lower F excavation area, at a depth of 6.5 meters below surface (Tooth et al. 2013).

Tooth et al. (2013) paired terrace description. Tooth named individual paleosol formations within his overbank alluvial succession the Lower Grey Paleosol, Red Paleosol, Upper Grey Paleosol, and Brown Paleosol (Tooth et al. 2013). The Lower Grey Paleosol is the stratigraphically lowest pedogenic event and superimposes the Upper Sandy Gravel with Bivalves. This unit is described as relatively well-consolidated with small (<1 cm) carbonate nodules interspersed among yellowish-brown and strong brown muddy sand with a mean silt and clay content of 62.20%. Slickenside structures coated with manganese oxides were described on individual ped structures, as was some evidence of bioturbation in the form of rodent burrows and root casts infilled with a secondary, sandy matrix. An OSL (MODD9) date of 42±3 ka and IRSL date of 29±2

both collected at 4.35 m below surface were recovered from the Lower Grey. Tooth et al. (2013) further noted that freshly exposed regions of the Lower Grey exhibited strong brown (7.5YR 5/6) and yellowish-brown (10 YR 5/6) coloration, however, surficial exposures effected by weathering appeared light grey in color hence the name "Lower Grey" (Tooth et al. 2013:547).

Tooth et al. (2013) named the next unit the Red Paleosol which is bounded by the Lower Grey Paleosol below and Upper Grey Paleosol above. The matrix was described as yellowish-red (5YR 5/6) to strong brown (7.5YR 5/6) in color, consisting of muddy sand, silts and clays. Small nodules and flecks of calcium carbonate were noted throughout the unit, and angular soil peds were described as manganese-stained and showing evidence for root bioturbation. Tooth et al. (2013) described the unit as thinning distally, pinching out towards the northern margin of the valley from 2.5 m to < .5 m in thickness. Both boundaries shared with the Lower Grey below and Upper Grey above were described as gradational. Samples collected at 2.75 m below surface in the Red Paleosol produced IRSL and OSL (MODD8) dates of 29±2 ka and 32±2 ka respectively (Tooth et al. 2013).

The Upper Grey Paleosol was described as making gradational contact with the Red Paleosol below and Brown Paleosol above. Well-consolidated, angular ped structures comprised of yellowish-brown (10YR 6/4) to brown (7.5YR 5/6) sandy mud with clear evidence of pedogenesis and bioturbation were observed. Manganese staining was also noted on slickenside structures and calcium carbonate ranging in size from flecks to nodules were found dispersed throughout the unit. Tooth et al. (2013) further described the Upper Grey as thinning distally to the north with a maximum thickness of 2

m, and found it to contain the highest mean silt and clay content of all four paleosols in the overbank sequence. No OSL or IRSL dates were recovered from this unit, however, Churchill et al. (2000) reported a single IRSL (ERF3) date of 25±1.2 ka collected from the Upper Grey from an unknown depth (Tooth et al. 2013; Churchill et al. 2000).

The Brown Paleosol was described as making gradational contact with the Upper Grey and in discrete cases, the Red Paleosol below, and is bounded by the Silty Sand or "Sand Cap" unit above. The Brown unit's matrix was characterized as muddy sand with brown (7.5YR 5/4) coloration and a mean silt and clay content of 62.7%. Angular soil peds were described as well-consolidated and interspersed with calcium carbonate flecks. The unit's thickness was described as relatively less than the underlying paleosol accumulations at >1 m. Though manganese-stained root traces were observed, Tooth et al. (2013) noted the Brown Paleosol appeared less impacted by bioturbation than lower units. No corresponding OSL and IRSL samples were collected.

Tooth et al. (2013) paleodonga fill description. Tooth et al. (2013) describe a weakly-structured Silty Sand and fluvially accumulated Paleodonga Fill as the second sedimentary unit at Erfkroon. The Silty Sand refers to silt- and sand-dominated channel-fill accruing in paleodongas that were once connected to channels of the Modder River. This unit bounds the alluvial sequence from above and forms a surface cap on all the geological deposits except where removed by recent erosion. They found that the sandy matrix was comprised of fine to medium sand grains, exhibiting little evidence for soil development. OSL dates of 0.39±0.03 ka (MODD5) and 1.5±0.2 ka (MODD4) were recovered at 1.5 and 5.5 m below surface respectively. One IRSL date of 11.2±0.8 ka at 5.5 m below surface was also recovered at locality MODD4. The Paleodonga fill refers to

structureless silty sand with a basal gravel lens occurring in paleodonga incisions thought to represent a single cut-and-fill episode of fluvial deposition (Tooth et al. 2013).

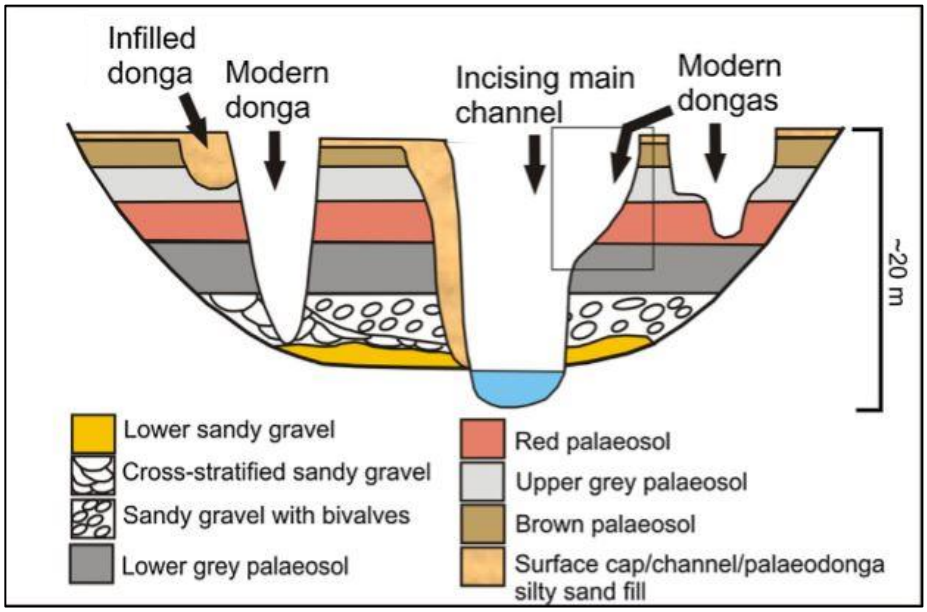

Fig. 4.3. Profile illustration of the single paired terrace and paleo-donga fill as described by Tooth et al. (2013) and published in Lyons et al. (2014). Outlined area refers to the Dating Profile sampled by Lyons et al. (2014).

Tooth et al. (2013) geochronology at Erfkroon. The second component of the Tooth et al. (2013) study was to produce a geochronology for the primary terrace sequence (Table 4.3). This was accomplished by implementing small aliquot OSL and IRSL methods to expand on dating efforts performed by Churchill et al. (2000) in previous years. Churchill used a combination of OSL and IRSL to produce the first dates for the study area, but only published two OSL dates (Churchill et al. 2000). Churchill's IRSL dates were finally published in Tooth's 2013 paper, associated with 3 of the 8 facies described in their study. These were collected from the Lower Sandy gravels (163±7 ka), Upper Sandy Gravel (113±6 ka), and the Upper Grey Paleosol (25±1.2 ka) (refer to Figure 4.2 for Churchill sample locales).

Table 4.3. Overbank facies IRSL and OSL dates published in Tooth et al. (2013:550); includes IRSL dates produced by Churchill et al. (2000) and published in Tooth et al. (2013).

Source	Facies Association	Sample no.	Depth (m)	IRSL Date (ka)	OSL Date (ka)
Tooth et al. 2013	Silty Sand	MODD5	1.5	n/a	0.39±0.03
Tooth et al. 2013	Silty Sand	MODD4	5.5	11.2±0.8	n/a
Churchill et al. 2000	Upper Grey	ERF3	n/a	25±1.2	n/a
Tooth et al. 2013	Red	MODD8	2.75	29±2	32±2
Tooth et al. 2013	Lower Grey	MODD9	4.35	42±3	42±2
Tooth et al. 2013	Upper sandy gravel w/ bivalves	MODD1	6.5	118±35	>71
Churchill et al. 2000	Upper sandy gravel w/ bivalves	ERF4	n/a	113±6	n/a
Tooth et al. 2013	Cross-stratified sandy gravels	MODD2	4.5	n/a	45- >70
Churchill et al. 2000	Lower sandy gravel	ERF1	n/a	163±7	n/a

Tooth et al. (2013) expanded the chronology by targeting the remaining, undated facies of the paired terrace and the paleodonga fill. Two channel facies were included in Tooth's study: Sample MODD2, the Cross Stratified Sandy Gravels, and sample MODD1, the Upper Gravels with Bivalves. MODD2 produced an OSL date ranging from >70 ka to 45 ka, and MODD1 produced an IRSL date of 118±35 ka and an OSL date of >70 ka. Sampled facies of the alluvial overbank sequence included the Lower Grey and Red Paleosols, where both IRSL and OSL methods were employed. Sample MODD9 (Lower Grey) produced an IRSL date of 42±3 ka and an OSL date of 42±2 ka. MODD8 (Red Paleosol) produced an IRSL date of 29±2 ka and an OSL date of 32±2 ka.

Estimating the age of the Paleodonga Fill was achieved by implementing both IRSL and OSL methods. The most-accepted date is associated with sample MODD5 which was used to create a minimum-age statistical model (see Galbraith et al. 1999). This sample was taken from the upper aspect of the silty sand facies and coincides with

an OSL date of 0.39±0.03 ka. MODD4, also sampled from the silty sand fill, was dated using large single aliquot IRSL estimates. This method produced an age of 1.5±0.2 ka but is considered an overestimate (Tooth et al. 2013:550).

Tooth et al. (2013) suggests that the close range of dates produced from the overbank facies reflects relatively continuous sedimentation over time. This is an alternative to another theory they propose in which periodic episodes of non-sedimentation and/or erosion separate each soil formation event. However, because of the tight chronology, the former accretionary model is accepted.

Tooth et al. (2013) present a 9-stage developmental scheme depicting the sedimentation and erosional episodes responsible for shaping Erfkroon's landscape as it is seen today (see Figure 4.4). Stages 1-3 are characterized by bedrock erosion and lateral migration of the paleo-river channel during which cut-and-fill sequences variably truncated fluvial deposits. The Lower Sandy Gravels, Cross-Stratified Sandy Gravels, and Upper Sandy Gravel with Bivalves accumulated as the result of intermittent fluvial deposition and channel migration. Stages 4-6 are characterized by restriction of lateral channel migration and subsequent increase in vertical aggradation. Tooth et al. (2013) suggest later channel sedimentation of the Upper Sandy Gravel with Bivalves occurred contemporaneously with the deposition of silty overbank alluvium, thereby providing the parent material for soil formation in the Lower Grey Paleosol. The Red, Upper Grey, and Brown Paleosols are stratigraphically stacked above the Lower Grey, indicating periodic aggradation of overbank alluvium was followed by abbreviated, yet consistent episodes of landscape stability preferential for pedogenic development.

Episodes of deep channel incision and donga formation characterize Stages 7-8. Tooth et al. (2013) suggest incision of the main channel initiated donga development into previously deposited overbank alluvium. Aggradation and backfilling of the main channel and dongas were subsequently followed by modern phases of incision which alter Erfkroon's landscape today (Tooth et al. 2013).

The Tooth et al. (2013) study potentially finds evidence for at least one unconformable contact within the overbank succession, but this is attributed to variations in overall thickness of sedimentation and/or obscuration via pedogenic overprinting. Thinning is observed in the Upper Grey Paleosol which is expressed in Tooth's transect 5 (see Figure 4.5). The Upper Grey stratum is described as pinching out distally to the north, away from the active river channel. The upper boundary of the Red Paleosol and lower boundary of the Brown make contact where the Upper Grey's thickness is significantly reduced/non-existent. If, as Tooth implies, the Upper Grey, Red, and Brown Paleosols represent individual soil formation events, then the contact between the Red and Brown Paleosols would be unconformable.

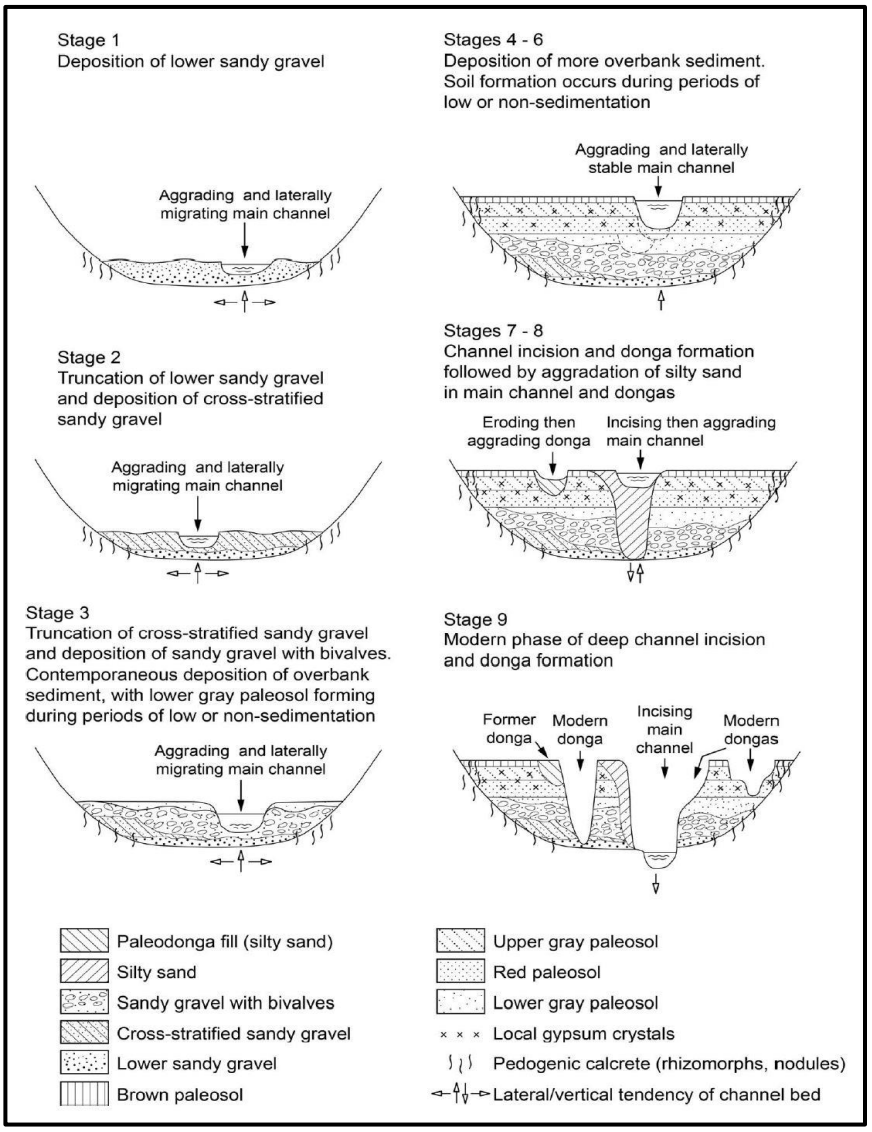

Fig. 4.4. Tooth et al. (2013) model for landscape development at Erfkroon (modified from Tooth et al. 2013:554).

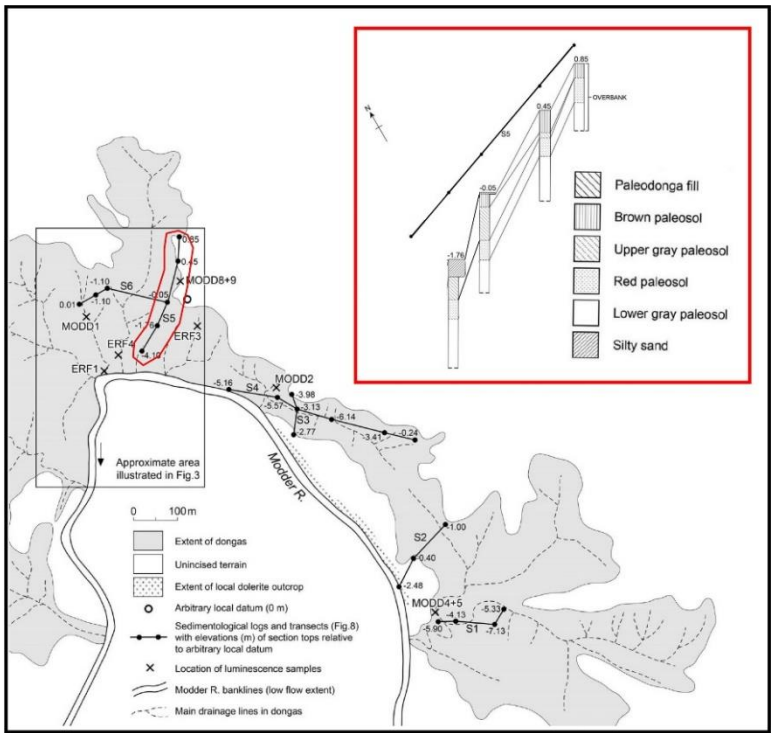

Fig. 4.5. Transect 5 illustrating "pinching-out" of Upper Grey Paleosol between the Brown and Red (outlined in red) (modified from Tooth et al. 2013).

The Lyons et al. (2014) Study

The Tooth et al. (2013) study was expanded by Richard Lyons (Lyons et al. 2014) to provide the first paleoenvironmental reconstruction associated with Erfkroon's history of alluvial deposition and pedogenic development. His study also provided a higher-resolution geochronology for the overbank paleosol sequence, ultimately fueling validation of Tooth's accretionary hypothesis. The results of the Lyons et al. (2014) study is a revised geochronology for the sequence, in addition to a paleoclimatic interpretation extracted from mineral magnetic susceptibility and diffuse reflectance spectroscopy (DRS) (Lyons et al. 2014).

Lyons et al. (2014) collected nine samples for dating from a single, prepared profile containing intact exposures of the Lower Grey, Red, Upper Grey, and Brown

paleosols as described in Tooth's overbank sequence (Figure 4.6). The sample exposure is referred to as the "Dating Profile" in later research, and the geochronology produced from it establishes the chronological control for this and previous studies (see Bousman & Brink 2014; Palmison 2014).

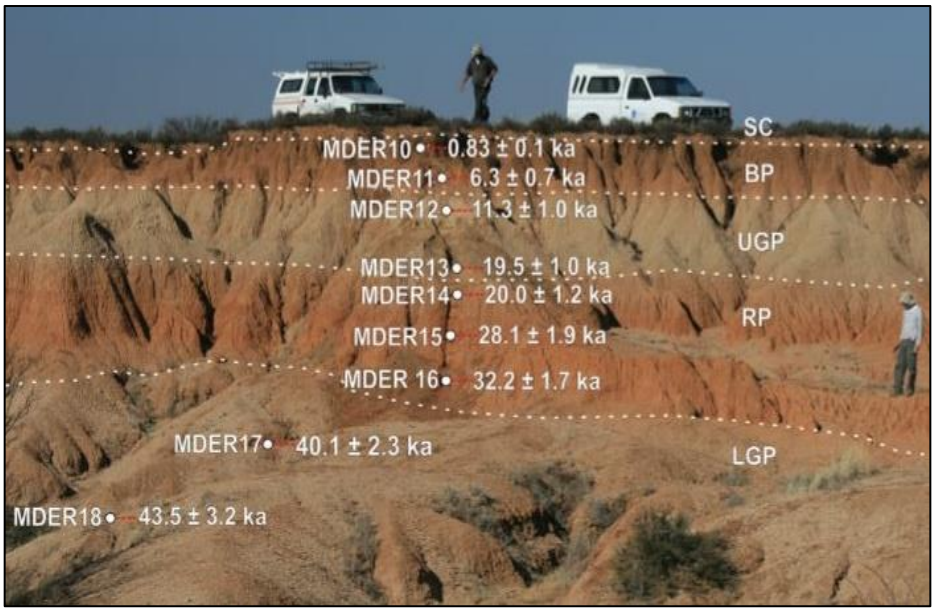

Fig. 4.6. OSL dates and corresponding accretionary paleosol sequence as reported by Lyons et al. (2014). Abbreviations: SC= Sandy Cap, BP= Brown Paleosol, UGP= Upper Grey Paleosol, RP= Red Paleosol, LGP= Lower Grey Paleosol. Dashed lines indicate general regions of gradational contact between lithostratigraphic units (image adapted from Lyons et al. 2014).

Lyons et al. (2014) extracted nine samples from the overbank paleosol sequence for single grain and small aliquot OSL dating. Samples were labeled with the prefix "MDER" and collected from the upper and lower boundaries of each paleosol, with the exception of the Lower Grey: Two samples from the middle (MDER18) and upper boundaries (MDER17) of the Lower Grey, three from the lower (MDER16), middle (MDER15), and upper (MDER14) aspect of the Red, two from the lower (MDER13) and upper (MDER12) boundaries of the Upper Grey, and two from the lower (MDER11) and

upper (MDER10) boundaries of the Brown were extracted. A review of the methods employed to process these dates can be found in Lyons et al. (2014:46).

Lyons' results offer a higher resolution chronology of the overbank sequence at Erfkroon and show that alluvial aggradation began around ~42 ka and proceeded until ~0.83 ka (Figure 4.7) (Lyons et al. 2014). Echoing Tooth's earlier sentiments, Lyons et al. (2014) interprets the close dating sequence from the Lower Grey through the Brown as validation of Tooth's accretionary model. Its argued that the relatively uniform increase in age down-profile is evidence for steady sedimentation (~0.15mm/yr). It is further suggested that the relative chronology provided by MSA (>25 ka) materials recovered from the Lower Grey, and LSA (<25 ka) materials from the Red, Upper Grey, and Brown, further supports the accretionary model (Lyons et al. 2014). Lyons et al. (2014) also asserts that there is "a lack of stratigraphic evidence for phases of cut-and-fill prior to ~0.83 ka, with no prolonged breaks in sedimentation or significant phases of erosion" (Lyons et al. 2014:56)— a statement based on Tooth's own observations published in 2013 since an independent description of the sequence was not conducted by Lyons et al. (2014).

Lyons et al. (2014) also provides a paleoenvironmental reconstruction based on inferred sedimentation and precipitation patterns interpreted from three geoproxies: Calcium carbonate ($CaCO_3$) development, degree of gypsum ($CaSO_4.2H_2O$) formation, and the relative persistence of hematite and goethite ferromagnetic minerals in sediment samples. Interpretations of these data assume the correctness of Tooth's (Tooth et al. 2013) accretionary model.

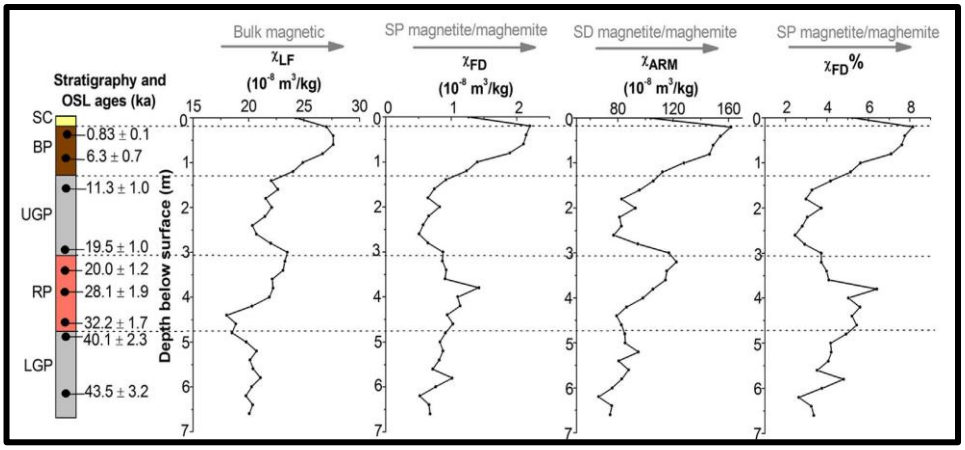

Fig. 4.7. Lyons et al. (2014) magnetic susceptibility and DRS results graphed with reference to OSL geochronology; N=33 (modified from Lyons et al. 2014).

The Lyons et al. (2014) Dating Profile reached 6.6 meters in depth and bulk samples for geoproxy analysis were collected every 20 cm (N=33). Magnetic susceptibility measurements, in addition to independent measurements of hematite and goethite ratios using UV-Vis DRS were taken from each sample (refer to Figure 4.7).

The Lyons et al. (2014) reconstruction consists of a three-phase sequence for paleoenvironmental change characterized by intervals of sedimentation and pedogenic development within the paleosol sequence. Phase 1 coincides with accumulation and weathering of the Lower Grey and Red paleosols (~46-28 ka). Relatively low ratios of magnetite/maghemite are interpreted as evidence for seasonal rainfall regimes and mild annual temperatures. Increased ratios of magnetite and maghemite around ~32-28 ka correspond with warmer, wetter conditions. Phase 2 coincides with the upper Red and a portion the Upper Grey Paleosol (~28-15.5 ka). Decreasing amounts of magnetite/maghemite concentrations are interpreted as reflections of cooler, drier climatic conditions. The lowest recorded rainfall estimates (>400mm/yr) coincide with the middle portion of the Upper Grey. Phase 3 coincides with the upper aspect of the

Upper Grey and Brown Paleosols and is characterized by higher concentrations of magnetite and maghemite. This is thought to reflect rising temperatures and increasing annual rainfall regimes at the Pleistocene-Holocene transition.

The Bousman & Brink (2014) Study

The Multiple Terrace Allostratigraphy Hypothesis refers to Britt Bousman and James Brink's proposed revision of Tooth and Lyons' single terrace accretionary model. This was developed in lieu of Bousman and Brink's own interpretation of Lyons' Dating Profile and following their collective observations of several geological profiles exposed during their archaeological excavations. Bousman and Brink implement pedological and allostratigraphic principles, in addition to conceptual principles of lithostratigraphy, to argue for the presence of three terrace landforms. In descending order of age, Bousman and Brink refer to these as the Erfkroon Terrace, Orangia Terrace, and Soetdoring Terrace.

Their model derives from the identification of unconformable boundaries noticed between Tooth's facies designations: The cross-stratified sands and gravels of the channel facies correspond with the Erfkroon Terrace, the overbank facies (Lower Grey, Red, Upper Grey, and Brown paleosols and the Sandy Cap) correspond with the Orangia Terrace, and the young, cut-and-fill sequence described by Tooth et al. (2013) as the "Paleodonga Fill" correspond with the Soetdoring Terrace.

Bousman and Brink (2014) characterize the Erfkroon Terrace as the oldest and least preserved alluvial unit in the study area. Its erosional edges are described as periodically visible across the landscape and are thought to comprise the valley edge, bounding sequentially younger deposits. The terrace is unconformably bounded by the

Orangia Terrace which insets into the Erfkroon Terrace, and by Ecca bedrock below. Bousman and Brink identify four lithostratigraphic units comprising the terrace: (1) the basal gravels, (2) cross-bedded sands, (3) a fine-grained overbank deposit, and (4) a petrocalcic horizon (Bousman & Brink 2014: Bousman et al. *in prep*).

The Soetdoring Terrace refers to the youngest terrace landform and contains sandy sediment deposits and weakly developed, buried soils. This terrace was primarily identifiable on the south side of the Modder River channel, though discrete deposits were also found along the northern bank, infilling bank incisions and dongas. Bousman and Brink (2014) correlate the Soetdoring Terrace with Tooth and Lyons' (Tooth et al. 2013; Lyons et al. 2014) Paleodonga fill (refer to Figure 4.8).

Bousman and Brink identify 24 pedo- and lithostratigraphic units within the Orangia Terrace. These are allocated into four allostratigraphic units (AU1-AU4) differentiated by unconformable boundaries, representing four separate phases of pedogenesis and/or sedimentation. Each unit roughly corresponds with lithofacies designations in the Tooth et al. (2013) and Lyons et al. (2014) accretionary model. Bousman and Brink retain some of Tooth and Lyons' previous lithofacies naming system, but augment as needed to better reflect pedogenic relationships. The stratigraphically youngest unit, AU1, consists of the Sand Cap. Next is AU2 which consists of the Brown Paleosol, Upper Grey, and Red Sandy Loam units. AU3 consists of the Red Paleosol and Lower Grey, and the oldest, AU4, consists of the Green Sands and Lower Gravels (refer to Table 4.4).

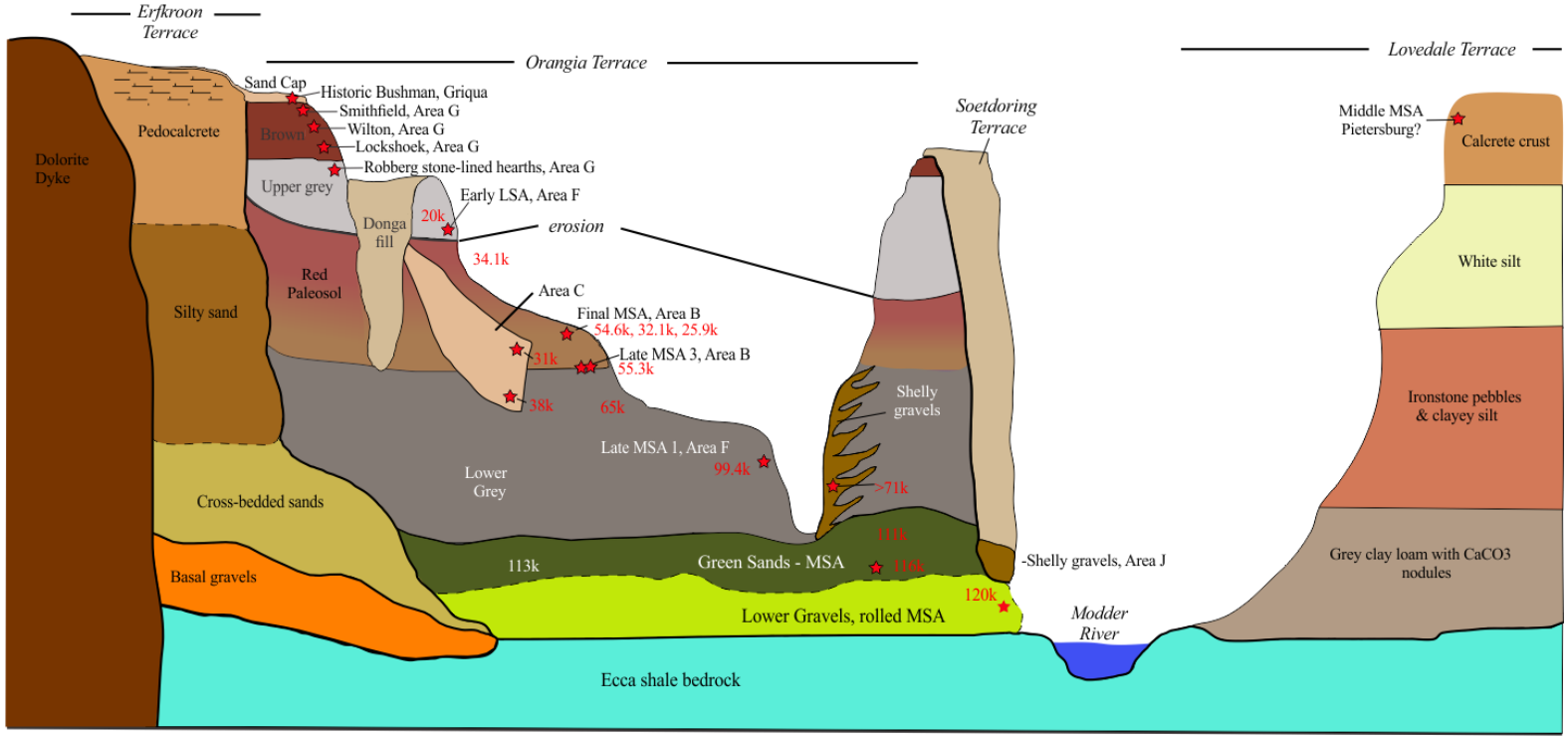

Fig. 4.8. Bousman & Brink's Multiple Terrace Allostratigraphy Model. Erfkroon study area consists of three terraces. In descending order of age: Erfkroon Terrace, Orangia Terrace, and Soetdoring Terrace. Red stars indicate dated sediments from previously tested archaeological and paleontological locales (image modified from Bousman & Brink 2014).

Table 4.4. Bousman et al. (*in prep*) and Bousman & Brink (2014) Orangia Terrace description. Allostratigraphic Unit (AU) boundaries correspond with bold black lines; conformable boundaries marked by dotted lines. Tooth et al. (2013) descriptions provided in far-right column for comparison.

AU	*Soil Horizon*	*Depth (cmbs)*	*Area or Profile*	*Description*	*Tooth et al. 2013 Description*
1	A	0-19	Dating Profile	Brown (7.5YR 5/4) slightly firm sandy loam, weak, medium-fine subangular blocky, common roots and rootlets, light surface vegetation and cover, abrupt smooth lower boundary.	Sandy Cap
	C	19-23	Dating Profile	Brown (7.5YR 5/4) friable silty sandy loam, very weak medium subangular blocky, few rootlets, abrupt smooth lower boundary-unconformity.	
2	2A1	23-55	Dating Profile	Dark brown (7.5YR 3.5/4) firm loam, strong-moderate medium subangular blocky, rootlets on ped faces, small manganese flecks on ped faces, smaller flecks in peds, gradual smooth lower boundary.	Brown Paleosol
	2AB	55-81	Dating Profile	Strong brown (7.5YR 4/6) firm loam, medium moderate subangular blocky, 1% $CaCO_3$ small nodules, gradual smooth lower boundary.	
	2Bk	81-130	Dating Profile	Strong brown (7.5YR 5/6) firm loam, 2% $CaCO_3$ nodules and flecks, some insect burrows, clear smooth lower boundary.	
	2Bkt	130-178	Dating Profile	Light yellowish-brown (10YR 6/4) firm loam, medium moderate subangular blocky 3-4% $CaCO_3$ nodules with interconnected filaments between nodules, very common (10%) insect burrows filled with strong brown (7.5YR 5/6) to yellowish red (7.5YR 5/6) firm loam, 2% $CaCO_3$ nodules and flecks, some insect burrows, clear smooth lower boundary.	Upper Grey Paleosol
	2Bt1	178-207	Dating Profile	Light yellowish-brown (10YR 6/4) slightly firm sandy loam, with very common (10%) yellowish-red (5YR 5/6) sandy loam infilling insect burrows, manganese flecks on ped faces, abrupt smooth lower boundary.	

Table 4.4. Continued

	2Bt2	207-262	Dating Profile	Pale brown (10YR 6/3) friable loam, crumb structure, common (5-8%) insect burrows infilled with strong brown (7.5YR 5/6) loam, $CaCO_3$ filaments along root pores, clear smooth lower boundary.	
	$2Bt3_3$	262-308	Dating Profile	Brownish-yellow (10YR 5.5/6) firm loam, medium, moderate to weak subangular blocky, manganese flecks on ped faces, no $CaCO_3$ clear to abrupt smooth lower boundary.	
	2Bt4	308-324	Dating Profile	Strong brown (7.5YR 5/6) firm sandy loam, coarse weak subangular blocky, <1% $CaCO_3$ nodules, gradual smooth lower boundary.	
	2Bw/C (*Red Sandy Loam*)	324-363	Dating Profile	Yellowish-red (5YR 5/6) firm sandy loam, coarse weak subangular blocky, common insect burrows, abrupt smooth lower boundary-unconformity.	
3	3Bw	363-414	Dating Profile	Yellowish-red (5YR 5/8) very firm sandy loam, coarse moderate subangular blocky, large manganese films on ped faces, clear to abrupt smooth lower boundary.	Red Paleosol
	3Btw	414-457	Dating Profile	Strong (7.5YR 5/6) firm clay loam, medium-fine moderate-strong angular to subangular blocky, clay films on ped faces, <1% manganese nodules, gradual, smooth lower boundary.	
	3Bkt	457-579	Dating Profile	Strong brown (7.5YR 5/6) firm (Friable when moist) clay loam grading down profile to sandy loam, medium moderate angular blocky, many (5%) large $CaCO_3$ nodules, gradual to clear smooth lower boundary.	
	3Bkt/C	579-614	Dating Profile	Light yellowish-brown (10YR 5/4) to yellowish -brown (10YR 5/6) alternating thin (1mm) sand and clay laminae, 2-3% $CaCO_3$ small nodules, lower boundary not observed.	Lower Grey Paleosol
4	Green Sands	N/A	Area I	Subangular to rounded coarse gravels to large cobbles, larger gravels are $CaCO_3$ and Ecca formation fragments constitute smaller sand-sized matrix.	
	Lower Gravels	N/A	Area I	Small fragments of Ecca formation shales and less frequently, $CaCO_3$ particles.	

Allostratigraphic units 1, 2, and 3 were described from the Dating Profile exposure, and AU4 was characterized at different locales across the landscape. AU1-AU3 collectively reflect the archaeology bearing strata in the study area and are the focus of proceeding discussions because of their direct correlation with the Tooth and Lyons' accretionary model for paleosol development.

Allostratigraphic units of the Orangia Terrace. Bousman and Brink's (2014) Allostratigraphic Unit 4 (AU4) is the stratigraphically oldest unit of the Orangia Terrace and contains the Lower Gravels and Green Sands. The Lower Gravels refer to the basal fluvial layer of the Orangia Terrace that unconformably rests on the Basal Gravels of the Erfkroon Terrace (Basal Gravels are comprised of Ecca Group shales, dolerite, and hornfels deposits). Gravel and cobble-sized clasts and a smaller, sand-sized matrix comprised of Ecca Formation shale fragments and calcium carbonate-encrusted gravels were observed in this unit. The Lower Gravels are conformably bound by the Green Sands above. The Green Sands are known for containing well-preserved fossil materials including mammals, reptiles, crustaceans, and fish, and consist of fine-grained, Ecca Formation shale fragments and sands. This unit is unconformably bound by the alluvial Lower Grey unit above (Bousman & Brink 2014).

Allostratigraphic Unit 3 (AU3) is unconformably bound by AU4 below, and above by the stratigraphically younger AU2. This represents the oldest visible allostratigraphic unit in the Dating Profile. AU3 contains the Lower Grey unit followed by the Red Paleosol above, where pedogenesis has modified their sediments. Together, the Lower Grey and Red are found to comprise a single soil formation interval described as a 3Bw-3Btw-3Bkt-3Bkt/C sequence (Bousman et al. *in prep*) (refer to Table 4.4). A

notable characteristic in the Lower Grey aspect of the unit is the presence of thinly stratified laminae comprised of sands, clay, and silts. Bousman and Brink (2014) and Bousman et al. (*in prep*) interpret these as evidence for laminar flow during the depositional event. The upper aspect of the unit, dominated by the Red, is characterized by fine-grained, homogenized, overbank sediment that is more heavily altered by pedogenesis. The conspicuous lack of an A-horizon was however, used to define the unit as a truncated paleosol, forming an unconformable boundary with AU2 above (Bousman et al. *in prep*).

Allostratigraphic Unit 2 (AU2) is unconformably bounded by AU3 below and the stratigraphically younger AU1 above. This unit contains the Red Sandy Loam, Upper Grey, and Brown units. Bousman and Brink (2014) suggest these form a single pedogenic sequence: 2A-2AB-2ABk-2Bkt-2Bt1-2Bt2-2Bt3-2Bt4-2Bw/C. Here, Bousman et al. (*in prep*) find that A-horizons comprising the stratigraphically youngest Brown unit are well-preserved and share conformable boundaries with the B-horizons of the Upper Grey and Red Sandy Loam units (Bousman et al. *in prep*). The stratigraphically oldest component, the Red Sandy Loam, is described as the 2Bw/C-horizon, representing a partially modified parent material of the AU2 pedogenic phase. This is interpreted as a lithologically and pedogenically unique unit for the Red Paleosol below. The contact between the Red Paleosol and Red Sandy Loam is described as abrupt and “scalloped”. Bousman et al. (*in prep*) suggest this is evidence for removal of the upper component of the Red Paleosol, followed by its replacement with a loamy overbank material (Red Sandy Loam) as a product of lateral stream migration.

Allostratigraphic Unit 1 (AU1) is bounded unconformably by AU2 below. The upper aspect of the unit corresponds with the modern surface. AU1 is comprised of the Sand Cap that collectively consists of an A-BC sequence. Bousman and Brink (2014) characterize this as a relatively young aeolian deposit, where the top aspect of the unit represents an actively weathering A-horizon.

Bousman and Brink's allostratigraphic model depicts an erosional gap between the Red Paleosol and Red Sandy Loam, and an extended period of non-sedimentation between the Brown Paleosol and Sandy Cap (Tooth's paleodonga fill). Both interpretations are supported by the presence of a temporal gap between OSL samples in the Lyons et al. (2014) geochronology. OSL samples MDER15 and MDER14 are separated by a temporal gap of approximately 7,000 years and coincide with what Bousman and Brink (2014) describe as an unconformable contact between the Red Paleosol and the Red Sandy Loam (between 27 ka and 20 ka) (AU3 from AU2). Dates of ~28 ka provided by Lyons et al. (2014) within the upper portion of the Red Paleosol below its contact with the Red Sandy Loam (2Bw/c) coincide with a 3Bw-horizon. The lack of an A-horizon within the Red Paleosol leads Bousman and Brink (2014) to hypothesize that erosion was responsible for its removal, followed by redeposition of red, loamy sediments (Red Sandy Loam) as the product of slope wash or as a result of lateral stream migration (Bousman & Brink 2014; Bousman et al. *in prep*).

Another temporal gap of roughly 400 years exists between the Brown unit (upper aspect of AU2) and the Sandy Cap (AU1). The age difference was noted between the Lyons et al. (2014) sample MDER10 (~0.83 ka) at the upper boundary of the Brown, and the Tooth et al. (2013) sample MODD5 (~.39 ka) from the Sandy Cap (refer to Figure 4.7

and Table 4.3 respectively). A physical "gap" in the sequence was also described by Bousman and Brink. Differences in texture, color, and ped development between the two units formed an abrupt boundary; a characteristic associated with unconformably bound horizons.

Bousman and Brink's allostratigraphic interpretation of the upper Orangia Terrace (AU1, AU2, & AU3) relies on the notion that soil formation was time transgressive (Bousman & Brink 2014; Bousman et al. *in prep*). This implies that each soil development sequence, while of a certain temporal interval, occurred in sediments of variable [older] ages as demonstrated by Lyons' geochronology and the dates produced from Bousman and Brink's archaeological locales. Bousman et al. (*in prep*) suggest the temporal gaps between unconformable boundaries are better temporal indicators for periods of landscape stability, rather than the OSL ages of the sediments themselves.

Summary & Discussion

Previous geological investigations at Erfkroon resulted in two disparate interpretations of the area's alluvial architecture. The Single Terrace Accretionary Hypothesis, developed by Tooth et al. (2013) and validated by Lyons et al. (2014), acknowledges only one terrace formation at Erfkroon. The upper, archaeology-bearing deposits are described as four accretionary paleosols that developed sequentially and during periods of slow, steady sedimentation over the course of ~47 ka. No evidence for erosion or extended periods of non-sedimentation were identified (Tooth et al. 2013; Lyons et al. 2014). The paleoenvironmental reconstruction modeled by Lyons et al. (2014) employs magnetic susceptibility which is used to estimate precipitation regimes and periods of enhanced pedogenic weathering.

Bousman and Brink's (2014) Multiple Terrace Allostratigraphy Hypothesis separates Tooth and Lyons' single terrace into three separate terrace formations. These are named the Erfkroon, Orangia, and Soetdoring terraces. The Orangia Terrace contains the region's archaeology-bearing deposits and is further separated into four allostratigraphic units (AU1-AU4). AU1, AU2, and AU3 encompass the deposits described as accretionary paleosols by Tooth and Lyons (Tooth et al. 2013; Lyons et al. 2014) but are described by Bousman and Brink as three separate periods of soil formation. The unconformable boundaries between each allostratigraphic unit are thought to correspond with episodes of prolonged landscape stability. This is supported by Bousman and Brink's own observations at the Dating Profile and other archaeological locales, and their interpretations of the Lyons et al. (2014) magnetic susceptibility results. Bousman and Brink view irregular spikes in mineral magnetic values ($\chi_{fd\%}$) produced from the Dating Profile sample population as evidence for unconformable boundaries between the Brown and the Sand Cap, and the Red Paleosol and Red Sandy Loam (Bousman & Brink 2014; Bousman et al. *in prep*).

The Single Terrace Accretionary Hypothesis and Multiple Terrace Allostratigraphy Hypothesis differ in three fundamental ways: (1) Theoretical framework in the characterization of strata, (2) the identification of unconformable boundaries, and (3) interpretation of magnetic susceptibility results. Tooth and Lyons (Tooth et al. 2013; Lyons et al. 2014) employ a lithostratigraphic framework designed to identify unique lithofacies units, where the subtleties of pedogenic weathering with regards to soil horizon differentiation are not necessarily acknowledged. Bousman and Brink (2014) employ pedological descriptive methods within an allostratigraphic framework to identify

if any, missing horizons; the absence of which are indicative of unconformable boundaries. Tooth's initial characterization of the upper alluvial overbank sequence at Erfkroon does not acknowledge the presence of erosional features nor periods of prolonged non-sedimentation. Alternatively, Bousman and Brink identify three unconformable boundaries in the upper overbank sequence alone.

The primary difference between Lyons et al. (2014) and Bousman and Brink's (2014) magnetic susceptibility interpretations derive from their disparate understanding of the paleosol succession. Tooth and Lyons base their interpretations on the idea that paleosol development was concomitant with sedimentation. Their model implies that each paleosol contains a full pedogenic sequence, where even ancient surface horizons (A-horizons) are still represented. From this, Lyons et al. (2014) view magnetic enhancements as a preserved reflection of climate (temperature and precipitation) in buried surface horizons (A-horizons) because they assume magnetic minerals in these contexts were able to reach steady-state equilibrium with respect to climatic conditions (Maher & Thompson 1995; Lyons et al. 2014).

Alternatively, Bousman and Brink's model characterizes the upper overbank sequence as a series of time-transgressive pedogenic events interrupted by erosion (between the Red Paleosol and Red Sandy Loam) and extended periods of sedimentation (between the Brown Paleosol and Sandy Cap). Their model informs their interpretation of magnetic enhancement, where the neoformation of magnetic particles is thought to coincide with enhanced magnetic values associated with A-horizons (induced by increased biological activity) and illuviated B-horizons. Enhancement trends are typically

gradual, therefore, sudden peaks in magnetic enhancement followed by sudden drops coincide with breaks in pedogenic weathering intervals.

The purpose of this study is to elucidate the validity of each hypothesis by conducting an independent investigation of the overbank alluvial sequence in the Orangia Terrace. This is accomplished through high-resolution sampling and descriptive characterization of five profiles exposed across the Erfkroon study area. Identifying the presence or absence of unconformable boundaries between strata is guided by the theoretical underpinnings of multiple geological perspectives.

5. MATERIALS & METHODS

A multi-proxy analytical approach involving the high-resolution characterization of strata was employed to explore the validity of the Allostratigraphy and Accretionary models for soil development at Erfkroon. Field methods included the exposure, description, and sampling of seven geological profiles, five of which are presented here.

Bulk sediment samples were collected from individually identified zones in each profile, and high-resolution bulk sediment samples were extracted at 5-cm increments in select profiles (Profiles 2A, 2B, and 2C). Sediment blocks for petrographic thin section preparation and analysis were also extracted from stratigraphic contexts identified in previous research as unconformable boundaries. Laboratory-based laser-sizer particle size analysis and magnetic susceptibility analysis were also employed.

Two field seasons were conducted over the months of July and August in 2017 and 2018. Seven profiles were cleaned, described, and sampled over the 2017 field season. In 2018, three of the seven profiles were re-exposed to extract higher-resolution samples to facilitate a more comprehensive understanding of the Orangia Terrace alluvial sequence. Profiles 1, 2A, 2B, 2C, 3 and 4 were exposed adjacent to previously tested geological or archaeological loci (refer to Figure 5.1 for profile locations). The only outlier, Profile 5, was excavated in a previously untested area to assess the sequence's lateral integrity across the Erfkroon study area.

Profiles were vertically cleaned by hand using a geological pick, rock hammer, and shovel. Outer, heavily weathered surface sediments were removed from each profile to expose strata unmarred by modern weathering processes and deformation. This

equated to the removal of ~80-100 cm of material. The typical width of each profile ranged from 80 to 100 cm, while vertical depths varied.

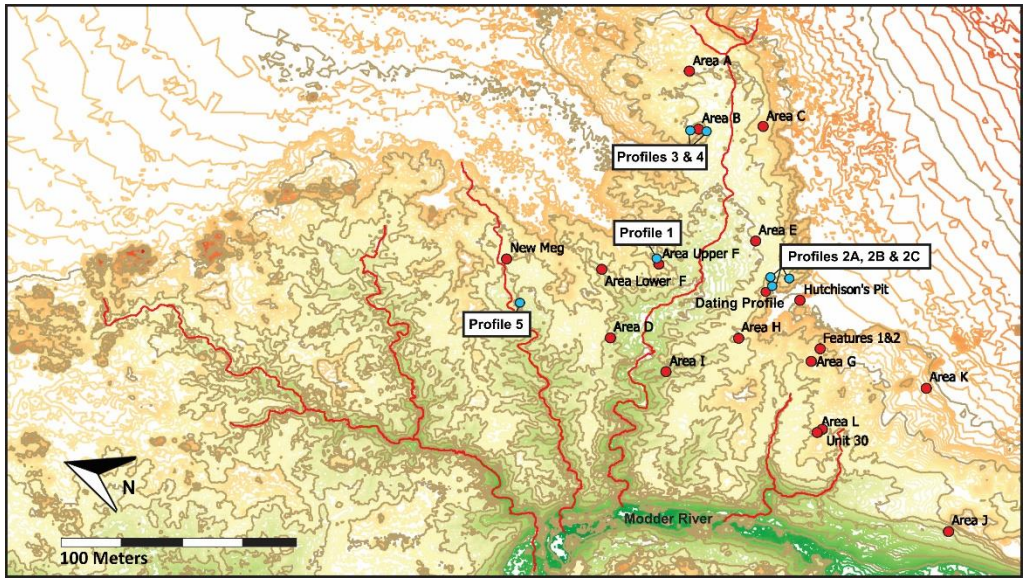

Fig. 5.1. Topographic map of Erfkroon illustrating profile locations in relation to previously excavated archaeological and paleontological locales.

Profile 1 was exposed approximately 5 meters northeast of area Upper F, an archaeological locale investigated in 2006, 2008, 2009 and 2010 by Bousman & Brink (2014). Profile 2 was excavated within three meters of the Dating Profile (see Tooth et al. 2013; Lyons et al. 2014; Bousman et al. *in prep*) but was subdivided into three juxtaposed profiles to expose as much of the alluvial sequence as possible. Resulting profiles (2A, 2B, 2C) were described and sampled individually. Profile 3 was excavated on an eastern exposure of an alluvial outcrop at Area B previously excavated by Bousman & Brink (2014) in 2006, 2008, 2009 and 2010. Profile 4 was also located in Area B and exposed another 4 vertical meters of sediment below Profile 3, along the southern face of the exposure. Profile 5 was excavated on a previously untested terrace exposure approximately 80 m northwest of Profile 1.

Of the seven excavated locales, only Profiles 1, 2A, 2B, 2C, and 5 are presented in this study. Future components of this research will include fluvial geomorphological analysis of the area's alluvial sequences, including a close characterization and spatial analysis of facies changes. Profiles 3 and 4, while almost certainly comprised of the same alluvial strata identified at the Dating Profile and elsewhere, contain different facies of the Lower Grey and Red units as described by Bousman and Brink in their 2010 geological analysis. These are suggestive of a more complex relationship between mode of deposition and discrete areas of the fluvial environment. Proper characterization of these exposures will require the use of analytical techniques outside the scope of this study. Results will be presented in future research and upon a more comprehensive understanding of the formation processes at work in the study area.

Profile Description

The United States Department of Agriculture's (USDA) *Field Book for Describing and Sampling Soils*, Version 3.0 (Schoeneberger et al. 2012), the USDA's *Soil Survey Manual* (Handbook No. 18) (Soil Science Division Staff 2017), and the *North American Stratigraphic Code* as published in the November 2005 AAPG bulletin (NASCN 2005) collectively provide standardized and comprehensive methodologies and descriptive terminology for characterizing soil pedons and sediments. The *Field Book for Describing and Sampling Soils* (Schoeneberger et al. 2012) and the *Soil Survey Manual* (Soil Science Division Staff 2017) are dedicated to the description of pedogenic characteristics and were used to guide in-field observations and descriptions of the profiles presented in this study. *The North American Stratigraphic Code* (NASCN 2005) provides descriptive terminologies for sedimentary units from a lithostratigraphic

perspective. Characteristics used to describe bedded sedimentary units were employed in this study to identify and describe, if any, sediments unaltered by pedogenic processes. Finally, the color guide, *Munsell Soil Color Book* (Munsell Color 2015), was used to estimate color value and chroma of pedofeatures and sediments.

Descriptive terminology and characteristics used to describe both pedogenic formation and the character of sedimentary units were adapted into a field form for profile-specific zone descriptions. The field form is provided in Appendix A and a comprehensive list of characteristics and associated definitions used in this study are provided in Appendix B.

Degree of Development Score

A standardized approach for describing profiles also facilitated qualitative mathematical comparisons within and between profile zones. A simple sum of the highest possible ranks among ordinal-data observations provided a score that measured the degree of development (DDS) as it relates to the relative advancement of pedogenic weathering. The greater the DDS (highest possible score of 113 points), the more closely a zone resembles a well-developed B-horizon versus stratigraphic beds or lamina unaltered by pedogenic processes. The DDS was calculated for each profile zone and used as a comparative method within and between profiles. DDS values were also calculated as a percent of the total possible DDS (113 points) and is referred to as DDS%. DDS% was also calculated for all profile zones. Raw DDS and DDS% values by profile are provided in Appendix C, and DDS% values are graphed with associated magnetic susceptibility results by profile in the following section, “Results.”

Sampling

Bulk sediment samples were extracted from all profile zones for laboratory analyses. High-resolution bulk sediment sampling was also conducted in Profiles 2A, 2B, and 2C. Approximately 5 g of sediment was extracted every ~5 cm up profile for magnetic susceptibility and particle size analysis. Zone provenience data presented by profile can be found in Appendix D and sample proveniences, and other associated measurements (grain size and magnetic susceptibly values) by profile are presented in Appendix E.

Field collection of micromorphology samples. Twelve sediment blocks were collected during the 2017 field season and 16 blocks were collected during the 2018 field season for petrographic thin section analysis. Blocks were extracted from both primary zones and zone boundaries in select profiles (refer to Appendix G for a complete list of thin section samples and associated proveniences presented in this study). Micromorphology blocks were collected by carving out a block of in situ sediment from select regions of each profile. Each block was wrapped with cloth-soaked plaster and left to dry in the field prior to extraction. Air-dried samples were then extracted and completely wrapped for transport to Texas State University.

Particle Size Analysis

Particle size refers to the relative size classes of particulates (clay, silt, and sand) comprising the inorganic fraction of a soil or sediment (Birkeland 1999:10). This method is employed to investigate the relative particle size of sediments comprising bulk and high-resolution samples as a means for comparing size classes within and between zones in each profile. Particle size is also known as texture analysis, which is a primary

descriptive characteristic presented in the *Soil Survey Manual* (Soil Science Survey Staff 2017). Texture classes referenced in this text derive from the USDA Textural Triangle, an illustration showing percentages of sand, silt, and clay as they conform with 12 primary texture classes (Figure 5.2).

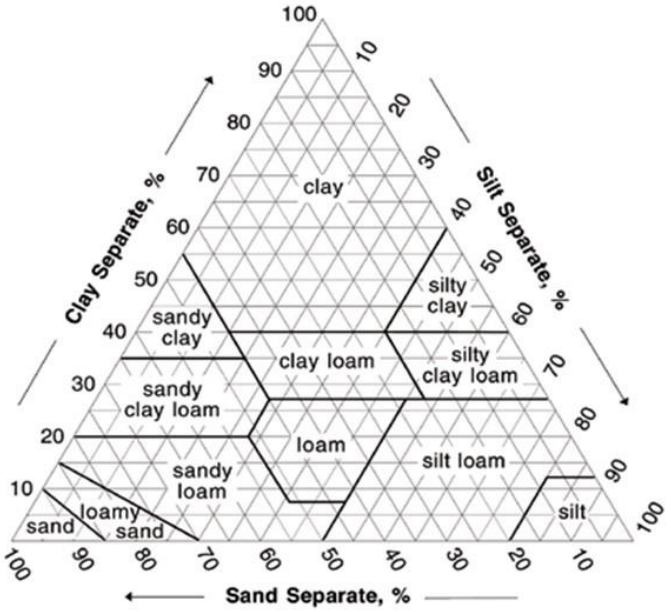

Fig. 5.2. Soil texture triangle illustrating particle size classes as ratios (% sand, silt, clay) (Soil Survey Staff 2012).

A LS 13 320 Laser Diffraction Particle Size Analyzer was utilized to measure the particle size ratio and diameter of grains in each sample. The instrument, designed to measure the diffraction pattern of a laser beaming through a suspension, calculates the proportional relationship of particle sizes within the suspension. This calculation is based the Fraunhofer diffraction theory which states that the intensity of light scattered by a particle is directly proportional to its size (McCave et al. 1986).

Samples for particle size analysis were drawn from bulk samples extracted from each profile over the course of the 2017 and 2018 field seasons. All samples were pre-treated to remove organic residues from the inorganic fraction. This was accomplished by

mixing each sample with a single pipette of hexametaphosphate and water mixture, followed by the addition of a single pipette of sodium hypochlorite after a period of heating. Hexametaphosphate is a disaggregating chemical that helps break down adhered conglomerates of fine sand and clay-sized particulates, and sodium hypochlorite refers to household bleach. The hexametaphosphate-water mixture was added to samples first, followed by heating of the mixture for 5-7 minutes on a hotplate at 150º C. Sodium hypochlorite was then added to the heated mixture after approximately 5 minutes, upon disaggregation of clumped particulates. Sample mixtures were then heated for an additional 20 minutes. Prolonged heating with the addition of sodium hypochlorite ensured any remaining organic fraction was neutralized prior to the sample entering the suspension well of the LS 13 320.

Thin Section Preparation & Analysis

Micromorphological analysis of petrographic thin sections can be a powerful tool for identifying the presence and state of pedogenesis in a buried soil (paleosol). This method was employed to elucidate the depositional context of sediments comprising the overbank sequence at Erfkroon, and to identify, if any, the presence of post-depositional processes indicative of past environmental conditions and changes.

Characterizing formation processes (in situ v. transported) associated with buried horizons, particularly the identification and characterization of buried in situ soils (paleosols) is of interest in this study. An in situ soil is recognized in thin section by continuous pedogenic characteristics such as undisturbed features created by soil biological activity (passage features etc.), consistent pedogenic microstructure, pedogenic

b-fabric, and/or the presence of one or more types of undisturbed pedofeatures (Stoops et al. 2010a:624).

B-fabric. An important component of this study is the characterization of fine fraction observed in thin section. This is referred to as the b-fabric, or "birefringence fabric" of a soil. The b-fabric refers to clay domains comprising the finest observable fraction in a micromass (the very finest fraction observed in thin section). Using cross polarized light, it is possible to observe primary b-fabric features such as clay orientation patterns and interference colors. The type and degree to which these features are observed can be telling of post-depositional processes such as clay illuviation. The b-fabric can also reveal characteristics of a strata's lithology (parent material), its degree of homogeneity, and the amount of weathering it has undergone (Stoops 2003:92).

Characterizing and comparing b-fabrics from sample to sample is also effective for identifying differences in parent material. It is expected that a soil horizon in a successive pedogenic sequence has a spatial and genetic relationship to both overlying and underlying horizons (Birkeland 1999). If a different parent material is observed in a bounding horizon, it could then be interpreted as an unconformity. In thin section, it is possible to detect the presence of different parent materials as a component of the b-fabric (Stoops 2003).

Pedogenic features. Other elements observable in thin section include pedogenic features indicative of specific soil horizons, especially B-horizons, and post-depositional environments. The B-horizon refers to a zone where subsoil materials have amassed through illuviation (translocation of materials into the B-horizon from stratigraphically higher A and/or E-horizons). This process typically occurs when a geomorphic surface

remains stable for a prolonged period. Illuvial substances refer to materials that can be mobilized, including fine, clay-sized particles, ions, chemical precipitates, and humus (fine organics). Illuviation occurs when percolating water carries mobile particles down-profile, where water soaks into B-horizon ped structures and illuviated materials are left behind as coatings on matrix particles, lining pores, or as coatings on ped faces. Illuvial materials may also accumulate as solid precipitates that form after ions are mobilized and transported into the B-horizon. Mineral weathering and accumulation of weathering elements such as Fe oxides are also common characteristics of B-horizons (Birkeland 1999).

The micromorphological expression of a B-horizon can be indicated by clay illuviation features, carbonate and/or gypsum features, and oxidation-reduction (redox) features. In thin section, clay illuviation is indicated by the presence of clay films. These manifest in several ways: Clay films coating individual grains, films coating clasts, and films lining ped surfaces or voids (Kovda & Mermut 2010).

Other pedogenic features indicative of B-horizon development include the accumulation of orthic or disorthic carbonates and ferrimagnetic minerals. These features are often indicative of long-term pedogenic development or the presence of environmental conditions conducive for oxidation or reduction (redoximorphic or redox features). Carbonate features can manifest as coarse or fine masses or nodules that develop within (orthic) or intrude (disorthic) into the groundmass or micromass. Orthic carbonate nodules, identified by their diffuse and irregular boundaries, typically form in situ and reflect prolonged periods of stable soil formation. Disorthic carbonate nodules

occur as “intrusive” features that were moved into place via pedoturbation processes such as the shrinking and swelling of clays in vertic environments (Durand et al. 2010).

Redoximorphic features can manifest as intrusive, impregnative, or depletion pedofeatures. All types, and the location in which they occur in profile, are indicative of degrees of water saturation. In the case of stratified soils, these features can sometimes occur in fine-grained horizons where water saturation is relatively short-lived and does not saturate macropores and channels along ped faces (Lindbo et al. 2010). Intrusive features refer to nodules that occur either as intrapedal Fe or Mn oxide nodules or coatings. Impregnative features form when iron (Fe) and/or manganese (Mn) accumulate in the matrix as oxidized nodules or coatings along voids or surrounding coarse grains (Stoops 2003). Depletion redox pedofeatures occur when Fe and/or Mn oxides and clays have been removed due to the reduction and mobilization of these materials (Schoeneberger et al. 2001; Vepraskas 2015).

Twenty-four micromorphology blocks were extracted from the field for petrographic thin section preparation and analysis over the course of the 2017 & 2018 field seasons. All samples were transferred from the Florisbad Quaternary Research Station in Soutpan, Free State, South Africa, to a USDA-approved foreign soils holding-area at the Center for Archeology Studies at Texas State University, San Marcos, TX. Samples were then transferred to another USDA-approved foreign soils lab where further preparation commenced. The lab, owned by Dr. Charles Frederick in Dublin, TX, was utilized to complete the first of two preparation phases.

Thin section preparation. The preparation of thin sections in this study occurred in two phases. The first phase was conducted in-house, and involved hardening sample

matrices with a polyester resin, followed by trimming of the hardened samples into "chips" or "billets" roughly the size of a 2-x-2-inch glass slide. This process is described in detail below. The second phase of preparation involves mounting sample chips onto slides. This process entails slicing, trimming, and grinding chips into thin (~30 microns thick) and optically flat samples. Phase 2 was achieved by outsourcing the process to Quality Thin Sections, a professional thin section preparation company located in Tucson, Arizona.

The first phase of thin section preparation was accomplished by following a three-step procedure augmented from Murphy's (1986) thin section preparation methodology: (1) Sample drying, (2) sample embedding and polymerization, and (3) slicing hardened samples into slide-sized chips. In step 1, raw samples were slow-dried in an oven at 80°C for 18 hours to remove any remaining moisture prior to embedding. Samples were then placed into individual, liquid-tight, plastic containers. Step two refers to polystyrene embedding and polymerization of samples. A polyester resin mixture comprised of unsaturated polyester resin, a stabilized styrene monomer, and methyl ethyl ketone was used to embed each sample. The mixture was poured around each sample until all but the very top of the sample was immersed in its plastic container. Each sample was then placed into a vacuum chamber for three, 1-minute intervals to facilitate complete resin saturation. Saturated samples were then immersed in the resin mixture and left to polymerize. Polymerization occurred in a well-ventilated, covered outdoor shed for 3 to 4 weeks. Following the drying interval, samples were placed in an oven set at 100ºC for 6-12 hours to ensure any remaining, "tacky" resin polymerized completely. Chips were then produced by slabbing polymerized sample blocks along vertical planes (from top to

bottom) into ~1-2 cm-thick pieces using a variety of diamond-tipped circular saws. Care was taken to clearly mark the stratigraphic top of each block with deeply embedded scores. All slabs were further trimmed into 2-x-2-inch chips.

Micromorphological analysis of the 17 thin sections selected for this study was accomplished using a Motic BA310 polarizing light microscope. Photomicrographs of pedogenic and sedimentary features were taken using a moticam 5.0 mp digital microscope camera and Motic Images Plus 3.0 ML software. Two sources: *Interpretation of Micromorphological Features of Soils and Regoliths* (Stoops et al. 2010a) and *Guidelines for Analysis and Description of Soils and Regolith Thin Sections* (Stoops 2003) guided interpretations.

Magnetic Susceptibility Analysis

Magnetic susceptibility refers to the relative magnetic properties of an unconsolidated material, where susceptibility values reflect the degree to which a material can be magnetized by an external magnetic source. In some cases, this method has been used as a proxy indicator for pedogenic development and climate-controlled depositional processes (Heller & Liu 1984; Maher et al. 1994; Liu et al. 1995; Dearing et al. 1996). Mass-specific magnetic susceptibility (expressed as χ) refers to the magnetic enhancement associated with a sample's dry mass, rather than density which can be variable. This measurement was used to identify magnetic enhancement indicative of pedogenic development and/or anomalous patterns suggestive of unconformities in the overbank alluvial sequence at Erfkroon.

Calculating mass-specific susceptibility. Mass-specific susceptibility was calculated per sample by dividing its volume susceptibility (k) by the sample's bulk

density (ρ), where bulk density was calculated by dividing a sample's mass by its volume. Sample volumes remained a constant 10 cm^3. Measurements obtained through these calculations are expressed as χ (chi), which is further expressed as both low (χ_{lf}) and high-frequency (χ_{hf}) values in units of 10^{-8} (Dearing 1999). Low and high-frequency susceptibility measurements were then used to calculate percentage frequency-dependent susceptibility ($\chi_{fd\%}$) using the following formula:

$$\chi fd\% = \left\{\frac{(\chi lf - \chi hf)}{\chi lf}\right\} * 100$$

Frequency-dependent susceptibility calculation, where $\chi_{fd\%}$ value is in units of $10^{-8}m^3kg^{-1}$ (Dearing 1999).

Mass-specific susceptibility measurements were taken on all bulk and high-resolution samples extracted from the study profiles using a Bartington Instruments MS2B Meter with a dual frequency well-sensor. Mass-specific susceptibility readings were taken at both low-frequency ($\chi_{lf;}$ 470 Hz) and high-frequency ($\chi_{hf;}$ 4700 Hz) measurements at room-temperature and used to calculate percentage frequency-dependent susceptibility.

Dried sediment from profile sample populations were packed into 10 cm^3 plastic cubes. Cube mass (g) was measured before and after packing to calculate sample bulk density (D=m/v, where D=density, m=mass, and v=volume) for mass-specific measurements. Samples were then placed in the Bartington well-sensor for measurement, only after a continuous air measurement of 0 was achieved. Samples were measured sequentially, where one air measurement was taken as a buffer between each frequency specific measurement. The sequence was performed as follows: (1) Air measurement, (2)

low-frequency measurement, (3) air measurement, (4) high-frequency measurement. This process was repeated for every sample. The difference between low- and high-frequency values was used to calculate frequency-dependent susceptibility (χ_{fd}, where $\chi_{fd} = \chi_{lf} - \chi_{hf}$), and percentage frequency-dependent susceptibility ($\chi_{fd\%}$) (see above equation) (Dearing 1999). Refer to Appendix D for a comprehensive list of χ_{lf}, χ_{hf}, and $\chi_{fd\%}$ values for all profile sample populations.

Magnetic behavior. The purpose of magnetic susceptibility analysis is to identify and characterize the magnetic behavior of minerals in depositional and post-depositional environments. Primary magnetic behaviors include ferromagnetism, ferrimagnetism, canted antiferromagnetism, paramagnetism, and diamagnetism (refer to Table 5.1 for a summary of definitions). Ferrimagnetism refers to the most common magnetic behavior found in the natural environment, where higher densities of ferrimagnetic minerals such as magnetite and other Fe-bearing minerals generate high magnetic susceptibility values (Dearing 1999).

Pedogenic ferrimagnets. The neoformation of pedogenic materials with ferrimagnetic properties most often manifest as magnetite. The presence of magnetite in pedogenic environments is attributed to the presence of iron-reducing bacteria that are common in organic rich, anoxic soils. Accumulations of magnetite also tend to occur in oxidizing environments where intermittently wet/dry soils are common (Maher 1998). Identifying the presence and relative degree to which a material is magnetically enhanced can also be used to correlate stratigraphy within a profile or across a landscape (Dalan & Banerjee 1998).

Table 5.1. Five primary magnetic behaviors identifiable with magnetic susceptibility analysis (Dearing 1999).

Magnetic Behavior	Definition
Ferromagnetism	Refers to materials with strong positive susceptibility (i.e. pure iron); magnetic domains are highly ordered and aligned in the same direction. Such materials are uncommon in the natural environment.
Ferrimagnetism	Refers to materials with strong positive susceptibility; such materials are commonly found in the natural environment (i.e. iron oxide, magnetite); magnetic domains are strongly aligned but occur as opposing, unequal forces.
Canted antiferromagnetism	Refers to materials with moderate positive susceptibility (i.e. iron minerals, haematite); magnetic domains are well-aligned and opposing, though the force of opposition is equal thus canceling each other out.
Paramagnetism	Refers to materials with weak positive susceptibility (i.e. biotite, pyrite); magnetic domains arise only when exposed to a magnetic field and occur because of the presence of manganese (Mn) and iron (Fe) ions.
Diamagnetism	Refers to materials with weak negative susceptibility produced when a magnetic field interacts with orbiting electrons. Minerals with no iron fall into this category (i.e. quartz, calcium carbonate); other diamagnetic materials include organic matter and water.

Low-frequency, high-frequency & frequency-dependent susceptibility. Magnetic susceptibility values of soils can be expressed in different ways by exposing a sample to low- and high-frequency magnetism, the results of which can be indicative of past climatic conditions, post depositional processes, and pedogenic weathering environments (Heller & Liu 1984; Maher et al. 1994; Liu et al. 1995; Dearing et al. 1996). Low-frequency mass-specific susceptibility (χ_{lf}) refers to the value calculated when a sample is exposed to a weak, external magnetic field (470 Hz). The ratio of material effectively magnetized is translated into a value (m^3kg^{-1}) quantifying the degree to which a substance can be magnetized. In soils, this is largely controlled by the mass concentration of

magnetite and maghemite (Dearing et al. 1996). High-frequency susceptibility (χ_{hf}) exposes a sample to a higher magnetic field (4700 Hz). Low-frequency values are coupled with high-frequency values to note the presence of superparamagnetic (SP) grains in a sample. If present, the susceptibility at high-frequency will be slightly lower than values measured at low-frequency. If no SP-grains are present, the two values will be the same (Dearing 1994).

Frequency-dependent susceptibility (χ_{fd}) refers to the difference between low- and high-frequency mass-specific magnetism values. This parameter indicates the presence of ultrafine grains of magnetic material occurring at the SD/SP boundary (SD=stable, single domain grains; SP=superparamagnetic grains). Superparamagnetic minerals (SP-grains) refer to ultrafine, single-domain grains that are thermally unstable but retain high susceptibility values. SP-grains tend to occur as secondary mineral components in a system, as a product of burning, pedogenesis, or bacterial action (Dearing 1999). In a modern soil, samples containing a significant amount of SP grains tend to have a frequency-dependent susceptibility percentage ($\chi_{fd\%}$) that is greater than 6%. A percentage of less than 5% suggests either no SP grains are present, or they occur as extremely fine particulates; this reflects the nature of the measurement which only identifies the presence of medium SP grains ranging between 0.013 to 0.027 micrometers in size (Dearing et al. 1996; Dearing 1999). The highest χ_{fd} values derive from grains within this range and decrease accordingly if grains fall outside (Dearing et al. 1996; Eyre 1997). While this size range is narrow, SP grains falling within it conform with secondary magnetic particles typically associated with biogenic and pedogenic activity, rather than primary magnetic grains within the parent material (Dearing et al. 1996).

6. RESULTS

Five geological profiles exposing the Orangia Terrace's alluvial overbank sequence were investigated to explore the validity of the Accretionary and Allostratigraphy hypotheses. Both paleopedological and lithostratigraphic approaches were employed to holistically characterize the gross morphology of profile strata, while soil horizon assignments were made after assessing concomitant patterns among geoproxy data sets. Results suggest that employing both paleopedological and lithostratigraphic approaches to describe Erfkroon's alluvial architecture is effective for identifying and characterizing patterns of sedimentation and pedogenic development.

Descriptive results pertaining to Profiles 1, 2A, 2B, 2C, and 5 are presented, followed by a brief discussion of identifiable patterns in their respective geoproxy datasets. All methodologies employed in this study are presented by profile, as assessing these data holistically drives pedogenic horizon designations. The pedological and sedimentary relationships among horizons within and between profiles are discussed in the following section, "Interpretations & Conclusions." Detailed provenience data for zones comprising each profile are presented in Appendix D. Sample provenience data, including grain size and magnetic susceptibility results are presented in Appendix E. Refer to Appendix F for profile description narratives and a summary of field form observations, and Appendix G for a comprehensive list of thin section samples and provenience data.

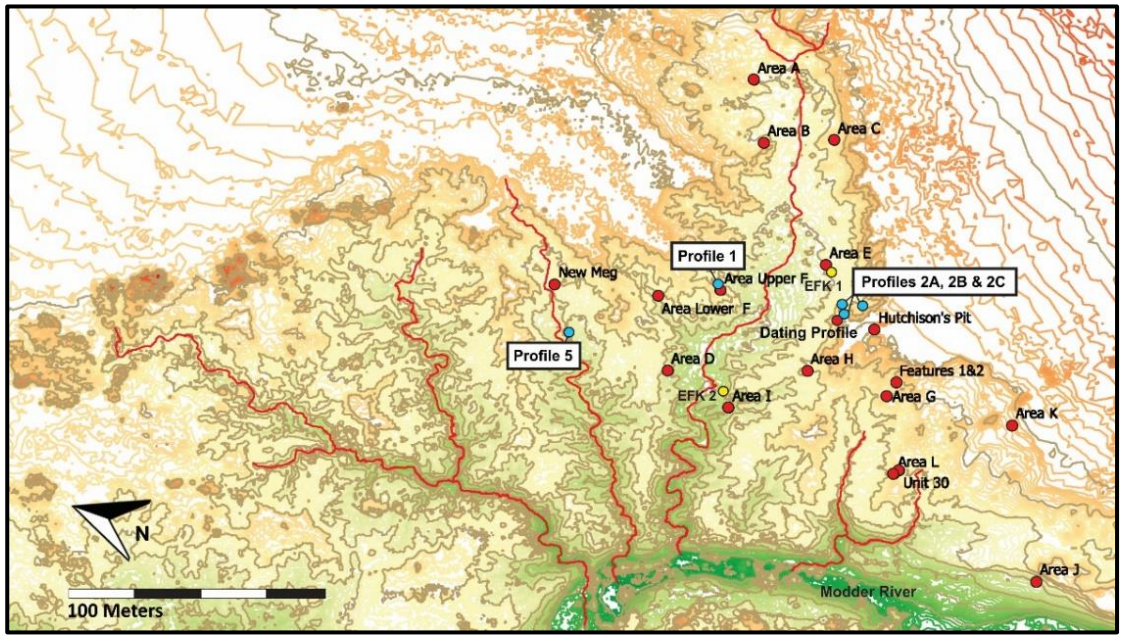

Fig. 6.1. Erfkroon study area and profile locations in relation to previously excavated archaeological locales and Dating Profile. Profiles included in this study: 1, 2A, 2B, 2C, & 5.

Profile 1 Results

Profile 1 was excavated along an eroded alluvial exposure in Area Upper F approximately 50 m north of the Dating Profile previously investigated by Tooth et al. (2013), Lyons et al. (2014), and Bousman and Brink (2014) (see Figure 6.1). Approximately 80 cm of the outer, heavily weathered and disturbed surface material was removed to expose relatively unaltered sediments. The excavated exposure reached a maximum depth of 3.89 m below surface, in which 11 stratigraphic zones were identified (Figure 6.2). Bulk samples, one from each zone, were extracted for particle size and magnetic susceptibility analysis. One micromorphology block straddling the contact between zones 4 and 5 was also extracted for thin section analysis (see Figure 6.3).

Field description of Profile 1 revealed 11 zones comprising an AB-CB-Bkt-Bw-Btss-Bw-Bw-Bw-Bw-Bk/C-C sequence. An illustration of Profile 1 with corresponding

zone and horizon designations are provided in Figure 6.3. Refer to Table 6.1 for a description of Profile 1 organized by zone. A summary of field description form results and a profile description narrative by zone is provided in Appendix F.

Fig. 6.2. Profile 1 exposure and sample areas.

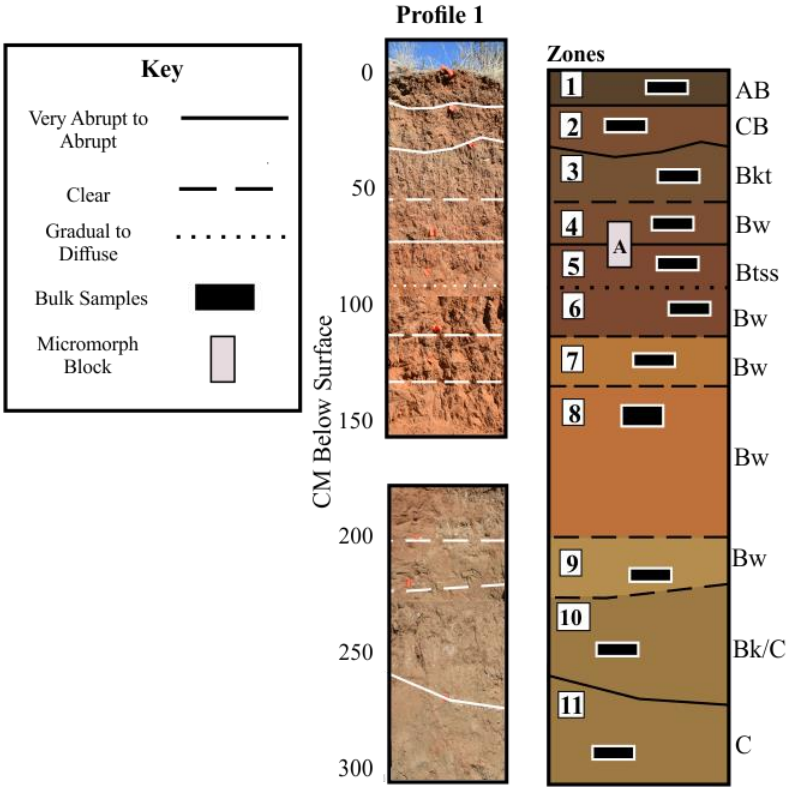

Fig. 6.3. Profile 1 horizons and sample locations. “A” corresponds with thin sections 44MM6S9A & 44MM6S9C (refer to Appendix G).

Table 6.1. Profile 1 description by zone.

Zone	Horizon	Depth (cmbs)	Description
1	AB	0-17.70	Fine, weak sub-angular blocky strong brown (7.5YR 5/6 dry) to brown (7.5YR 4/4 moist) loam matrix. Matrix consistence ranges from hard (dry) to friable and plastic (moist). Few very fine to fine carbonate filaments and many fine to very fine roots occur throughout matrix. Lower boundary abrupt and wavy.
2	CB	17.70-38.10	Medium, weak subangular blocky peds comprised of alternating strong brown (7.5YR 4/6) to brown (7.5YR 5/3) bedded, silty loam matrix. Matrix consistence ranges from soft (dry) to slightly plastic and very friable (moist). Ped structure deforms bedding that is characterized by very thin to medium laminations comprised of very fine sands, silts and moderately well-sorted pebbles. Sandy/silty laminae are separated by strong brown clay drapes. Many discontinuous, distinct clay bridges occur on ped faces. Few, very fine, dendritic roots between ped faces. Pedofeatures include few very fine irregular pores, few fine carbonate masses, few discontinuous and platy carbonate laminations, and bioturbation in the form of insect casts, burrows and root voids. Few fine vertical rhyzoliths occur near top of zone. Lower boundary abrupt and wavy.

Table 6.1. Continued

3	Bkt	38.10-61.10	Fine, moderately strong, prismatic peds comprised of yellowish-brown (10YR 5/4 dry) to dark yellowish-brown (10YR 4/4) silty loam matrix. Matrix consistence ranges from medium hard (dry) to firm and plastic (moist). Ped faces strongly effervesce when exposed to 10% HCl solution, no reaction within ped matrix. Pressure faces and clay films are distinct, discontinuous and common on ped faces. Sand films, discontinuous and distinct, accumulate on pressure faces and clay films. Very few specs of soft manganese occur discretely on ped faces and in matrix. Very fine carbonate filaments infilling cracks and pores are common. Very fine, cubic to reticulate carbonate nodules occurring in pores, cracks and adhering to matrix along ped faces in bottom of zone are common. Bioturbation in the form of root voids, insect burrows and worm casts are common. Fine, vertically oriented rhyzoliths are common and occur in bottom of zone. Lower boundary gradual and wavy.
4	Bw	61.10-82.90	Fine, moderately strong wedge-shaped peds comprised of strong brown (7.5YR 4/6 dry and moist) silty loam matrix. Matrix consistence ranges from moderately hard (dry) to loose and non-plastic (moist). Ped faces and matrix slightly effervesce when exposed to 10% HCl solution. Continuous, prominent sand films occur on all ped faces. Film grains match color of matrix (7.5YR 4/6). Very few, fine carbonate filaments infill cracks and pores on ped faces in localized areas at top of zone. Very few, fine carbonate masses occur discretely on ped faces. Bioturbation in the form of worm channels, insect casts, and root voids are common. Fine roots and pores with moderate vertical continuity, dendritic and vertical in shape, commonly occur on ped faces. Lower boundary clear and smooth.
5	Btss	82.90-101.10	Coarse, strong prismatic peds comprised of yellowish-red (5YR 5/6 dry; 5YR 4/6 moist) silty loam matrix. Matrix consistence ranges from moderately hard (dry) to friable and plastic (moist). Sand films and slickensides are prominent and patchy on ped faces. Very fine dendritic and tubular pores are many and occur on ped faces. Bioturbation in the form of cylindrical, linear worm channels are many, and contain a strong brown (7.5YR 5/4) infilled matrix. Channels are pervasive throughout zone. Insect burrows and casts, some containing fecal pellets, are also common. Live termites observed in profile. Black Mn masses occurring in dendritic and thread-like filaments are common on ped faces. Platy, very fine Mn masses are many and occur on ped faces and in parting planes. Very fine FeMn nodules occur commonly in matrix and on ped faces. Very few fine carbonate filaments observed in cracks on ped faces. Lower boundary clear and smooth.

Table 6.1. Continued

6	Bw	101.1-119	Medium, weak, wedge-shaped peds comprised of yellowish-red (5YR 5/6 dry; 5YR 4/6 moist) loam matrix. Matrix consistence ranges from soft (dry) to loose and non-plastic (moist). Ped faces and matrix are nonreactive to 10% HCl solution. Clay films in secondary, bioturbated regions are few. Few, distinct, discontinuous clay films also observed between sand grains in matrix of peds. Sand films, discontinuous and distinct, are many and occur on ped faces. Few, vertical to dendritic pores observed on ped faces, with low vertical continuity. Bioturbation in the form of linear, cylindrical worm channels containing brown (7.5YR 5/4) matrix are many. Root voids and insect burrows are common. Very few, very fine carbonate filaments observed in cracks on ped faces. Lower boundary clear and smooth.
7	Bw	119-135	Fine, weak, wedge-shaped peds comprised of strong brown (7.5YR 5/8 dry; 7.5YR 5/6 moist) loam matrix. Matrix consistence ranges from soft (dry) to loose (moist). Ped faces and matrix are nonreactive when exposed to 10% HCl solution. Very fine, dendritic to vertical roots with low vertical continuity are common throughout peds. Few very fine dendritic and vertical pores are common on ped faces. Few hard FeMn nodules occur in pores, cracks, and bioturbated areas of peds. Dark brown/black masses of Mn in very fine to fine, spherical to platy formations, are common on ped faces and throughout matrix. Mn masses in the form of filaments (vertical and dendritic) also occur on ped faces. Very few carbonate infilled burrows and very fine filaments in cracks observed. Bioturbation in the form of linear, cylindrical worm channels penetrate zone and contain light yellowish-brown (10YR 6/4) matrix. Lower boundary clear and smooth.
8	Bw	135-216.70	Fine, very weak wedge-shaped peds comprised of strong brown (7.5YR 5/8 dry; 7.5YR 5/6 moist) sandy loam matrix. Matrix consistence ranges from soft (dry) to loose and non-plastic (moist). Very few pores with low vertical continuity occur on ped faces. Bioturbation in the form of linear worm channels and insect burrows are very few and infilled with light yellowish-brown (10YR 6/4) matrix containing fine to very fine sands and pebbles. Lower boundary clear and smooth.
9	Bw	216.70-243.40	Fine, weak subangular blocky peds comprised of light yellowish-brown (10YR 6/4 dry; 10YR 5/4 moist) loam matrix. Matrix consistence ranges from soft (dry) to loose and non-plastic (moist). Very fine to very coarse, dendritic and vertical roots with moderate vertical continuity are common. Bioturbation in the form of linear, cylindrical worm channels and insect burrows are very many, nearly obscuring ped structure throughout zone. Worm channel matrix is strong brown (7.5YR 5/6). Few, fine dendritic to vertical carbonate filaments occur on ped faces and in cracks. Few, very fine carbonate masses (flecks) occur on vertical ped faces. Lower boundary clear and wavy.
10	Bk/C	243.40-276.50	Fine, weak subangular blocky peds comprised of pale brown (10YR 6/3) loam matrix. Matrix consistence ranges from soft (dry) to loose and non-plastic (moist). Ped faces and matrix slightly effervesce when exposed to 10% HCl solution.

Table 6.1. Continued

10 (cont.)			Fine, dendritic and vertical roots with low vertical continuity are few. Few, very fine pores on ped faces. Very fine to fine, irregular to spherical carbonate masses and irregular concretions, very fine nodules, and lenticular carbonate "flecks" are common throughout matrix and on ped faces. Top and bottom of zone bounded by a 2cm thick carbonate bed. Thin and very thin laminae characterized by fining upward sands and silts are commonly disrupted by pedo- and bioturbation. Bioturbation in the form of insect burrows and linear worm channels infilled with reddish-yellow (7.5YR 6/8) matrix are very common. Clay films commonly line interior channel boundaries. An abrupt, wavy lower boundary is formed by a thin carbonate lens (~2mm thick).
11	C	276.50-389.90	Loose, single-grain light yellowish-brown (10YR 6/4 dry) to yellowish-brown (10YR 5/4 moist) non-plastic loam matrix. Zone is characterized by very thin to thin beds of parallel to cross-bedded sands, silts, and well-sorted sub-rounded pebbles. Bedding is comprised of many fining-upward sequences. Base of zone (lower 20 cm of exposed profile) contains fine to coarse gravels and pebbles, moderately sorted and sub-rounded to angular in shape, embedded in fine sandy matrix. Bioturbation in the form of insect burrows (live ants observed in matrix) alter zone. Infilled burrows contain strong brown (7.5YR 5/6) matrix. Zone is bounded above by carbonate bed (2cm thick); no carbonates observed in matrix below. Bedding at base of zone slopes downwards at 30-45º angle to the east. Lower boundary unobserved; base of profile exposure.

Particle size, magnetic susceptibility & degree of development results. Particle size and magnetic susceptibility analyses were conducted on the 11 representative bulk samples extracted from Profile 1. The distribution of sand, silt, and clay (measured in phi) by zone with respective frequency-dependent susceptibility ($\chi_{fd\%}$) values are presented in Figure 6.4. Particle size means and standard deviations by zone are presented in Figure 6.5. Raw numeric particle size ratios, standard deviations, means, and magnetic susceptibility values by sample are tabulated in Appendix E.

Ordinal characteristics recorded during morphological description of Profile 1 were utilized to calculate degree of development scores by zone. Zone scores illustrate

stratigraphic regions of the profile that reflect well-developed B-horizons indicative of buried phases of pedogenic development (paleosols). Degree of development scores and percentage calculations (DDS%) are presented in Appendix C and zone DDS% calculations are graphically portrayed with associated frequency-dependent magnetic susceptibility values in Figure 6.6. A side-by-side comparison between degree of development and susceptibility results show frequency-dependent magnetic enhancement coincides with relatively high DDS% values, suggesting soil magnetism is, in part, driven by pedogenic weathering and perhaps clay illuviation associated with buried B-horizons.

In summary, observations suggest Zone 1 is characterized by modern surface residuum altered by bio- and pedoturbation. Zone 1 and Zone 2 form an abrupt boundary, made apparent by remnant sedimentary structures including pedogenically altered laminations of sands, silts, and clays. Magnetic enhancement in Zone 1 corresponds with visual observations of illuviating clays that contribute to its characterization as an AB-horizon. A reduction in magnetic values associated with Zone 2 correlates with its expression as a slightly modified C-horizon.

Visible sedimentary structure attests the relatively unaltered nature of Zone 2 and implies that it shares no pedogenic relationship with the well-structured Bkt-horizon in Zone 3 below. Susceptibility values reflect pedogenic development in this circumstance. Low $\chi_{fd\%}$ (3.32) is associated with the modified C-horizon in Zone 2, and a slightly higher $\chi_{fd\%}$ (4.044) occurs in Zone 3; a visibly abrupt boundary separates Zone 3's well-developed argillic horizon from the weakly developed, partially laminated C-horizon in Zone 2. Zones 4 and 5 are also characterized as B-horizons and correspond with increasing ratios of silt in the profile matrix (refer to Figure 6.4). Degree of development

scores swing from relatively high, to low, then back to high in zones 3-5 respectively. This confirms in-field B-horizon designations for these zones, but also helps to illustrate comparatively less pedogenic development in Zone 4. Higher DDS% associated with zones 3 and 5 coincide with $\chi_{fd\%}$ enhancement. DDS% and $\chi_{fd\%}$ then decline into Zone 6 (refer to Figure 6.6 and Appendix C).

Magnetic susceptibility and DDS% values plummet into Zone 7, where a lower DDS% score appears to be a function of reduced calcium carbonate in the matrix, and generally weak ped structural development. Magnetic enhancement increases into Zone 8, while DDS% continues to decline. This relationship is opposite to those observed between DDS% and $\chi_{fd\%}$ in zones 3 and 5. Zone 8's DDS% score reflects weak pedogenic development, a general lack of redoximorphic features, and a decline in visually observable calcium carbonate features. A lack of these combined characteristics suggests higher susceptibility values are driven by something other than advanced pedogenic development.

Particle size results for Zone 8 reveals a matrix comprised of a higher ratio of coarse fraction than observed in stratigraphically higher zones which might account for its enhanced magnetic signature. One possibility is that the zone's coarse fraction is comprised of iron-enriched particles of magnetite— a condition of the matrix receiving weathering inputs of magnetic particles from an igneous (doleritic) parent material. This is plausible given the numerous dolerite koppies found near the project area. A slight decrease in susceptibility values, higher ratios of fine silts and clays in the profile matrix, and a higher DDS% score coincides with the transition into Zone 9. Zone 9, a Bw-

horizon, is characterized by relatively weak pedogenic development and a matrix containing finely disseminated carbonates.

Zone 10 is characterized by magnetic enhancement and slightly greater pedogenic development, while Zone 11 coincides with a decline in susceptibility and a DDS% that plummets into the negatives. A defining characteristic of Zone 10 is the increased presence of calcium carbonate. The matrix itself contains finely disseminated carbonate, while fine, nodular and platy carbonates also occur. Fine, platy carbonate lenses form along ped faces, and a 1-2mm-thick carbonate lens forms an abrupt boundary between zones 10 and 11. Zone 11 is characterized by a negative DDS% score and an extremely low susceptibility value, both characteristics of a pedogenically unaltered, sedimentary C-horizon. The zone's matrix is comprised of unconsolidated, fining upward sands and silts that form thin and very thin laminae.

Micromorphology Results. Micromorphology Block A was extracted from the boundary between zones 4 and 5 (refer to Figure 6.3). Two thin sections were prepared for further analysis. Thin section 44MM6S9A derives from Zone 4, just above its boundary with Zone 5, and slide 44MM6S9C derives the upper 6 cm of Zone 5, just below the Zone 4-5 boundary. Descriptive results of micromorphological analysis are presented in Table 6.2 and representative photomicrographs are illustrated in Figure 6.7.

In summary, thin sections reveal slight differences between matrix particle size compositions and b-fabric. Zone 4 is primarily comprised of sub-angular to sub-rounded fine to medium sand-sized quartz with a gefuric to close-porphyric c/f related distribution. Clays are light yellow in color, and the b-fabric is stipple-speckled and in some areas, undifferentiated, with few occurrences of granostriated coarse fraction.

Pedofeatures include carbonate hypocoatings along insect channels. Such features are commonly described among soils developing in arid and semi-arid conditions (Seghal & Stoops 1972; Courty 1990; Monger et al. 1991). Zone 5 is dominated by very fine sands and silts forming single- to double-spaced porphyric c/f related distributions. Well-oriented, fine clay and silt fractions are dark yellow in color, and the b-fabric is primarily stipple-speckled and parallel and granostriated. Such features are typical of vertisols and shrink/swell action. Unlike the above zone, the coarse fraction in Zone 5 is considerably less rounded, ranging from sub-angular to angular in shape (refer to Figure 6.7).

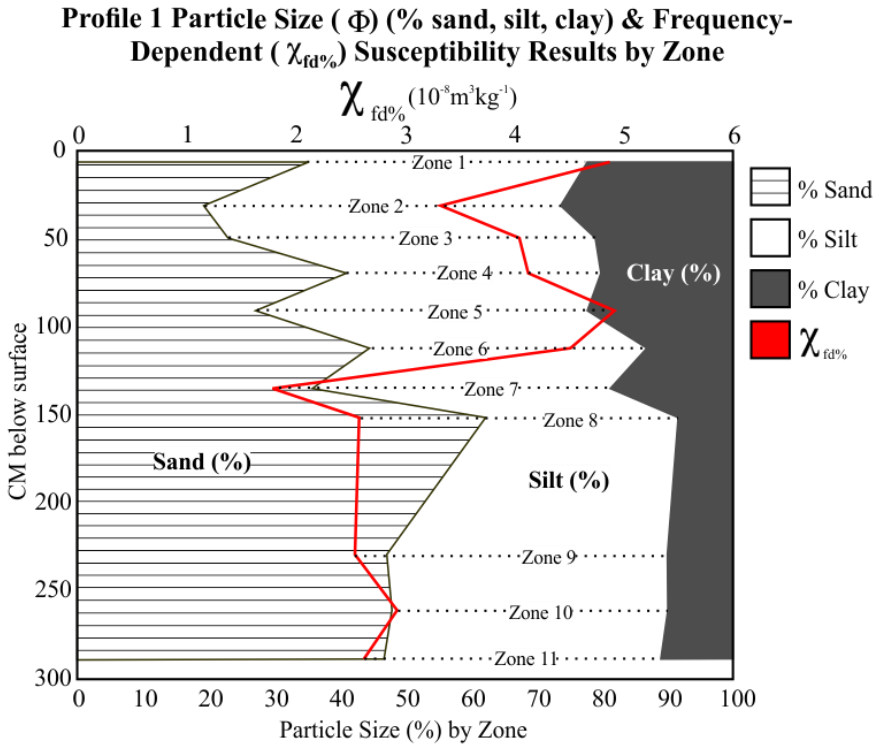

Fig. 6.4. Profile 1 particle size distribution (% sand, silt, clay) & frequency-dependent susceptibility results by zone. Dotted lines indicate zone-specific sample locations. Refer to Appendix D for zone boundary provenience data.

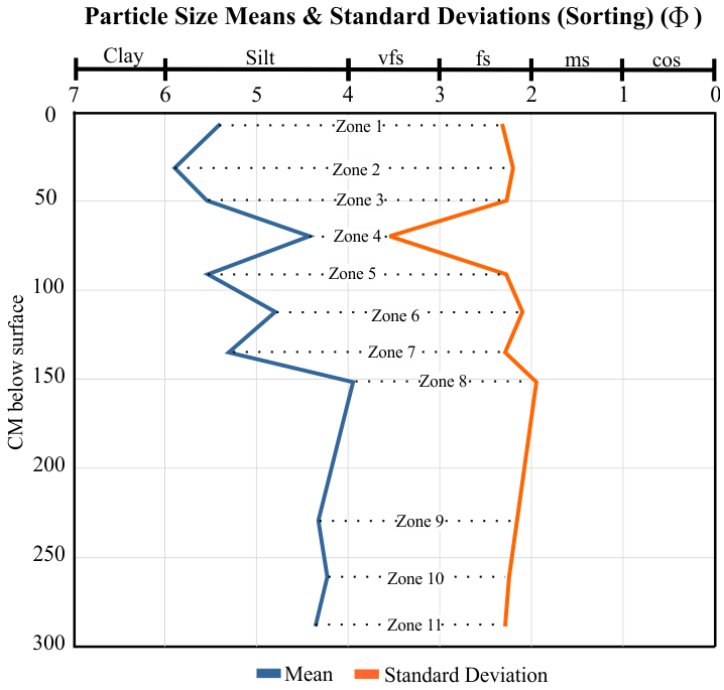

Fig. 6.5. Profile 1 particle size means and standard deviations by zone. Abbreviations: cos=coarse sand, ms=medium sand, fs=fine sand, vfs=very fine sand. Dotted lines indicate zone-specific sample locations. Refer to Appendix D for zone boundary provenience data.

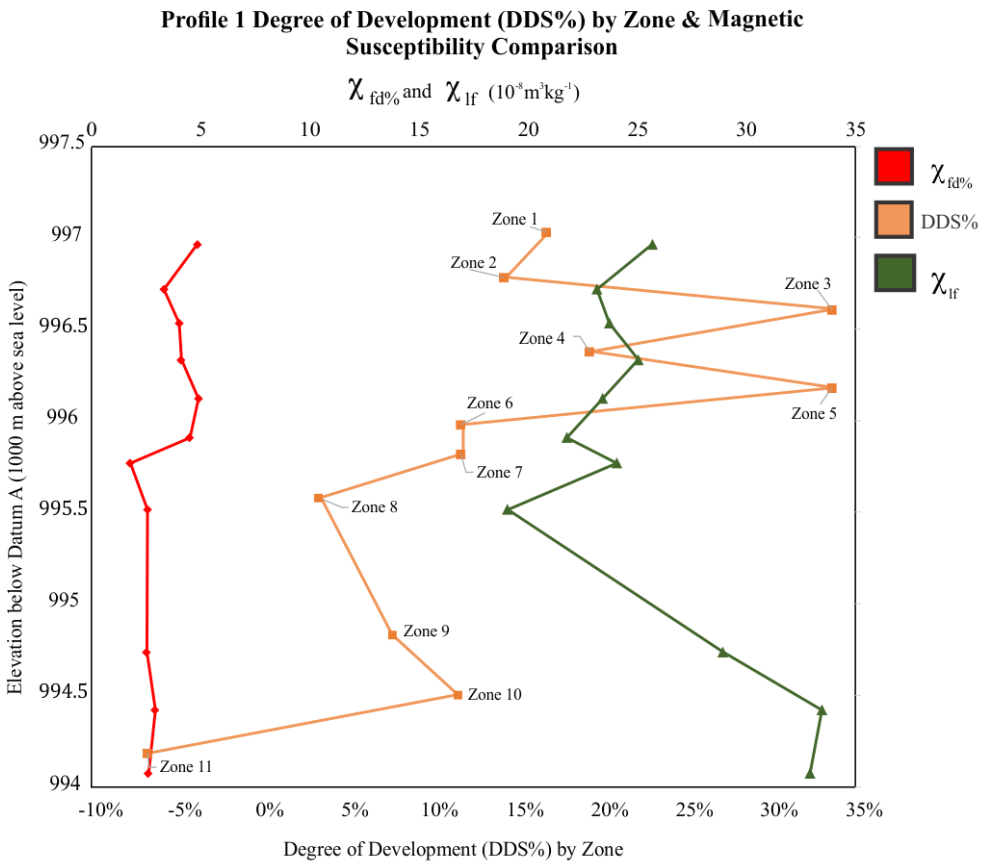

Fig. 6.6. Profile 1 degree of development percent (DDS%) by zone & magnetic susceptibility comparison.

Table 6.2. Profile 1 micromorphological analysis results.

Block	Zone	Slide ID	Description	Figure
A	4	44MM6S9A	**c/f related distribution:** Close to single-space porphyric and in some places, gefuric**.** **Structure & voids:** Channel microstructure with vesicles, chambers and simple and compound packing voids. **Coarse Fraction:** Moderate to well-sorted, sub-angular to sub-rounded fine to very fine sand-size quartz (dominant), augite (common); very fine sand-sized quartz (common), augite and magnetite (few), subrounded and rounded feldspar (very few); coarse sand-sized quartz (few), augite (very few). **Fine Fraction:** Light yellow clays, stipple-speckled and undifferentiated b-fabric; in a few places, granostriated b-fabric and calcareous b-fabric surrounding fine and very fine grains (typical b-fabric in passage features and comprising fecal pellets)**.**	6.7

Table 6.2. Continued

		44MM6S9A (continued)	**Pedofeatures:** Passage features with calcareous, stipple speckled parallel striated b-fabric in fecal pellets; Fe-Mn staining on grains (few); impregnative, orthic carbonate nodules with diffuse boundaries containing very fine grains of coarse fraction.	
A	5	44MM6S9C	**c/f related distribution:** Single- and double-space porphyric and in some areas, close porphyric. **Structure & Voids:** Subangular blocky and channel microstructure with vesicles and chambers. **Coarse fraction:** Moderately sorted fine sub-angular to angular very fine sand and silt-sized quartz (dominant), feldspar (common), augite (few), very fine to silt-sized quartz (common), feldspar and augite (few), magnetite (very few); Coarse and very coarse sand-sized quartz, augite and feldspar (few to very few). **Fine fraction:** Strong yellow to reddish-yellow clays and stipple-speckled and granostriated b-fabric. **Pedofeatures:** Passage features partially and completely infilled with calcareous, crystallitic b-fabric containing fine to very fine quartz, feldspar, and augite; dense calcareous fecal pellets with dusty yellowish-brown clay films; limpid dark reddish-brown clay infillings in few vesicles; dark (black) organic material lining channels and voids.	6.7

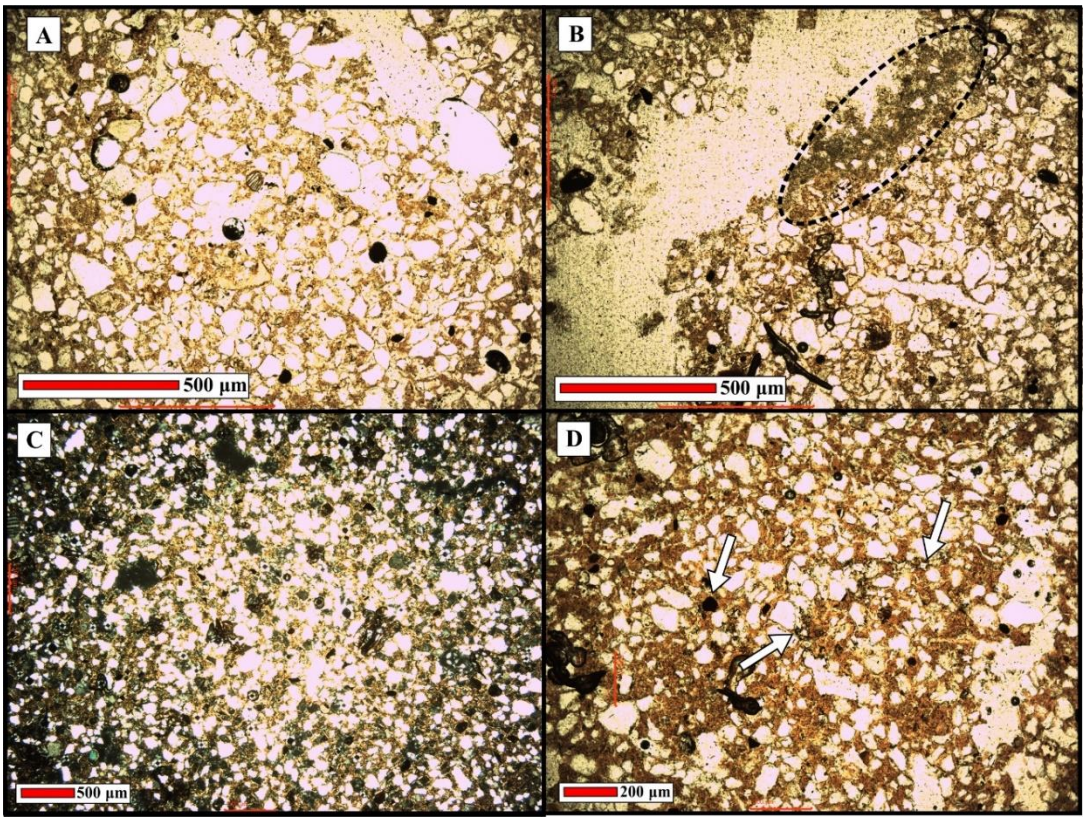

Fig. 6.7. Profile 1 thin sections 44MM6S9A & 44MM6S9C. (A) Zone 4 (44MM6S9A), typical b-fabric and c/f related distribution (xpl, 40x); (B) Zone 4 (44MM6S9A), orthic carbonate formation surrounding coarse fraction along void boundary (circled area); (C) Zone 5 (44MM6S9C), typical c/f related distribution orthic and disorthic FeMn nodules (black) (xpl, 20x); (D) Zone 5 (44MM6S9C), typical c/f related distribution with organic matter lining channels and voids (white arrows) (ppl, 40x).

Profiles 2A, 2B & 2C Results

Three profiles (2A, 2B & 2C) were exposed adjacent to each other along the northeastern perimeter of Erfkroon's primary donga (refer to Figures 6.8 and 6.9). The locality was chosen for its proximity to the previously described and tested Dating Profile (Lyons et al. 2014; Bousman & Brink 2014). Profile 2A was positioned along a vertical exposure ~3.8 m in vertical depth, located 3.5 m west of the Dating Profile. The 2A exposure was comprised of the upper four alluvial units (Sandy Cap, Brown Paleosol, Upper Grey Paleosol, and Red Paleosol) of the Tooth et al. (2013) lithostratigraphic

sequence, alternatively referred to as Allostratigraphic Units 1-3 of the Orangia Terrace as described by Bousman and Brink (2014).

Profiles 2B and 2C were exposed to the east and southeast of Profile 2A respectively. Profile 2B was positioned approximately 4 m east of 2A along a vertically eroding wall of the donga that exposed lower components of the overbank sequence. This profile acted as a vertical extension of Profile 2A, containing aspects of the Upper Grey, Red, and Lower Grey units as characterized by Tooth et al. (2013), or, as described by Bousman and Brink (2014), AU2 and AU3 of the Orangia Terrace. Profile 2C was exposed around the corner, ~ 8 m southeast from Profiles 2A and 2B. This exposure contained the Upper Grey and Red units as described by Tooth et al. (2013), alternatively referred to as the Upper Grey, Red Sandy Loam, and Red Paleosol (the boundary between AU2 and AU3) as described by Bousman and Brink (2014).

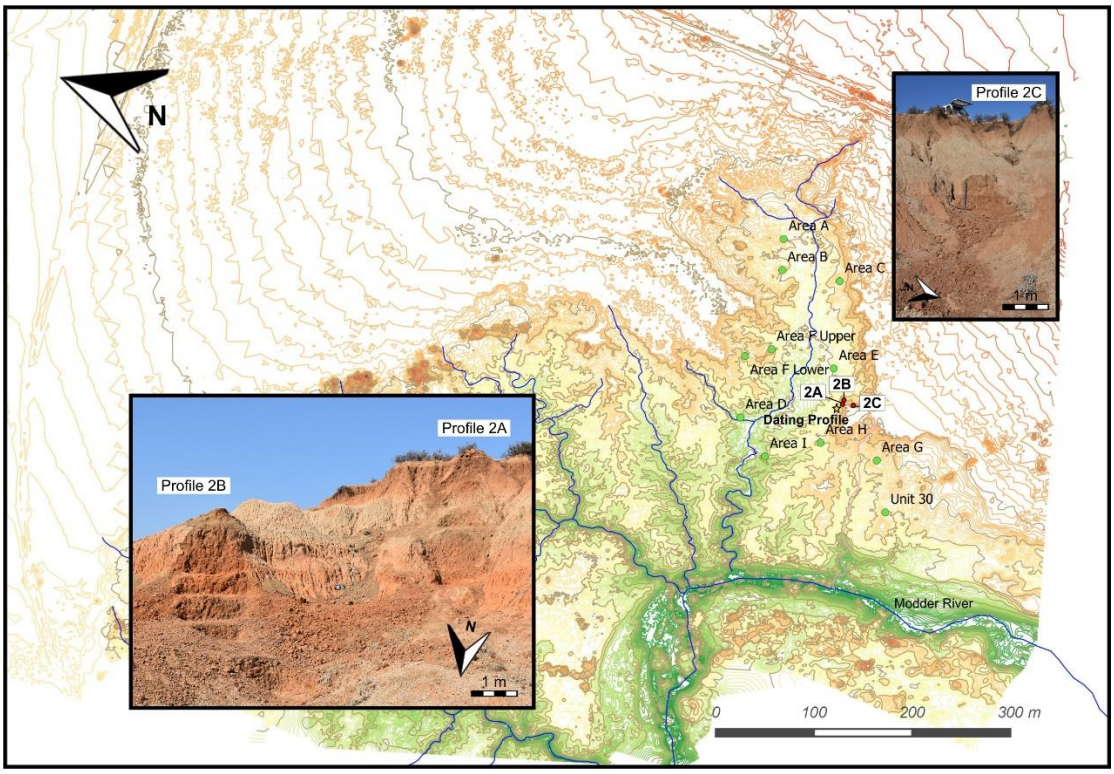

Fig. 6.8. Mapped location of Profiles 2A, 2B & 2C.

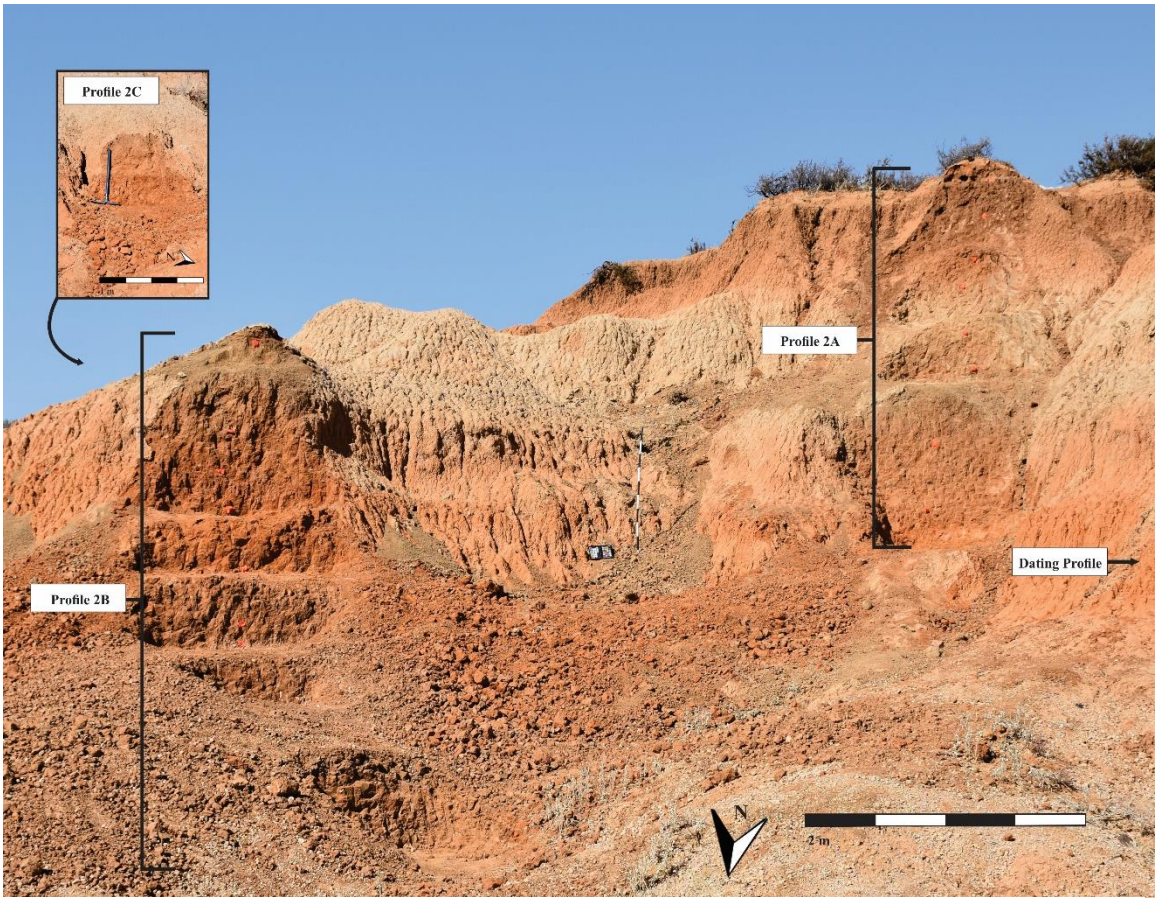

Fig. 6.9. Profiles 2A, 2B & 2C exposures with reference to Dating Profile. Dating profile occurs ~3.5 m west of Profile 2A along primary donga wall.

Profile 2A Results

Profile 2A measured ~3.5 m in vertical depth and was originally cleared and described during the 2017 field season. At the time, ten zones were identified and single representative bulk samples were extracted by zone. Four micromorphology blocks were also extracted from zone boundaries previously characterized by Bousman and Brink (2014) as erosional unconformities. However, preliminary analysis of these samples revealed the need for a higher-resolution sampling strategy and for additional thin sections representative of each zone proper, rather than zone transitions. Both issues were addressed over the course of the 2018 field season during which the 2A profile was re-

exposed, described and sampled at 5-cm increments up profile. Eleven rather than ten zones were identified, and 67 high-resolution bulk samples and four additional micromorphology blocks were collected.

The 11 identified zones comprising Profile 2A form an A-AC-ABt-Btk-Bkt-Bk-Bts-Bt-Bt-Bt-Bw sequence (see illustration in Figure 6.10 and description in Table 6.3). Refer to Appendix F for field form descriptive summaries by zone, and profile description narrative.

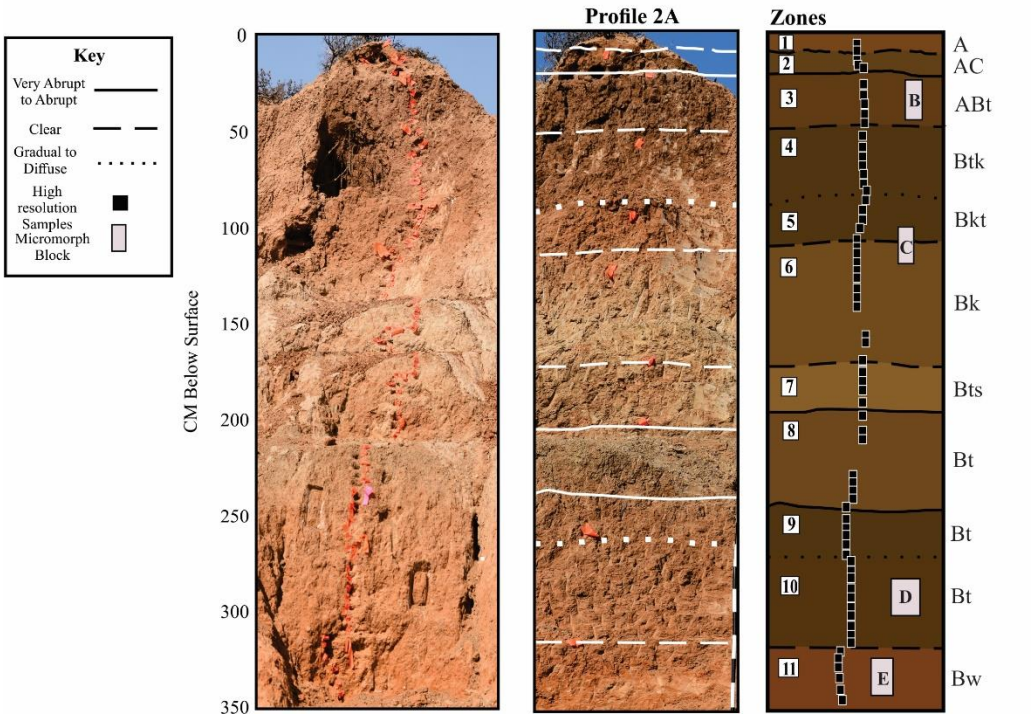

Fig. 6.10. Profile 2A horizons and sample locations. High-resolution sample locales indicated by orange flagging tape in image of profile exposure (N=67).

Table 6.3. Profile 2A description by zone.

Zone	Horizon	Depth (cmbs)	Description
1	A	0-8.69	Fine, loose, non-plastic yellowish-brown (10YR 5/4 dry; 10YR 4/6 moist) sandy loam with no structure. Matrix consistence is loose both dry and moist, and nonreactive when exposed to a 10% HCl solution. Fine and very fine, dendritic and vertical roots observed throughout zone with moderate vertical continuity. Bioturbation in the form of rodent burrows ranging in size from 5-8 cm in diameter and fine to very fine insect casts and burrows are common. Vegetation in the form of drought resistant grasses and acacia grow along surface of zone. Lower boundary gradual and smooth.
2	AC	8.69-21.13	Medium, weak, granular peds with yellowish-brown (10YR 5/4 dry; 10YR 4/2 moist) loam matrix. Matrix consistence ranges from soft (dry) to extremely friable and very slightly plastic (moist). Matrix very slightly effervesces when exposed to 10% HCl solution. Very fine to fine roots with moderate vertical continuity are many. Coarse, vertical roots with high vertical continuity are few. Bioturbation in the form of insect casts, burrows and rodent burrows are common. Krotovina are 6-7cm in diameter. Lower boundary abrupt and smooth.
3	ABt	21.13-47.46	Medium, strong angular blocky peds with brown (7.5YR 5/4 dry; 7.5YR 4/3 moist) silty loam matrix. Matrix consistence ranges from moderately hard (dry) to firm and slightly plastic (moist). Ped size increases to coarse down profile. Ped faces and matrix very slightly effervesces when exposed to 10% HCl solution. Very weak, distinct, discontinuous pressure faces are common and on horizontal ped faces. Very fine irregularly shaped FeMn nodules, soft in consistence, and fine, irregularly shaped Mn masses are common on ped faces, separation planes and in matrix. Cracks in ped are infilled with FeMn staining (7.5YR 3/3). Many very fine and fine, vertical and dendritic roots with moderate vertical continuity occur throughout zone. Coarse roots with high vertical continuity are few. Bioturbation in the form of insect casts and worm channels infilled with organic debris from above zone are common. One large (~30 cm in diameter) krotovina obscures western side of zone. Very few, very fine gypsum crystals accumulate in cracks along ped faces. Lower boundary clear and smooth.
4	Btk	47.46-86.76	Medium, moderate, subangular blocky peds with brown (7.5YR 5/4 dry; 7.5YR 4/4 moist) silty clay loam matrix. Matrix consistence ranges from hard (dry) to firm and plastic (moist). Ped faces and matrix slightly effervesce when exposed to 10% HCl solution. Very fine and fine, vertically continuous roots commonly grown between and along ped faces. Few, discontinuous, faint FeMn stains (7.5YR 3/3) appear on and between peds. Very fine, hard, spherical FeMn nodules are common on ped faces. Fine and very fine carbonate nodules spherical and cylindrical in shape are few to common. Carbonates increase in frequency down profile. Few cracks and pores are lined with carbonate. Very few fine carbonate nodules present in matrix. Very fine carbonate filaments on ped faces are few. Lower boundary gradual and smooth.

Table 6.3. Continued

5	Bkt	86.76-108.30	Coarse, moderate subangular blocky peds with brown (7.5YR 4/6 dry; 7.5YR 4/4 moist) silty loam matrix. Matrix consistence ranges from slightly hard (dry) to friable and slightly plastic (moist). Many very fine pores occur on ped faces and separation planes. Subangular, medium to very fine pebbles are common in matrix. Discontinuous distinct sand films are common on ped faces. Bioturbation in the form of worm channels bisect zone horizontally and obliquely. Worm channels are infilled with a strong brown (7.5YR 5/8) matrix. Very fine to fine vertical and dendritic roots infiltrate peds. Very few medium to coarse roots grow between vertical ped faces. Very fine to fine, carbonate "flecks" and spherical to cylindrical carbonate nodules occur commonly on ped faces and in matrix. Very few fine carbonate filaments occur among cracks, pores, and worm channels. Few fine to very fine, irregularly shaped Mn masses occur in cracks, lining pores, and on ped faces. Few fine, cylindrical and vertical rhyzoliths occur in pores. Few, discontinuous, faint patches of FeMn staining occurs on ped faces (7.5YR 3/2). Lower boundary clear and smooth.
6	Bk	108.3-170.93	Moderate, weak subangular blocky parting to granular peds comprised of light yellowish-brown (10YR 6/4 dry) to brown (10YR 5/3 moist) silty loam matrix. When dry, matrix is slightly hard. When moist, matrix is friable and plastic. Ped faces and matrix are nonreactive when exposed to 10% HCl solution. Common inclusions on ped faces include very fine, black, hard, spherical to cylindrical FeMn nodules. Few very fine pores, few containing very fine roots also occur on ped faces. Very fine and fine carbonate filaments and very fine subrounded carbonate nodules are common. Carbonate filaments occur in cracks, pores, and bioturbated areas, and nodules occur within the matrix and in bioturbated areas. Bioturbation in the form of worm channels are many and contain strong brown (7.5YR 5/8) matrix with very fine, hard FeMn nodules. Lower boundary clear and smooth.
7	Bts	170.93-195.21	Moderate, weak subangular blocky parting to granular peds comprised of light yellowish-brown (10YR 6/4 dry) to brown (10YR 5/3 moist) silty loam matrix. Matrix consistence ranges from slightly hard (dry) to friable and plastic (moist). Ped faces and matrix are nonreactive when exposed to 10% HCl solution. Very fine, black, hard, spherical to cylindrical FeMn nodules commonly adhere to ped faces. Few very fine pores and very fine roots also occur on ped faces. Few carbonate filaments form in cracks, pores, and bioturbated areas. Many worm channels partially obscure peds throughout zone and contain strong brown (7.5YR 5/8) matrix. Worm channel matrix also contains very fine, hard FeMn nodules. Lower boundary abrupt and smooth.

Table 6.3. Continued

8	Bt	195.21-244.91	Fine, weak, granular peds with dark yellowish-brown (10YR 4/4) to brown (7.5YR 4/4) silty loam matrix. Matrix consistence ranges from moderately hard (dry) to very friable and plastic (moist). Ped faces strongly effervesce when exposed to 10% HCl solution, matrix slightly effervesces. Bioturbation in the form of worm channels are common and contain a matrix mixed with very fine pebbles, including semi-rounded to flat sub-mm fragments of Ecca shale. Moderately developed, distinct, discontinuous pressure faces and clay films are common on ped faces. FeMn staining occurs discontinuously but commonly among worm channels, pores, and ped faces. Soft, fine to very fine irregularly shaped Mn masses adhere to pressure faces. Very fine to fine carbonate filaments are common and form in cracks, pores and voids on ped faces. Lower boundary abrupt and smooth.
9	Bt	244.91-266.51	Medium, moderately strong prismatic peds parting to subangular blocky peds comprised of yellowish-brown (10YR 5/4 dry) to brown (7.5YR 4/4 moist) silty loam matrix. Matrix consistence ranges from slightly hard (dry)to friable and plastic (moist). Ped faces and matrix are non-reactive when exposed to 10% HCl solution. Moderate, distinct, discontinuous pressure faces occur on vertical ped faces. FeMn staining is also discontinuous and common on ped exteriors and lining cracks and pores. Very few, discontinuous, distinct ferriargillans occur on ped faces. Very few Mn masses (black in color and irregular in shape) occur discontinuously on vertical ped faces. Bioturbation in the form of worm channels are common and contain strong brown (7.5YR 5/8) matrix mixed with very fine pebbles, including sub-mm flat, subangular fragments of Ecca shale. Few very fine gypsum crystal clusters form in cracks along ped faces. Few very fine, dendritic and vertical roots with very low vertical continuity infiltrate peds and occur on ped faces. Very few, very fine to fine carbonate nodules and 'flecks' adhere to ped faces. Very few fine sub-rounded, hard carbonate nodules occur between ped faces. Few carbonate filaments line pores and infill cracks on ped faces. Lower boundary abrupt and smooth.
10	Bt	266.51-313.42	Coarse, strong, subangular blocky peds comprised of brown (7.5YR 5/4 dry; 7.5YR 4/4 moist) loam matrix. Matrix consistence ranges from slightly hard (dry) to slightly plastic and loose (moist). Ped faces and matrix are non-reactive when exposed to 10% HCl solution. Features on ped faces include many, fine to very fine pores, and few very fine to medium roots vertically oriented with moderate vertical continuity. Irregularly shaped and oval insect voids are common. FeMn staining on ped faces is distinct and discontinuous. Few, very fine to fine Mn masses occur within bioturbated areas. Very few, very fine carbonate nodules occur on ped faces and very few, fine vertically oriented carbonate filaments infill cracks and pores. Many worm channels alter the zone and contain a reddish-yellow (7.5YR 6/6) matrix. Lower boundary clear and smooth.

Table 6.3. Continued

11	Bw	313.42-339.17	Medium, strong prismatic parting to angular blocky peds comprised of yellowish-red (5YR 4/6 dry; 5YR 5/8 moist) silty loam matrix. Matrix consistence ranges from semi-hard (dry) to friable and non-plastic (moist). Ped faces and matrix are nonreactive to 10% HCl solution. Very distinct, discontinuous FeMn staining occurs commonly along ped faces. Bioturbation in the form of worm channels are many and contain a brown (7.5YR 5/4) matrix. FeMn films line the interior of worm channels. Very fine, few dendritic and vertical roots occur between and through peds. Ped matrix and pores contains few, very fine, soft to semi-hard Mn masses. Few, very fine gypsum crystals occur in clusters on ped faces. Very few, very fine vertical carbonate filaments infill cracks on ped faces. Lower boundary unobserved; base of profile.

Particle size, magnetic susceptibility & degree of development results. Particle size and magnetic susceptibility analyses were conducted on the high-resolution sample population extracted from Profile 2A (N=67). The distribution of sand, silt, and clay (measured in phi) by sample is tabulated in Appendix E and illustrated in Figure 6.11. Also illustrated in Figure 6.11 are frequency-dependent ($\chi_{fd\%}$) susceptibility values by sample. Particle size mean and standard deviation results calculated by sample are presented in Figure 6.12. Raw particle size ratios, standard deviations, means, and magnetic susceptibility values by sample are also tabulated in Appendix E. Ordinal characteristics recorded during in-field description of Profile 2A were utilized to calculate degree of development scores by zone. Degree of development scores and percentage calculations (DDS%) are presented in Appendix C. DDS% calculations by zone are compared with associated magnetic susceptibility values in Figure 6.13.

In summary, relatively high frequency-dependent susceptibility ($\chi_{fd\%}$) values and DDS% scores correspond with zones 3, 5, 8, and 11 in Profile 2A. Enhanced values corresponding with Zone 3 coincide with relatively high fine clay and silt fractions, and

gross morphological characteristics consistent with greater pedogenic development (pressure features, clay coats, strong ped structure etc.). In Zone 5, enhanced susceptibility values and its relatively high DDS% score coincide with a general increase in calcium carbonate frequency and size. In Zone 8, increased susceptibility values appear to be driven by illuviated clay as indicated by the presence of illuviation features such as pressure faces, argillans, and clay films. Redox features are also considerably more prevalent in Zone 8 than observed in stratigraphically higher zones (6 and 7). A similar pattern appears to drive high susceptibility values and DDS% scores in Zone 11. Gross morphological characteristics contributing to its high DDS% score include well-defined ped structure and more distinct illuviation features such as clay films, and the common presence of well-defined redox features such as ferriargillans, manganese masses, nodules, and dendritic filaments. Redox features appear to be controlling high susceptibility values more so than relative particle sizes. Zone 11 is primarily comprised of a coarse-grained matrix consisting of fine to medium sands rather than the finer silt populations forming the parent material in zones 9 and 10.

Micromorphology results. Micromorphology blocks B, C, D and E extracted from Profile 2A produced five thin sections representing zones 3, 5, 6, 10 and 11. Refer to Table 6.4 for thin section descriptive results and associated figures (Figures 6.14, 6.15, 6.16, and 6.17). Micromorphological characteristics identified from the Zone 3 thin section (Figure 6.14) validate the in-field ABt-horizon designation. This is supported by the presence of illuviating clay features indicative of B-horizon development, but also the persistence of relic pores and channels infilled with organic debris typically associated with A-horizonation. The thin section prepared from Zone 5 contains clay illuviation

features, but also impregnated FeMn nodules, FeMn quasi- and hypocoatings, and in places, parallel-striated clays characteristic of formerly active slickensides. Other features include a partially calcitic b-fabric and the presence of embedded, orthic carbonates. Combined, these features are indicative of a subsurface B-horizon forming in vertic environment, conforming to its Bkt-horizon designation. Also, the prevalence of Fe-Mn oxide features implies changing oxidation states occurred during the pedogenic formation interval. This process is associated with cycling wet-dry conditions. A slide analyzed from Zone 6 illustrates many of the same features, but with a higher ratio of crystallitic b-fabric associated with a greater amount of calcium carbonate in the matrix. The increased presence of carbonate may be a pedogenic feature associated with mobilization and recrystallization of carbonate down profile, or it could be a vestige characteristic of a calcareous parent material (sediment that contained pedogenic carbonates from a secondary, erosional context).

In thin section, Zone 10 is characterized by features indicative of a subsurface B-related horizon that developed in a stable, vertic environment. The c/f related distribution is best described as open and double-spaced porphyric, where coarse (sand-sized) grains are relatively poorly sorted and spaced apart. The b-fabric is predominantly characterized by a crystallitic b-fabric. This type of b-fabric is associated with secondary carbonate enrichment, or as an inherited feature of the parent material. In the latter scenario, it is possible that the parent material derived from redeposited sediments from another terrace. The older, nearby Erfkroon Terrace identified by Bousman and Brink (2014) contains indurated petrocalcic horizons. If the terrace was eroded at some point in the past, it is possible that carbonates formed pedogenically within became incorporated into

redeposited sediments now comprising the Orangia Terrace. Other pedofeatures, such as granostriated coarse fraction, are suggestive of clay illuviation and B-horizonation. Biotic features, namely worm channels containing calcareous fecal pellets, indicate the zone has been heavily altered by biogenic processes (see Table 6.4 and Figure 6.16).

In thin section, Zone 11 is characterized as a weakly developed, subsurface B-related horizon that contains weak clay illuviation features in a matrix dominated by coarse fraction. This is indicated by a single-spaced to close porphyric c/f related distribution containing moderately to poorly sorted fine sand-sized quartz grains. What clay occurs is reddish-yellow in color and the b-fabric is relatively undifferentiated with the occasional occurrence of grainostriation. Pedofeatures include strongly and weakly embedded Fe-Mn oxide nodules, disorthic carbonates, and worm-channel bioturbation containing pellets comprised of calcareous b-fabric (see Figure 6.17).

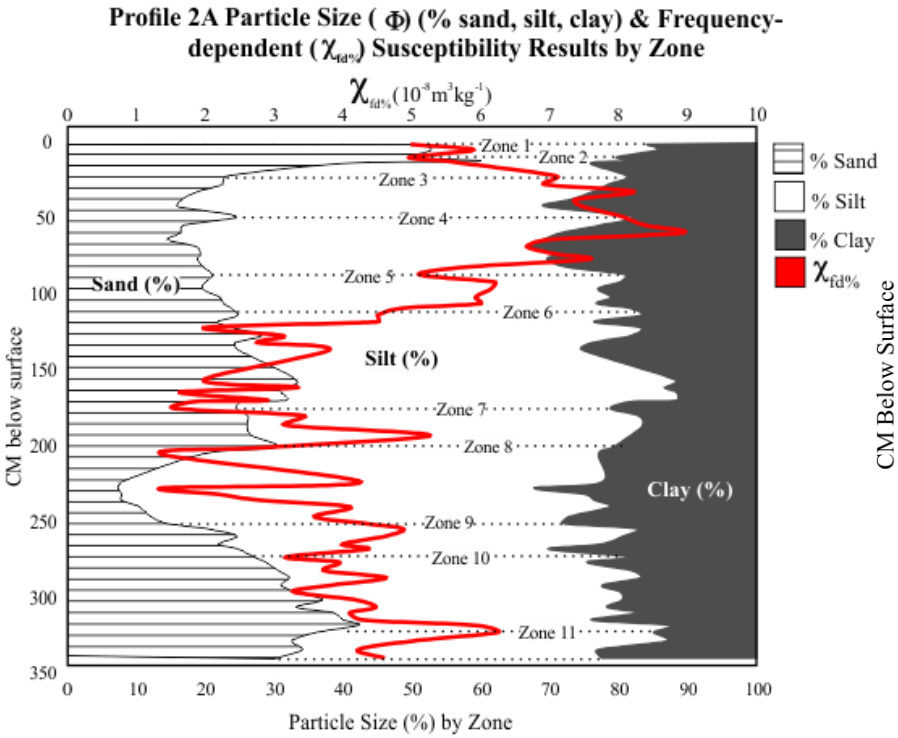

Fig. 6.11. Profile 2A particle size ratios (% sand, silt, clay) by sample & frequency-dependent susceptibility results. Dotted lines mark zone upper boundaries.

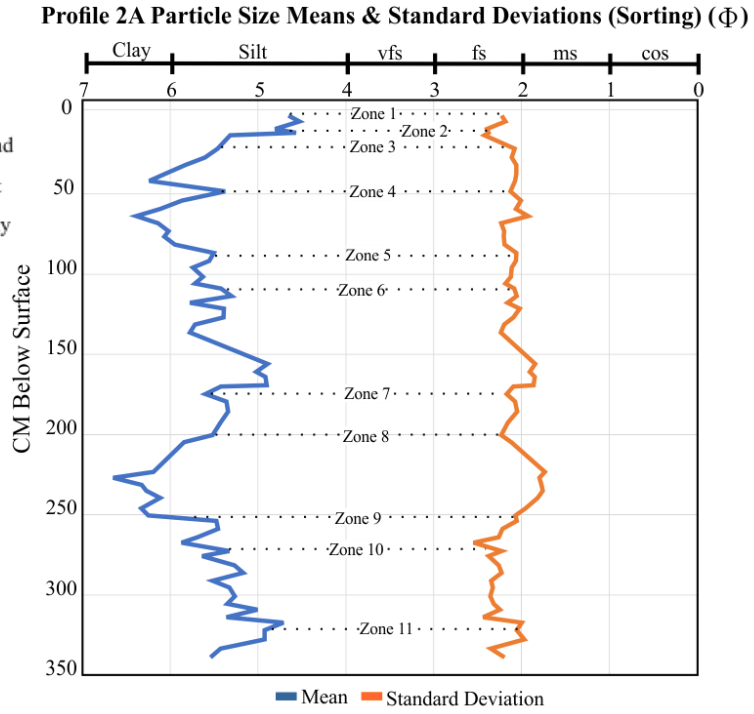

Fig. 6.12. Profile 2A particle size mean & standard deviation results by sample. Dotted lines mark zone upper boundaries. Abbreviations: cos=coarse sand, ms=medium sand, fs=fine sand, vfs=very fine sand.

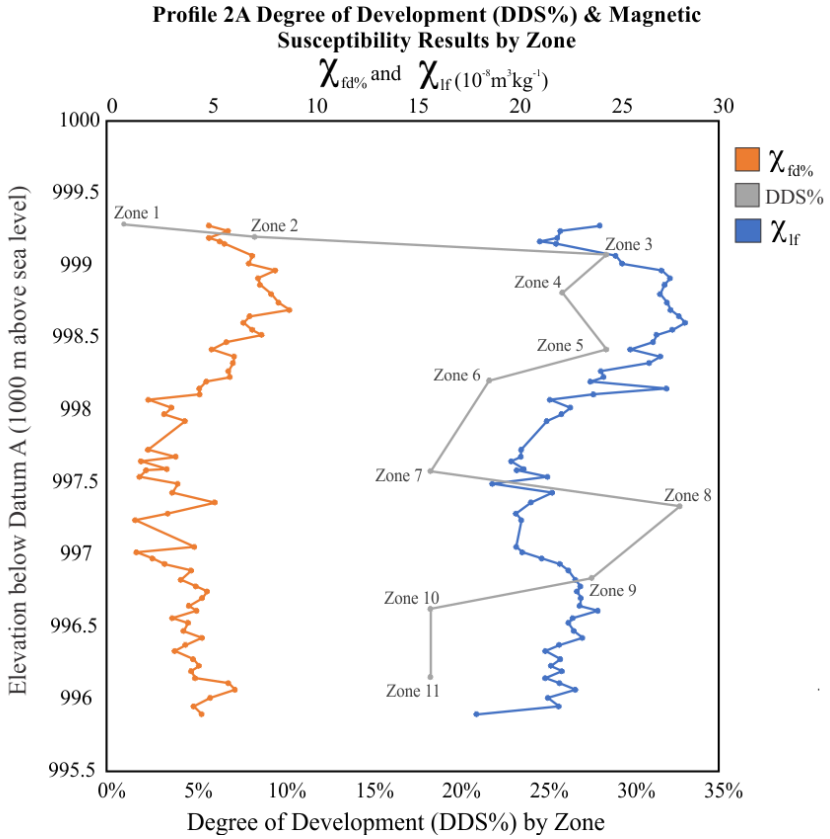

Fig. 6.13. Profile 2A degree of development (DDS%) calculations by zone & magnetic susceptibility comparison by sample.

Table 6.4. Profile 2A micromorphological analysis results.

Block	Zone	Slide ID	Description	Figure
B	3	MM8P2AZ3B	**c/f related distribution:** Close and single-space porphyric**.** **Structure & voids:** Strongly separate, accommodated angular blocky microstructure (dominant) and channel microstructure (common). Vesicles and chambers common. **Coarse Fraction:** Moderately sorted fine to very fine sand-sized subangular and sub-rounded quartz grains (dominant), augite (few); very fine subangular sand-sized quartz (common), augite and magnetite (few); coarse sub-angular to sub-rounded augite and quartz (few); fine subangular feldspar (very few). **Fine Fraction:** Medium yellowish-brown clay with granostriated stipple-speckled b-fabric (dominant); light yellow clay and parallel striated b-fabric (few); granostriated stipple-speckled b-fabric (common).	6.14

Table 6.4. Continued

		MM8P2AZ3B (continued)	**Pedofeatures:** Strong reddish-brown dusty clay coatings lining channels and voids; Fe-oxide hypo- and quasi-coatings lining channels, voids, and coating coarse fraction; passage features lined with Fe-oxide and dusty strong reddish-brown clay coatings; worm fecal pellets comprised of dark yellowish-brown clay and crystallitic b-fabric; rounded coarse-sand sized orthic carbonate nodules (few to common); moderately and weakly impregnated orthic Fe-Mn oxide nodules (common); limpid dark reddish-brown clay coats and films (few); dislodged strong reddish-brown striated clay coats in channels; calcium oxalate phytoliths in channels and voids (few).	
C	5	38MM10S6A	**c/f related distribution:** Chitonic and close porphyric (both common). **Structure & voids:** Channel and subangular blocky microstructure with simple and compound packing voids, weakly separated channels, and vesicles. **Coarse fraction:** Moderate to poorly sorted angular and subangular medium to very fine quartz (dominant), feldspar and augite (few), magnetite (few); coarse subangular and angular quartz grains (few); very fine angular and subangular quartz (common), augite (very few), and magnetite (few). **Fine fraction:** Light yellowish-brown clay with granostriated, stipple-speckled b-fabric and in places, calcitic crystallitic b-fabric (in passage features). **Pedofeatures:** Linear passage features containing calcitic crystallitic b-fabric embedded with fine sand-sized angular and subangular quartz, reddish-brown clay hypo- and quasi-coats around grains; weakly embedded orthic Fe-Mn oxide nodules; Fe-Mn oxide quasi-coats around grains and lining channels and voids; weakly embedded orthic carbonate nodules containing coarse fraction; light yellow clay coats lining channels and voids**.**	6.15
C	6	38MM10S6C	Same as above but with slight increase in amount of calcareous b-fabric and increased frequency of orthic carbonate nodules.	N/A

Table 6.4. Continued

D	10	MM10P2AZ9A	**c/f related distribution:** Open and double-spaced porphyric and in places, single-spaced porphyric. **Structure & voids:** Weakly separated, subangular blocky to granular microstructure, with channel microstructure, regular vughs, vesicles, and simple and compound packing voids.	6.16
			Coarse fraction: Moderately sorted **v**ery fine sand and coarse silt-sized subangular and angular quartz (dominant), feldspar (common), augite and magnetite (few); fine sand-sized quartz (common) and magnetite (few)**.** **Fine fraction:** Dark yellowish-brown to greyish-brown clay and dusty greyish-brown clay with crystallitic, calcitic and stipple speckled b-fabric and in some places, parallel striated b-fabric**.** **Pedofeatures:** Dark reddish-brown dusty clay coatings surrounding grains, carbonate hypocoatings and quasicoatings around grains, voids, and channels; orthic carbonate with embedded ground mass; fine to very fine disorthic Fe-Mn oxide nodules, Fe-Mn hypocoatings around grains and lining channels, passage features with loose granitic infilling, strongly and moderately impregnated orthic Mn oxide nodules, and Mn oxide hypocoatings on grains and voids.	
E	11	MM12P2AZ11B	**c/f related distribution:** Chitonic to close porphyric and less commonly, single-space porphyric. **Structure & voids:** Weakly separated subangular blocky and channel microstructure with regular vughs and simple and compound packing voids. **Coarse fraction:** Moderately sorted very-fine sand-sized subangular to angular quartz (dominant), feldspar (common), augite and magnetite (few); coarse sand-sized angular quartz (few)**.** **Fine fraction**: Reddish-yellow clay and undifferentiated b-fabric (dominant); in places, stipple-speckled and granostriated b-fabric (less common). **Pedofeatures:** Weakly and strongly embedded orthic Fe-Mn oxide nodules, sub-rounded coarse to fine sand-sized disorthic carbonate nodules, Fe-Mn oxide hypocoatings on grains; dark reddish-brown dusty clay films and quasi-coats on grains; ovoid worm fecal pellets in channels with calcitic and greyish- brown to yellowish-brown clay with stipple speckled b-fabric; few coarse disorthic carbonates containing coarse quartz fraction.	6.17

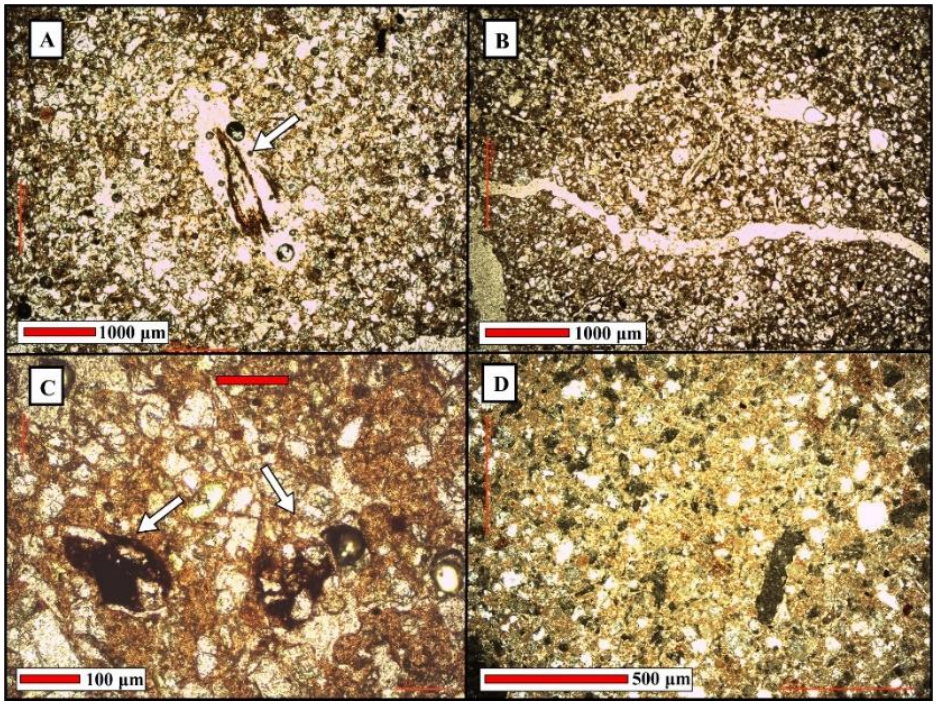

Fig. 6.14. Profile 2A Zone 3, block B, thin section MM8P2AZ3B. (A) Organic matter (root debris) in void surrounded by worm fecal pellet organic matter lining void boundary (xpl, 20x); (B) planar void creating angular blocky microstructure (ppl, 10x); (C) inherited FeMn oxide nodule containing coarse fraction (ppl, 100x); (D) typical c/f related distribution, close and single-space porphyric (xpl, 40x).

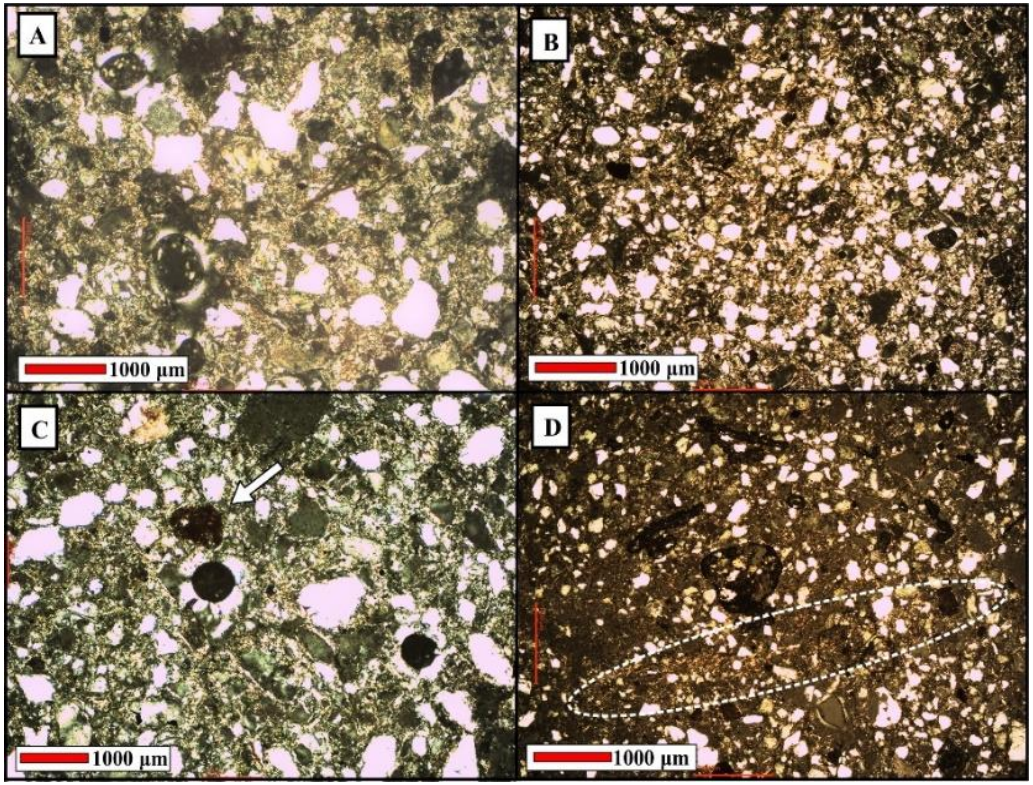

Fig. 6.15. Profile 2A Zone 5, block C, thin section 38MM10S6A. (A) Typical stipple-speckled b-fabric and moderately sorted c/f related distribution (xpl, 100x); (B) moderately to poorly sorted c/f related distribution, stipple speckled and granostriated b-fabric (xpl, 40x); (C) granostriated and stipple speckled b-fabric, Fe/Mn oxide nodule with regular outline (white arrow (xpl, 100x); (D) poorly sorted coarse fraction and parallel striated b-fabric (white circle) (xpl, 40x).

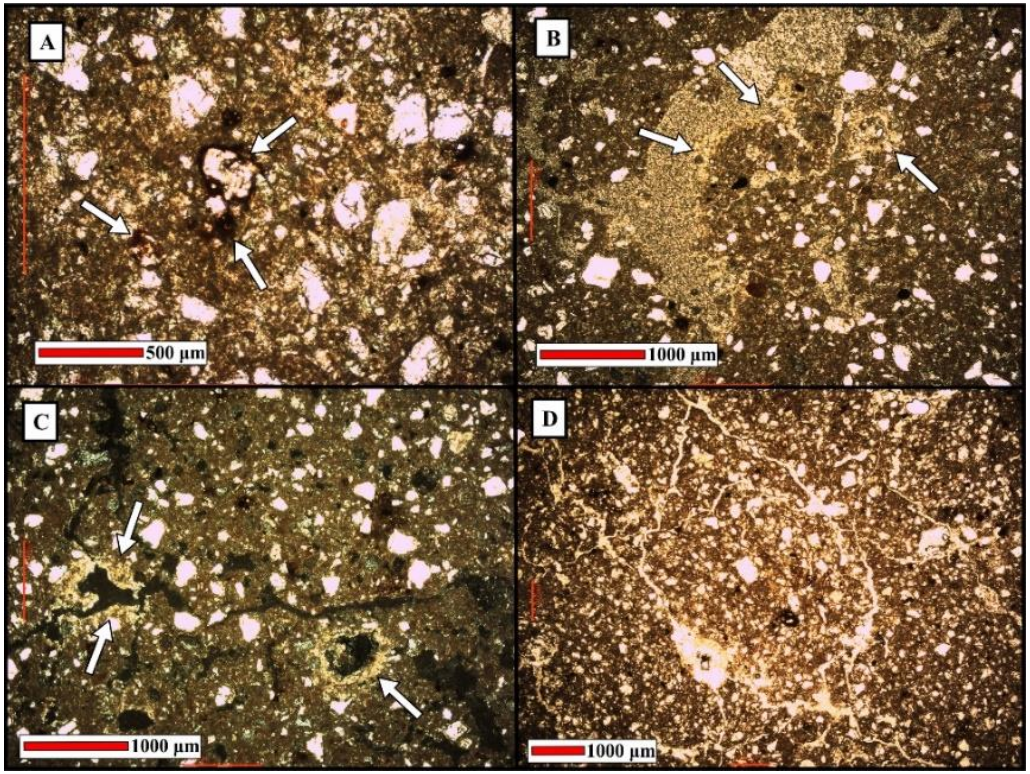

Fig. 6.16. Profile 2A Zone 10, block D, thin section MM10P2AZ9A. (A) FeMn oxide hypocoating around quartz grains (100x, ppl); (B) calcium carbonate hypocoating along planar void, calcium carbonate hypocoatings around coarse fraction (white arrows) (40x, xpl); (C) typical double space/open porphyric c/f related distribution, channel microstructure & carbonitic b-fabric, calcium carbonate hypocoatings on channels & pores (white arrows) (40x, xpl); (D) channel & vesicular microstructure with disorthic/orthic FeMn nodules and FeMn hypocoatings (20x, ppl).

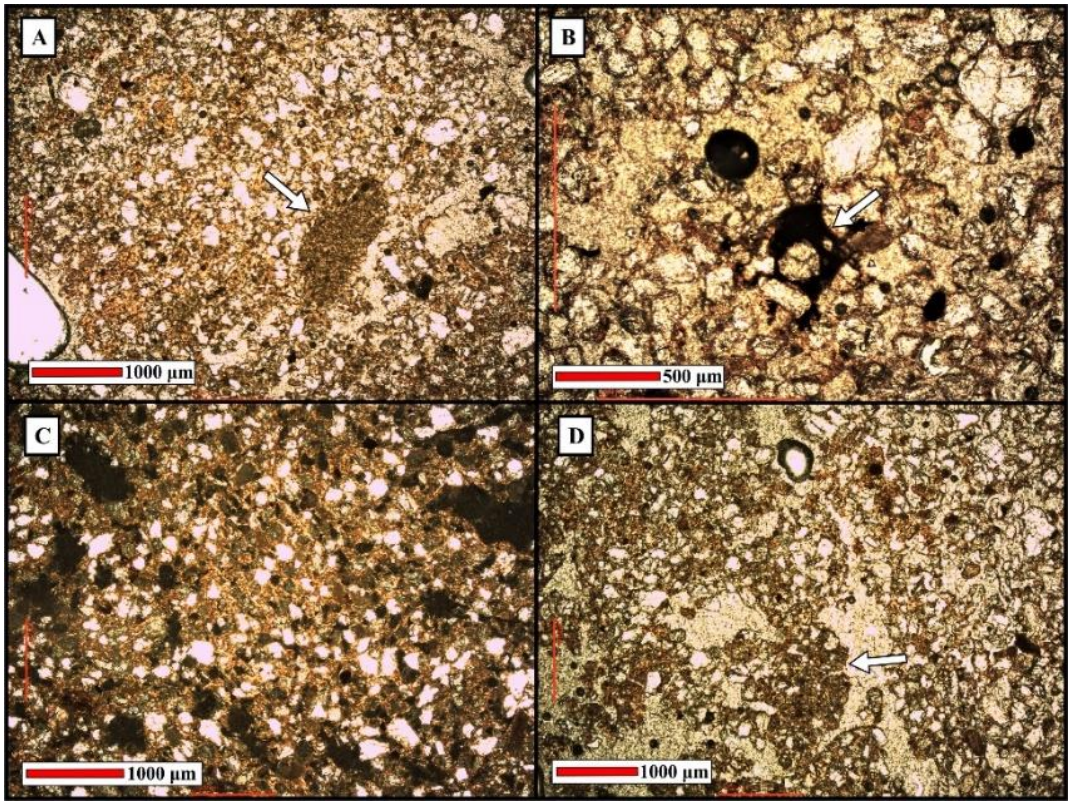

Fig. 6.17. Profile 2A Zone 11, block E, thin section MM12P2AZ11B. (A) Typical chitonic and single-space porphyric c/f related distribution and coarse disorthic carbonate nodule (white arrow) (40x, ppl); (B) strongly embedded orthic FeMn nodule (100x, ppl); (C) typical stipple-speckled/granostriated b-fabric (40x, xpl); (D) calcitic worm fecal pellet lodged in channel (40x, ppl).

Profile 2B Results

Profile 2B was cleared ~4.5 m east of Profile 2A to expose the latter aspect of the Upper Grey and Red units, in addition to the Lower Grey unit as previously described by Tooth et al. (2013) and Bousman and Brink (2014). The eroded surface of the profile occurred ~1.97 m below the modern surface and top of Profile 2A. The entire exposure reached a maximum vertical depth of 3.5 m. Approximately 80 to 100 cm of weathered colluvium was removed prior to description and sampling. A total of 64 high-resolution samples ranging in weight from 5-8 g were extracted every ~5 cm up profile. Refer to Appendix E for a comprehensive list of sample provenience data and associated particle size and magnetic susceptibility results. Elevations in the following profile description and those presented in figures and tables reflect arbitrary elevations starting at 0 cm below surface. Elevations as they relate to the top of Profile 2A are provided in Appendix D.

Field description of Profile 2B revealed ten zones that comprise an A/Bky-Btk-Bty-Bs-Btk-Btk-Bkt/C-Bkss/C-Bkt/C-BwC sequence (see profile exposure and illustration in Figure 6.18). Refer to Table 6.5 for a description of the profile by zone and Appendix F for a profile description narrative and field-form description summaries by zone.

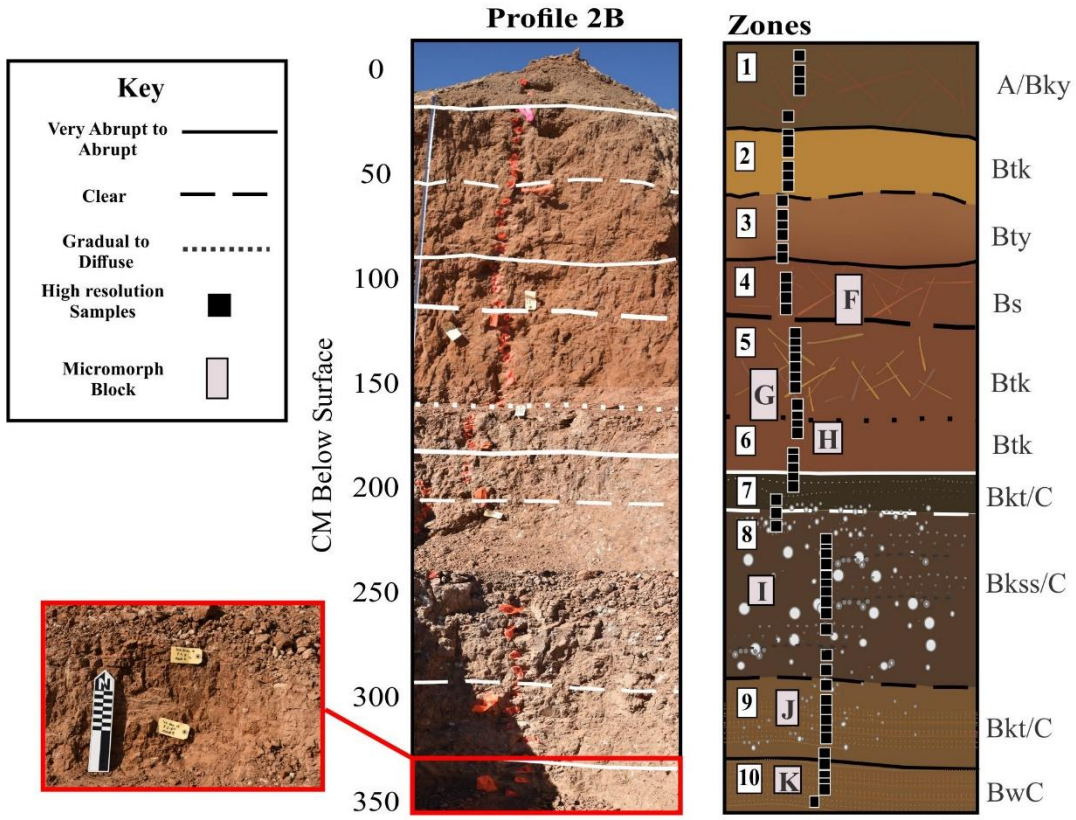

Fig. 6.18. Profile 2B horizons & sample locations. High-resolution sample locales indicated by orange flagging tape in image of profile exposure (N=64).

Table 6.5. Profile 2B description by zone.

Zone	Horizon	Depth (cmbs)	Description
1	A/Bky	0-44.81	Coarse, moderate, granular peds comprised of brown (10YR 5/3 dry; 10YR 4/3 moist) silty loam. Matrix consistence ranges from moderately hard (dry) to friable and plastic (moist). Carbonate films along ped faces (interior/exterior) strongly effervesce when exposed to 10% HCl solution. Few, fine to very fine gypsum crystal clusters occur along ped faces, accumulating in cracks. Very few, fine cylindrical $CaCO_3$ nodules occur in matrix and adhere to ped faces. Very fine $CaCO_3$ filaments and films are discontinuous and common on ped faces. Few discrete, discontinuous, carbonate coats occur on ped faces. Bioturbation including insect casts and cylindrical worm channels (1-2cm in diameter) are very common and intercept zone vertically and horizontally. In-filled casts contain yellowish-red matrix (5YR 4/6). Lower boundary abrupt and smooth.

Table 6.5. Continued

2	Btk	44.81-77.15	Fine, weak to moderately strong subangular blocky brown (7.5YR 5/6) silty loam. Matrix consistence ranges from slightly hard (dry) to plastic and very friable (moist). Ped faces and matrix slightly effervesce when exposed to 10% HCl solution. Redox features are common and include FeMn staining (dark brown, 7.5YR 3/2) that occurs discontinuously on ped faces, and weak, discontinuous ferriargillans. Few, distinct ferriargillans also occur along pores and cracks. Discontinuous, distinct patchy pressure faces, and clay films are common on ped faces. Fine to very fine dendritic $CaCO_3$ filaments are common and form along ped faces and in cracks and pores. Few, very fine cylindrical carbonate nodules form on ped faces and cover ~5-15% of the ped surface area. Nodules are discrete and soft. Bioturbation in form of insect burrows and worm tunnels are many. Mn concretions are few and heavily localized in bioturbated areas (lining boundaries of worm tunnels). Few, very fine gypsum crystals also form within bioturbated regions. Lower boundary clear and smooth.
3	Bty	77.15-103.62	Fine, strong, prismatic peds comprised of reddish-brown (5YR 4/4 moist; 5YR 5/8 dry) loam. Matrix consistence ranges from soft (dry) to very plastic and friable (moist). Patchy, discontinuous FeMn stains occur on peds covering > ~5% of ped surface area. Few discontinuous clay films occur on ped faces. Few, distinct patchy pressure faces occur along horizontal planes. Few very fine, soft, discrete FeMn nodules occur within the matrix. Few carbonate filaments occur on ped faces and very few, very fine gypsum crystals form along vertical and horizontal planes. Very few, fine and very fine, soft carbonate nodules adhere to ped faces. Lower boundary abrupt and smooth.
4	Bs	103.62-129.93	Medium, strong prismatic parting to subangular blocky peds comprised of yellowish-red (5YR 4/6 moist & dry) silt loam matrix. Matrix consistence ranges from moderately hard (dry) to slightly firm and moderately plastic (moist). Ped faces strongly effervesce when exposed to 10% HCl solution, ped matrix nonreactive. Discontinuous, distinct clay films and pressure faces commonly occur on all ped faces. Few, thin, discontinuous ferriargillans are also present on ped faces. Few fine and very fine roots penetrate zone vertically and occur between ped faces. Distinct, very common FeMn stains occur on ped faces. Black Mn masses commonly accumulate around pore openings. Dendritic Mn filaments also form commonly along cracks and grooves on ped faces. Few, very fine carbonate filaments and discontinuous, patchy films also occur on ped faces. Bioturbation in the form of insect burrows and worm channels are common. Channels and voids are infilled with a yellowish-red matrix (5YR 4/6 to 5YR 5/8). Very few, very fine, soft FeMn nodules line burrows, pores and accumulate on ped faces. Lower boundary clear and smooth.
5	Btk	129.93-173.69	Coarse, hard, prismatic parting to angular blocky peds comprised of yellowish-red (5YR 4/6 moist & dry) loam. Matrix consistence ranges from hard (dry) to friable and slightly plastic (moist). Matrix very slightly effervesces when exposed to 10% HCl solution.

Table 6.5. Continued

5 (cont.)			Many distinct ferriargillans occur on ped faces covering ~75% of ped surface area. Prominent, continuous FeMn staining and fine to very fine FeMn nodules and Mn masses are common on ped faces. FeMn masses increase in frequency and firmness (turning nodular) down profile. Prominent, discontinuous clay films and pressure faces commonly occur on ped faces, few are observed lining pores and insect/worm channels. Bioturbation in the form of ovoid insect burrows and linear worm channels are common. Channels infilled with matrix ranging in color from strong brown (7.5YR 5/6) to greyish-brown (10YR5/4), and dark greyish-brown (10YR 4/2). Channel frequency increases to many down- profile. Oblate and spherical, fine and very fine, moderately hard to rigid carbonate nodules are few to common. Nodules adhere to ped faces and increase in frequency down profile. Very fine and fine carbonate filaments are few to common, increasing in frequency down profile. Lower boundary gradual and smooth.
6	Btk	173.69-205.98	Extremely coarse, strong prismatic parting to coarse angular blocky peds comprised of yellowish-red (5YR 5/8 dry; 5YR 4/6 moist) silty loam. Matrix consistence ranges from hard (dry) to firm (moist). Ped faces violently effervesce and matrix is non-reactive when exposed to 10% HCl solution. Very distinct, discontinuous ferriargillans cover ~80% of ped faces. Distinct, discontinuous pressure faces occur commonly on ped faces and interior parting planes. Few, prominent, discontinuous, striated and undulating slickensides occur on vertical and horizontal ped faces. Few, very fine gypsum crystals form between horizontal ped faces. Discontinuous, common carbonate plates "cap" ped faces. Carbonate filaments are common along vertical ped faces and infilling cracks and pores. Fine and medium, hard, oval and spherical carbonate nodules are few. Nodule frequency increases down profile. Many prominent, discontinuous FeMn stains and ferriargillans occur on ped faces and parting planes. Dendritic Mn filaments commonly accumulate in cracks and pores. Very fine, soft Mn nodules are very common in matrix. Mn nodules become harder and more rhombic in shape down profile. Few nodules occur on ped faces down profile. Many linear worm channels bisect zone. Lower boundary abrupt and smooth.
7	Bkt/C	205.98-233.54	Medium, strong prismatic peds comprised of strong brown (7.5YR 5/6 dry & moist) silty clay loam. Matrix consistence ranges from hard (dry) to friable, sticky and very plastic (moist). Ped faces and matrix non-reactive when exposed to 10% HCl solution. Ferriargillans are discontinuous and common on ped faces, covering ~30-40% surface area. FeMn staining and clay films are also discontinuous and commonly occur on ped faces and along interior ped planes. Horizontal, linear worm channels are common. Fine to medium cylindrical and spherical carbonate nodules are common in upper half of zone and occur between horizontal ped faces. Coarse carbonates are few. Frequency/density of coarse carbonates increase down profile (become most frequent at ~225 cmbs). Very few carbonates occur in matrix.

Table 6.5. Continued

7 (cont.)			Carbonate coatings along ped faces are few and patchy. Thin sedimentary laminae disrupted by ped development occur commonly and contain sub cm-sized pebbles, fine sands and few rigid, fine and medium FeMn nodules. Sandy/silty laminae are bounded above and below by very thin clay drapes. Laminae are partially to mostly obscured by pedogenesis but are distinct in localized areas (at ~215 cmbs and 225 cmbs). Thickness of lamina bands range from ~ 5-7 cm. The upper most laminae are dominated by horizontal bands of fine to medium carbonates and pebbles, marking the zone's upper boundary. Few, very fine gypsum crystals occur between ped faces. Lower boundary clear and smooth.
8	Bkss/C	233.54-313.51	Extremely coarse, strong prismatic peds comprised of brown (7.5YR 5/4 dry & moist) clay loam matrix. Matrix consistence ranges from hard (dry) to friable, sticky and plastic (moist). Ped faces and interior parting planes strongly effervesce when exposed to 10% HCl solution. Distinct, common, continuous FeMn stains ped faces (brown; 7.5YR 4/3). Obliquely striated slickensides occur commonly between horizontal ped faces, and prominent, continuous ferriargillans covering ~90% of ped surface area. Fine and very fine, hard FeMn nodules commonly adhere to ped faces. Few, black Mn masses occur in fine to very fine, amorphous accumulations and as dendritic filaments on ped faces. Ped matrix inclusions include spherical, very fine carbonate nodules, fine to very fine pebbles, some coated in carbonate and fine to medium, linear, worm channels containing reddish orange (5YR 4/6) matrix and lined with black Mn masses and FeMn stains. Carbonate nodules are common to many throughout zone. Fine and very fine carbonate nodules occur on and within peds; coarse to very coarse spherical and irregularly shaped nodules, commonly featuring concentric formation increase in frequency down profile into Zone 9 and occur between horizontal ped faces. Thin to very thin laminae containing fine sands, fine to very fine carbonate nodules, FeMn nodules, and rounded and subangular pebbles (including very fine fragments of green Ecca shale) bisect zone at ~378-388 cmbs. Laminae are heavily altered/obscured by pedogenesis. Lower boundary clear and smooth.
9	Bkt/C	313.51-343.23	Coarse, weak to moderate subangular blocky peds comprised of reddish-yellow (7.5YR 6/6 dry) to brown (7.5YR 5/4 moist) silty clay loam matrix. Matrix consistence ranges from moderately hard (dry) to friable and plastic (moist). Ped faces and interior parting planes strongly effervesce when exposed to 10% HCl solution. FeMn masses cover ~75% ped surface area (brown; 7.5YR 4/4). Hard, fine and very fine FeMn nodules adhere to ped faces and are common. Few, distinct, patchy ferriargillans and pressure faces occur on vertical ped faces. Matrix inclusions include few, fine to very fine subangular and rounded pebbles coated in carbonate and very fine to medium dendritic pores and voids commonly infilled with carbonate filaments. Coarse, concentric, oval and spherical carbonate nodules are few and occur throughout ped matrix and between ped faces.

Table 6.5. Continued

9 (cont.)			Irregular, medium and coarse dendritic rhyzoliths are few. Sedimentary features include thin to very thin laminae comprised of fine-very fine, angular-subangular pebbles, carbonate nodules, and fine sands. Laminae are separated by thin clay drapes and are heavily obscured by pedogenesis. Laminae occur throughout zone, increasing in frequency and distinctness down profile. Lower boundary abrupt and smooth.
10	BwC	343.23-349.97	Fine, very weak, subangular blocky breaking down to granular peds comprised of brown (7.5YR 4/4 dry & moist) matrix alternating between silty loam and clay loam. Different textures comprise thin to very thin, horizontal/obliquely bedded laminae bounded by thin clay drapes. Laminae consist of fine to very fine silt and sands, fine pebbles coated in carbonate, and fine to very fine carbonate nodules. Few, distinct ferriargillans and FeMn stained masses occur discontinuously between laminations. Clay films are common, discontinuous and distinct on ped faces. Carbonate nodules occur commonly at boundaries between laminae. Laminae range in color, alternating between brown (10YR 4/3) clay-dominant drapes and light yellowish-brown (10YR 6/4) fine silty loam. Lower boundary unobserved; base of profile exposure.

Particle size, magnetic susceptibility & degree of development results. Particle size and magnetic susceptibility analyses were conducted on the high-resolution sample population extracted from Profile 2B. Distribution of sand, silt, and clay (measured in phi) by sample is tabulated in Appendix E and illustrated in Figure 6.19. Frequency-dependent ($\chi_{fd\%}$) susceptibility values by sample are also illustrated in Figure 6.19. Particle size means and standard deviations calculated by sample are presented in Figure 6.20. Numeric particle size values, standard deviations, means, and magnetic susceptibility values (both $\chi_{fd\%}$ and χ_{lf}) by sample can also be found in Appendix E. Ordinal characteristics recorded during field description of the profile were utilized to calculate degree of development scores by zone. Degree of development scores and percentage calculations (DDS%) are presented in Appendix C. DDS% calculations by

zone are also presented with sample-specific magnetic susceptibility results in Figure 6.21.

Magnetic susceptibility values calculated for the 2B sample population correlate closely with DDS% scores and particle size results. Frequency-dependent susceptibility values ($\chi_{fd\%}$) gradually enhance from Zone 1 to the middle of Zone 2, then decline at the boundary of Zone 3 (~80-90 cmbs). Values then decrease through Zone 3 until the boundary of Zone 4, where susceptibility increases at ~109 cmbs. Enhancing susceptibility values also coincide with fining grainsize distributions, where relatively high $\chi_{fd\%}$ corresponds with influxes of finer grained materials (silts and clays). Degree of development increases from Zone 1 (35%) to Zone 2 (34%) and appears to be driven by an increase in matrix plasticity and frequency of carbonates. This is followed by a decrease into Zone 3 (27%), primarily driven by a slight reduction in carbonate presence. A relatively higher degree of development score coincides with Zone 4, mirroring enhanced $\chi_{fd\%}$ values associated with the Zone 4 sample population at ~110 cmbs.

A similar pattern occurs between zones 4 through 6. Enhanced $\chi_{fd\%}$ values corresponding with the upper boundary of Zone 4 gradually decline through Zone 6 until the boundary with Zone 7. A $\chi_{fd\%}$ value of 2.8 corresponding with the latter 3 samples extracted from Zone 6 climbs to 4.0 among samples extracted from the upper boundary of Zone 7. Magnetic enhancement generally declines from Zone 7 to Zone 10. The "chatter" in these data is likely related to residual C-horizon materials occurring in these zones. Thin, laminated silts and clays occur throughout this aspect of the profile, where laminae of coarse fraction are bounded by thin clay/silt drapes. Sedimentary features are especially visible in thin section.

Micromorphology results. Five micromorphology blocks were extracted from Profile 2B (blocks F, H, I, J and K) and were processed to produce thin sections representative of zones 3, 5, 6, 10 and 11. Descriptive results are presented in Table 6.6 and illustrated in Figures 6.22, 6.23, 6.24, 6.25, 6.26 and 6.27.

The thin section prepared from Block F, Zone 4 is characterized by close and single-space porphyric c/f related distributions, where the coarse fraction is primarily moderate to well-sorted and comprised of very fine sand-sized quartz and coarse silts. Fine fraction consists of reddish-yellow clay and stipple-speckled b-fabric. Parallel and granostriated b-fabric, including relict slickenside features manifesting as parallel striated clays are also observed. Zone 4 also contains many dislodged, limpid yellow, parallel-striated clay films and coatings. Clay coats themselves are characteristic of luvisol (illuvial) development. However, fragmented clay coats are suggestive of a disruption in the pedogenic sequence that may be associated with erosional truncation (Fedoroff et al. 2010). Clay films observed in a secondary context surrounded by different colored clay coatings might further suggest an illuvial phase occurred *after* the initial disturbance event.

The c/f related distribution and b-fabric characteristics observed in Zone 4 are also found in Zone 5, but with a few important exceptions. Zone 5 generally lacks dislodged clay films. Instead, it contains coarse fraction with two different clay hypocoatings: yellowish-brown dusty clay hypocoatings superimposed on dusty reddish-brown clay coatings. FeMn oxide nodules are also more common in Zone 5, as are areas of calcitic, crystallitic b-fabric (refer to Table 6.6 and Figure 6.23).

Finely laminated sands bounded by fine silts and clay drapes predominantly characterize the parent material throughout zones 7-10, though pedogenic weathering obscures most sedimentary structures. An important characteristic of the sedimentary features are thin laminae comprised of a limpid yellow clay coatings and infillings that superimpose laminae comprised of coarse fraction. This pattern may reflect short periods of stasis, followed by even shorter periods of sedimentation. Collectively, these are disrupted by the intrusion of coarse carbonates, calcitic b-fabric and the inundation of reddish-brown to yellowish-red dense clay coatings that surround impregnative redox (FeMn) features and coarse fraction (refer to Table 6.6 and Figures 6.24, 6.25, 6.26 and 6.27).

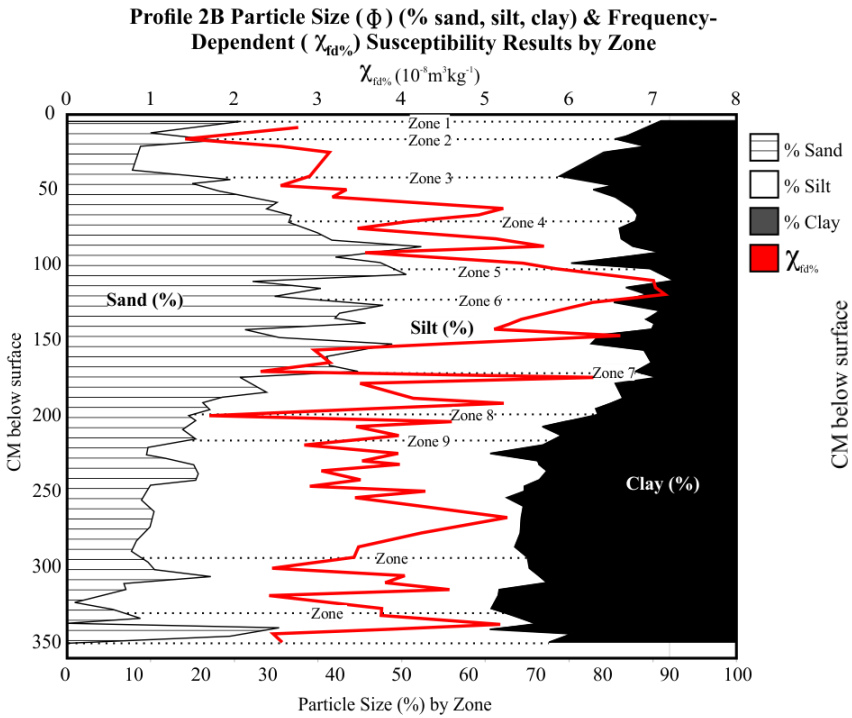

Fig. 6.19. Profile 2B particle size (% sand, silt, clay) & frequency-dependent susceptibility ($\chi_{fd\%}$) results by sample (N=64). Dotted lines mark zone upper boundaries.

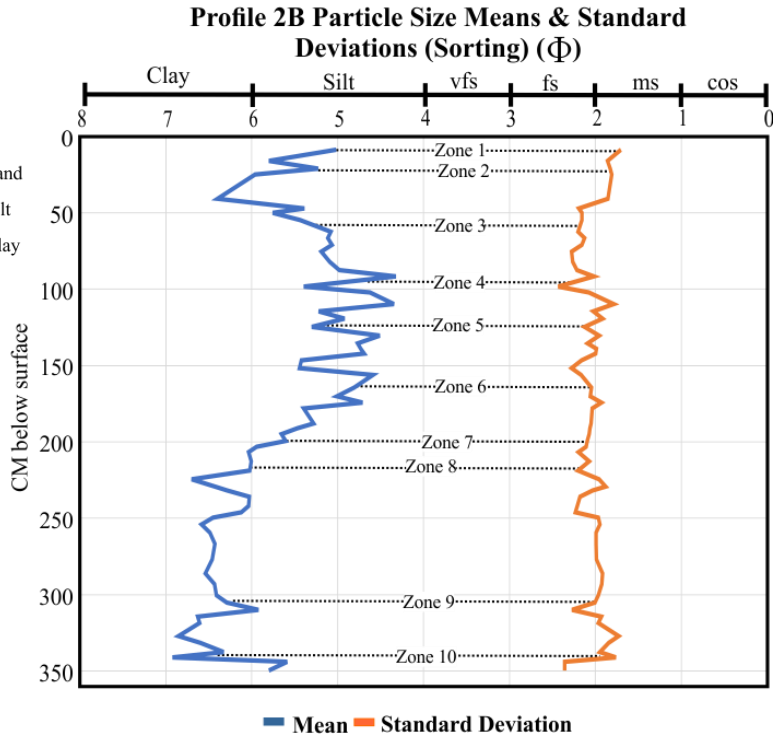

Fig. 6.20. Profile 2B particle size mean & standard deviation results by sample (N=64). Dotted lines mark zone upper boundaries.

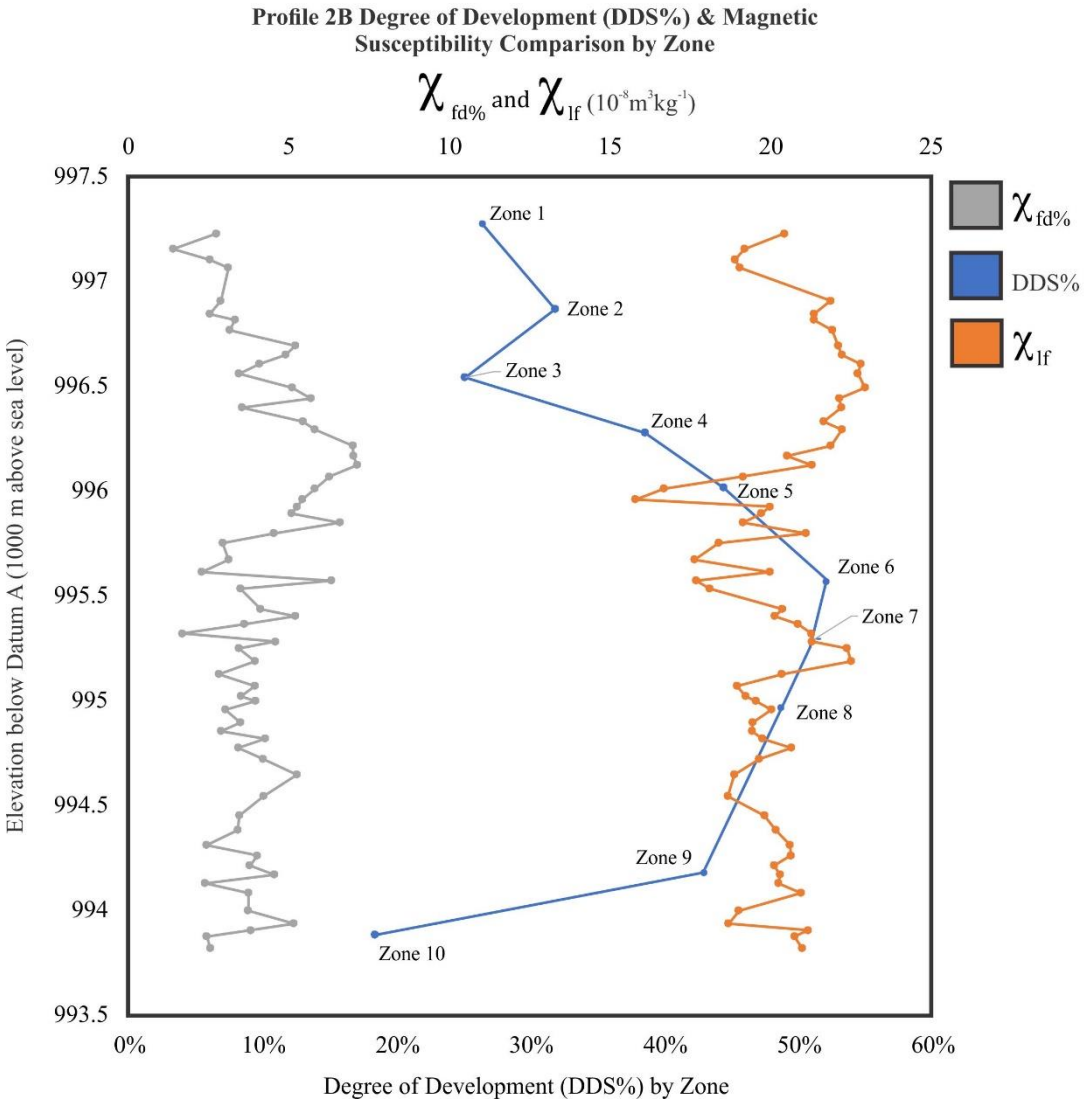

Fig. 6.21. Profile 2B degree of development (DDS%) by zone & magnetic susceptibility comparison by sample (N=64).

Table 6.6. Profile 2B micromorphological analysis results.

Block		Slide ID	Description	Figure
F	4	MM7P2BZ11	**c/f related distribution:** Close and single-space porphyric. **Structure & voids:** Weakly separated channel and subangular to angular blocky microstructure, simple and compound packing voids and vesicles. **Coarse Fraction:** Moderate to well-sorted subangular to subrounded fine to very fine sand-sized quartz (dominant), augite (few), magnetite (few); coarse subangular to subrounded apatite (few) (2) subangular very fine sand sized quartz (common), augite (very few), apatite (very few); fine quartz, magnetite, apatite (few), augite (very few); subrounded coarse sand-sized apatite and quartz (very few). **Fine Fraction:** Reddish-yellow to yellowish-brown clay with stipple speckled, granostriated and in places, parallel striated b-fabric. **Pedofeatures:** Disorthic subangular calcite nodules; orthic and disorthic FeMn oxide nodules strongly embedded; limpid strong reddish-brown to dark yellowish-brown clay coats dislodged in passage features and lining grains; dusty reddish-brown clay films on grains; fecal pellets with carbonitic b-fabric containing very fine quartz grains, orthic calcite nodules (coarse to massive in size) forming around subangular to angular fine quartz (common) and augite (few); FeMn oxide hypocoats and quasicoats around grains and lining voids, limpid reddish-brown clay films on grains, parallel striated clay hypocoatings along channels, redeposited limpid yellowish-brown to reddish-brown clay coats.	6.22
G	5	MM1P2BZ12B	**c/f related distribution:** Close and single-space porphyric. **Structure & voids:** Weakly separated subangular blocky and channel microstructure; channels, voids and vughs and planar voids. **Coarse fraction:** Well-sorted subangular, very fine sand and silt-sized oblate and planar quartz (dominant); subangular to sub-rounded very fine sand to silt-sized triaxial and oblate augite (few); subangular to sub-rounded very fine sand to silt-sized equant and oblate feldspar and magnetite (very few). **Fine fraction:** Reddish-brown clay with granostriated and stipple speckled b-fabric, in places, calcitic, crystallitic and porostriated b-fabric.	6.23

Table 6.6. Continued

		MM1P2BZ12B (continued)	**Pedofeatures:** Dusty reddish-brown clay coatings on voids and individual grains; coarse orthic, typic and alteromorphic carbonate nodules, microgranular channel infillings (very fine sand and silt-sized quartz cemented by calcite and single-grains); black Fe-Mn oxide hypo-coatings and quasi-coatings on channels, voids and individual grains; weak to moderately impregnated Fe-Mn oxide orthic aggregate nodules in groundmass; vertical passage features few with dark reddish brown dusty clay coatings; yellowish-brown clay hypocoatings superimposed on dusty reddish-brown clay hypocoatings.	
H	7	MM3P2BZ14B	**c/f related distribution:** Close porphyric (dominant), single-space porphyric (common). **Structure and voids:** Moderately separated, partially accommodated angular blocky and channel microstructure (dominant), compound packing voids (few). **Coarse fraction:** Moderately sorted, subangular to sub-rounded fine sand-sized quartz (dominant), medium and coarse sand-sized quartz (few), subangular fine to very fine sand sized magnetite (common), subangular fine and very fine sand-sized augite and feldspar (few), coarse sand-sized rounded dolerite (very few). **Fine fraction:** Dark yellowish-brown clay with stipple-speckled and calcitic crystallitic b-fabric, and in places, granostriated and parallel striated b-fabric. **Pedofeatures:** Dark reddish-brown dusty clay coatings on voids and channels and laminating grains; passage features with loose continuous infillings and ellipsoidal fecal pellets; passage features with dense complete infillings that contain dark reddish-brown clay with stipple-speckled b-fabric and medium sand-sized quartz (dominant) and fine-sand sized augite (common); FeMn oxide hypocoatings along channels and passage features; strongly impregnated Fe-Mn oxide nodules with dark reddish-brown dusty clay coatings; orthic and disorthic carbonate nodules with Fe-Mn oxide films.	6.24
I	8	MM4P2BZ15	Very thin bedding/banded b-fabric where 3 distinct bands containing unique c/f related distributions are observed. Types are labeled 1, 2 and 3 in the following description. **c/f related distribution:** (1) Monic (dominant) and gefuric (common); (2) single and double-spaced porphyric (3) open and double-spaced porphyric.	6.25

Table 6.6. Continued

		MM4P2BZ15 (continued)	**Structure and voids:** (1) Loose/no microstructure and in some cases, crumb microstructure with simple and compound packing voids; (2) weakly separated granular to crumb microstructure with weakly separated channels, vesicles and compound packing voids; (3) accommodated to partially accommodated granular microstructure with planar voids and vesicles. **Coarse Fraction:** (1) Moderately sorted, fine to very fine sand-sized subangular quartz (dominant), apatite (few), magnetite (lining bottom of zone and separating laminae 1 from 2), augite and feldspar (few); coarse sub-rounded quartz (very few); (2) well-sorted subangular very fine sand sized quartz (dominant), silt-sized quartz (common), very fine augite and magnetite (few); very fine silt sized feldspar (very few); (3) well sorted silt-sized subangular quartz (dominant), very fine quartz (common), very fine to silt-sized augite and magnetite (few). **Fine fraction:** (1) Light yellowish-brown clay with granostriated, stipple speckled b-fabric (dominant), crystallitic b-fabric in discrete areas; (2) yellow clay with stipple speckled, granostriated b-fabric and in places, crystallitic b-fabric; (3) dusty, dark reddish-brown and yellowish-brown clay with undifferentiated b-fabric. **Pedofeatures:** (1) carbonate hypocoats on grains; disorthic carbonate nodules; reddish-brown clay quasicoats on quartz grains (very few); (2) Fe-Mn oxide coats on grains; dusty dark reddish brown clay films on grains; carbonate in-filled channels; dusty Grey carbonate films on grains (few); (3) strongly embedded orthic Fe-Mn nodules in limpid and stipple speckled dark reddish-brown b-fabric; disorthic sub-rounded carbonate nodules; strongly embedded orthic carbonate nodules in limpid clay b-fabric, parallel striated clay coats with alternating dusty reddish-brown and stipple speckled clay striae; carbonate coats along channels.	
J	9	MM6P2BZ16B	Three distinct types of banded b-fabric with differing coarse fraction observed. Types named 1, 2, and 3 in the following description. **c/f related distribution**: (1) Close porphyric, (2) gefuric and enaulic; (3) open porphyric (all laminae overprinted by channel and subangular blocky microstructure that separate pedofeatures).	6.26

Table 6.6. Continued

		MM6P2BZ16B (continued)	**Structure & voids:** (1) Channel and crumb microstructure (dominant) and in places, weak granular microstructure; simple and compound packing voids and vesicles, (2) loose grains, (3) partially accommodated granular microstructure with planar voids, channels and vesicles; microstructure moderately separated. **Coarse Fraction:** (1 & 2) Moderately sorted subangular to subrounded fine to very fine sand-sized quartz (dominant), augite (few), magnetite (few); coarse subangular to subrounded apatite (few) (3) subangular very fine sand sized quartz (common), augite (very few), apatite (very few); fine quartz, magnetite, apatite (few), augite (very few); subrounded coarse sand-sized apatite and quartz (very few). **Fine Fraction:** (1) Yellowish-brown clay with stipple speckled and calcitic crystallitic b-fabric; (2) very weak yellowish-brown clay quasicoats around grains (no substantial b-fabric); (3) dense, dusty to limpid reddish-brown ground mass with parallel and granostriated b-fabric intermixed with crystallitic b-fabric. **Pedofeatures:** (1) Disorthic subangular calcite nodules (coarse in size); disorthic FeMn oxide nodules strongly embedded; limpid strong reddish brown to dark yellowish-brown clay coats dislodged in passage features and lining grains; dusty reddish brown clay films on grains; fecal pellets with carbonitic b-fabric containing very fine quartz; (2) disorthic carbonate nodules, disorthic Fe-Mn oxide nodules, dark reddish-brown clay coat fragments (3) orthic calcite nodules (coarse to massive in size) forming around subangular to angular fine quartz (common) and augite (few); disorthic, rounded FeMn oxide nodules; orthic FeMn oxide nodules moderately to strongly embedded; FeMn oxide hypocoats and quasicoats around grounds and lining voids, limpid reddish-brown clay films on grains; bright yellowish-brown parallel straited b-fabric in disarticulated clay coats; passage features.	
K	10	MM5P2BZ17B	Very fine to fine bedding creates banded b-fabric of two distinct types. Types are labeled 1 and 2 in the following description. **c/f related distribution:** (1) Double-spaced porphyric; (2) monic (dominant) and in places, chitonic (common). **Structure & voids:** (1) Strongly separated, accommodated granular and channel microstructure; (2) loose; no microstructure (dominant), crumb microstructure in discrete areas.	6.27

Table 6.6. Continued

MM5P2BZ17B (continued)	**Coarse Fraction:** (1) Poorly sorted subangular and subrounded medium to very fine sand sized quartz (dominant), augite and magnetite (few); fine to very fine subangular appetite (few); (2) moderately sorted subangular, fine quartz (dominant), magnetite, augite, apatite (few), very fine quartz and feldspar (common), magnetite and augite (very few). **Fine fraction:** (1) Dark reddish-brown clay with stipple-speckled b-fabric and in some places, parallel striated b-fabric; (2) yellowish-brown clay with crystallitic and granostriated b-fabric. **Pedofeatures:** (1) Strongly embedded orthic carbonate nodules some containing very fine quartz coarse fraction; strongly embedded orthic Fe-Mn oxide nodules; limpid dark reddish-brown clay films on grains, hypo- and quasicoatings on grains; (2) carbonate hypo- and quasi coats on grains; few dusty dark reddish-brown clay coats on grains, FeMn oxide hypocoatings on grains and lining channels; passage features; disorthic carbonate nodules; strongly embedded orthic FeMn oxide nodules.

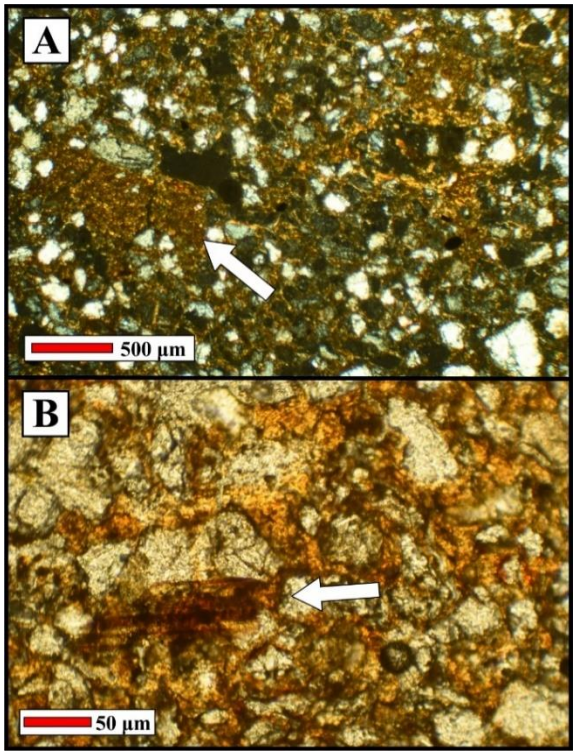

Fig. 6.22. Profile 2B Zone 4, block F, thin section MM7P2BZ11. (A) Typical granostriated b-fabric with redeposited clay coats (white arrow) (xpl, 40x); (B) dislodged clay film (white arrow) with superimposed dusty red clay hypocoatings around coarse fraction (ppl, 100x).

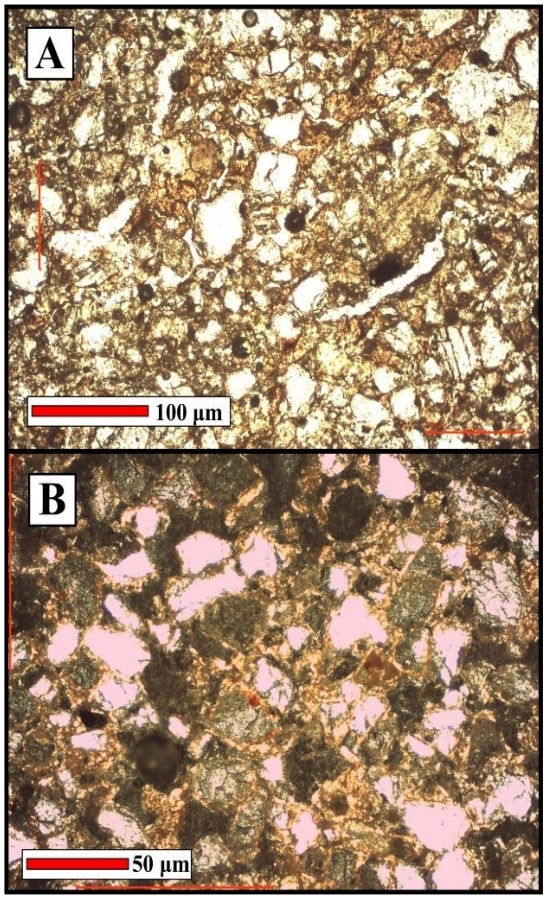

Fig. 6.23. Profile 2B Zone 5, block G, thin section MM1P2BZ12B. (A) Typical c/f related distribution (ppl, 40x); (B) typical granostriated b-fabric (xpl, 100x).

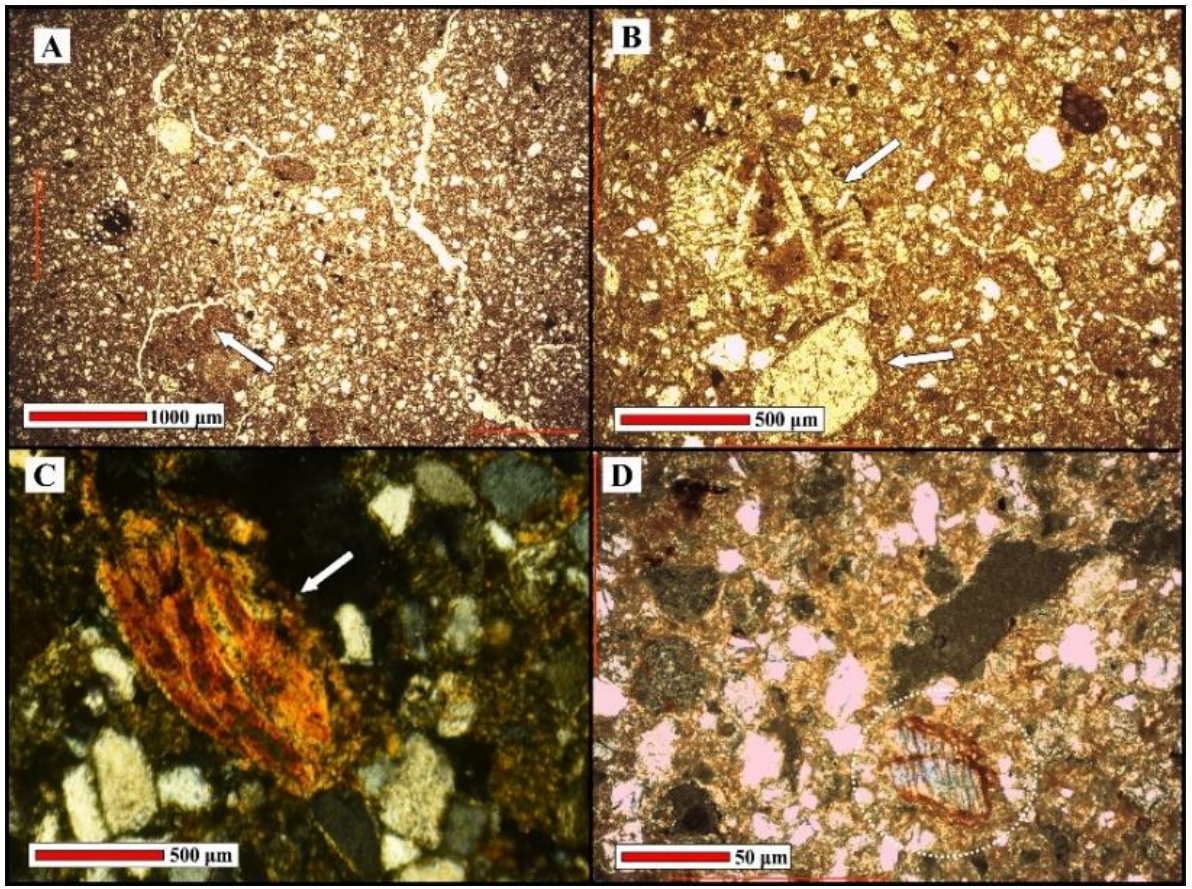

Fig. 6.24. Profile 2B Zone 7, block H, thin section MM3P2BZ14B. (A) Typical angular blocky microstructure, redeposited clay coat fragments (white arrow) & disorthic FeMn oxide nodule with regular boundaries (circled) (ppl, 20x); (B) coarse fraction (dolerite/appetite) covered with dusty red clay film (arrow) (ppl, 40x); (C) dense complete infilling of void with clay coat fragment (arrow) (xpl, 40x); (D) coarse fraction with two clay hypocoats- oldest=light yellow-brown clay, youngest=reddish-brown clay (circled area) (possible illuviation from above horizon) (xpl, 100x).

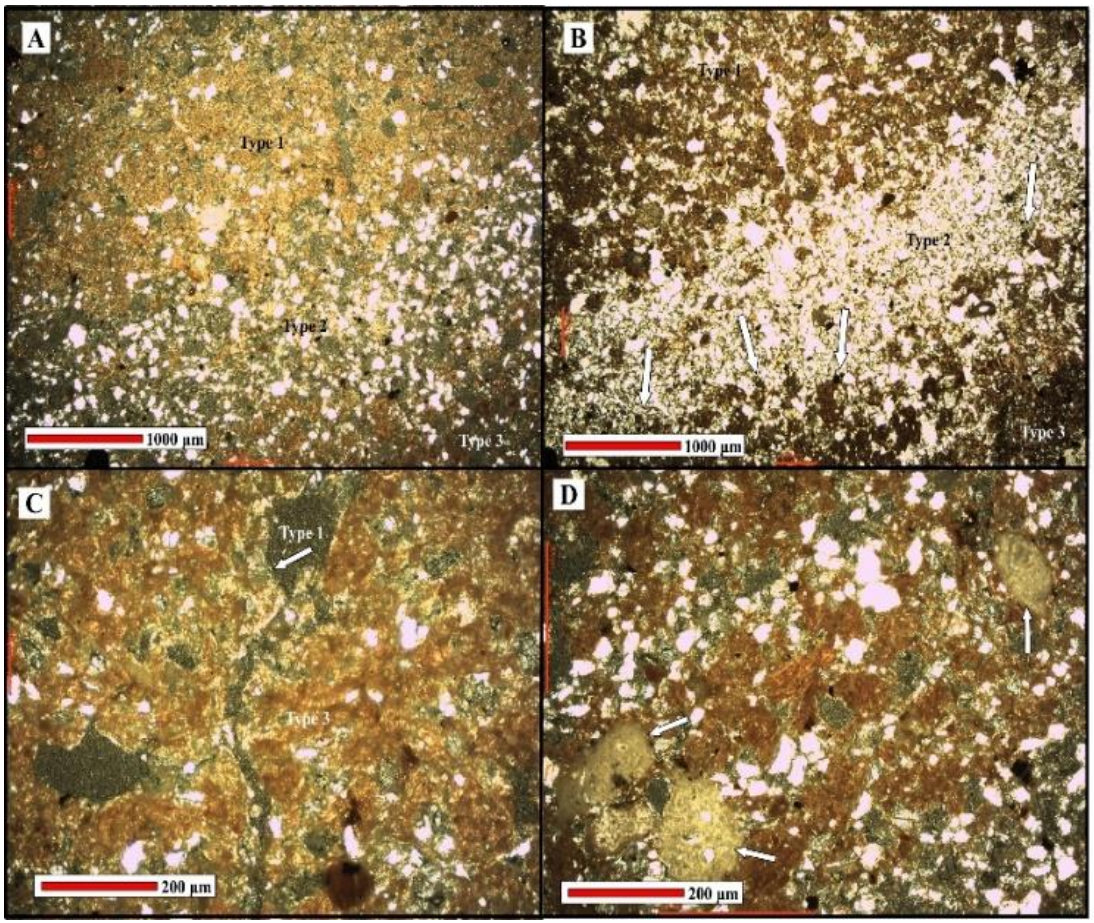

Fig. 6.25. Profile 2B Zone 8, block I, thin section MM4P2BZ15. (A) Typical banded b-fabric; Type 1 (upper half), Type 2 (middle), Type 3 (very bottom right) (xpl, 20x); (B) Type 1 (upper) and Type 2 (middle) with parallel oriented magnetite grains lining abrupt boundary between bands (arrows) (ppl, 20x); (C) Type 3 fabric with Type 1 clay hypocoatings lining channels (xpl, 40x); (D) Type 3 b-fabric with disorthic carbonate nodules (arrows) and very thin parallel oriented Type 2 coarse fraction (xpl, 40x).

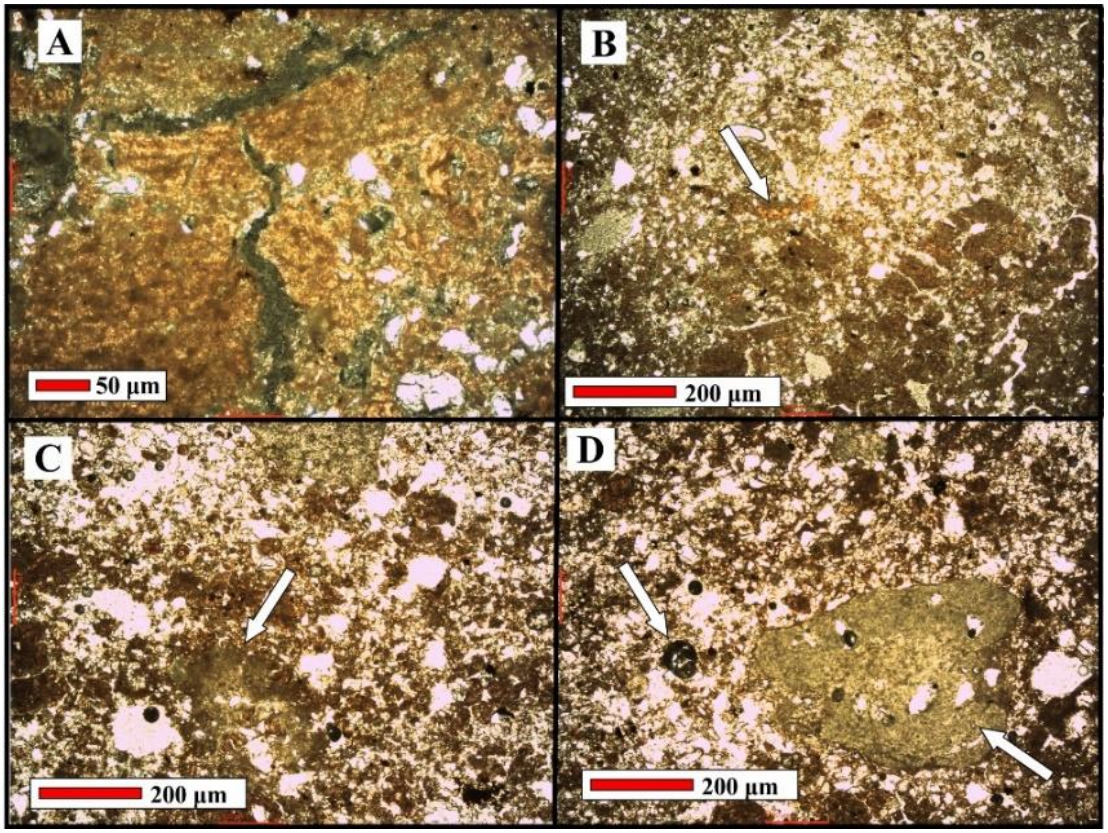

Fig. 6.26. Profile 2B Zone 9, block J, thin section MM6P2BZ16B. (A) Typical Type 1 b-fabric (xpl, 100x); (B) typical Type 2 b-fabric superimposed on Type 3 b-fabric, contains fragment of Type 1 clay coat (arrow) (xpl, 40x); (C) disorthic carbonate nodule in Type 3 band (ppl, 40x); (D) disorthic carbonate & Fe-Mn oxide nodules (arrows) in Type 2 band (ppl, 40x).

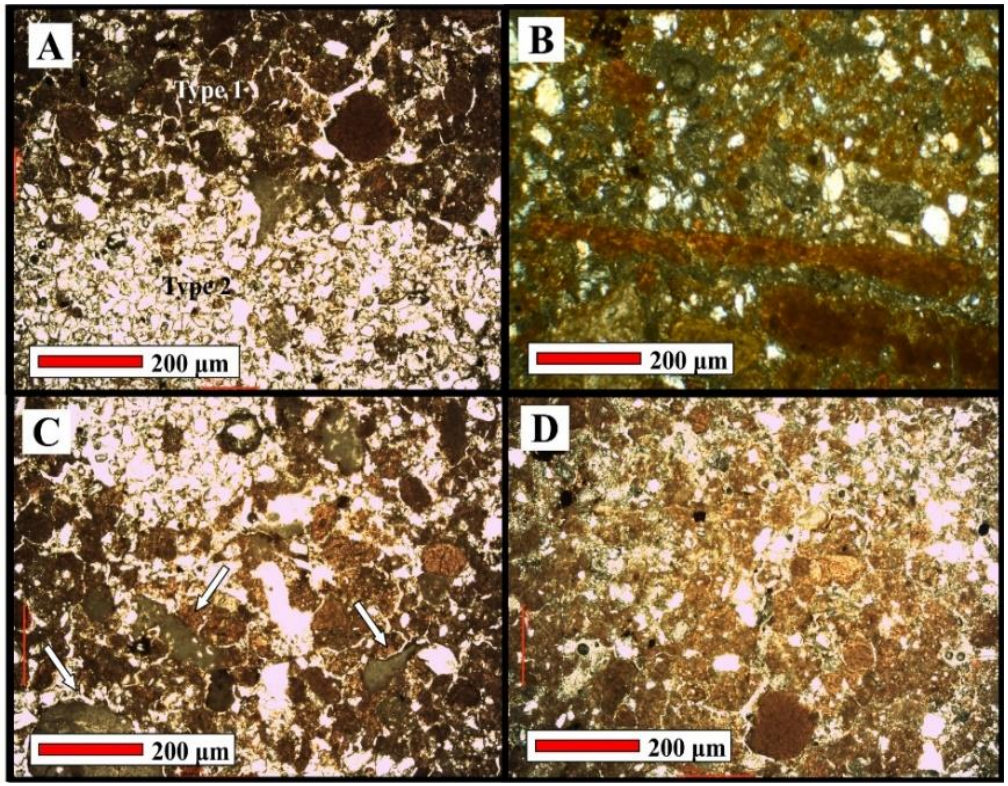

Fig. 6.27. Profile 2B Zone 10, block K, thin section MM5P2BZ17B. (A) Type 1 (upper clays) & Type 2 (lower coarse fraction) bands (ppl, 40x); (B) fragmented, parallel striated clay coats bounded abruptly by redeposited clays and coarse fraction (xpl, 40x); (C) redeposited clay coat fragments and disorthic carbonates (arrows) (typical features of Type 1 bands) (xpl, 40x); (D) illuviating and fragmented clays in Type 1 band (xpl, 40x).

Profile 2C Results

The Profile 2C exposure occurs approximately 8 m south of Profiles 2A and 2B, along an eastern facing slope along the main donga wall. Approximately 80 to 100 cm of heavily weathered surface sediment and loose, colluvial detritus was removed from the vertical face to expose the Upper Grey and Red contact as initially described by Tooth et al. (2013), and referred to as the Upper Grey and Red Sandy Loam contact by Bousman and Brink (2014). The entire 2C exposure reached a vertical depth of ~75 cm, where the surface corresponding with Zone 1 occurred 257.68 cm below the modern surface and top of Profile 2A (refer to Appendix D). The following profile description presents arbitrary elevations starting at 0 cm below surface associated with the eroded surface of Profile 2C. A total of 15 high-resolution samples ranging in mass from 5-8 g were extracted at ~5 cm intervals up profile. Two micromorphology blocks were also extracted. Block L was taken from the center of Zone 2 and Block M from the center of Zone 3 (refer to Figure 6.30 and Appendix G). Though this exposure was relatively small compared to others in the study, it provides a high degree of visibility between the Grey and Red unit boundaries defined by Bousman and Brink (2014) as an erosional, allostratigraphic unconformity (refer to Figures 6.28 and 6.29). The three zones identified in profile form a Bt-Bt-Bss sequence. Refer to Table 6.7 for a summarized description Profile 2C and Appendix F for the descriptive narrative by zone and summary of field form observations.

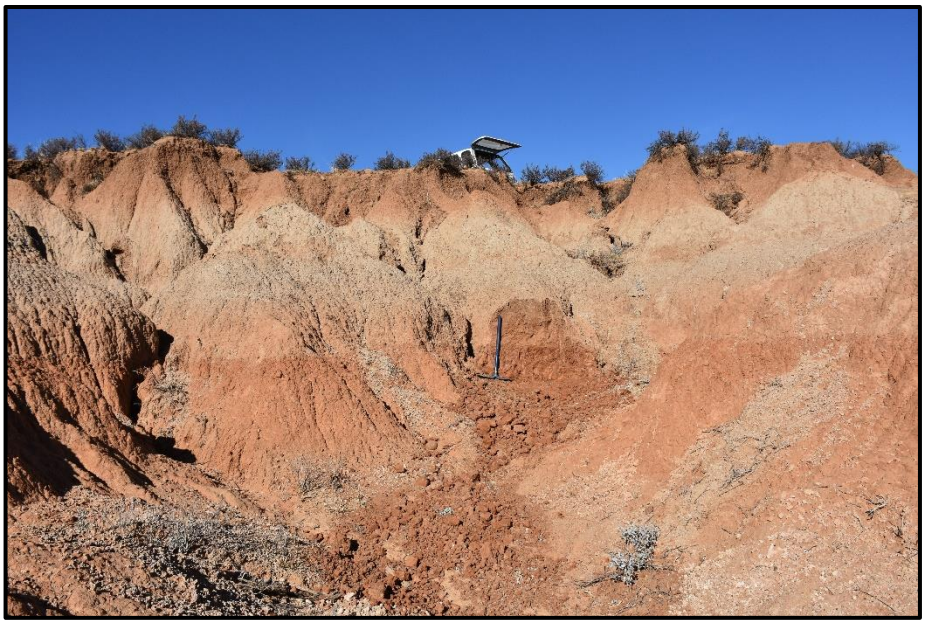

Fig. 6.28. Profile 2C exposure along eastern-facing slope of Erfkroon's primary donga.

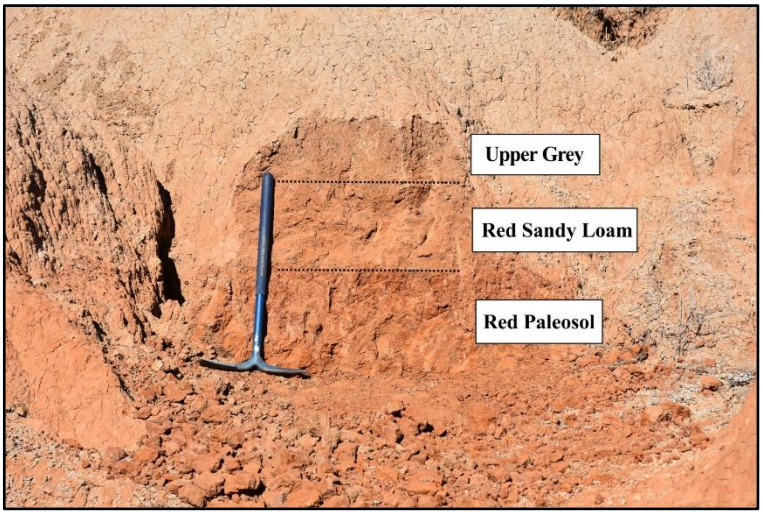

Fig. 6.29. Visibility of the boundary between the Upper Grey and Red units in Profile 2C.

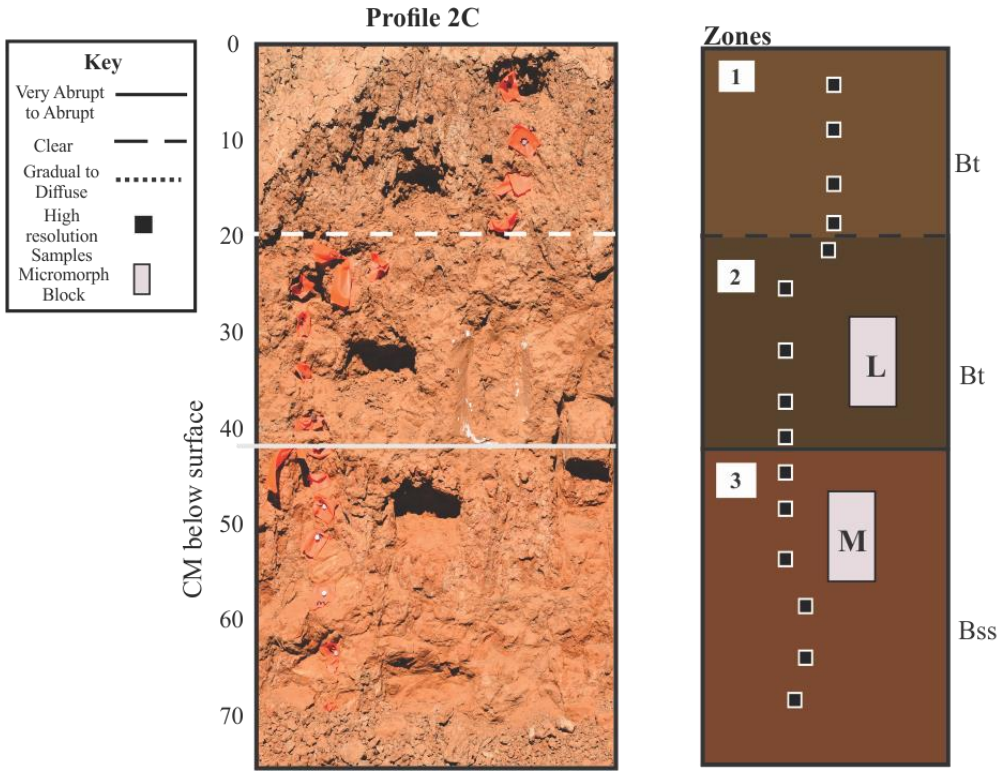

Fig. 6.30. Profile 2C horizons and sample locations (N=15).

Table 6.7. Profile 2C description by zone.

Zone	Horizon	Depth (cmbs)	Description
1	Bt	0-21.68	Fine, moderate, subangular blocky parting to coarse granular peds comprised of yellowish-brown (10YR 5/4 dry) to dark yellowish-brown (10YR 4/4) silty loam matrix. Matrix consistence ranges from semi-hard (dry) to plastic and friable (moist). Ped faces and matrix slightly effervesce when exposed to 10% HCl solution. Discontinuous, distinct FeMn staining is common on ped faces and parting planes. Black, irregularly shaped Mn masses and dendritic filaments are also common on ped faces. Mn films commonly line pores and worm channels. Bioturbation in the form of worm channels are common and contain strong brown (7.5YR 5/8) matrix. Discontinuous, thin carbonate films line worm channels. Lower boundary smooth and clear.
2	Bt	21.68-42.51	Medium, moderate, subangular blocky peds comprised of strong brown (7.5YR 4/6 dry; 7.5YR 4/4 moist) loam matrix. Matrix consistence ranges from semi-hard (dry) to very friable and plastic (moist). Fine, dendritic and tubular roots are common and occur through peds. Roots have low vertical continuity. Common, discontinuous, distinct FeMn staining observed on ped faces. Fine, dendritic and vertical Mn filaments are common on ped faces and lining cracks and pores.

Table 6.7. Continued

2 (cont.)			Soft, irregular Mn nodules are common throughout matrix. Few, very fine to fine gypsum crystals form between ped faces. Few, fine to very fine carbonate filaments occur in vertical pores and lining worm channels. Few fine, soft, irregular carbonate nodules occur in lower aspect of zone. Bioturbation in the form of worm channels are common. Lower boundary smooth and abrupt.
3	Bss	42.51-72.41	Strong, coarse prismatic peds with yellowish-red (5YR 4/6 dry; 5YR 4/4 moist) silty loam matrix. Matrix consistence ranges from hard (dry) to friable and plastic (moist). Discontinuous, common, prominent slickensides occur on horizontal ped faces. Discontinuous, very distinct ferriargillans common on ped faces. Irregular, black, fine to very fine Mn masses occur commonly on slickensides and ferriargillans. FeMn continuous on ped faces. Many dendritic filaments of Mn infill cracks and voids on ped faces. Strong brown (7.5YR 5/8) sand coats occur discontinuously on ped faces (18-20% coverage). Fine, dendritic carbonate filaments are common and infill pores, voids, and cracks in ped faces. No roots observed. Bioturbation in the form of worm channels common, channel matrix ranges from strong brown (7.5YR 5/6) to light yellowish-brown (10YR 6/4). Lower boundary unobserved; base of profile exposure.

Particle size, magnetic susceptibility & degree of development results. Particle size and magnetic susceptibility analyses were conducted on the high-resolution sample population extracted from Profile 2C (N=15). Distributions of sand, silt, and clay (measured in phi) by sample are tabulated in Appendix E and illustrated in Figure 6.31. Figure 6.31 also illustrates frequency-dependent ($\chi_{fd\%}$) susceptibility values by sample. Particle size means and standard deviations calculated by sample are illustrated in Figure 6.32. Numeric particle size ratios, standard deviations, means, and magnetic susceptibility values for the sample population are also tabulated in Appendix E. Ordinal characteristics recorded during field description of the profile were utilized to calculate degree of development scores by zone. Degree of development scores and percentage calculations (DDS%) are presented in Appendix C. DDS% calculations by zone are also graphically presented with low-frequency and frequency-dependent susceptibility results

in Figure 6.33. Overarching patterns in these combined data sets suggest enhanced pedogenic development (primarily driven by ped structure, illuvial clay content, and the presence of redox features) corresponds with relatively high $\chi_{fd\%}$ values.

Micromorphology results. Micromorphology blocks L and M were extracted from Profile 2C and correspond with zones 2 and 3 respectively. A micromorph sample was not extracted from Zone 1 due to the friability of its matrix and the zone's proximity to the modern, heavily weathered surface. Thin section descriptions are presented in Table 6.8 and provenience information is tabulated in Appendix G. In summary, Zone 2 shares similar b-fabric characteristics with those described in Profile 2A, Zone 10. Comparable characteristics include weakly separated channel microstructure with yellowish-gray clay, calcitic stipple-speckled, undifferentiated to weakly granostriated b-fabric, and single-spaced and close porphyric c/f related distributions (refer to Figure 6.34). The thin section described from Profile 2C, Zone 3 is characterized by well-developed, angular blocky microstructure with reddish-yellow clays and stipple-speckled, granostriated b-fabric (refer to Figure 6.35). These characteristics more closely reflect gross morphology observed in Profile 2B, zones 4 and 5; the latter aspect of the "Red Paleosol" as described in Bousman and Brink's (2014) characterization of the Dating Profile.

Lateral Continuity between Profiles 2A, 2B & 2C

Visual observations made in the field and through an inter-profile comparison of magnetic susceptibility and degree of development calculations confirm lateral continuity between Profiles 2A, 2B, and 2C. In summary, Profile 2C Zone 1 is laterally contiguous with Profile 2B Zone 2 and Profile 2A Zone 9, Profile 2C Zone 2 is laterally contiguous with Profile 2B Zone 3 and 2A Zone 11, and Profile 2C Zone 3 is laterally contiguous

with Profile 2B Zone 4. Figure 6.36 provides an illustrative summary of the lateral continuity between profiles, and Figure 6.37 illustrates an inter-profile comparison of magnetic susceptibility values and DDS% scores by profile sample populations. The lateral integrity of Profile 2 horizon designations is discussed at greater lengths in the next section, “Interpretations & Conclusions.”

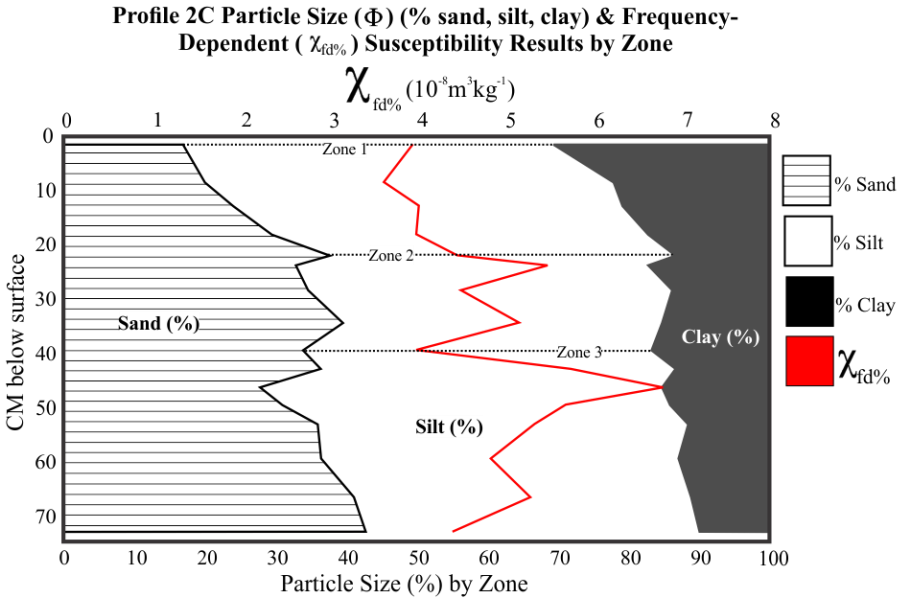

Fig. 6.31. Profile 2C particle size (% sand, silt, clay) & frequency-dependent susceptibility results (N=15). Dotted lines mark zone upper boundaries.

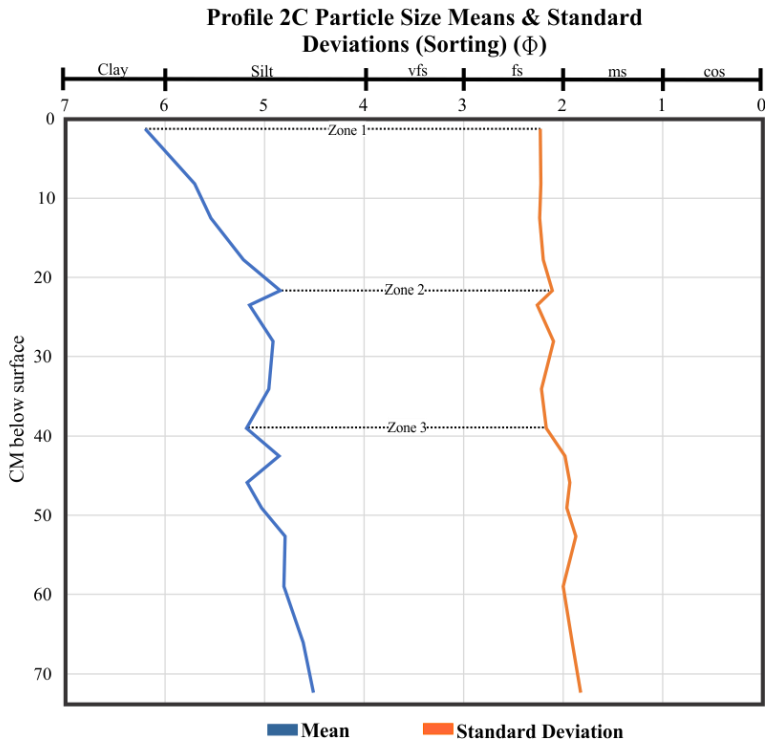

Fig. 6.32. Profile 2C particle size mean & standard deviation results by sample (N=15). Dotted lines indicate zone upper boundaries.
Abbreviations: cod= coarse sand, ms= medium sand, fs= fine sand, vfs= very fine sand. Dotted lines mark zone upper boundaries.

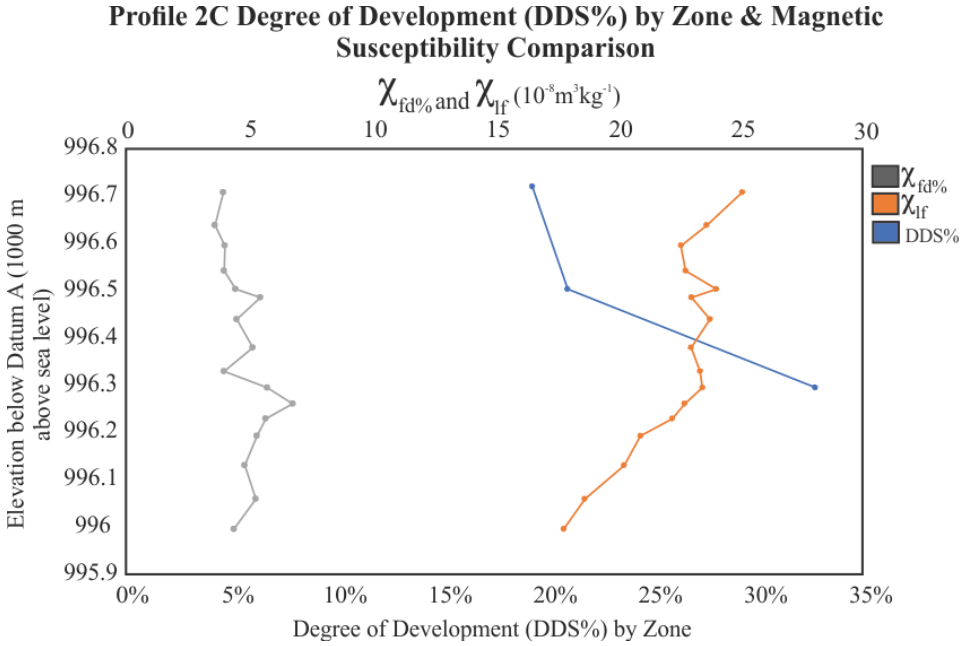

Fig. 6.33. Profile 2C DDS% by zone and magnetic susceptibility comparison.

Table 6.8. Profile 2C micromorphological analysis results.

Block	Zone	Slide ID	Description	Figure
L	2	MM14P2DZ2B	**c/f related distribution:** Single-spaced porphyric (dominant); in some places close porphyric. **Structure & voids:** Weakly separated granular and channel microstructure with simple and compound packing voids and vesicles. **Coarse fraction:** Moderate and poorly sorted sub-angular to sub-round very fine quartz (dominant), augite, apatite, and feldspar (very few), silt-size magnetite (few), subrounded fine sand-sized quartz (common), feldspar and augite (very few), Coarse sub-rounded quartz and augite (very few). **Fine fraction:** Yellowish-gray to weak brownish-yellow clay with stipple speckled and calcitic b-fabric; very calcareous ground mass. **Pedofeatures:** Passage features, dusty yellow to greyish-brown clay films on grains, dusty dark reddish-brown clay films on grains, Fe-oxide coats on grains and lining channels, irregular Fe-Mn oxide nodules, Fe oxide hypocoating around grains and voids; chambers completely infilled with dense ground mass comprised of silt-sized quartz grains and yellow stipple speckled b-fabric.	6.34
M	3	MM15P2DZ3A	**c/f related distribution:** Close porphyric (dominant), in some places gefuric**.** **Structure & voids:** Strongly separated angular blocky microstructure; planar channels, vesicles, regular vughs and chambers. **Coarse fraction:** Moderately sorted, subangular silt-size quart grains (dominant), feldspar, magnetite, augite (few); fine sand-size quartz (common), apatite (few), magnetite, augite and feldspar (very few). **Fine fraction:** Reddish-yellow clay and stipple speckled, granostriated b-fabric overprinted by dark reddish-brown limpid clay. **Pedofeatures:** All channels, chambers, vesicles, and planar separation voids are coated or partially infilled with reddish-yellow clay; passage features containing fecal pellets comprised of carbonate-crystallitic b-fabric and fine to very fine subangular quartz grains; needle fiber calcite hypocoatings and calcite hypocoating in non-calcareous ground mass; Fe-oxide hypocoatings around voids; illuvial clay coatings on channels and voids; typic impregnative Fe/Mn oxide nodules.	6.35

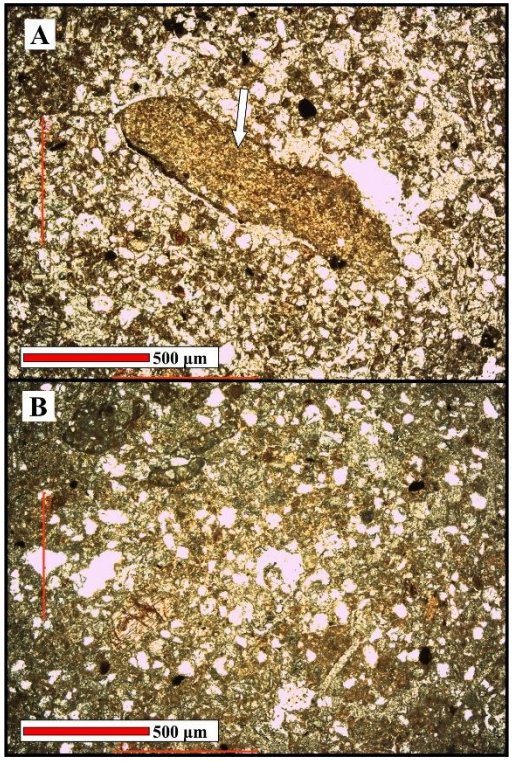

Fig. 6.34. Profile 2C Zone 2, block L, thin section MM14P2DZ2B. (A) Typical close porphyric c/f related distribution and dense, complete infilling (white arrow) (ppl, 40x); (B) typical stipple speckled b-fabric and area of single and double-space porphyric c/f related distribution (xpl, 40x).

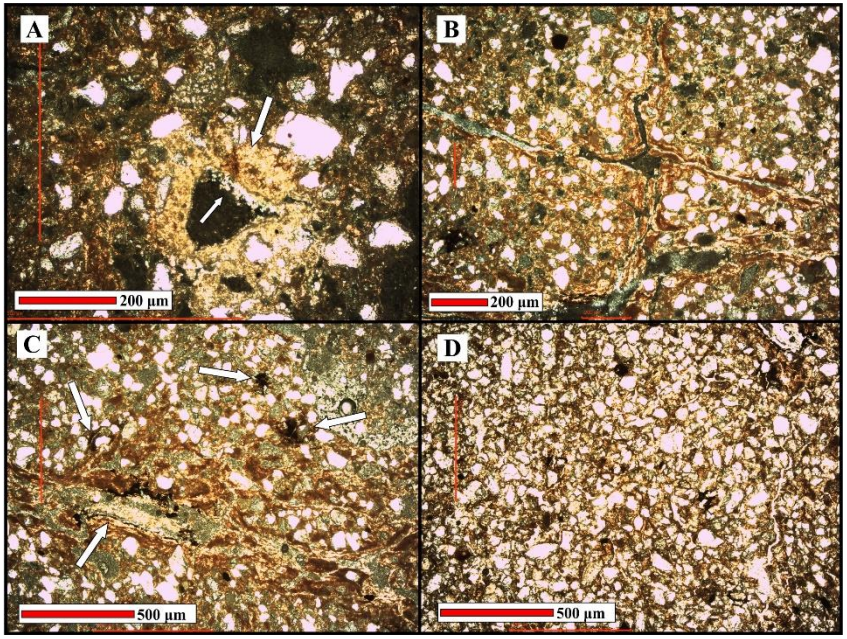

Fig. 6.35. Profile 2C Zone 3, block M, thin section MM15P2DZ3A. (A) Regular vughs with calcite hypocoatings in non-calcareous groundmass (white arrows) (xpl, 100x); (B) strongly separated planar voids creating angular blocky microstructure, planar voids bounded by reddish-brown ferriargillans and illuviated clays; FeMn oxide accumulations also present. Pedofeatures include disorthic FeMn oxide nodules (xpl, 40x); (C) typical separation planes covered with ferriargillans and infilled with bright yellow stipple speckled b-fabric, FeMn oxide hypocoatings and orthic FeMn oxide nodules also present (white arrows) (xpl, 40x); (D) typical close porphyric c/f related distribution and commonly occurring orthic and disorthic FeMn nodules (ppl, 40x).

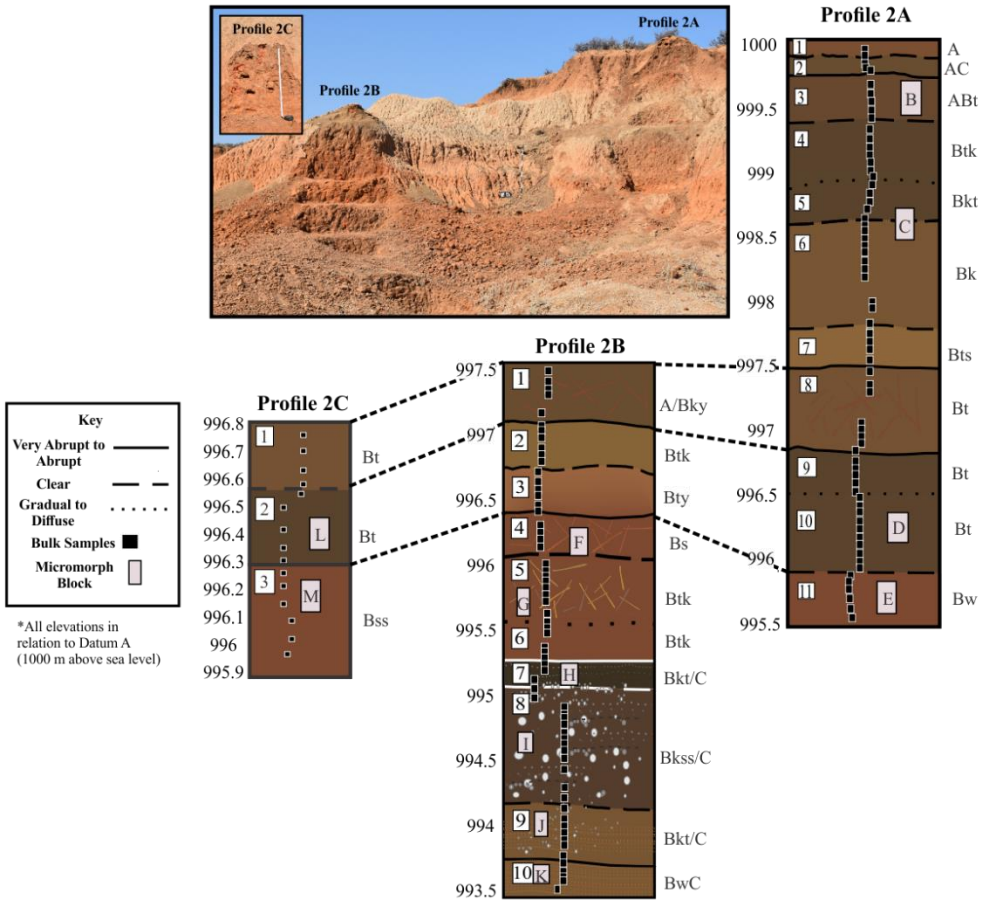

Fig. 6.36. Lateral continuity between zones in Profiles 2A, 2B and 2C. Dashed lines connect upper boundaries of laterally contiguous zones between profiles.

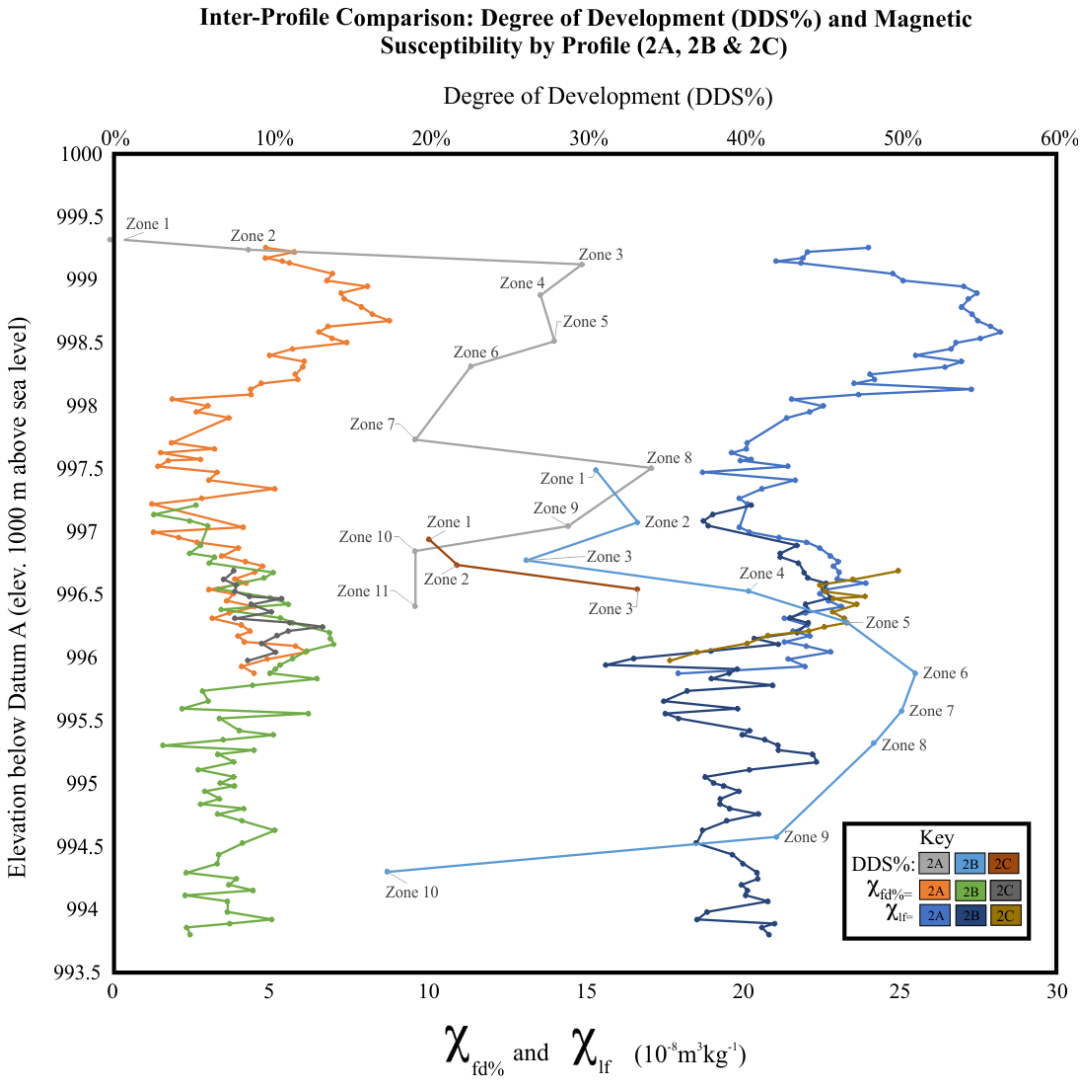

Fig. 6.37. Profiles 2A, 2B, and 2C inter-profile comparison of magnetic susceptibility results by sample and DDS% by zone. Left aligned graphic= frequency-dependent susceptibility values by sample, center graphic= DDS% scores by zone, and right-aligned graphic= low-frequency susceptibility values by sample.

Profile 5 Results

Profile 5 was exposed during the 2017 field season, approximately 500 m northwest of the Dating Profile and the Profile 2 Complex, at a locale untested during previous geological, archaeological, and paleontological investigations. The exposure was cleared along the northwestern face of an eroding terrace bench, now disconnected

from the main terrace wall. This particular exposure was chosen because of its near vertical scarp revealing intact components of the Brown, Upper Grey, and Red units of the primary alluvial overbank sequence (refer to Figure 6.38). The profile's lateral distance from other profiles in this and other studies provided an opportunity to examine the lateral continuity of the overbank sequence.

The vertical extent of the profile measured ~3 m, where the surface of the profile occurred at 997.03 m above sea level in relation to Datum A (1000 m above sea level). Elevations presented in the following description coincide with an arbitrary elevation of 0 cm below surface, however, both arbitrary elevations and those associated with Datum A are provided in Appendix D. Nine bulk samples (one representative sample per zone) were extracted for laboratory analysis, and one micromorphology block was extracted from the boundary between zones 3 and 4 (Block M) for thin section analysis. Figure 6.39 provides an illustration of zone boundaries and sample locations. Zone provenience data is provided in Appendix D, while particle size and magnetic susceptibility values by sample are tabulated in Appendix E. In-field examination of the profile revealed nine zones that comprise an A/Bw-A/Bt-A/Bk-Btk-Btss-Bty-Btky-Bs-Btk sequence. Refer to Table 6.9 for a descriptive summary of the profile by zone, and Appendix F for a detailed descriptive narrative and summary of field form observations.

Fig. 6.38. Profile 5 exposure. Identified zones marked by orange flagging tape (N=9).

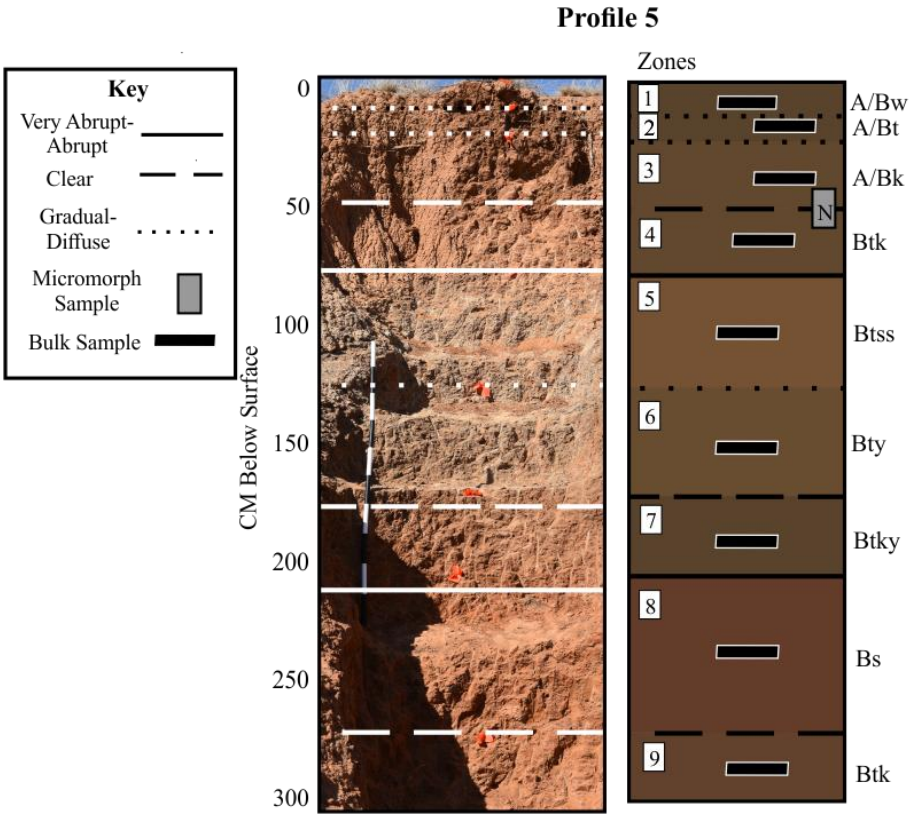

Fig. 6.39. Profile 5 horizons & samples locations (N=9).

Table 6.9. Profile 5 description by zone.

Zone	Horizon	Depth (cmbs)	Description
1	A/Bw	0-13.0	Medium, moderate subangular blocky peds comprised of strong brown (7.5YR 5/6 dry) to brown (7.5YR 4/4) silty loam. Matrix consistence ranges from soft (dry) to loose and non-plastic (moist). Ped faces very slightly effervesce when exposed to 10% HCl solution and matrix is nonreactive. Ped faces and matrix contain many fine and very fine dendritic, tubular and interstitial pores with high vertical continuity. Many fine and medium, dendritic and tubular roots with high vertical continuity penetrate peds. No stress features, RMF features, or carbonates observed. Bioturbation in the form of root sheaths, insect casts, and worm channels are many. Lower boundary gradual and smooth.
2	A/Bt	13.0-27.90	Fine, strong prismatic peds comprised of strong brown (7.5YR 4/6 dry; 7.5YR 4/4 moist) silty loam. Matrix consistence ranges from moderately hard (dry) to friable and very plastic (moist). Ped faces slightly effervesce when exposed to 10% HCl solution. Vertical ped faces contain common, discontinuous, distinct pressure faces with undulating "pocked" surfaces. Waxy clay films are distinct, discontinuous and few on ped faces. Few, very fine, dendritic to interstitial pores with moderate vertical continuity occur on ped faces. Many very fine and fine dendritic roots with moderate vertical continuity occur on ped faces and penetrate peds. Few very fine gypsum crystal masses occur on ped faces. Very fine, few thread-like, dendritic carbonate filaments and masses occur in cracks and infill pores on vertical ped faces. Few very fine spherical carbonate nodules occur on ped faces. Bioturbation in the form of insect casts, linear and tubular worm channels, and root sheaths are common. Few contain observable accumulations of fecal pellets. Lower boundary gradual and smooth.
3	A/Bk	27.90-59.10	Fine, weak wedge-shaped peds comprised of strong brown (7.5YR 5/6 dry) to brown (7.5YR 4/4) silty loam. Matrix consistence ranges from moderately hard (dry) to very friable and slightly plastic (moist). Ped faces are slightly effervescent when exposed to 10% HCl solution, ped matrix is nonreactive. Very few fine dendritic roots occur through peds. Very few, fine dendritic root pores with low vertical continuity occur on ped faces. Medium to fine spherical and reticulate carbonate nodules commonly occur on vertical ped faces. Fine, dendritic and thread-like carbonate filaments are few and occur in cracks and lining surfaces of pores on and between vertical ped faces. Bioturbation in the form of insect burrows and worm channels are few. Few fine, dendritic rhyzoliths observed on ped faces and infilling pores. Lower boundary clear and smooth.

Table 6.9. Continued

4	Btk	59.10-95.80	Medium, moderate wedge-shaped peds comprised of strong brown (7.5YR 5/6 dry) to brown (7.5YR 4/4 moist) silt. Matrix consistence ranges from slightly hard (dry) to friable and plastic (moist). Ped faces and matrix are nonreactive when exposed to 10% HCl solution. Distinct, loose, fine sand (7.5YR 5/6) coats on ped faces are discontinuous and common. Few very fine irregular and dendritic root pores with low vertical continuity occur on ped faces. Fine, dendritic and tubular roots with moderate vertical continuity are few and occur between ped faces. Few distinct discontinuous Mn masses accumulate as platy masses on ped faces. Few soft, fine spherical FeMn nodules adhere to vertical ped faces. Very fine and fine, cubic and spherical carbonate nodules commonly adhere to matrix on vertical ped faces. Irregular, dendritic, and thread-like carbonate filaments and masses are common in cracks, lining surfaces of pores, and accumulating around pore openings. Fine rhyzoliths are few and occur in root voids and pores. Bioturbation in the form of root sheaths, insect burrows and linear, tubular worm channels are common. Lower boundary abrupt and smooth.
5	Btss	95.80-154.20	Medium, strong angular blocky peds comprise of a yellowish-brown (10YR 5/4 dry; 10YR 5/6 moist) silty loam matrix. Matrix consistence ranges from moderately hard (dry) to friable and very plastic (moist). Ped faces very slightly effervesce when exposed to 10% HCl solution, ped matrix is nonreactive. Yellowish-brown (10YR 5/4) fine silt coats are common, distinct and patchy on ped faces. Pressure faces and slickensides are common, discontinuous and distinct on horizontal ped faces. Very fine to medium root pores, root casts, and very fine tubular pores with moderate vertical continuity occur on ped faces and through ped matrix. Mn masses, spherical and thread-like in shape are common and accumulate in pores, along cracks on ped faces, and on slickensides. Many very fine carbonate masses and thread-like filaments accumulate in pores, along cracks, and lining surfaces and openings of pores. Bioturbation in the form of linear worm channels, insect burrows, and root pores are common. Very few, fine tubular and dendritic rhyzoliths infill pores. Lower boundary gradual and smooth.
6	Bty	154.20-200.10	Coarse, strong prismatic peds comprised of yellowish-brown (10YR 5/4 dry) to brown (10YR 4/3) silty loam. Matrix consistence ranges from moderately hard (dry) to friable and plastic (moist). Ped faces strongly effervesce when exposed to 10% HCl solution, ped matrix is nonreactive.

Table 6.9. Continued

6 (cont.)			Distinct, discontinuous fine dark yellowish-brown (10YR 4/4) silty films commonly cover vertical ped faces. Many discontinuous, prominent slickensides commonly mottled with fine Mn masses occur on ped faces. Distinct, discontinuous, prominent pressure faces and ferriargillans occur on ped faces and on parting planes. Few, very fine dendritic and tubular roots with moderate vertical continuity occur lining ped faces. Many distinct and discontinuous platy Mn masses occur on ped faces, and as dendritic and thread-like filaments lining cracks and pores. Fine, slightly hard FeMn nodules also occur on ped faces and slickensides. Thin, very fine filaments infilling cracks on ped faces, accumulating around pore openings, and lining pores are common. Very fine gypsum crystals commonly accumulate in pores and cracks on and within peds. Bioturbation in the form of linear, cylindrical worm channels, insect burrows, and root sheaths are common. Fine, dendritic and tubular rhyzoliths are also common between ped faces. Lower boundary clear and smooth.
7	Btky	200.10-226.10	Medium, strong, prismatic peds comprised of brown (7.5YR 5/4 dry; 7.5YR 4/4 moist) silty loam matrix. When dry, matrix is slightly hard, when moist, matrix is very friable and plastic. Ped faces and matrix very slightly effervesce when exposed to 10% HCl solution. Weak, discontinuous and distinct pressure faces are common on ped faces. Fine dendritic and tubular pores with moderate vertical continuity are also common on ped faces. Mn masses are many and occur as platy, dendritic, and thread-like masses on ped faces, in cracks, lining pores, and accumulating along pore openings. Fine, platy carbonate flakes, fine cubic and spherical carbonate nodules, and dendritic, thread-like filaments are common and occur within matrix on ped faces and accumulate in cracks and pores on ped faces. Fine, gypsum crystals commonly occur as clusters infilling pores and cracks on ped faces. Bioturbation in the form of insect burrows, linear worm channels, and very fine root sheaths are few. Fine, tubular rhyzoliths are few. Lower boundary abrupt and smooth.
8	Bs	226.10-270.50	Medium, strong prismatic peds comprised of yellowish-red (5YR 5/7 dry; 5YR 4/6 moist) loam. Matrix consistence ranges from slightly hard (dry) to friable and plastic (moist). Ped faces and matrix very slightly effervesce when exposed to 10% HCl solution. Discontinuous, patchy, fine silty coats commonly occur on ped faces. Strongly developed, discontinuous pressure faces commonly occur on all ped faces and parting planes. Very fine, dendritic and tubular pores with low vertical continuity also common on ped faces. No roots observed. Medium platy Mn masses commonly occur on ped faces. Soft spherical FeMn nodules and thread-like dendritic filaments commonly infill pores and cracks along ped faces.

Table 6.9. Continued

8 (cont.)			Few, fine thread-like and dendritic filaments infill pores and cracks on ped faces and bioturbated areas. Bioturbation in the form of linear, cylindrical worm channels and insect burrows are many. Lower boundary clear and smooth.
9	Btk	270.50-290.50	Medium, moderately strong subangular blocky peds comprised of strong brown (7.5YR 5/6 dry) to brown (7.5YR 4/4 moist) silty loam matrix. Matrix consistence ranges from slightly hard (dry) to firm and slightly plastic (moist). Ped faces and matrix very slightly effervesce when exposed to 10% HCl solution. Strong brown (7.5YR 5/6) sandy coats on ped faces are common, discontinuous and distinct. Weak, discontinuous, distinct pressure faces common on ped faces. Very fine tubular and irregularly shaped pores are common on ped faces, with moderate vertical continuity. No roots observed. Mn masses commonly occur as fine platy rosettes and thread-like filaments on ped faces, within cracks, and lining pores. Carbonates commonly occur as very fine platy "flecks" and thread-like filaments adhering to matrix on ped faces, within cracks, and lining pores. Few, very fine spherical carbonate nodules occur between ped faces. Bioturbation in the form of linear, cylindrical worm channels and insect burrows are many. Lower boundary unobserved; base of profile exposure.

Particle size, magnetic susceptibility & degree of development results. Magnetic susceptibility and particle size analyses were conducted on the nine bulk samples extracted from Profile 5 (refer to Figure 6.40). Particle size ratios compared with frequency-dependent magnetic susceptibility results are presented in Figure 6.40, while particle size means and standard deviations by sample are illustrated in Figure 6.41. These data are also provided in Appendix E. Degree of development (DDS%) scores by zone are presented with both low-frequency and frequency-dependent susceptibility results in Figure 6.42. Numeric values used to calculate DDS and DDS% by zone are provided in Appendix C.

In Profile 5, gross morphological characteristics and general patterns observed among its geoproxy data are similar to those observed among stratigraphically comparable zones in Profile 2A. These similarities suggest Profile 5 horizons correlate with the Brown, Grey, and Red units as described in other profiles and in previous studies (Tooth et al. 2013; Bousman & Brink 2014).

In Profile 5, the Brown occurs in zones 1-6. The top of the Brown corresponds with the modern surface (upper boundary of Zone 1) which has been altered by developmental upbuilding— a scenario where sediment is added to existing pedogenic development, but additions accumulate slow enough that pedogenesis is able to keep pace with the incorporation of new material into the existing matrix (Johnson 1985). In-field observations of modern aeolian deposition and surface detritus intermixed with the upper Brown horizons in Profile 5 suggest pedogenesis is still very much active. The Upper Grey unit manifests in well-developed B-related horizons in zones 5 and 6, and zones 7 and 8 coincide with the latter aspect of the Upper Grey and Red Sandy Loam as described by Bousman and Brink (2014). Zone 9 correlates with Bousman and Brink's (2014) Red Paleosol.

In Profile 2A, frequency-dependent susceptibility values ($\chi_{fd\%}$) decrease from the top of the Brown (Zone 3) into Zone 4, followed by an upward swing in magnetic enhancement into Zone 5, a well-developed Btk-horizon. A similar pattern is observed between zones 1-4 in Profile 5. A relatively higher susceptibility value associated with Zone 1 declines into Zone 2, followed by an increase in value into Zone 3. This corresponds with a higher degree of pedogenic development score, reflecting the relatively well-developed Bk-horizon attributes observed in Zone 3.

The Grey unit as described by Tooth et al. (2013) and Bousman and Brink (2014) corresponds with zones 5 and 6 in Profile 5. Susceptibility values decline from Zone 4 into Zone 6, which corresponds with increasing silt ratios in the profile matrix. The lowest susceptibility value observed in Profile 5 is 2.44 ($10^{-8}m^3kg^{-1}$), which occurs in Zone 6 at ~174.70 cm below surface. The opposite trend is observed among degree of development scores which consistently rise from Zone 3 to Zone 6, but then decline into Zone 7.

Zones 7-9 correspond with the Red unit collectively described as one paleosol sequence by Tooth et al. (2013) and Lyons et al. (2014), but by Bousman and Brink (2014) as an unconformable boundary separating AU2 and AU3 (at the Red Sandy Loam and Red Paleosol contact). Frequency-dependent susceptibility values associated with samples extracted from zones 7 through 8 consistently increase, where magnetic enhancement peaks in Zone 8 at a high of 10.26 ($10^{-8}m^3kg^{-1}$) at ~244.60 cm below surface. This susceptibility peak corresponds with an increase in sand and silt ratios (49.5% and 42.13% respectively) in the matrix, but also corresponds with a lower DDS%. DDS% scores are relatively lower than stratigraphically higher zones due to a reduction in overall clay content, relatively less calcium carbonate in the matrix, and generally smaller ped sizes. Frequency-dependent susceptibility values decrease in Zone 9 to 5.25 ($10^{-8}m^3kg^{-1}$) but correspond with a slightly higher DDS% score and matrix silt content than Zone 8.

Micromorphology results. Two thin sections were prepared from block N extracted from the boundary between zones 3 and 4 in Profile 5. The block's location in profile is illustrated in Figure 6.39 and descriptive results are presented in Table 6.10.

Zone 3 exhibits characteristics consistent with both A and B horizonation. A-horizon characteristics include passage features, organic debris accumulations in channels and voids, and limpid clay infillings suggestive of clay illuviation down profile. B-horizon characteristics include blocky microstructure, areas of granostriation in the stipple-speckled clay b-fabric, and multiple layers of clay hypocoatings around the coarse fraction (refer to Figure 6.43). These combined features mirror similar features observed in the upper Brown unit of Profile 2A, Zone 3. A noticeable reduction in the presence of limpid clay and organic infillings characteristic of A-horizon development coincides with Zone 4. Instead, clearly separated planar voids and channels creating subangular blocky microstructure, and pedofeatures such as orthic FeMn oxide nodules and hypocoatings, and illuviated, disorthic calcium carbonate nodules collectively reflect well-developed, sub-surface B-horizonation (refer to Figure 6.44).

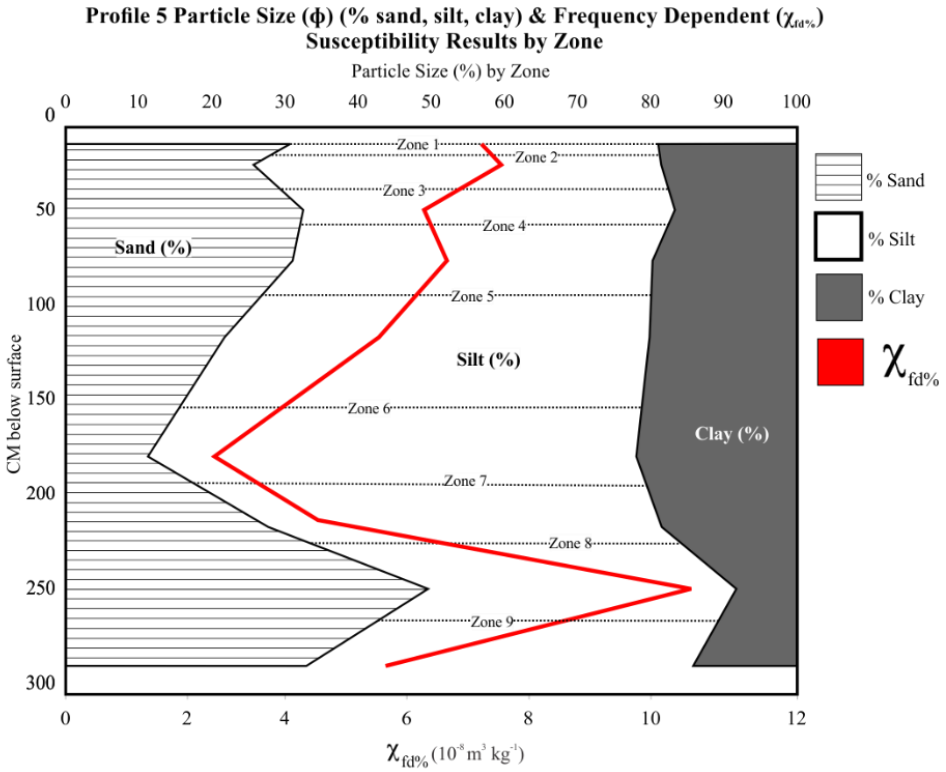

Fig. 6.40. Profile 5 particle size (% sand, silt, clay) & frequency-dependent susceptibility results. Dotted lines mark zone upper boundaries.

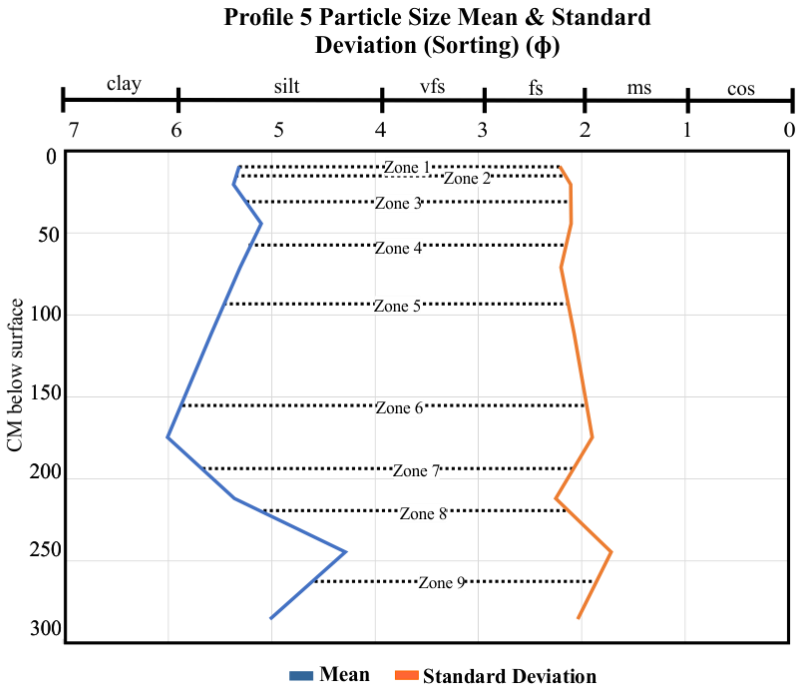

Fig. 6.41. Profile 5 particle size means & standard deviations by zone. Dotted lines mark zone upper boundaries.

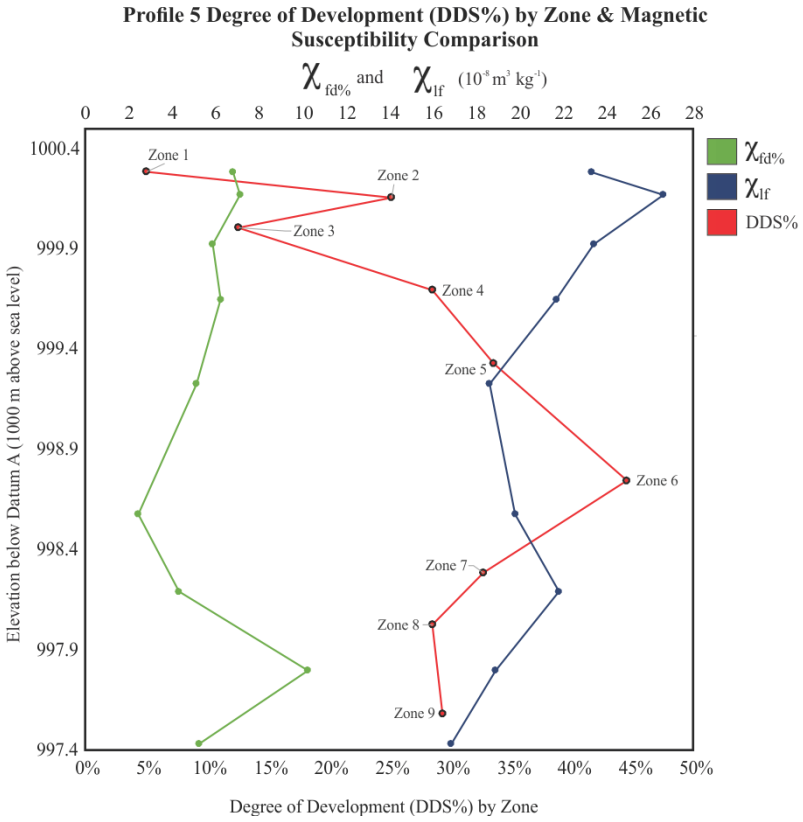

Fig. 6.42. Profile 5 DDS% by zone and magnetic susceptibility comparison.

Table 6.10. Profile 5 micromorphological analysis results.

Block	Zone	Slide ID	Description	Figure
N	3	40MM5S3A	**c/f related distribution:** Close and single space-space porphyric. **Structure & voids:** Subangular blocky and channelitic microstructure with simple and compound packing voids. **Coarse fraction:** Moderately well-sorted fine and very fine sand-sized quartz (dominant), fine and very fine sand-sized dolerite and feldspar (few), very fine sand-sized, angular and sub angular augite (very few), medium sand-sized quartz (few), coarse sand-sized quartz very few**.** **Fine fraction:** Yellowish-brown well-oriented limpid clay and stipple speckled b-fabric with areas of parallel and granostriated b-fabric. **Pedofeatures:** Limpid yellow and yellowish-brown clay infillings, dense complete infillings in channels and passage features; limpid yellow and dusty yellowish-brown clay coatings along channel and void boundaries; dusty yellow clay and silt hypocoatings around coarse fraction; dusty yellow clay coatings with microlaminations; organic matter accumulations along channel boundaries and passage features (very fine silt-sized oblate and spherical fecal pellets).	6.43
N	4	40MM5S3B	**c/f related distribution:** Close and single space-space porphyric. **Structure & voids:** Subangular blocky and channelitic microstructure (dominant), simple and compound packing voids (common). **Coarse fraction:** Moderately well-sorted fine and very fine sand-sized quartz (dominant), fine and very fine sand-sized dolerite and feldspar (few), very fine sand-sized, angular and sub angular augite (very few), medium sand-sized quartz (few), coarse sand-sized quartz (very few)**.** **Fine fraction:** Dusty yellow clay and stipple speckled b-fabric, and in areas granostriated b-fabric. **Pedofeatures:** Ovoid passage features (common), medium sand-sized disorthic calcium carbonate nodules containing coarse fraction (few), fine and very fine disorthic FeMn nodules with sharp boundaries (few), organic debris (common), dusty yellow silt and clay hypocoatings around coarse fraction and lining channels (common).	6.44

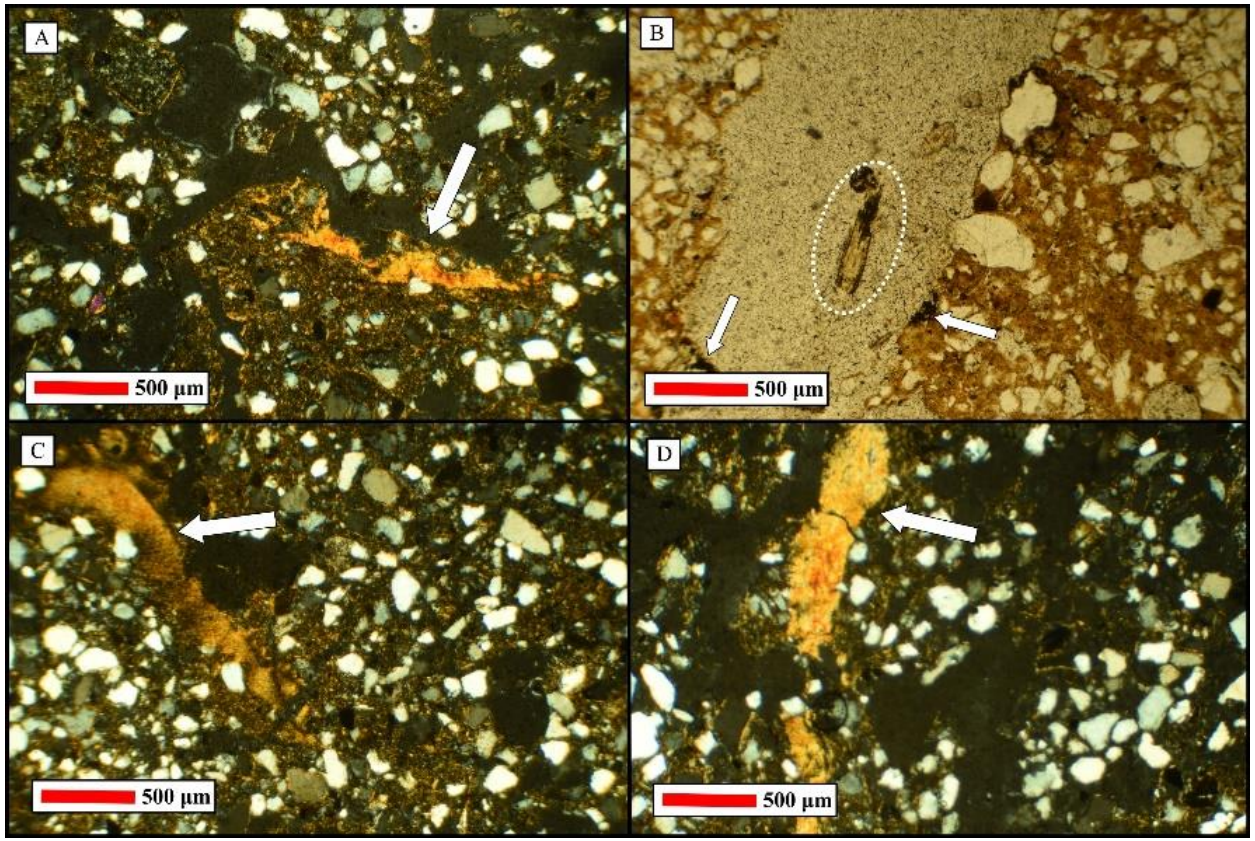

Fig. 6.43. Profile 5 Zone 3, block N, thin section 40MM5S3A. (A) Limpid clay hypocoat and infilling (xpl, 40x); (B) typical channel microstructure containing root fragment (circle), channel contains organic debris (white arrows) (ppl, 40x); (C) well-oriented dusty clay and silt infilling in channel (xpl, 40x); (D) dense complete limpid clay infilling (xpl, 40x).

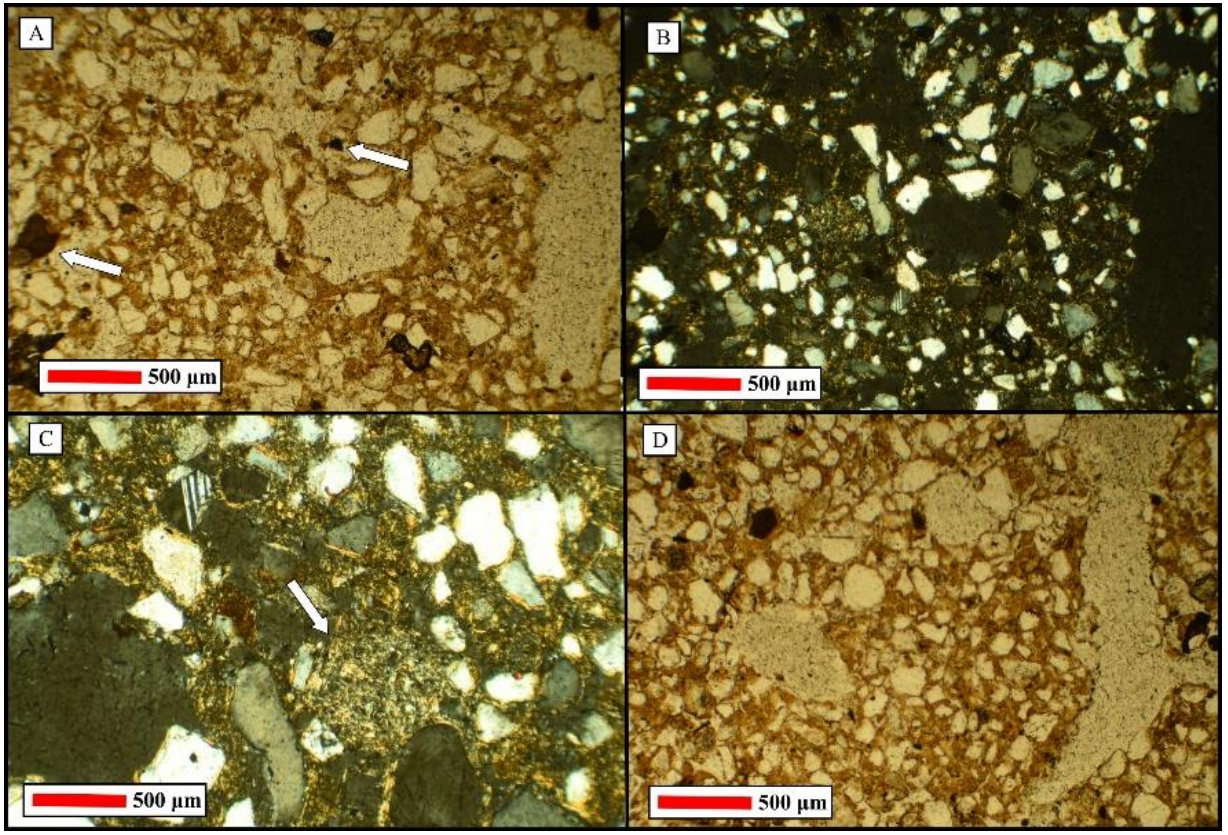

Fig. 6.44. Profile 5 Zone 4, block N, thin section 40MM5S3B. (A) Dusty silt coatings around coarse fraction, typical close and single spaced porphyric c/f related distribution, fine and very fine FeMn nodules (arrows) (ppl, 40x); (B) typical stipple-speckled b-fabric (xpl, 40x); (C) disorthic carbonate nodule (arrow) and dusty clay and silt hypocoatings around coarse fraction (xpl, 40x); (D) typical voids and passage features (ppl, 40x).

7. INTERPRETATIONS & CONCLUSIONS

Overbank sediments deposited by avulsive (flood) events and the post depositional alteration and weathering of such deposits creates varied, often complex, geological architecture (Behrensmeyer 1987; Brown & Kraus 1987, Farrell 1987, Sinha & Friend 1999). The alluvial overbank sequence comprising the upper Orangia Terrace at Erfkroon is no exception. Two prevailing yet opposing interpretations regarding the history of pedogenesis within the study area demonstrate the nature of this complexity (refer to Tooth et al. 2013; Lyons et al. 2014; Bousman & Brink 2014). However, both interpretations (The Single Terrace Accretionary Hypothesis and the Multiple Terrace Allostratigraphy Hypothesis) are based on information provided by a single profile exposure; a relatively narrow perspective when the spatial extent and variability of Erfkroon's terrace systems are considered. Description and analysis of five profile exposures in this study allows for a more comprehensive look into pedogenic and lithostratigraphic relationships at Erfkroon and enables inter and intra-profile comparative analyses between multiple geoproxy datasets. Ultimately, results of these analyses provide the foundation for a higher-resolution characterization of the Orangia Terrace's alluvial sequence, while offering additional, clarifying insights regarding pedogenic relationships, stable geomorphic intervals, and phases of sedimentation.

Accretionary Hypothesis v. Allostratigraphy Hypothesis: Review & Expectations

The Tooth and Lyons Single Terrace Accretionary Hypothesis identifies four paleosols within Erfkroon's primary overbank sequence. The model asserts that paleosol formation is the result of ongoing pedogenesis interrupted rarely or occasionally by slowly accreting sedimentation. It implies that enhanced pedogenic development in

buried horizons is a function of paleoclimate (higher moister regimes and rainfall patterns) rather than a function of time. Bousman and Brink's Multiple Terrace Allostratigraphy Hypothesis alternatively argues for periodic intervals of geomorphic stability (stable land surfaces) interrupted by events facilitating erosion and redeposition of sediments. They argue enhanced pedogenic development within buried horizons are a function of time and coincide with time transgressive intervals of soil formation, which may correspond to periods of paleoclimatic change but not necessarily so. Their model implies that sedimentation and resultant pedogenic development occurred during prolonged periods of geomorphological stability. In either case, validation of the respective models would necessitate the presence of certain patterns, or expectations, within geoproxy datasets representative of the Orangia Terrace sequence. Table 7.1 provides a list of expectations regarding evidentiary patterns in the proxy data that would be considered in support of the accretionary versus allostratigraphy models.

Table 7.1. Summary of Expectations: Accretionary Hypothesis v. Allostratigraphy Hypothesis.

Accretionary Hypothesis	***Allostratigraphy Hypothesis***
Presence of complete pedons.	Incomplete pedons.
Gross morphological identification of buried A-horizons.	Missing/Eroded A-horizons.
Diffuse/gradual contact between bounded horizons within a complete pedon/weathering profile.	Clear/abrupt contact between vertically bounded horizons.
Vertically consistent parent material; textural changes associated with successive pedogenic development (clay illuviation).	Inconsistent parent materials, abrupt textural changes associated with temporally disparate sedimentation or pedogenic episodes between vertically bounded horizons.
Gradual fluctuations in magnetic susceptibility between vertically bounded horizons.	Abrupt changes in magnetic susceptibility between vertically bounded horizons.
High magnetic susceptibility values coincide with horizons containing redoximorphic features (features indicative of increased rainfall/moisture regimes).	Higher magnetic susceptibility values correlate with greater pedogenic development (function of time) in an incomplete, buried sequence.
Continuous pedofeatures between bounded horizons identified as a buried, successive pedons.	Discontinuities in pedofeatures between vertically bounded horizons identified as paleosols.

Accretionary Hypothesis expectations. Slow, progressive pedogenesis provides the foundation for Tooth and Lyons' accretionary model and derives from Tooth's identification of four paleosol sequences in the upper Orangia Terrace overbank deposits (Tooth et al. 2013). This description, founded on a lithostratigraphic conceptual framework, assumes that sedimentation and pedogenesis occurred relatively simultaneously, and that parent material remained mineralogically homogenous over time. Processes such as developmental upbuilding or cumulic soil formation would coincide with specific depositional characteristics made manifest in the geoproxy data.

Validation of the Accretionary model would first require the identification of four buried paleosols as complete solums within the overbank sequence; all horizons, including the uppermost A-horizon of each pedogenic interval would need to be present. Second, from a magnetic susceptibility standpoint, magnetic values would be expected to rise and fall with respect to soil horizonation. If Tooth and Lyons' interpretations are accurate, values would be enhanced in A-horizons as these tend to accumulate biogenic magnetic particles. Susceptibility values would then be expected to gradually decrease with respect to eluviation (leached) horizons stratigraphically below, followed by another gradual increase in susceptibility associated with clay illuviation in lower B-horizons. Another gradual decline would be expected among the lowest horizons which are typically comprised of less pedogenically altered parent material.

Third, gross morphological and micromorphological characteristics of B-horizons in the Red Paleosol as defined by Tooth et al. (2013) would need to exhibit features indicative of higher moisture regimes consistent with the Lyons et al. (2014) enhanced

rainfall model. Specific characteristics would include higher concentrations of redoximorphic pedofeatures observed in thin section.

Finally, it would be expected that vertically bounded horizons visually characterized as the same pedogenic sequence would contain continuous micromorphological pedofeatures and exhibit expected c/f related distribution transformations down profile. For instance, Stoops et al. (2010b) find that pedogenic alteration of quartz dominated, sandy and silty parent materials in pedogenically related horizons will undergo specific microstructural changes down profile. When fine fraction materials are added to a soil's parent material as a function of pedogenic weathering, coarse and fine fraction spatial relationships tend to follow a specific progression. Stratigraphically higher, less pedogenically weathered surface horizons typically exhibit enaulic c/f related distributions. As weathering advances, sub-surface horizons tend to give rise to chitonic or gefuric, followed by porphyric c/f related distributions. Increasingly advanced stages of weathering, particularly with respect to enhanced fine fraction illuviation down-profile in sub-surface B-horizons, tend to produce increasingly spaced apart distributions once the porphyric phase is reached. In these scenarios, single-spaced porphyric often gives rise to double-spaced porphyric distributions (Chadwick & Nettleton 1994; Stoops et al. 2010a).

Allostratigraphy Hypothesis expectations. Bousman and Brink's (2014) allostratigraphic interpretation of the Orangia Terrace overbank sequence implies pedogenic events were buried and, in some cases, truncated and modified via pedogenic overprinting and diagenetic processes. Instead of four complete soil pedons, they identify one complete pedon, and a paleosol displaying evidence for truncation prior to burial in

the Red unit, where B-horizons are all that remain. Unconformably bounded pedogenic intervals that formed in sediments of varying age are the results of these processes.

Validation of Bousman and Brink's (2014) allostratigraphic model would be possible if certain patterns emerged from the geoproxy data. From a gross morphological perspective, it would be expected that buried soils, if any, would be truncated. Missing A-horizons would be indicative of this scenario. If horizons were missing, visually clear or abrupt boundaries marking said unconformities would also be expected. From a micromorphological perspective, atypical microstructural progressions would also be expected. Inconsistencies between parent material composition might also be observable if two horizons are unconformably bound. Differences, if any, would be observable in thin section and among particle size results.

Discontinuous pedofeatures from one horizon to the next would also be expected if two horizons were separated by an unconformity. For instance, microlaminations of temporally discrete clay illuviation events might occur in one horizon, but not among stratigraphically higher, bounding horizons. Inherited pedofeatures from an unrelated pedogenic interval from above might also occur; this might manifest as vertically illuviated particles in separation planes and voids from an above horizon no longer present. With regards to Bousman and Brink's suggestion that redeposition of previously, pedogenically altered sediments occurred after the Red Paleosol truncation event, horizons above and/or below the unconformity might exhibit evidence for disruption or mixing.

From a magnetic susceptibility perspective, high frequency-dependent susceptibility values would be expected of B-horizons containing illuviated clays. The

presence of redoximorphic features, while capable of strengthening soil magnetism, would not necessarily drive magnetic enhancement. When compared from a spatial perspective, magnetic susceptibility fluctuations might also form laterally traceable patterns across the landscape, and any "peaks" would likely correspond with advanced pedogenic development (as indicated by relatively high DDS and DDS% scores).

Bousman and Brink (2014) also argue that Tooth and Lyons' OSL ages for the overbank sequence are not necessarily representative of soil formation and periods of geomorphic stability. Because they view pedogenesis at Erfkroon as time-transgressive, the age of sedimentary units providing the parent material for pedogenic intervals says little about the age of said intervals themselves. Only two pedogenic phases are identified in their model which implies OSL dates correspond with phases of sedimentation antecedent to prolonged periods of stability. Because sediments are mixed and varied across the landscape, Bousman and Brink suggest they make for ineffective, confusing chronological markers. Instead, they suggest that periods of non-sedimentation, traceable across the landscape as allostratigraphic unconformities, make for more accurate temporal markers.

Pedogenic & Lithostratigraphic Interpretations

Dominant pedogenic and sedimentary relationships within and between profiles at Erfkroon were characterized by comparing multiple, profile-specific data sets. Holistic analysis of these data, which included magnetic susceptibility analysis, particle size analysis, gross morphological profile description, micromorphological analysis, and degree of development scoring revealed five overarching patterns: (1) Zones with relatively high $\chi_{fd\%}$ values tend to coincide with fine-textured matrices, (2) zones

producing higher DDS% scores tend to coincide with high $\chi_{fd\%}$ values and fine fraction-dominant matrices, (3) enhanced low-frequency (χ_{lf}) susceptibility values occur in zones with relatively low DDS% scores, (4) $\chi_{fd\%}$ values "peak" in zones producing relatively high DDS% scores, and (5) visually clear and abruptly bounded horizons coincide with abrupt changes in $\chi_{fd\%}$ and in some cases, dramatic textural fluctuations.

The above observations suggest there is a correlation between enhanced magnetic susceptibility values, relatively high degree of development scores, and higher percentages of fine fraction. The relationship between high $\chi_{fd\%}$ values and relatively high DDS% suggests higher ratios of moderate-sized SP grains tend to occur in zones exhibiting B-horizon characteristics. I infer, therefore, that soil magnetism is largely driven by advanced pedogenic development. Additionally, both conditions tend to occur in zones comprised of fine matrices, a characteristic associated with clay illuviation. These patterns substantiate field characterizations of buried B-horizons across the study area, which are indicative of advanced pedogenic development associated with periods of geomorphic (land surface) stability. The question then becomes, what contextual, pedogenic, and sedimentological relationships do periods of soil formation share with bounding horizons?

The presence of buried, stable geomorphic surfaces has important paleoenvironmental and archaeological implications. The preservation state of past surfaces imparts information about the contextual integrity and nature of the environment during which the soil was formed and/or altered. The same features can also speak volumes about the preservation of archaeological materials, but also contextualize paleoenvironmental conditions associated with evidence for human occupation. A buried

surface signifies a period of landscape stability, but also instability— when the geomorphic surface of a soil becomes truncated and/or buried. Intervals of instability can be initiated by a variety of events including drought, flooding, fire, or glaciation (Catt 1990). Such events are catastrophic in the sense that they change the landscape, but preserved evidence for said changes provide clues regarding periods of environmental instability. Buried and/or truncated soils are evidence for dynamic landscape change and may shed light on what environmental pressures, if any, would have impacted human populations at the time. At Erfkroon, Bousman and Brink (2014) have noted differences with respect to the spatial distribution of sites and technological changes between MSA assemblages and those of the Early LSA and LSA. Discerning whether periods of instability coincide with these patterns is important for understanding the complex relationship between paleoenvironmental change and the trajectory of human adaptation from the terminal Pleistocene into the Holocene.

The following interpretations regard a pedogenic sequence as incomplete if no associated A-horizon was identified stratigraphically above a buried pedogenic interval (B-horizon). Missing horizons imply removal by an external force— erosion via fluvial or aeolian processes being the most plausible in the study area. The contact between stratigraphically bounded horizons were therefore determined unconformable if multiple characteristics in the following list were observed: (1) vertically bounded horizons share a visually clear or abrupt boundary, (2) mass-specific frequency-dependent susceptibility values suddenly fluctuate between two vertically bounded horizons, (3) differences in micromorphological c/f related distributions coincide with b-fabric differences in vertically bounded horizons, (4) gross morphological/micromorphological pedofeatures

are discontinuous between vertically bounded horizons, and (5) pedogenic discontinuities coincide with a lithological discontinuity identified via particle size analysis and inert component comparisons of skeletal data (clay-free sand and silt).

Profile 1 Interpretations

Profile 1 consists of an AB-CB-2Bkt-2Bw-3Btss-3Bw1-3Bw2-3Bw3-3Bw4-3Bk/C-3C sequence. Field description and comparative analysis of geoproxy datasets reveal patterns consistent with unconformable boundaries and three episodes of pedogenic development (see Figure 7.1). The Surface Pedon refers to the youngest phase of pedogenesis, forming an AB-CB sequence. This reflects active pedogenic deformation occurring at the modern surface in zones 1 and 2. The Surface Pedon unconformably bounds the second phase of pedogenic development at a lithological and pedogenic discontinuity separating zones 2 and 3. This is called Paleosol 1, a truncated 2Bkt-2Bw sequence that occurs in zones 3 and 4. Paleosol 1 forms in its own sedimentary unit bracketed by lithological discontinuities LD2 and LD3 (see Figure 7.2). Paleosol 1 unconformably bounds the second buried pedogenic phase, Paleosol 2, below. This forms a 3Btss-3Bw1-3Bw2-3Bw3-3Bw4-3Bk/C-3C sequence in zones 5 through 11. Evidence suggests Paleosol 2 formed in 3 texturally unique sediments separated by 2 lithological discontinuities (LD4 and LD5). Refer to Figure 7.1 for an illustration of the profile with modified horizon nomenclature and unconformable boundaries, and Figure 7.2 for an inert-component line plot illustrating the stratigraphic context of lithological discontinuities.

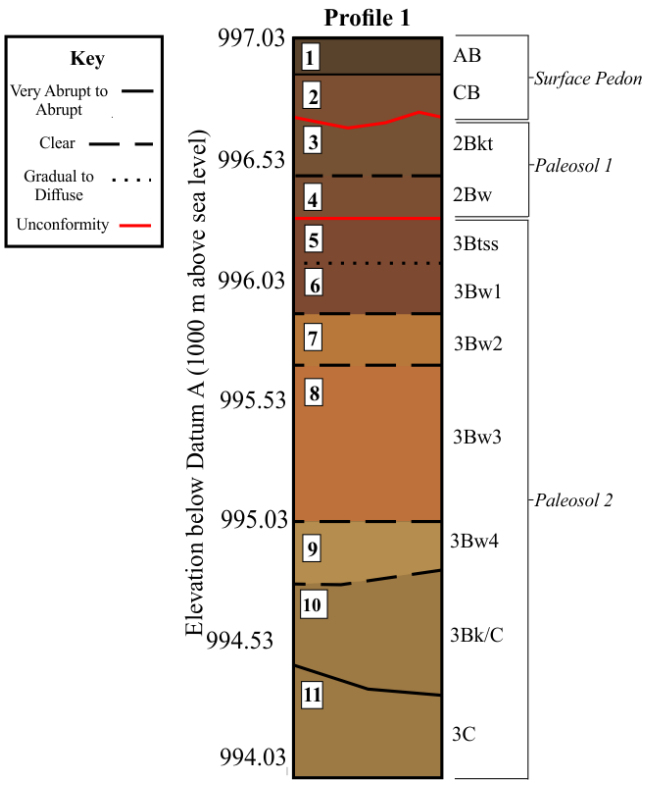

Fig. 7.1. Profile 1 interpretive illustration with unconformable boundaries. Three pedogenic sequences are observed: (1) The Surface Pedon, (2) Paleosol 1, & (3) Paleosol 2.

Surface Pedon. The Surface Pedon refers to pedogenic development occurring in modern surface sediments comprising zones 1 and 2. These form an AB-CB pedon and the youngest, active [modern] phase of pedogenesis observed in profile. The sequence is characterized by ped development in modern aeolian sediments that have begun to alter a finely laminated, fluvial sedimentary unit comprising Zone 2. The Zone 2 deposit contains many fine and very fine sandy and silty laminae bounded by very thin clay drapes consistent with sheet wash. While laminae can be clearly seen in profile, they are disrupted by vertically penetrating ped development from the surface horizon. The lower boundary of Zone 2 is unconformable with the upper boundary of Zone 3, representing a pedogenic and lithological discontinuity between the Surface Pedon and Paleosol 1 (see LD2 in Figure 7.2).

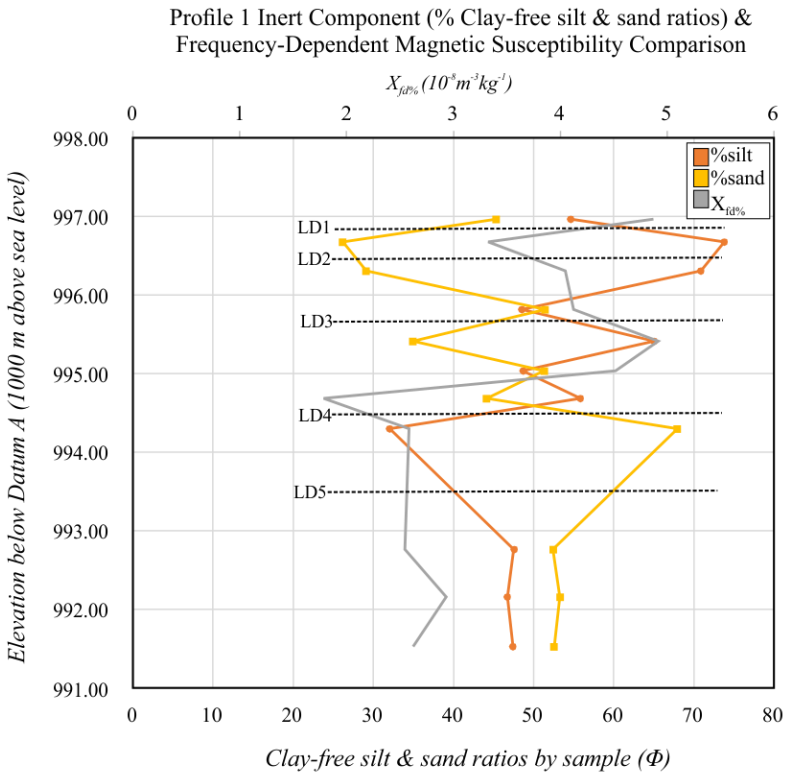

Fig. 7.2. Profile 1 inert-component comparison of clay-free sand and silt-sized particle ratios by zone. Dotted lines approximate locations of lithological discontinuities (LD1-5).

Paleosol 1. Paleosol 1 refers the youngest buried phase of pedogenesis in Profile 1. It consists of a truncated 2Bkt-2Bw sequence in zones 3 and 4, and is unconformably bounded by the Surface Pedon above and Paleosol 2 below. The first (youngest) unconformity is indicated by an abrupt boundary separating this pedogenic sequence from the Surface Pedon. Disparate gross morphological characteristics between bounding zones, patterns observed among magnetic susceptibility and particle size data, and observations of a missing A-horizon support this interpretation. These data further suggest the boundary was created by an erosional event that removed the paleosol's surface horizons prior to burial. The presence of a second unconformity separating Paleosol 1 from Paleosol 2 is indicated by similar patterns in the geoproxy data, with the

addition of micromorphological characteristics also indicative of an unconformable boundary.

Because of the missing A-horizon in Paleosol 1, a pedogenically weathered sub-surface B-horizon helps to form an abrupt boundary with a significantly less altered CB horizon forming the base of the Surface Pedon. The abruptness of this contact is a condition of markedly different pedogenic weathering characteristics and differences in parent material composition between the two bounding zones; Zone 2, the lower aspect of the Surface Pedon, and Zone 3, the upper aspect of what remains of Paleosol 1. Zone 2 is characterized by sandy, friable peds altering finely laminated sands and silts. This zone sits abruptly on top of the dense, rubified, clay-rich Bkt-horizon in Zone 3. Morphologically, Zone 2 represents a slightly modified C-horizon, and Zone 3 resembles a pedogenically developed, argillic, B-horizon.

Inert-component analysis, a comparison of clay-free sand and silt populations between parent materials, illustrates clear textural differences between matrices comprising zones 2 and 3. Such differences are characterized as lithological discontinuities, indicating separate episodes of sedimentation provided a unique parent material for each soil formation interval. Textural, rather than lithological discontinuities are common among fluvial environments where sediments vary with respect to speed and rate of deposition, rather than mineralogical composition. “LD2” in Figure 7.2 illustrates the lithological discontinuity separating the Surface Pedon from Paleosol 1 below. The difference between the two zones is further accentuated by their respective magnetic susceptibility values. Zone 2 yields a relatively low frequency-dependent susceptibility measurement ($\chi_{fd\%}$ value of 3.33), while Zone 3 produces a higher value ($\chi_{fd\%}$ value of

4.044). Coupled with advanced pedogenic weathering characteristics observed in Zone 3, magnetic enhancement in this aspect of the profile appears to coincide with clay illuviation; a distinct feature of a well-developed B-horizon. Similar discrepancies in texture and morphology help to validate the presence of a second unconformity separating Paleosol 1 from Paleosol 2 below.

Paleosol 2. Paleosol 2 represents the second and oldest buried pedogenic phase in the sequence. Paleosol 2 extends from Zone 5 to the base of the profile in Zone 11, forming a 3Btss-3Bw1-3Bw2-3Bw3-3Bw4-3Bk/C-3C sequence. Like Paleosol 1, Paleosol 2 is missing an A-horizon and the combined body of geoproxy data suggests Paleosol 2 was truncated via erosional processes prior to burial. Zones 5, 6, and 7 are all that remain of the paleosol's near surface horizons. These are characterized as B-horizons as indicated by their well-developed, angular blocky and prismatic ped structures comprised of rubified silty loam and varying degrees of Stage I and II carbonate development (Soil Survey Staff 2013). The paleosol's lower horizons (zones 8-11) are characterized by discernably less pedogenic development, and tend to display progressively more C-horizon characteristics down-profile. Variability of sedimentary characteristics portrayed in lower zones of the paleosol coincide with suspected lithological discontinuities. These separate the Paleosol 2 sequence into chronologically older sedimentary units, suggesting its pedogenic formation interval occurred after multiple phases of sedimentation. Patterns among particle size and magnetic susceptibility data suggest Paleosol 2 developed in three lithologically unique parent materials differentiated by texture rather than mineralogy (see LD4 and LD5 in Figure 7.2).

The upper aspect of Paleosol 2 is separated from Paleosol 1 at an unconformable boundary between zones 4 and 5. Differences with respect to matrix particle size ratios, pedogenic development, micromorphological characteristics, and magnetic susceptibility values between the two zones supports the presence of a pedogenic and lithological unconformity.

First, from a gross morphological perspective, no discernable A-horizon in Paleosol 2 suggests the sequence is only partially represented by its sub-surface B-horizons, the first of which is characterized as a pedogenically advanced Btss-horizon in Zone 5 (B-horizon with increased presence of illuviating clays and vertic slickenside features). Zone 5 shares a visually clear boundary with the lowest horizon in Paleosol 1, a Bw-horizon, made apparent by their disparate morphologies. Unlike the strong, prismatic ped structures characterizing Zone 5, Zone 4 consists of relatively weakly defined subangular blocky peds with little to no differentiation, and shows little evidence for clay illuviation. Second, textural data suggests bounding zones are comprised of different parent materials. Zone 4, the latter aspect of Paleosol 1, consists of a predominantly sandy matrix comprised of 41.1% sand, 38.8% silt, and 20.1% clay (refer to Appendix E and Figure 7.3). This stands in contrast to the predominantly silty matrix comprising Zone 5 which contains 50.6% silt, 27.2% clay, and 22.2% sand.

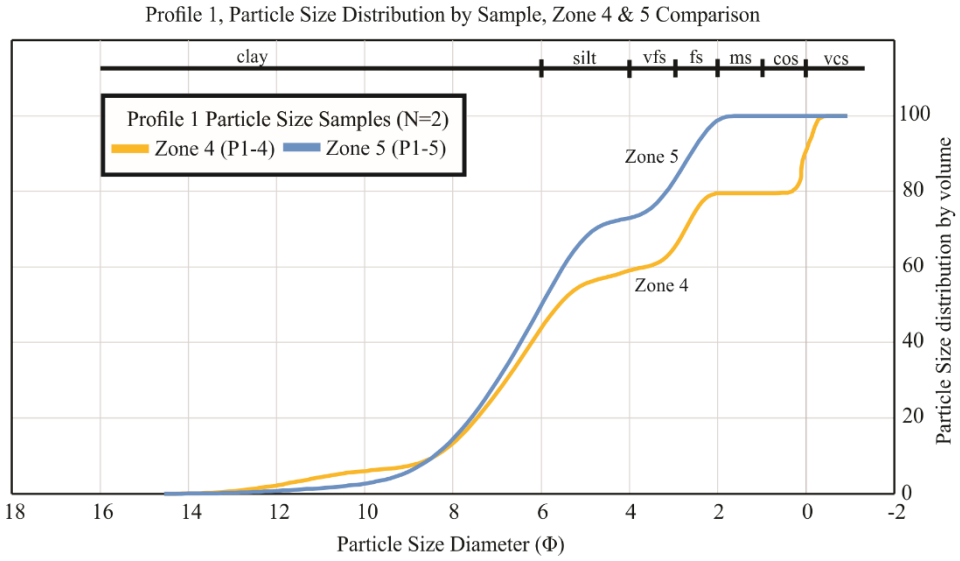

Fig. 7.3. Profile 1 particle size distribution by sample, Zone 4 & 5 comparison. Sand, silt and clay amounts are calculated as percent of total sample volume. Abbreviations: vfs= very fine sand, fs=fine sand, ms=medium sand, cos=coarse sand, vcs=very coarse sand.

Parent material is often best preserved in a soil's coarse fraction, therefore, coarse fraction characteristics such as clay-free ratios of sand and silt particulates, and physical characteristics of matrix particles such as shape, size, and relative mineralogy, can be used to trace parent material continuity from one horizon to the next (Stoops et al. 2010a). Therefore, in addition to textural analysis, parent material differences were further evaluated via thin section analysis, and various comparative analyses using inert-component, magnetic susceptibility, and degree of development data.

Thin sections prepared from the Zone 4-5 boundary revealed differences with respect to c/f related distributions, particle size, and mineral composition between the two zones (see Figure 6.2 and Table 6.2). Zone 4 was primarily comprised of sub-angular to sub-rounded fine to medium sand-sized quartz with gefuric to close-porphyric c/f related distributions. Alternatively, Zone 5 was dominated by very fine sands and silts that formed single- and double-spaced porphyric c/f related distributions. Coarse fraction

ranged from sub-angular to angular in shape. While both zones were dominated by quartz, Zone 5 contained higher ratios of very fine sand- and silt-sized feldspars than Zone 4.

Other micromorphological differences were noted with respect to b-fabric and pedofeatures. The fine fraction in Zone 4 was comprised of light-yellow clays and very fine silts, and exhibited a stipple-speckled, calcareous and undifferentiated b-fabric. Some granostriation suggestive of clay illuviation was observed along coarse fraction, but was not a dominant b-fabric characteristic. This contrasts with the dark yellowish-brown to reddish-brown clays and stipple-speckled, parallel striated, and in places, heavily granostriated b-fabric observed in Zone 5. Zone 5 also contained an abundance of disorthic FeMn nodules and well-oriented clay coatings and infillings.

Zone 4's calcareous b-fabric, combined with observations of carbonate hypocoatings along channels and voids, are indicative of pedogenic development in arid and semi-arid conditions (Kovda & Mermut 2010; Khün et al. 2010). Relatively weak pedogenic development and generally sandier, subangular and subrounded coarse fraction observed in thin section may also reflect an aeolian derived parent material that was altered during the formation interval of Paleosol 1. Alternatively, Zone 5's clay-rich fine fraction and heavily granostriated b-fabric is consistent with advanced clay illuviation and persistent shrink-swell action; typical characteristics of vertisols which are known to form in seasonally wet-dry, savannah-like climates (Weider & Yaalon 1982; Seghal & Stoops 1972; Courty 1990; Monger et al. 1991). An abundance of disorthic FeMn nodules in Zone 5 are also indicative of fluctuating oxidation and reduction conditions

typical in climates with wet-dry seasonality (Schwertmann & Fanning 1976; Vepraskas 2015).

Texturally driven differences were also observed between the two paleosols (refer to Figure 7.2). The lithological discontinuity indicated by LD3 in Figure 7.2 occurs at the boundary between zones 4 and 5. This comparison, which removes mobile clay-sized particles out of the particle size datasets, illustrates a fluctuation from a heavily silt-dominated parent material in Zone 5 to one comprised of relatively equal parts sand and silt in Zone 4. This would suggest that Paleosol 1 and the upper horizons of Paleosol 2 are comprised of texturally unique parent materials.

Relatively advanced pedogenic development in Paleosol 2 subsides at the boundary between zones 7 and 8, where strong ped development and the presence of clay illuviation features in Zone 7 abruptly give rise to a similarly rubified, but more massive, heavily bioturbated horizon in Zone 8. This occurs in tandem with a fluctuation in susceptibility enhancement, where Zone 7, producing a relatively low $\chi_{fd\%}$ value of 1.79 increases to 2.58 in Zone 8 (refer to Appendix E). The slight increase in susceptibility into Zone 8 may reflect slightly higher percentages of SD particles associated with unique parent material mineralogy or texture size, rather than pedogenic development. A matrix particle size comparison between the two zones suggests Zone 8 is comprised of a texturally unique matrix from Zone 7. Figure 7.4 demonstrates that fine silt and very fine sand makes up the majority of Zone 7's matrix, while a predominantly sandy matrix comprises Zone 8. Zone 8's texture is similarly differentiated from zones 9 through 11, suggesting Zone 8 is comprised of its own parent material, representing a separate phase of sedimentation altogether.

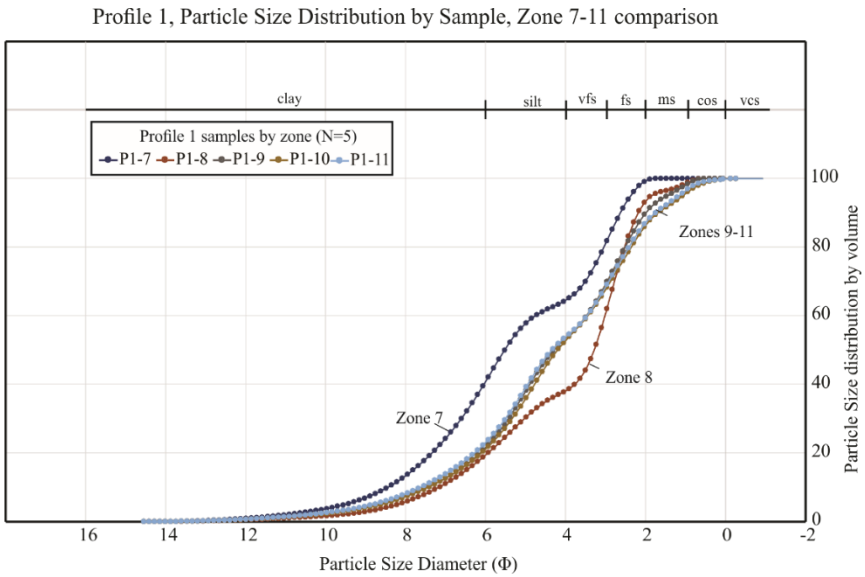

Fig. 7.4. Profile 1 particle size distribution by sample, Zone 7-11 comparison. Sand, silt and clay amounts are calculated as percent of total sample volume. Abbreviations: vfs= very fine sand, fs=fine sand, ms=medium sand, cos=coarse sand, vcs=very coarse sand.

Zones 8 through 11 form the latter, less pedogenically weathered aspect of the Profile 2 sequence. In addition to LD4 separating Zone 8's lithology from Zones 5-7 above, LD5 separates Zone 8 from zones 9-11. Zones 9-11 collectively form the stratigraphically oldest, least pedogenically weathered sedimentary unit in Paleosol 2. Gross morphological observations combined with comparative analyses among geoproxy datasets suggest zones 8 through 11 maintain pedogenic continuity with the upper horizons of Paleosol 2, but represent discrete intervals of sedimentation prior to Paleosol 2's development interval. As illustrated in Figure 7.4, the Zone 8 matrix is dominated by very fine and medium sands (62.3%), while zones 9-11 are composed primarily of silts, showing very little deviation among their respective silt particle size ratios (Zone 9= 42.80%, Zone 10=42.07%, and Zone 11= 64.4%). Only subtle differences were noted

with respect to degrees of pedogenic development, where differing scores appear to be driven by the relative abundance of calcium carbonate from one zone to the next. In the absence of micromorphological samples representative of zones 8-11, textural differences between parent materials are determined to be lithological (textural) rather than pedogenic in origin. Taken in context with stratigraphically higher lithological discontinuities, it appears at least three phases of sedimentation occurred prior to the onset of the Paleosol 2 formation interval.

Interpretations of the Profile 2 Complex

Profile exposures 2A, 2B, and 2C correlate with the Dating Profile previously described by Tooth et al. (2013) and Bousman and Brink (2014). Inter and intra-profile analysis of geoproxy data sets accompanied by field observations led the identification of three pedogenic phases. Rather than use previous lithostratigraphic terminologies developed by Tooth et al. (2013) and implemented by Bousman and Brink (2014), new descriptive names are used to avoid confusion between these and previous interpretations. From stratigraphically youngest to oldest, pedogenic phases are named the Surface Pedon, Paleosol 1, and Paleosol 2 (see Figure 7.5). Refer to Table 7.2 for a comparison between pedogenic unit designations assigned in this study, and litho- and allostratigraphic units assigned by Tooth et al. (2013) and Bousman and Brink (2014).

The oldest pedogenic phase, Paleosol 2, is visible to some degree in all profiles, but is best represented in Profile 2B as a 3Bs-3Btk1-3Btk2-3Bkt/C1-3Bkss/C-3Bkt/C2-3BwC sequence that formed in multiple sedimentary units. Paleosol 2 is unconformably bounded by Paleosol 1 above at a lithological and pedogenic discontinuity. Paleosol 1, the stratigraphically younger of the two buried pedogenic phases, is best represented in

Profile 2A where it forms a 2ABt-2Btk-2Bkt-2Bk-2Bts-2Bt1-2Bt2-2Bt3 sequence. The Paleosol 1 formation interval occurred in at least two different parent materials. The upper boundary of Paleosol 1 terminates just below the surface at a second unconformable boundary. This is shared with the lower boundary of the Surface Pedon which forms an A-AC sequence and represents the youngest, active pedogenic phase in profile (see Figure 7.5).

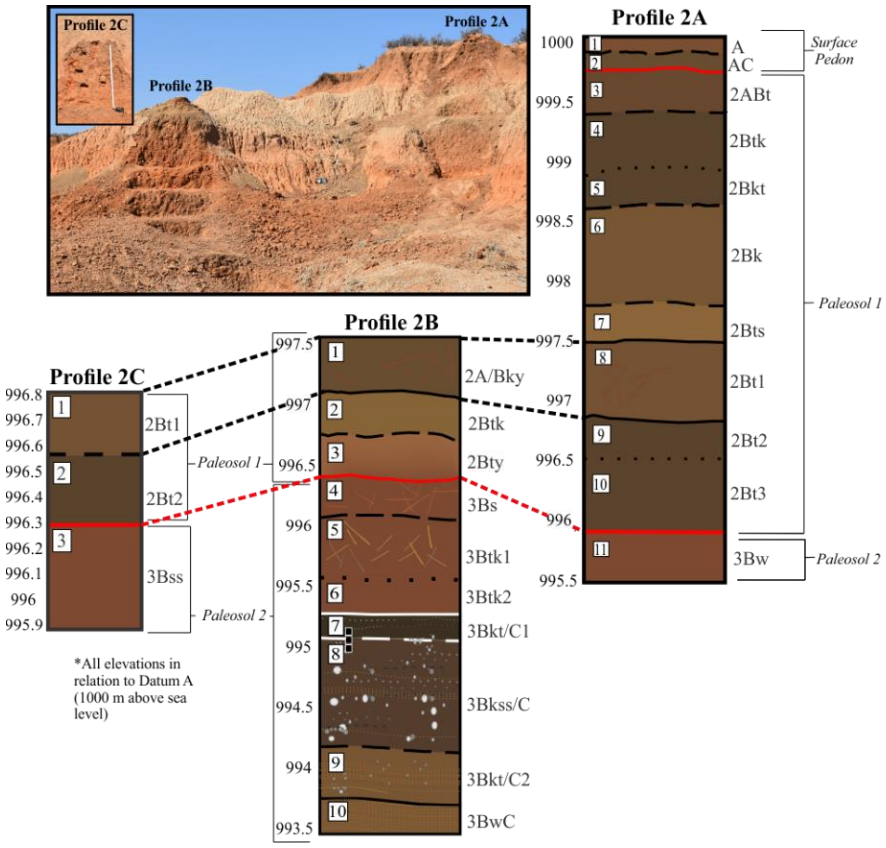

Fig. 7.5. Profile 2 Complex interpretive illustration. Three pedogenic sequences are recognized: Surface Pedon, Paleosol 2, & Paleosol 3. Dotted lines approximate connections between laterally correlated horizons in profiles 2A, 2B and 2C. Red lines indicate pedogenic unconformities. One succession of numeric prefixes is utilized to demonstrate lateral continuity between horizons.

Patterns observed in the geoproxy data suggest six lithological discontinuities (LD's) occur in the Profile 2 complex. This implies sedimentation episodes occurred prior to major pedogenic weathering phases. LD's are numbered 1 through 6 in stratigraphic order of appearance and are summarized in Figures 7.6, 7.7 and 7.8. Each figure illustrates the approximate location of LDs among plots comparing inert, clay-free sand and silt-sized particle ratios by sample, with corresponding frequency-dependent susceptibility values. Also refer to Table 7.3 for a summary of LD's by profile, and their respective stratigraphic zone correlations.

Table 7.2. Comparison of current & previous interpretations of the Profile 2 Complex and Dating Profile. Profile 2 Complex is synonymous with the Dating Profile locale. Bold solid lines mark unconformable boundaries and thin solid lines indicate lithological discontinuities. Arabic numerals designate pedogenic discontinuities. Designation of master and subordinate soil horizons conform to standards published in the *Soil Survey Manual* (Soil Survey Staff 2012). Highlighted regions correspond with Tooth et al. (2013) lithostratigraphic nomenclature, and perforated boxes encompass Bousman & Brink's (2014) allostratigraphic unit designations.

Current Study Interpretations						Previous Dating Profile Interpretations	
Profile 2 Complex						*Tooth et al. (2013)*	*Bousman & Brink (2014)*
Profile 2A						Lithostratigraphy	Allostratigraphy
Zone	*Horizon*						
1	A					Sandy Cap	AU 1
2	AC						
3	2ABt					Brown Paleosol	
4	2Btk						
5	2Bkt						
6	2Bk	**Profile 2B**		**Profile 2C**			
7	2Bts	*Zone*	*Horizon*	*Zone*	*Horizon*		AU 2
8	2Bt1	1	2A/Bky	1	2Bt	Upper Grey Paleosol	
9	2Bt2	2	2Btk	2	2Bt		
10	2Bt3	3	2Bty				Red Sandy Loam
11	3Bw	4	3Bs	3	3Bss		Red Paleosol
		5	3Btk1			Red Paleosol	
		6	3Btk2				
		7	3Bkt/C1				
		8	3Bkss/C				AU 3
		9	3Bkt/C2			Lower Grey Paleosol	
		10	3BwC				

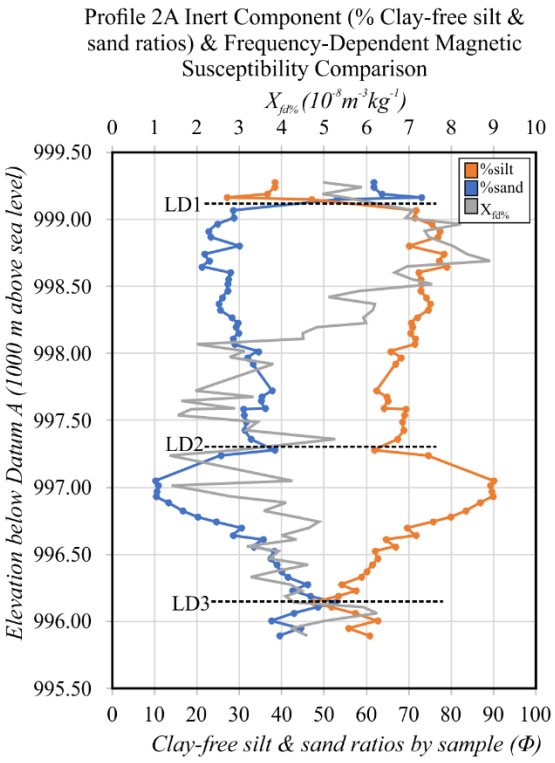

Fig. 7.6. Profile 2A inert component (% clay-free silt and sand) & frequency-dependent magnetic susceptibility comparison by sample. Lithological discontinuity (LD) marked by dotted lines.

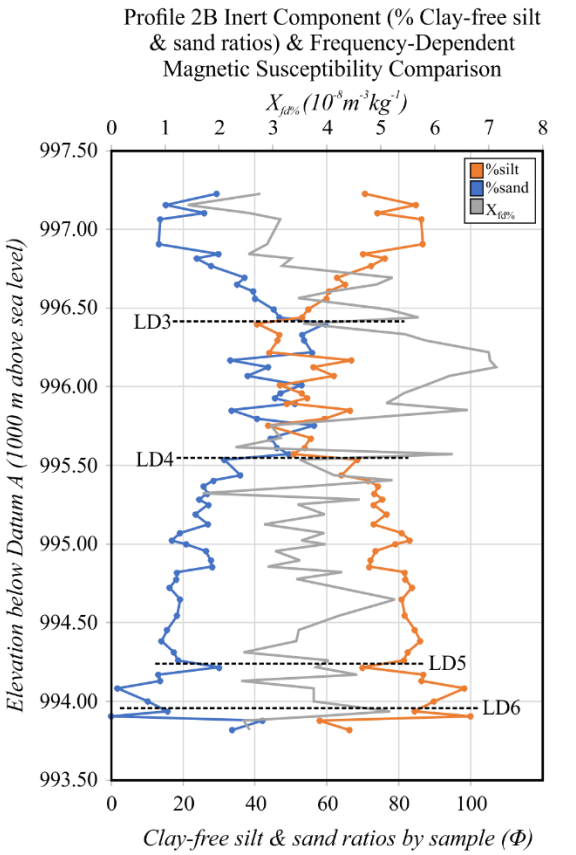

Fig. 7.7. Profile 2B inert component (% clay-free silt and sand) & frequency-dependent magnetic susceptibility comparison by sample. Lithological discontinuity (LD) marked by dotted lines.

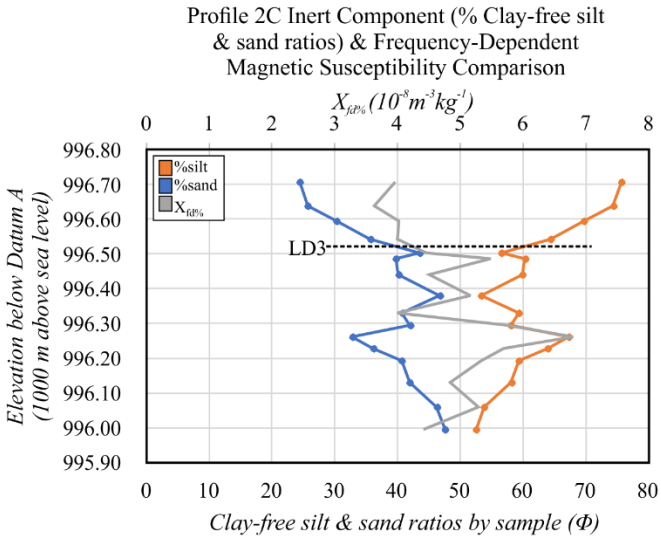

Fig. 7.8. Profile 2C inert component (% clay-free silt and sand) & frequency-dependent magnetic susceptibility comparison by sample. Lithological discontinuity (LD) marked by dotted line.

Table 7.3. Profile 2 Complex lithological discontinuities (LD1-LD6). Approximate stratigraphic context corresponds with zone boundaries.

Lithological Discontinuity (LD)	Pedogenic Discontinuity Present?	Approx. stratigraphic context by Profile		
		2A	*2B*	*2C*
1	Yes	Zone 2/3	n/a	n/a
2	No	Zone 7/8	n/a	n/a
3	Yes	Zone 10/11	Zone 3/4	Zone 2/3
4	No	n/a	Zone 5/6	n/a
5	No	n/a	Zone 8/9	n/a
6	No	n/a	Zone 9/10	n/a

Surface Pedon. The Surface Pedon, only observed in Profile 2A, refers to the youngest pedogenic unit in the Profile 2 complex. This refers to a complete A-AC pedon (zones 1-2) of aeolian origin that continues to undergo pedogenic alteration along the surface. The unit forms most of the modern surface across the study area and conforms with the Tooth et al. (2013) "Sandy Cap" and Bousman and Brink's (2014) AU1. The unit is actively weathering into an A-horizon in Zone 2, but terminates at an unconformable boundary with the top of a well-developed, clay- and organic rich ABt-horizon that forms the stratigraphically highest (youngest) zone of Paleosol 1.

Paleosol 1. Paleosol 1 is visible to some degree across all three profiles, but is best represented in Profile 2A as a 2ABt-2Btk-2Bkt-2Bk-2Bts-2Bt1-2Bt2-2Bt3 sequence (zones 3-10). The paleosol is unconformably bounded by the Surface Pedon above and Paleosol 2 below. Stratigraphically, this sequence corresponds with Tooth's Brown Paleosol and the upper aspect of the Red Paleosol, and Bousman and Brink's AU2 (refer to Table 7.2). Gross morphological observations, magnetic susceptibility analysis, and micromorphological observations indicate this sequence represents one pedogenic weathering interval that occurred within at least two older sediments lithologically differentiated by texture.

The upper aspect of Paleosol 1 (2ABt-2Btk-2Bkt-2Bk-2Bts, zones 3-7) is generally well-preserved and consists of near surface horizons containing many oxidation features and those indicative of clay illuviation. These appear to have formed in a silty loam parent material that becomes finer (siltier) in conformably bounded B-horizons comprising the latter half of the sequence (2Bt1-2Bt2-2Bt3). All B-horizons exhibit varying degrees of carbonate development and evidence for advanced clay illuviation.

Inert component analysis of clay-free sand and silt-sized particle ratios were plotted with frequency-dependent susceptibility values to elucidate, if any, changes in lithology within the Paleosol 1 sequence. This comparison revealed a potential lithological discontinuity between zones 7 and 8 (refer to LD2 in Figure 7.6). The sample population associate with zones 3 through 7 in Profile 2A consist of a relatively sandy matrix. A sudden change in slope indicating a difference in texture occurs between this sample population and those comprising zones 8-9. The sand dominant parent material in Zone 7 and above suddenly becomes silt dominant within Zone 8.

Gross morphological characteristics are also suggestive of a lithological difference between the upper and lower horizons in Paleosol 1. For instance, Profile 2A's Zone 7 and Zone 8 share a visually abrupt boundary made apparent by differing ped structures, and to some extent, matrix color. The Zone 8 matrix is comprised of a finer, more calcareous matrix than Zone 7. This corresponds with an acute fluctuation from low and high susceptibility values at the 7-8 boundary. That said, an overarching decline in magnetic enhancement from stratigraphically higher horizons (Zone 7 and above) into Zone 9 is consistent with pedogenic correlation between the zones. The area of susceptibility "chatter" appears to be driven by the presence of distinct oxidation features

such as FeMn nodule accumulations, ferriargillans, and clay cutans along ped faces observed in Zone 8. The increased presence of these features also drives Zone 8's comparably high DDS% value.

Textural discontinuities are not uncommon among fluvial settings where changes in depositional energy within the same sedimentological regime are known to occur (Soil Survey Staff 2010). The presence of a discontinuity in Paleosol 1 suggests there were two intervals of sedimentation prior to pedogenic development. The first [oldest] sedimentary unit observed in Profile 2A occurs between LD3 and LD2 and provides the parent material for zones 10 through 8. The latest [youngest] sedimentary unit occurs between LD2 and LD1 and comprises the parent material for zones 7-3.

Evidence suggests the two sedimentation episodes occurred in relatively rapid succession prior to the Paleosol 1 formation interval. This is suggested by the succession of pedogenic development observed down profile from the upper aspect of Paleosol 1 in Zone 3, to the base of the sequence in Zone 10. The Paleosol 1 sequence follows an expected developmental trend down profile. The upper A and B-horizons exhibit advanced pedogenic weathering characteristics, while the lower horizons (Zones 9 and 10) exhibit less pedogenic development consistent with less modified C-horizons (that manifest as weak Bt-horizons today). This would suggest that any geomorphic stability to occur after the first sedimentation event was not long enough to facilitate pedogenic weathering prior to the second.

That said, it is possible Zone 8 (the top of the first sedimentation episode) was once exposed to the surface prior to burial, in which case, it may represent a brief period of stability. This might account for the magnetic susceptibility "chatter" observed at the

7-8 boundary. The upper aspect of Zone 8 could represent a biomantle that became buried, then welded to a later pedogenic phase. A welded paleosol refers to a shallowly buried soil that becomes pedogenically overprinted by a downward developing soil phase (Ruhe & Olson 1980). Though no thin section representative of the zone was created, micromorphology would be an effective method for identifying, if any, characteristics indicative of prior pedogenic development and/or soil welding at the LD2 boundary.

As previously mentioned, Paleosol 1 is unconformably bounded by Paleosol 2 at a pedogenic and lithological unconformity. This unconformity coincides with LD3 as marked in Figures 7.6, 7.7, and 7.8. In Profile 2A, the unconformity occurs between Zone 10 (2Bt3), the final horizon in Paleosol 1, and Zone 11 (3Bw), the upper aspect of Paleosol 2. In Profile 2B, the same unconformity occurs between zones 3 and 4 (2Bty-3Bs), and in Profile 2C, between zones 2 and 3 (2Bt-3Bss) (see Figure 7.5). The unconformity is best represented in Profile 2B, but visual acuity of the boundary is most clearly observed in Profile 2C. Here, the unconformity can be viewed at high resolution on individual ped structures (see Figure 7.9).

Profiles 2B and 2C, exposed just east of 2A, provide views of the terrace's lower horizons and a clear view of the hypothesized discontinuity between the lower boundary of Paleosol 1 and the top of erosionally truncated Paleosol 2. Profile 2B forms a 2A/Bky-2Btk-2Bty-3Bs-3Bkt1-3Bkt2-3Bkt/C1-3Bkss/C-3Bkt/C2-3BwC sequence. This exposure provides a clear view of the unconformity separating Paleosol 1 (2A/Bky-2Btk-2Bty) from the Paleosol 2 sequence below (3Bs-3Bkt1-3Bkt2-3Bkt/C1-3Bkss/C-3Bkt/C2-3Bw/C). Stratigraphic elevations associated with the Paleosol 2 sequence coincide with Tooth's Red and Lower Grey Paleosols, and Bousman and Brink's AU3.

Fig. 7.9. Profile 2C ped structure illustrating unconformable boundary between zones 2 & 3 (Bousman & Brink's hypothesized erosional unconformity at the AU2-AU3 boundary). Note weakly developed, granular structure (Zone 2) abruptly bounding well-developed blocky ped (Zone 3) with visible cutans forming on vertical faces.

Bousman and Brink argue that AU2 and AU3, as defined in their geological interpretation of the Orangia Terrace, are separated by an erosional unconformity that was formed when an erosional event led to the truncation of AU3 prior to its burial. Stratigraphically speaking, this occurs in the upper aspect of the Red Paleosol, at its contact with their Red Sandy Loam unit. They suggest the upper portion of AU3 was quickly reburied by Red Sandy Loam sediments after its truncation. Red Sandy Loam sediments would have effectively capped, then preserved, B-horizons of the Red Paleosol below, and would have provided a portion of the parent material for later pedogenic development associate with the Paleosol 1 formation interval (Bousman & Brink 2014). Thus, according to Bousman and Brink (2014), the AU2-AU3 boundary and vestige traces of the Red Paleosol would represent a temporal gap, or interval of geomorphic stability that facilitated soil development for a prolonged period prior to a major truncation and burial event. Tooth et al. (2013) and Lyons et al. (2014) alternatively suggest the Red Paleosol (all rubified sediments within the overbank sequence)

represents a complete soil pedon that formed in one lithological unit that accreted slowly and consistently over time.

The boundary between Paleosols 1 and 2 stratigraphically conform with Bousman and Brink's erosional unconformity. Their interpretation of the boundary representing an erosional/burial event is supported by geoproxy evidence observed within and between exposures of the Profile 2 complex. The most compelling evidence comes from observed patterns in the magnetic susceptibility and DDS% data, as well as observable differences in grain size populations and micromorphological characteristics between horizons bounding the unconformity.

Frequency-dependent susceptibility fluctuations ($\chi_{fd\%}$) indicative of an unconformity between zones 10 and 11 in Profile 2A form a unique fluctuation pattern also observed in laterally correlating zones in Profiles 2B and 2C. In Profile 2A Zone 10, $\chi_{fd\%}$ generally declines in value from ~270 to ~300 cm below surface. This trend reverses with the onset of Zone 11, where $\chi_{fd\%}$ consistently (with some variation) increases. The same pattern clearly occurs at the Zone 2-3 boundary in Profile 2C, and at the Zone 3-4 boundary in Profile 2B. The most dramatic $\chi_{fd\%}$ fluctuation occurs at the boundary between zones 3 and 4 in Profile 2B (see samples P2B-16 through P2B-20 in Appendix E). Sudden magnetic fluctuations from high to low up profile, and the stratigraphic traceability of this pattern across all three profiles complies with unconformity expectations described in previous sections.

Other proxies demonstrate the lateral continuity of these patterns, all of which conform with those expected to occur at an unconformity. Grain size data presented in a percent-by-volume graph illustrates visible differences between grain size populations

forming zones 10 and 11 in Profile 2A (see Figure 7.8). Zone 10 is primarily comprised of clays and fine silts, where Zone 11 is dominated by very fine and fine sands (a significantly coarser matrix). Similar differences among matrix particle size populations are observed between laterally correlating zones in Profiles 2B and 2C; horizons stratigraphically above the unconformity are comprised of finer parent materials than horizons below (see Figures 7.10, 7.11 and 7.12). Other evidence indicative of a lithological discontinuity includes differences between clay-free sand and silt populations comprising zones 10 and 11 in Profile 2A. Figure 7.6 provides an inert component (clay-free sand and silt ratios) comparison between zone sample populations. Sudden slope change occurs at the junction between zones 10 and 11 (refer to "LD3" in Figure 7.6). The Zone 11 sample population contains a greater sand fraction than the very silt dominant matrix comprising Zone 10.

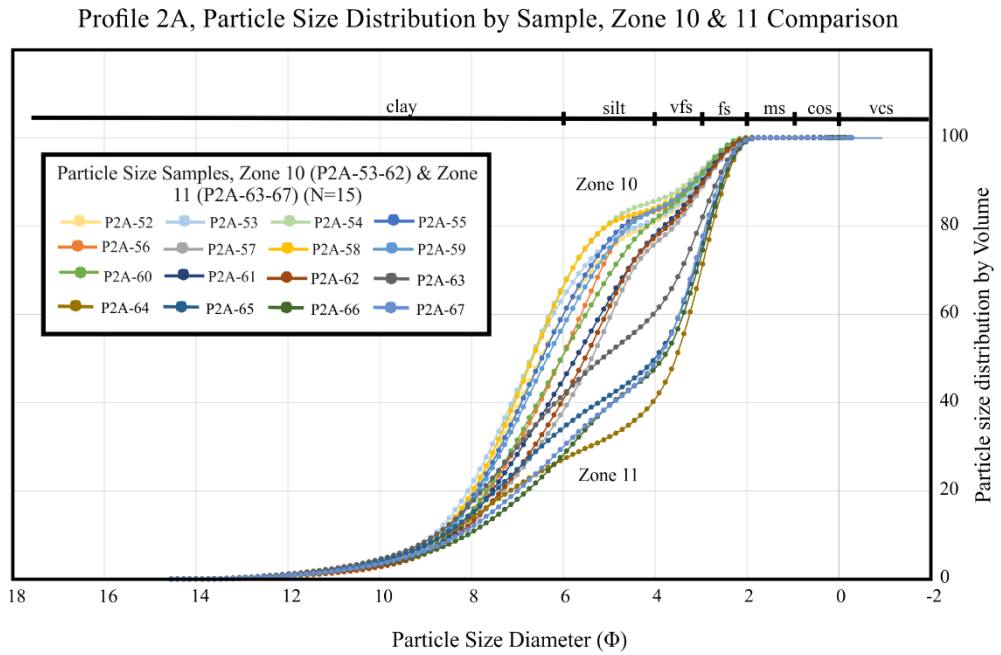

Fig. 7.10. Profile 2A particle size distribution by sample, Zone 10 & 11 comparison. Sand, silt and clay ratios calculated as percent of total sample volume. Abbreviations: vfs= very fine sand, fs=fine sand, ms=medium sand, cos=coarse sand, vcs=very coarse sand.

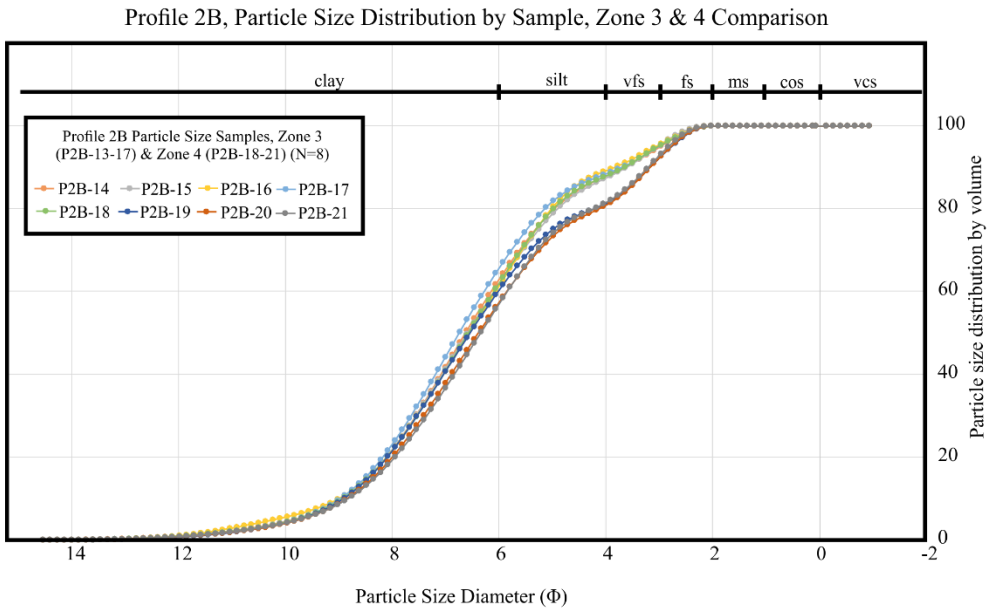

Fig. 7.11. Profile 2B particle size distribution by sample, Zone 3 & 4 comparison. Sand, silt and clay ratios are calculated as percent of total sample volume. Abbreviations: vfs= very fine sand, fs=fine sand, ms=medium sand, cos=coarse sand, vcs=very coarse sand.

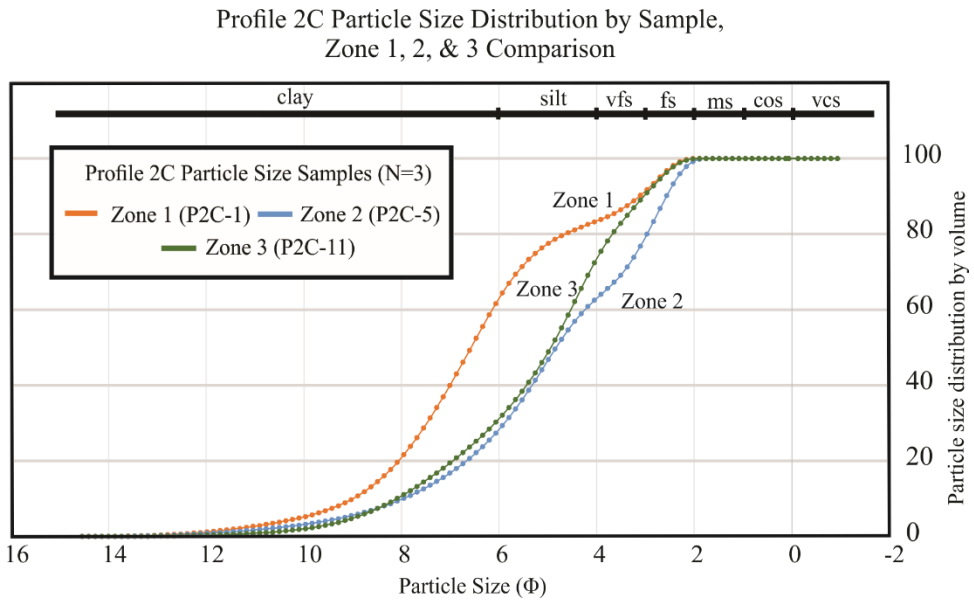

Fig. 7.12. Profile 2C particle size distribution by sample, Zone 1-3 comparison. Sand, silt and clay ratios are calculated as percent of total sample volume. Abbreviations: vfs= very fine sand, fs=fine sand, ms=medium sand, cos=coarse sand, vcs=very coarse sand.

Chadwick and Nelton (1994) report on the typical grainsize evolution associated with weathering sequences observed in profile and suggest certain patterns can be expected between conformable, vertically bounded horizons comprised of the same/similar parent material. The trend is typically associated with a mass transfer from coarse to fine fraction as fine fraction undergoes displacement and illuviation down profile into a forming B-horizon. These trends, observed in thin section, manifest in changes among the c/f related distribution. The typical evolution (enaulic/chitonic/gefuric → porphyric → single/double/open-spaced porphyric) would be expected between Profile 2A zones 10 and 11 if the horizons were conformable and unaffected by disturbances. However, Zone 10 contains an open porphyric c/f related distribution, while Zone 11 ranges from chitonic to close porphyric. This would be considered an atypical progression (refer to Table 6.4 and Figures 6.16 & 6.17).

Disparities in coloration of fine clays and characteristics of b-fabric further differentiate horizons forming the boundary between Paleosols 1 and 2. The lowest horizon in Paleosol 2 is best represented in Profile 2A Zone 10. This contains dark, yellowish-brown clays and granostriated b-fabric with areas inundated by a crystallitic b-fabric consistent with advanced carbonate precipitation. Such features can be associated with prolonged periods of aridity or the combined effect of carbonate formation occurring in an already calcareous parent material (a possible scenario if the parent material was eroded from the petrocalcic horizons of the Erfkroon Terrace then redeposited). Carbonate nodules, albeit few, occur as orthic, embedded features. By contrast, the upper most horizon of Paleosol 2 (Zone 11 in Profile 2A, Zone 4 in Profile 2B, and Zone 3 in Profile 2C), is characterized by a reddish-yellow fine fraction and an undifferentiated b-

fabric with no calcareous element except for a few carbonate hypocoatings around pores and voids (viewed in Profile 2C Zone 3 thin section). Other carbonate features include secondary, rounded disorthic nodules with very sharp boundaries. These may have been introduced from an illuviating horizon above that is no longer represented in profile, or moved into place through bioturbation or mixing. Field inspection of zones forming the upper most horizons of Paleosol 2 were found to be inundated by linear worm channels containing darker red matrix infillings consistent with matrixes of stratigraphically lower horizons. Refer to Figures 6.34 and 6.35 for photomicrographs of zones 2 and 3 in Profile 2C, and Figures 6.16 and 6.17 for photomicrographs of Profile 2A, zones 10 and 11.

Other micromorphological characteristics are indicative of an unconformity at the Paleosol 1-2 boundary. Dislodged, limpid yellow, parallel-striated clay coats occur as intrusive features in the upper most horizons of Paleosol 2. In Profile 2B Zone 4, dislodged, fragmented clay coatings were observed between and superimposed on coarse fraction (refer to Figure 6.22). Clay coats themselves are textural features related to luvisol development (clay illuviation). If found in situ as drapes, infillings, or coatings surrounding coarse fraction, they become suggestive of a well-preserved A-horizon or near surface B-horizon. If disarticulated or dislodged, the same feature can be indicative of a few scenarios, namely, post depositional disturbances, or a feature inherited via illuviation/pedoturbation associated with a bounding near-surface horizon. In the case of depositional disturbance, fragmented features allude to mass transportation and redeposition of an earlier illuvial event (Fedoroff et al. 2010). If clay coatings are inherited, a vertically bounding, near-surface horizon would be expected to contain in situ

versions of the clay coatings, with evidence for illuviation or pedoturbation down profile (Stoops et al. 2010a).

The latter scenario is observed in Zone 4, the upper most preserved horizon of Paleosol 2 in Profile 2B (see Figure 6.22). Clay coats occurring in Zone 4 are fractured, disarticulated and mixed either within the coarse fraction, or as disarticulated features lodged in separation planes and voids. Their color and consistence do not match any in situ pedofeatures. Many of the disarticulated clay coatings are also draped with multiple hypocoating layers. The first (oldest) layer consists of a reddish-brown dusty clay, while the second (younger) layer consists of a dusty, dark gray to grayish-brown clay. It is implied, therefore, that the two superimposed hypocoatings represent at least two younger illuviation intervals, and the limpid yellow coatings themselves derive from an even older vertically bounding, near-surface horizon that would have contained similar pedofeatures. Of the two hypocoatings observed, the outer most (youngest) dusty grayish-brown coatings display coloration and texture similar to the fine fraction observed in Profile 2C Zone 2, and Profile 2A Zone 10 (refer to figures 6.34 and 6.16 respectively). This suggests illuviating clays from the Paleosol 1 pedogenic interval accumulated in the Paleosol 2 horizons below, *after* illuviation of the dusty red clay hypocoatings. The presence of characteristically different, superimposed clay coatings suggests the older, reddish-brown clay coating and the dislodged clay coats themselves derive from an A or near surface B-horizon no longer represented in the Paleosol 2 sequence.

Paleosol 2. Paleosol 2 refers to oldest recognizable pedogenic interval identified in the Profile 2 complex (see Figure 7.5). It is represented in Profile 2A as a single 3Bw

horizon (Zone 11), in Profile 2B as a 3Bs-3Btk1-3Btk2-3Bkt/C1-3Bkss/C-3Bkt/C2-3BwC sequence (zones 4-10), and in Profile 2C as a single 3Bss horizon (Zone 5). The Paleosol 2 sequence appears to represent a truncated soil that formed in previously altered sediments of varying ages.

Previous interpretations place Paleosol 2 in varying lithological contexts. From Tooth and Lyons' perspective, this sequence falls within the lower aspect of the Red and the entirety of the Lower Grey Paleosol. However, they interpret the Lower Grey as lithologically and pedogenically separate from the Red, and as a complete pedon unto itself. Bousman and Brink alternatively interpret the Lower Grey as an extension of the pedogenic sequence also forming the Red Paleosol (AU3); an interpretation consistent with those presented in this study.

Field observations and geoproxy evidence indicate the upper horizons of Paleosol 2 are unconformably bounded by Paleosol 1 above at a pedogenic and lithological discontinuity (LD3) as described in the previous subsection. This unconformity is observable across the Profile 2 complex between zones 11 and 10 in Profile 2A, zones 4 and 3 in Profile 2B, and zones 3 and 2 in Profile 2C. Upper horizons of Paleosol 2 are comprised of a rubified B-horizon sequence that manifest across the Profile 2 Complex as Zone 11 in Profile 2A, zones 4 through 6 in Profile 2B, and Zone 3 in Profile 2C. The lower horizons of the paleosol are comprised of more calcareous, silt-rich parent materials that collectively form a series of B/C-horizons only observed in Profile 2B. In Profile 2B, these occur in zones 7 through 10 (3Bkt/C1-3Bkss/C-3Bkt/C2-3BwC). Field observations and geoproxy datasets further suggest the Paleosol 2 formation interval occurred in at least four unique sedimentary units of older, variable ages. These are

separated by lithological discontinuities (LD3-LD6) primarily differentiated by texture rather than mineralogical composition, but also by brief interludes of pedogenic development. Lithological discontinuities (LD's) in Paleosol 2 are numbered sequentially from youngest to oldest in continuous succession from those observed in Paleosol 1 (refer to Table 7.3 and Figure 7.7).

As previously described, LD3 forms the major unconformable boundary (both lithological and pedogenic discontinuity) separating Paleosol 1 from Paleosol 2. In Profile 2A, this occurs between zones 10 and 11, in Profile 2B, between zones 3 and 4, and Profile 2C, between zones 2 and 3. The three additional lithological discontinuities also occur in Paleosol 2, but are only observed in Profile 2B. These occur at the following boundaries: LD4 between zones 5 and 6, LD5 at the boundary between zones 8 and 9, and LD6 at the boundary between zones 9 and 10 (see Table 7.3). The presence of each discontinuity was determined by the combined results of inert component analysis, field observations, and magnetic susceptibility patterns which collectively suggest textural, rather than mineralogical breaks occur throughout the Profile 2B sequence.

LD4 occurs between zones 5 and 6. This discontinuity separates relatively sandy, rubified sediments between LD4 and LD3 in Profile 2B, from the heavily weathered, clay-and carbonate-rich sand and silt laminae associated with fluvial aggradation in zones 7-10, between LD4 and the base of the profile. Zone 6, a transitional horizon between these disparate sedimentary phases, forms a loamy biomantle that may represent a brief period of non-sedimentation prior to the influx of rubified sediments between LD4 and LD3. Biomantle formation would have occurred only after sedimentary phases between

the base of the profile and LD4 ceased. The horizons between LD4 and LD6 conform with the upper aspect of Tooth's (2013) Lower Grey Paleosol.

Textural differences between parent material above and below LD4 provides the main evidence for a lithological discontinuity, but field observations of unique calcium carbonate features in the same stratigraphic location also allude to a lithological discontinuity. While describing Profile 2B, a thin, horizontal layer (lens) of calcium carbonate nodules was observed at the Zone 6-7 boundary, a few centimeters stratigraphically below the approximated location of LD4. Zones directly below the carbonate lens were silt and clay-rich, forming strongly developed prismatic and blocky ped structures. This contrasted with the slightly finer prismatic peds comprised of sandier matrices in zones 3-5. It is well-known that the precipitation and illuviation of carbonate can be slowed by textural changes (e.g. Buol & Yesilsoy 1964; Stuart & Dixon 1973) (Schaetzl & Thompson 2015). The carbonate lens at the Zone 6-7 boundary may reflect carbonate precipitation during the Paleosol 2 formation interval that was blocked on its way down profile by the sudden textural change at LD4. The carbonate lens is bounded above by the sandy, rubified matrix of Zone 5, and below by heavily weathered, horizontal laminae of sands and fine, subrounded gravels. The sedimentological nature of these laminae are heavily obscured by pedogenic weathering and clay enrichment, which would imply that the carbonate lens itself is a feature of pedogenic overprinting.

Laminae observed in zones 7-8 characterize a relict sedimentary unit that accumulated between LD4 and LD5, prior to the sedimentation event responsible for the sandier parent material found in Paleosol 2's upper horizons between LD3 and LD4. Evidence for intermittent phases of clay illuviation between fine sandy laminae are

visible in thin sections created from zones 7 and 8. Sediments forming the parent material between LD5, LD6, and the base of Profile 2B are markedly sandier than those found between LD4 and LD5 (see Figure 7.8). These contain less modified C-horizon laminae, but also demonstrate evidence for discrete depositional hiatuses and short intervals of pedogenic development like those observed among sediments between LD4 and LD5.

Bulk sample populations extracted from horizons bounding LD6 and LD5 demonstrate dramatic $\chi_{fd\%}$ fluctuations. Sudden magnetic changes are one of the defining characteristics of an unconformity, but in these contexts, likely reflect periodic intervals of sediment aggradation followed by pedogenic development. Micromorphological evidence for clay illuviation observed between finely laminated sands and silts support this interpretation. Laminated sands and silts were found to be separated by fine clay drapes intermingled with clay coatings and infillings throughout zones 10-7 in Paleosol 2. Such pedofeatures, observed between sedimentation phases, suggest polygenetic processes were at work in the Lower Grey, far before Paleosol 2 was formed— dynamic phases of aggradation and pedogenesis were responsible for forming the Lower Grey unit prior to the sedimentation interval between LD4 and LD3 *and* the Paleosol 2 pedogenic interval (refer to Figures 6.25 through 6.27). While the Paleosol 2 formation interval ultimately weathered all sediments in the Red and Lower Grey units, previous, albeit short, intervals of pedogenic weathering in the Lower Grey occurred. This would suggest the Lower Grey is a multiphase soil that was impacted by several pedogenic weathering intervals prior to the prolonged period of stability that facilitated pedogenic development of Paleosol 2.

Profile 5 interpretations

Profile 5 consists of a 2A/Bw-2A/Bt-2A/Bk-2Btk-2Btss-2Bty-2Btky-3Bs-3Btk sequence that is comprised of two pedogenic intervals (see Figure 7.13). The first and youngest interval is referred to as Paleosol 1 which comprises a 2A/Bw-2A/Bt-2A/Bk-2Btk-2Btss-2Bty-2Btky sequence (zones 1-7). Paleosol 1 is perhaps best described as a near surface or exhumed paleosol because modern surface weathering actively alters its upper horizons, infiltrating previously weathered sediments associated with its initial formation. At least one lithological discontinuity (LD1) separating two texturally unique sedimentation intervals occurs in the sequence, suggesting the paleosol formed in sediments of varying ages (see Figure 7.14). Paleosol 1 unconformably bounds the second and oldest phase of pedogenic development known as Paleosol 2 at a lithological and pedogenic unconformity. Paleosol 2 refers to a buried, truncated soil that manifests as a 3Bs-3Btk sequence in zones 8 and 9.

Paleosol 1. Paleosol 1 occupies the modern surface and extends through Zone 7 before terminating at an abrupt, unconformable boundary with Zone 8 (top of Paleosol 2). As mentioned in "Results," the Paleosol 1 sequence occupies what previous interpretations have referred to as the Brown and Upper Grey Paleosols (Tooth et al. 2013; Lyons et al. 2014; Bousman & Brink 2014). Near surface horizons (zones 1-3) appear heavily altered by modern pedogenic weathering while also displaying pedogenically advanced B-horizon characteristics. This is not uncommon for shallowly buried soils which tend to become pedogenically overprinted by active, downward soil development from above horizons. In this scenario, modern aeolian sediments undergoing active pedogenic weathering have become welded to Paleosol 1 such that the

paleosol retains characteristics of its original soil formation interval, while exhibiting A-horizon characteristics. A-horizon features are associated with modern weathering. Clay illuviation from the surface can be seen penetrating voids and obscuring previous episodes of clay illuviation in Figure 7.14.

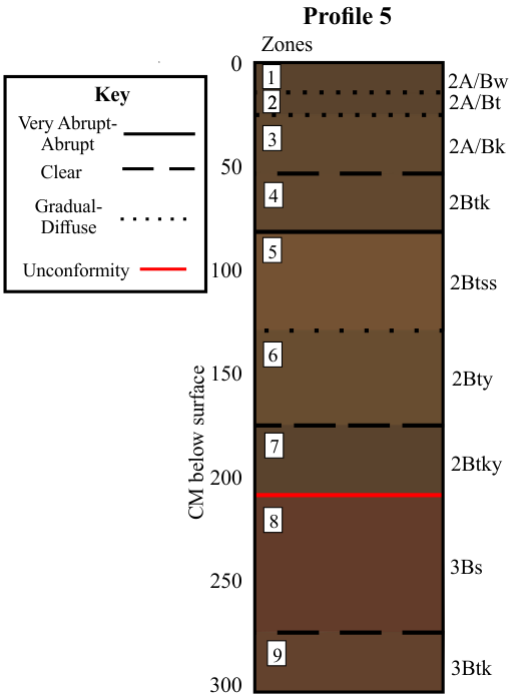

Fig. 7.13. Profile 5 interpretive illustration.

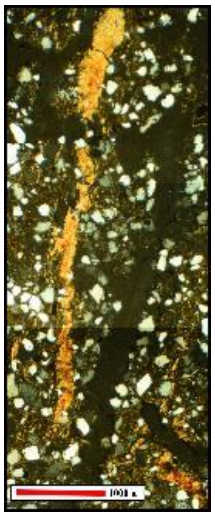

Fig. 7.14. Profile 5, Zone 3 thin section. Limpid yellow, well-oriented clay illuviation infilling voids and creating hypocoats along previously coated coarse fraction (xpl, 40x).

Particle size comparisons between skeletal data suggests Paleosol 1 formed in at least two older sediments. These are separated by one lithological discontinuity (LD1). LD1 is best illustrated by the sudden slope change between zones 4 and 5 in Figure 7.15. The first and youngest sediment provides the parent material for zones 1 through 4 and consists of a relatively sandier matrix than the vertically bounding unit below. Increasingly siltier matrices comprise stratigraphically lower horizons, where the highest silt to sand ratio occurs at the boundary between zones 5 and 6 before transitioning to a

sandier matrix in Zone 7. An abrupt color change is also indicative of an LD at the 4-5 boundary. The upper, near surface horizons of Paleosol 1 are dominated by brown sediments. At the zone 4 and 5 transition, the matrix becomes more carbonate rich; a condition contributing to a shift in chroma between zones. Stand alone, such observations might be considered a pedogenic discontinuity. However, a gradual increase in clay content from Zone 5 into Zone 7, combined with a mutual increase in pedogenic carbonate and advancing degrees of ped development (particularly size and grade) down profile is consistent with a single weathering interval. However, pedogenic progression suddenly stops at the LD2 boundary which coincides with the only unconformity identified in profile. This separates Paleosol 1 from preserved remnants of Paleosol 2 below.

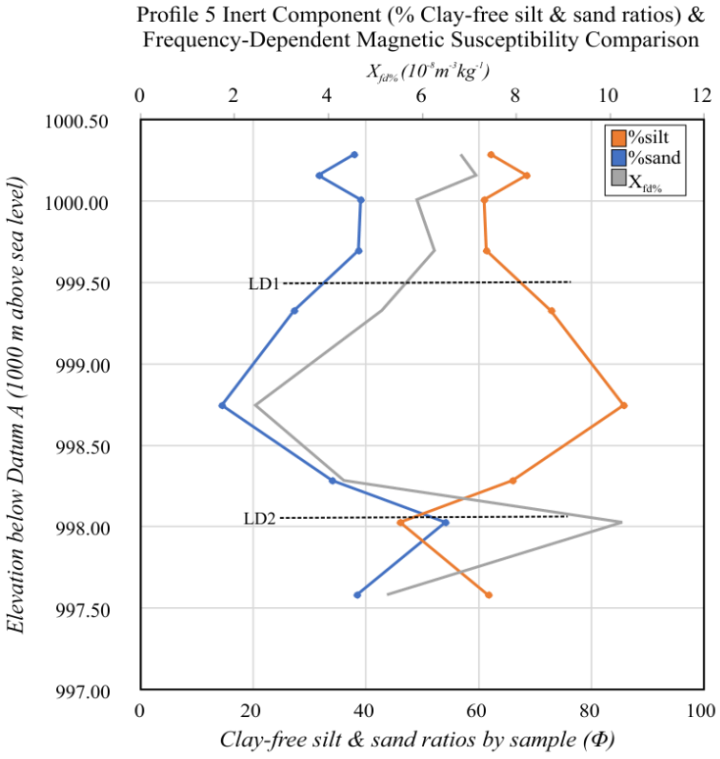

Fig. 7.15. Profile 5 inert component (% clay-free silt and sand) & frequency-dependent susceptibility comparison by zone (N=9). Lithological discontinuities (LD) indicated by dotted lines.

Paleosol 2. Paleosol 2 occupies zones 8 and 9, forming a 3Bs-3Btk sequence. Its upper boundary forms a pedogenic and lithological discontinuity (unconformity) with the base of Paleosol 1. Paleosol 2 is characterized by rubified, loamy sediments that form remnant subsurface horizons of a once complete soil pedon. These are expressed as isolated B-horizons exhibiting accumulations of either illuviated or residual sesquioxides in a distinctively reddish-brown matrix. The presence of black, FeMn oxidation features coating the faces of ped structures suggests the paleosol was affected by fluctuating redox conditions within a relatively long-weathered pedogenic interval. The abruptness of the paleosol's upper boundary (Zone 8) with Paleosol 1 above, in addition to a missing A-horizon in the sequence, suggests Paleosol 2 was truncated then buried by chronologically younger sediments (the sedimentary unit bounded by LD1 and LD2 in Paleosol 1). Erosional truncation, typically an effect of a mass movement event, is indicative of a period of environmental/climatic instability when a once stable geomorphic surface was partially removed or altered prior to burial.

The presence of an unconformity between zones 7 and 8 are supported by other geoproxy patterns. Fluctuating magnetic susceptibility values and discernable differences in parent material composition between zones collectively suggest zones 8 and 9 represent a separate lithological unit altogether. Skeleton particle size data representative of each parent material is presented with frequency-dependent susceptibility results in Figure 7.15. LD2 refers to the lithological discontinuity separating the two paleosols. A textural discontinuity occurs at the Zone 7-8 boundary, where the silt parent material comprising most of Paleosol 1 suddenly transitions to a sandier matrix comprised of

nearly equal parts sand and silt in Zone 8. The same two samples also produce disparaging frequency-dependent susceptibility values, made most apparent by a dramatic low-high value fluctuation.

Magnetic enhancement in Paleosol 1 follows a trend expected of gradual pedogenic enhancement down profile— $\chi_{fd\%}$ values are enhanced in well-developed, near surface B-horizons, then gradually decline as clay illuviation and other advanced weathering characteristics decrease among subsurface horizons. That said, susceptibility values at the LD1 boundary plummet despite associated zones containing pedogenic characteristics indicative of advanced development. Low susceptibility values in this context suggests soil magnetism is driven first by a general decline in magnetically enhanced SD particles in the parent material, more so than expressions of advanced pedogenesis. This is followed by a slight increase in $\chi_{fd\%}$ in Zone 7, then by a significant spike at the LD2 textural discontinuity and unconformity at the Zone 7-8 boundary. This is perhaps another example of magnetic enhancement being driven by parent material and textural change in addition to pedogenic development.

Discussion

Validation of the Tooth and Lyons' Accretionary Hypothesis warrants the application of lithostratigraphic nomenclature in characterizing sedimentary and pedogenic development at Erfkroon. This perspective assumes four complete soil pedons exist in the upper Orangia Terrace and exhibit characteristics indicative of accretionary pedogenic formation; soil cumulation and/or developmental upbuilding being the most likely forms of accretionary pedogenesis to occur in an alluvial context. Their model further implies that soil formation occurred progressively and at a consistent rate over

time. In other words, intervals of landscape stability and sedimentation remained constant enough to facilitate ongoing pedogenesis.

Alternatively, Bousman and Brink's Multiple Terrace Allostratigraphy Hypothesis applies allostratigraphic nomenclature to describe episodic soil formation in sediments of varying ages. Their model alludes to the presence of a dynamic fluvial system at Erfkroon, and relies on the combined presence of lithological and pedogenic discontinuities to assign periods of landscape stability. In the case of the overbank alluvial sequence in the Orangia Terrace, Allostratigraphic Units 1, 2 and 3 coincide with three pedogenic interludes within an otherwise active sedimentary landscape.

While there is some evidence to suggest accretionary pedogenic formation occurred in a few localized cases (Paleosol 2, zones 7-10 in Profile 2B and Paleosol 1; zones 1-3, Profile 5), the vast body of data supports the Allostratigraphic Hypothesis. Periodic interludes of pedogenic development disrupted by phases of sedimentation is made apparent by the identification of only two buried pedogenic intervals within multiple sedimentary deposits.

The two paleosols identified in each profile of this study exhibit commonalities across datasets, enough to argue for lateral continuity among horizons. The most noticeable patterns are illustrated by frequency-dependent magnetic susceptibility values where signature vertical fluctuations associated with Paleosols 1 and 2 occur in similar ways and stratigraphic contexts across profiles. Also significant is the traceability of patterns associated with unconformable boundaries separating the Surface Pedon from Paleosol 1, and Paleosol 1 from 2 (Figure 7.16). Pedogenic and sedimentary intervals

bounded by laterally continuous unconformities are best characterized as allostratigraphic units (Figure 7.17).

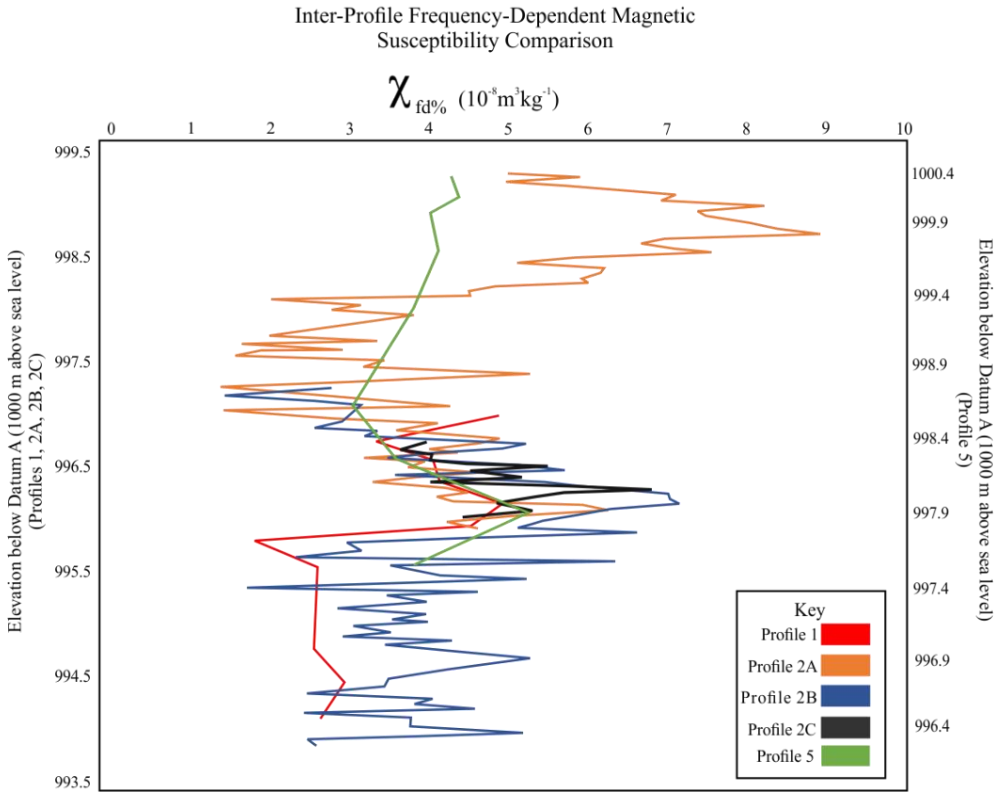

Fig. 7.16. Inter-profile frequency-dependent magnetic susceptibility comparison.

Allostratigraphy & Geochronology

A body of evidence demonstrates the existence of lateral continuity between two unconformably bounded paleosols and one surface pedon in Erfkroon's overbank sequence (see Figure 7.17). The paleosols are comprised of chronologically older and texturally heterogenous sediments, and are traceable across the study area. Each pedogenic interval represents an allostratigraphic unit— bodies of sedimentary rock that are identified and defined by bounding unconformities, where unconformable boundaries represent a land surface modern or otherwise (NASCN 2005).

The Surface pedon represents Allostratigraphic Unit (AU) 1 and conforms with Bousman and Brink's AU1, and Tooth and Lyons' "Sandy Cap". Paleosol 1, a buried paleosol expressed as a full pedon in profiles 2A and 5, as a truncated sequence in Profile 1, and as a partially exposed sequence in profiles 2B and 2C, represents AU2. Paleosol 1 conforms with Bousman and Brink's AU2, but its vertical extent differs from Tooth and Lyons' interpretations. Instead of the Brown, Upper Grey, and Red Paleosols representing individual pedogenic phases, the Brown and Upper Grey, and the upper portion of the Red comprise one pedogenic interval that formed in at least two sedimentary units. Paleosol 2 is observable in lower horizons of all profiles and represents AU3. This conforms with Bousman and Brink's AU3, but differs from Tooth and Lyons' interpretation. Tooth and Lyons identify the Red and Lower Grey units as two separate paleosols. However, evidence suggests the mid and lower aspect of the Red and all of the Lower Grey comprise one major phase of pedogenic development that occurred in multiple sedimentation intervals defined by their own brief histories of non-sedimentation and pedogenic weathering.

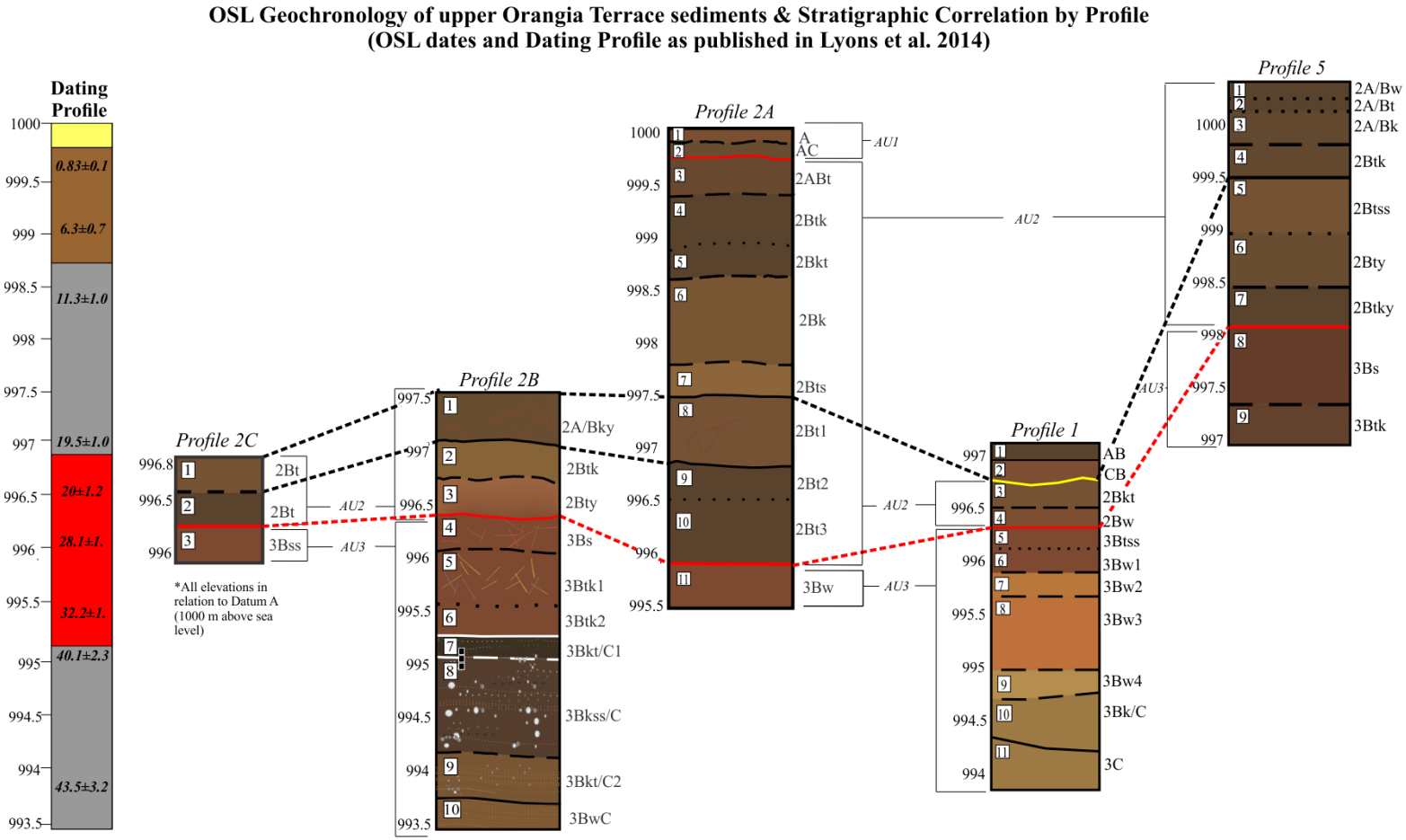

Fig. 7.17. OSL geochronology of the upper Orangia terrace sediments & stratigraphic correlations between profiles. Allostratigraphic units (AU) are indicated by bold red lines, local unconformity is indicated by bold yellow line. Perforated lines approximate lateral correlation between horizons. Dates illustrated in Dating Profile derive from Lyons et al. (2014) and correspond with OSL samples MDER 18-MDER10 in ascending age (43.5 to 0.83 ka).

Geochronology. Chronological contexts for phases of sedimentation, pedogenesis, and erosion at Erfkroon are estimated using Tooth and Lyons' OSL geochronology and some OSL dates published by Bousman and Brink (2014). Sediment ages vary spatially despite similar stratigraphic contexts, further indicating pedogenesis at Erfkroon is time transgressive. OSL assays, sample depths, and lithological and allostratigraphic correlations are provided in Table 7.4.

Table 7.4. Geochronological context of allostratigraphic units, OSL dates as published in Lyons et al. (2014) & Bousman and Brink (2014). Double lines indicate unconformities, dotted lines approximate locations of lithological discontinuities (LD).

Source	Sample	OSL Age	Standard Deviation	Depth (cm)	AU	Litho-nomenclature	Profile/ Area
Bousman & Brink (2014)	11067	0.02	0.03	10	1	Sandy Cap	HistBush
Lyons et al. 2014	MDER 10	0.83	0.09	30	2	Brown Paleosol	Dating Profile
Lyons et al. 2015	MDER 11	6.32	0.67	90	2	Brown Paleosol	Dating Profile
Lyons et al. 2016	MDER 12	11.3	0.98	160	2	Upper Grey Paleosol	Dating Profile
Bousman & Brink (2014)	11057	18.8	1.5	253	2	Upper Grey Paleosol	Upper F
Bousman & Brink (2014)	11058	19.9	1.9	264	2	Upper Grey Paleosol	Upper F
Bousman & Brink (2014)	11059	27.2	1.6	282	2	Upper Grey Paleosol	Upper F
Lyons et al. 2017	MDER 13	19.5	1.04	300	2	Upper Grey Paleosol	Dating Profile
Lyons et al. 2018	MDER 14	20	1.2	340	2	Red Paleosol	Dating Profile
Lyons et al. 2019	MDER 15	28.1	1.93	390	3	Red Paleosol	Dating Profile
Lyons et al. 2020	MDER 16	32.2	1.74	460	3	Red Paleosol	Dating Profile
Lyons et al. 2021	MDER 17	40.1	2.3	490	3	Lower Grey Paleosol	Dating Profile
Lyons et al. 2022	MDER 18	43.5	3.18	620	3	Lower Grey Paleosol	Dating Profile

Paleosol 2 (AU3) consists of sediments spanning 43.5 (MDER18) to 28.1 ka (MDER15). Its lower B/C-horizons represent ~11.5 ka of sedimentation punctuated by short weathering intervals consistent with low to moderate energy stream aggradation. The two oldest sediment units bounded by LD6 and LD5, and LD5 and LD4 were deposited shortly before 43.5 ka, and between 43.5 and 40 ka respectively.

An ~8 ka period between LD5 and LD4 conforms with observations of intermittent soil formation and sedimentation prior to the third and final sedimentation phase bounded by LD4 and LD3, prior to the Paleosol 2 formation interval. The LD4 boundary coincides with a brief period of stasis before being buried then obliterated by advanced pedogenic overprinting after ~32 ka. This pedogenic phase would have been responsible for the development of Paleosol 2, the first of two prolonged periods of stasis (major pedogenic formation intervals in AU2 and AU3). Dates associated with sediments just above and below the AU2-3 unconformity provide an estimate for the actual Paleosol 2 weathering interval. This occurred prior to 20.1 ka but after 28 ka. The ~7.5 ka gap in time between samples likely coincides with the depositional hiatus, when geomorphic stability facilitated pedogenic development prior to the paleosol's truncation and burial.

The first (oldest) sedimentation interval in Paleosol 1 (AU2) occurs between LD2 and LD3. Two dates, 20 and 19.5 ka, represent the age of sediments upon deposition. This suggests Paleosol 2 (AU3) was truncated sometime before 20.1 ka, but was quickly buried as indicated by the close chronological interval associated with the LD2-LD3 deposit. The fine-textured nature of the deposit is indicative of overbank deposition via lateral stream migration. Stratigraphically higher dates of ~11.5 ka suggest sedimentation persisted until the Paleosol 1 soil formation interval. The latest sediment age corresponds

with MDER10 at ~850 years ago, however, the proximity of the sample to the surface may prove misleading. The 6.32 ka date at MDER11 is probably a better estimate, placing the interval of geomorphic stability facilitating Paleosol 1's formation between ~6 ka and 850 years ago.

The unconformable boundary between AU1 and AU2 (the Surface Pedon and Paleosol 1) was created upon burial of the AU2 surface by aeolian sediments. This provides the parent material for the Surface Pedon. A single OSL date of ~20 years old was produced by Bousman and Brink (see Bousman and Brink 2014, Table 2), however, an age estimate of a few hundred years old is more likely. At one site in the study area, Bousman and Brink (2014) report nineteenth century artifacts including European gun flints, Khoi ceramics, and fiber-tempered Bushman pottery eroding from the basal aspect of the Surface Pedon.

OSL dates stratigraphically bracketing allostratigraphic unconformities suggest periods of stability were relatively prolonged, and occurred in the intervening years between sedimentation phases. Comparative review of the OSL chronology also confirms the variability of ages within these sediments, as it appears sediment ages vary across the landscape. As suggested by Bousman and Brink (2014) and Bousman et al. (*in prep*), it has become increasingly clear that periods of geomorphic stability and non-sedimentation make for more accurate temporal markers than the sediments themselves. Interludes of prolonged landscape stability marked by laterally traceable unconformities coincide with a set time interval, variability of sediment phases aside. This alone has important implications with regards to paleoenvironmental and human technological changes mentioned in previous studies.

Paleoenvironmental & Archaeological Implications

All profiles in the study area offer compelling evidence for two major phases of pedogenic development that occurred with the onset of the LGM and late Holocene. In addition, the Profile 2 Complex offers evidence for at least one discrete period of stability that dates to the Late Pleistocene. Each interlude brings with it subtle yet important implications regarding the relationship between paleoclimate and the history of human occupation at Erfkroon. Interestingly, periods of stasis identified in this study correspond with prevailing changes in climate and in some cases, unique, temporally specific human adaptive responses.

Bousman and Brink (2014) conducted soil carbon and nitrogen isotope analyses on samples from several Erfkroon localities over the course of previous investigations. Stable carbon isotope results demonstrated that plant communities fluctuated between C_4 and C_3 communities throughout the alluvial overbank sequence. However, specific fluctuations between photosynthetic pathways were found to occur in certain depositional contexts consistent with intervals of stability. Samples laterally correlating with archaeological contexts or collected from excavation areas also coincide with artifact frequencies that might be indicative of human adaptive responses to regional climate change patterns.

Bousman and Brink's $\delta^{13}C$ results for the Dating Profile were compared with inert-component particle size ratios calculated for Profiles 2A and 2B. A direct comparison was possible because their sample from the Dating Profile (N=15) stratigraphically correlate with horizons identified in this study (Bousman and Brink used the same Datum A to map zone elevations in their description of the Dating Profile). In

graphing these data, Dating Profile sample depths were averaged then plotted with reference to Datum A (1000 m above sea level) (refer to Figure 7.18).

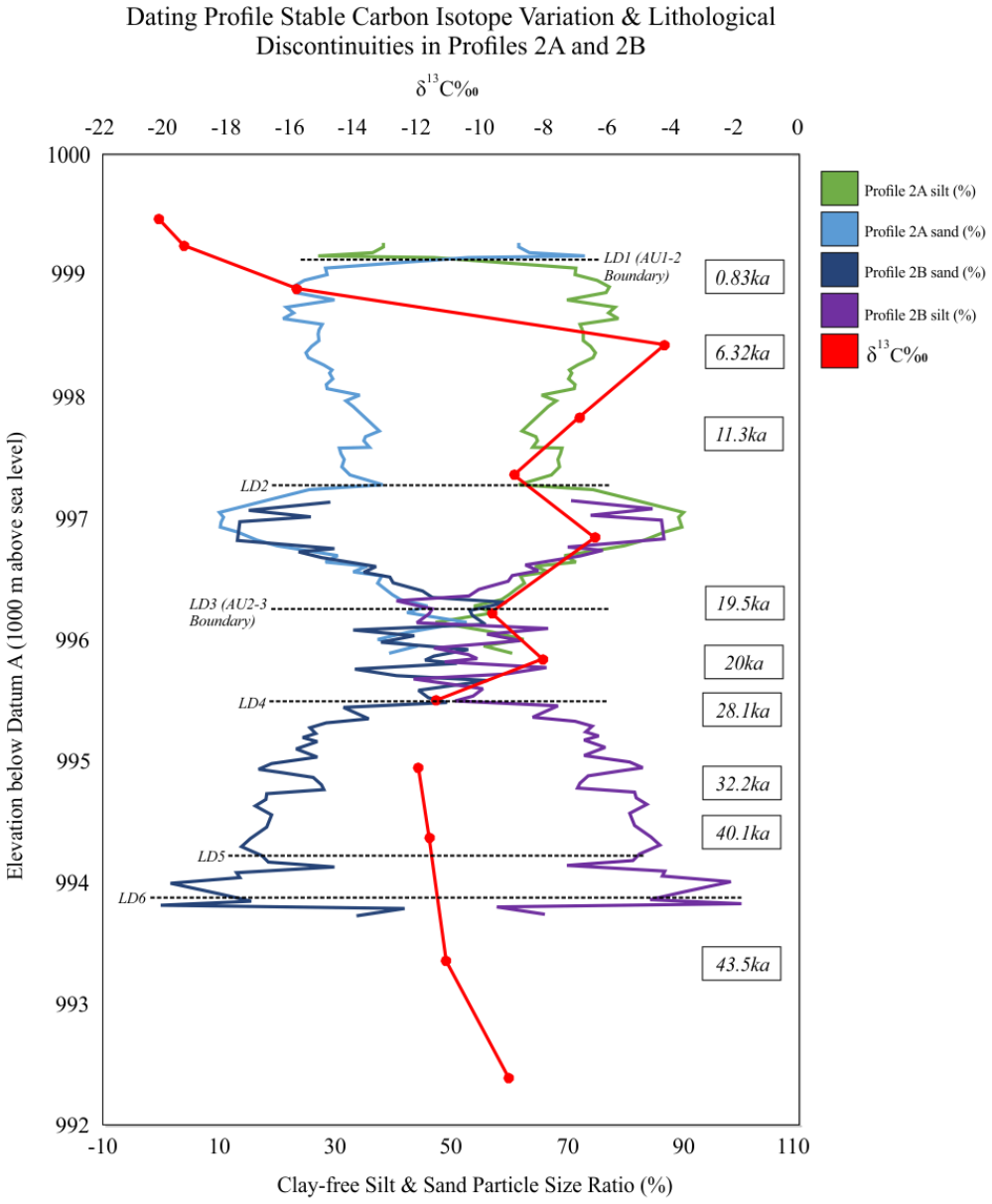

Fig. 7.18. Dating profile $\delta^{13}C$ soil stable carbon isotope results (Bousman & Brink 2014) & inert component comparisons from Profile 2A and 2B. Lithological discontinuities (LD) indicated by black dashed line, Lyons et al. (2014) OSL chronology right aligned.

Late Pleistocene paleoenvironment & archaeology at LD4. Sediments forming the lower horizons of Paleosol 2 in the Lower Grey began accreting sometime before ~43.5 ka (see Lyons et al. 2014). Remnant sedimentary structures within the horizons are characteristic of lateral stream/donga migration. This type of accretion persisted for a few thousand years as demonstrated by Late Pleistocene-age (~43-40 ka) OSL dates associated with the LD6 and LD4 discontinuities in Profile 2B. At LD4, noticeable textural changes and evidence for biomantle formation occurs at the boundary between the Lower Grey sediments and those of the lower Red unit above. Associated horizons (zones 6 and 7 in Profile 2B) offer evidence for at least two phases of illuviation, suggesting a period of non-sedimentation occurred prior to the third sedimentation interval, which was followed by the onset of pedogenic weathering associated with Paleosol 2.

Slight fluctuations from C_4 to C_3 plant communities occurred prior to the depositional event marked by the LD4 boundary in Profile 2B. This suggests there was a period of stasis when temperate climate conditions favored slightly more cool-adapted plant species. Micromorphological observations suggest higher moisture regimes occurred during this phase. Short intervals of standing water or higher water tables are indicated by the prevalence of impregnative FeMn nodules forming within the matrix of Zone 7 in Profile 2B, at the LD4 boundary.

Seasonal rainfall regimes are also a characteristic of vertic environments. High clay content within the upper aspect of the Lower Grey exhibit slickenside structures and clay cutans indicative of shrink-swell processes typical of seasonally enhanced moisture regimes. Also, an extremely slow sedimentation rate of 3.8 cm/1000 years was calculated

between MDER16 and MDER15 (OSL samples at and just above LD4) by Bousman and Brink (2014). This suggests the distinctly vertic features within the Lower Grey began their formation prior to the onset of Paleosol 2's primary pedogenic interval. This stands in contrast to a rate of 38.2cm/1000 years calculated between MDER18 and MDER17, the samples bracketing sediments within the LD6-LD4 boundaries (Bousman & Brink 2014). Sedimentation dramatically slowed at and just after the LD4 discontinuity, suggesting any sediment accumulation was likely worked into the biomantle observed in Profile 2B, Zone 6.

Though no archaeology has been recovered from the Dating Profile or from the Profile 2 Complex, AU boundaries and some lithological discontinuities are traceable across the landscape at known archaeological locales. This appears to be the case for the LD4 boundary identified in Profiles 1 and 2B (refer to Figures 7.20 and 7.21 respectively). As part of their archaeological excavation of Upper F, Bousman and Brink established an OSL chronology for archaeology-bearing sediments and extracted samples for soil stable carbon isotope analyses. The sampled excavation area occurred within a few meters of Profile 1, allowing for correlation between horizons identified in this study, and their Upper F sample locations. Stable isotopes produced from the Upper F locale indicate a shift from C_4 to C_3 plant species leading into the LD4 boundary in Profile 1. Stratigraphically, the LD4 boundary in Profile 1 is laterally consistent with LD4 in Profile 2B. However, it bears mentioning that a facies difference is noted between the two locations with respect to the LD4-LD3 sedimentation interval. A difference in texture and degree of pedogenic weathering between the two locales suggests different

sedimentation energies were responsible for their respective deposition. How these relate from a fluvial geomorphology perspective is beyond the scope of this study.

The stratigraphic context of LD4, now known to represent a period of stability with generally cooler regional temperatures during the Late Pleistocene, correlates with the Lower Grey-Red boundary. The same geological context is associated with an abundance of recovered late MSA artifacts, including many from in situ occupations. Few Early LSA occupations have also been documented, but these occur stratigraphically above LD4 (Bousman & Brink 2014).

Stable carbon isotope values among samples within the Lower Grey, stratigraphically below the LD4 boundary, suggest the prevailing climate accommodated a mixed C_3/C_4 plant community. Many of the older MSA occupations identified at Erfkroon were excavated from these contexts and were characterized by the production of large points constructed from flake blades. Bousman noted that a high percentage of the blades showed signs of unifacial retouch, or resharpening, along one side of the tool. He also found evidence for alternate beveling, a technique where both sides of the tool are alternately sharpened and resharpened presumably to accommodate a hafting component. Alternate beveling is considered a unique characteristic of the MSA assemblage at Erfkroon as such tools are not widely found in the South African archaeological record. In addition, Late MSA 1 occupations were also found to contained large, alternately beveled flake blades with strangulated forms. Perhaps high frequencies of these and other formal tools reflect availability of large game, the prevalence of which was supported by productive floral communities and higher moisture regimes in the paleoenvironmental context prior to LD4 in the Lower Grey.

LGM paleoenvironment & archaeology at AU3. The second interval of stability coincides with the formation of Paleosol 2 in AU3. OSL dates of 28.1 ka and 20 ka (MDER15 & MDER14) correspond with sediments just below and above LD3 (AU2-AU3 boundary). Both dates closely bracket the LGM, which occurred ~25 ka.

Dramatic carbon isotope fluctuations correspond with the Paleosol 2 pedogenic interval. A slight trend towards cooler C_3 conditions at the LD4 interlude suddenly fluctuates to accommodate arid/warm-adapted C_4 species above the LD3 boundary (Bousman & Brink 2014). This occurs during a period of extremely slow sedimentation indicative of the Paleosol 2 weathering/erosional phase (6.2cm/1000 years) (Bousman & Brink 2014). These conditions are supported by the micromorphology. Extremely rubified sediments comprising the b-fabric in thin section samples from the upper aspect of the Red are indicative of warm, dry conditions following a moist interval. Other features such as carbonate hypocoatings along voids are also indicative of fluctuating water tables (Seghal & Stoops 1972). Moisture regimes either became increasingly seasonal, or generally declined at the AU2-3 boundary. Such conditions further suggest that plant communities at Erfkroon were sensitive to paleoclimatic fluctuations since C_3-dominant conditions appear relatively short lived; values trend towards C_4 communities by the onset of sedimentation forming AU2, delaying the onset of the next pedogenic phase (Paleosol 1).

LD3, the boundary between AU2 and AU3, corresponds with a dynamic fluctuation from cool conditions with higher prevailing moisture regimes, towards increasingly arid conditions brought on by the LGM. A dramatic shift in the

technological repertoire among archaeological assemblages also occurs (Bousman & Brink 2014).

Evidence for Early LSA occupations occur in Erfkroon's archaeological record around ~20 ka. Bousman and Brink's (2014) and Bousman's (personal communication 2018) observations of several ELSA locales indicate occurrences postdate Paleosol 2's active phase of pedogenesis. Because these occur in tandem with a warming trend, technological patterns may reflect human adaptive responses to the suite of paleoenvironmental changes characterizing the time interval. This is loosely suggested by Bousman and Brink's statistical comparison of chipped stone characteristics among ELSA and MSA assemblages (see Bousman & Brink 2014).

It was mentioned previously that Erfkroon's MSA assemblages are dominated by points showing evidence for extensive core reduction strategies and modification. This stands in contrast to the relatively expedient, and less carefully prepared tools of the ELSA. At occupations such as Upper F, ELSA assemblages consisted of grinding stones and bipolar flakes (Bousman & Brink 2014). The same tool types have since been observed in similar stratigraphic contexts in other areas (Bousman, personal communications 2018). Experimental recreations of bipolar flakes suggest these may have been used for breaking into marrow cavities of mammal long bones. Bousman and Brink (2014) suggest the practice might explain the prevalence of broken grinding stones, as these may have been used as hammerstones in the marrow extraction process.

That said, the appearance of grinding implements is important unto itself as it suggests a shift towards plant processing at the beginning of the ELSA. Ethnobotanical studies in the Western Free State have demonstrated that few plants are ground for

consumption among local Tswana communities. Instead, the grinding process is reserved for preparation of medicinal plants (Thornton-Barnett 2013). Perhaps, as suggested by Bousman and Brink, the introduction of groundstone into the ELSA toolkit represents increasing reliance on medicinal plants at times of paleoclimatic uncertainty.

Holocene paleoenvironment & archaeology at AU2. The Paleosol 1 formation interval in AU2 occurred after at least two sedimentation events buried the truncated remnants of Paleosol 2. The influx of sediment forming the parent material is predominantly silt, suggesting slow-moving water breached an embankment, depositing very fine sediments. Rates of sedimentation for the first interval bounded by LD3 and LD2 (see Figure 7.18) are the highest calculated for the sequence at 80cm/1000 years (Bousman & Brink 2014). This suggests sedimentation accrued rapidly enough to where pedogenic weathering, if any, was not enough to establish a formal biomantle prior to the final sedimentation event. The second interval accreted significantly slower than the first, averaging 19cm/1000 years (Bousman & Brink 2014). This suggests pedogenic formation likely underwent some degree of upbuilding within the upper horizons of Paleosol 1 (the upper Brown unit). A similar scenario was observed at the Profile 5 locale.

Bousman and Brink's (2014) carbon isotope data shows photosynthetic pathways fluctuated between C_3/C_4 but trended towards C_4 dominant communities up profile in Paleosol 1. The strongest C_4 signature occurs within the upper 3 horizons of the Brown unit. Micromorphological observations associated with the lower horizons of Paleosol 1 contain crystallitic, calcareous b-fabric and extensive accumulations of carbonate as hypocoatings, infillings, and orthic impregnations. Such features coincide with prolonged

periods of aridity (Monger & Daugherty 1991). However, thin section characteristics allude to more seasonality with respect to moisture regimes in Zone 5 and above. Parallel striated clays in the b-fabric are consistent with vertic condition while periods of saturation and/or high water-tables are indicated by FeMn hypocoatings and intrusive FeMn nodule formation (Hseu & Chen 1999; Kyuma 2004).

Daryl Codron in Bousman and Brink (2014) conducted stable carbon and oxygen isotope analyses on a suite of faunal enamels representative of the alluvial sequence. His results also point toward increasing aridity after the LD3 boundary (Red Paleosol). Well-represented grazers such as black wildebeest (*Connochaetes gnou)* demonstrated increasing $\delta^{13}C$ values through the Late Pleistocene. Such species are known for eating a mixed C_3/C_4 diet but relatively higher, and steadily increasing values suggest a growing reliance on arid adapted plants for consumption.

It appears Paleosol 1 formed against a backdrop of fluctuating climatic conditions, so it is not surprising that it contains increasingly dense and varied LSA occupations. The earliest of these coincide with the Robberg (Palmison 2014) industry which is characterized by the production of microlithic blades. At Erfkroon, Robberg assemblages were excavated from the Upper Grey and lower Brown units. The Robberg then gave way to a suite of other technocomplexes including Lockshoek, Wilton, and Smithfield. Palmison (2014) excavated a Lockshoek assemblage in the lower and mid Brown unit. Technological variability within and between these complexes appear to be an expression of human adaptation, and function of a dynamically changing landscape into the Holocene.

Conclusions

The question of lithostratigraphy versus allostratigraphy is central to understanding the interplay between sedimentation and pedogenic weathering among Late Quaternary alluvial architecture in South Africa's continental interior. In exploring the complex overbank alluvium at Erfkroon, it can be demonstrated that allostratigraphic nomenclature is not only applicable, but critical for the accurate interpretation of non-sedimentation intervals. The detailed analysis undertaken in this thesis indicated the presence of multiple sedimentation intervals within single weathering profiles, suggesting breaks in sedimentation (intervals of geomorphic stability) are more accurate temporal markers than the sediments themselves. This condition is expected among time-transgressive pedogenic formation intervals.

The Erfkroon case study demonstrates the efficacy of coupling in-field gross morphological description with multiple lines of pedogenic and lithostratigraphic macro and micro evidence. Magnetic susceptibility analysis, micromorphological analysis, and particle size analysis were useful for the identification of buried pedogenic intervals and phases of sedimentation in otherwise heavily weathered, ubiquitous deposits. Field description also facilitated the comparison of ordinal data to evaluate the relative degree of pedogenic development within and between profiles (degree of development scores). The culmination of data was able to illuminate discontinuities and unconformities, the presence of which guided final interpretations.

In evaluating the Tooth et al. (2013) and Lyons et al. (2014) Single Terrace Accretionary Hypothesis and Bousman and Brink's (2014) Multiple Terrace Allostratigraphy Hypothesis, it was found that two major pedogenic intervals and one

modern interval of soil formation occur in the upper alluvial sediments of the Orangia Terrace. Results ultimately validate Bousman and Brink's Allostratigraphy model, where it was determined that pedogenic phases forming within multiple sediments were best characterized as allostratigraphic units. Three allostratigraphic units were identified, correlating (stratigraphically and spatially) with those previously proposed by Bousman and Brink (2014). In demonstrating the validity of their model, it was also found that localized regions of some study profiles exhibited accretionary pedogenic development, but not to the spatial nor vertical extent that would suggest this type of weathering was a primary driver of pedogenesis through time. Finally, data supports Bousman and Brink's preliminary identification of a brief pedogenic interlude dating to the Late Pleistocene, and an erosional unconformity at the boundary between the two major pedogenic phases dating to the LGM and early Holocene. Results strongly indicate the LGM pedogenic phase was truncated, then buried by rapid sedimentation alluding to increasing paleoenvironmental dynamism in South Africa's continental interior leading into the Holocene.

APPENDIX A: Field Description Form.

Profile: | **Zone #:** | **Photo #'s:**

Horizon: | **Thickness (cm):** | **Matrix Color (moist/dry):**

Consistence

Texture	*Plasticity*	*% gravel*
S COS FS FSL VFSL	po ps	0 <10 10
VFS LCOS LS SIL SCL	p VP	25 30 50
LS LFS CL SICL	Other:	>75 n/a
COSL SL SC SIC C		

Rupture Resistance

Dry	*Moist*	*Cemented*
L S SH	L VRF FR	n/a NC EW
MH HA VR	FI VFI EF	VW W M
EH R VR	SR R VR	ST VS I

HCl response: NE VS; SL ST; VE

Ped Structure

Unit structure	*Size*	*Grade*
gr abk sbk	vf f	0
lp pl wg	m co	1
pr cpr	vc ec	2
sg m n/a		3

Ped. Features

Coats & Films	*Coat distinct.*
CAF SIF CLF	F D P n/a
BRF GBF GYF	*Coat %*
OSF OAF SNF	vf f c
SLF SKF n/a	m vm n/a

Film Distinct.	*Coat Continuity*
F D P n/a	C D P n/a
Film %	*Film Continuity*
vf f c m	C D P n/a
vm n/a	

Stress Features (SF)	*SF Continuity*
PRF SS	P D C n/a
SSG n/a	*SF Loci in Ped*
SF Distinctness	n/a PF BF TF
n/a F D P	TC VF T

Roots/Pores

Root Size
VF F M
C VC n/a

Root Shape: DT IG TU; VE IR n/a

Root Loci in ped: PF BF TF; TC VF n/a

Pore Shape: DT IG TU; VE IR n/a

Root Quant.: f c m n/a

Pore Size: VF F M C VC n/a

Pore Quantity: f c m n/a

Pore loci in ped	*Vertical Continuity*
PF BF TF	Pore: L M H n/a
TC VF n/a	Root: L M H n/a

Other loci
BG BK BR
CC N RF n/a
SS SP SC TR

Redox (RMF) Features: n/a RMX CLD FED FM; JAM MNM FMM FSN FEF; JAN FMN PLN FMC MNF

RMF Shape: CU C D I L; PE P R RO S T n/a

RMF Quantity: f c m n/a

RMF Distinct.: F D P n/a

RMF Loci in Ped: PF BF TF TC VF; BG BK BR CC N; RF SS SP SC TR

RMF Color

Notes:

CaCO3

CaCO3 Dev. Stage
I II
III IV
V VI
n/a

Carbonate Location
PF BF TF TC
VF BG BK BR
CC NO RF SS
SP SC TR n/a

CaCO3 Nod. Shape
CU C D
I L PE
P R RO
S T n/a

Nodule Size
f m c
vc ec
Nodule Quantity
n/a f c m

CaCO3 Filam. Sz.
n/a vf f c
c m
Filam.Quantity
n/a f c m

CaCO3 Concentration Locations

Matrix	*Peds*	*Pores*	*Other*
MAT MAD	BPF MPF	MPO LPO	CRK TOH
MAD MAC	APF HPF	SPO RPO	ARF BRF
TOT n/a	VPF n/a	n/a	SSS ALS n/a

Concentrations

Finely Disseminated
FDC FDS FDG n/a
Masses (noncemented)
BAM CAM GYM CBM
SIM GBM SAM GNM n/a

Other Nodules
OPN ORT
GBN DNN n/a
Other:

Concretions
CAC SIC GBC
TIC n/a
Other:

Crystals
SAX CAX GYX SEC
n/a
Other:

Crystal Quantity
f c m
n/a
Other:

Size: 1 2 3 4; 5 n/a

Color

CaCO3/Concen. Notes

Biological Conc.

Biological Concentrations
DIB RSB FPB SFB ICB
SSB PPB WCB n/a
Other:

Miscellaneous
CBA CBE CAL CAO
CAP CRC n/a
Other:

Bio. Quantity	*Misc. Quantity*
f c m	f c m
n/a	n/a
Notes:	

Sedimentary Characteristics

Bedding
VTNL TNL ML THL
VTHL VTNB TNB MB
THB VTHB n/a

Sorting: 1 2 3 n/a; *Notes:*

Rounding: A SA R SR; n/a; Other:

Zone Boundaries: | *Distinctness* | *Upper: C D G n/a* | *Lower: C D G n/a* | *Topography* | Upper: S W I B n/a | Lower: S W I B n/a

APPENDIX B: Field form gross morphological characteristics, abbreviations & definitions.

Characteristic	Abbreviation	Definition	Data Type	Ranking
Consistence				
Texture	S	sand	nominal	n/a
	COS	coarse sand	nominal	n/a
	FS	fine sand	nominal	n/a
	VFS	very fine sand	nominal	n/a
	LCOS	loamy coarse sand	nominal	n/a
	LS	loamy sand	nominal	n/a
	LFS	loamy fine sand	nominal	n/a
	COSL	coarse sandy loam	nominal	n/a
	SL	sandy loam	nominal	n/a
	FSL	fine sandy loam	nominal	n/a
	VFSL	very fine sandy loam	nominal	n/a
	LS	loamy sand	nominal	n/a
	SIL	silt	nominal	n/a
	SCL	sandy clay loam	nominal	n/a
	CL	clay loam	nominal	n/a
	SICL	silty clay loam	nominal	n/a
	SC	sandy clay	nominal	n/a
	SIC	silty clay loam	nominal	n/a
	C	clay	nominal	n/a
Plasticity	po	non-plastic	ordinal	0
	ps	slightly plastic	ordinal	1
	p	plastic	ordinal	2
	vp	very plastic	ordinal	3
Percent Gravel	0	refers to % gravel within the matrix of given horizon.	ordinal	0
	<10		ordinal	1
	10		ordinal	2
	25		ordinal	3
	30		ordinal	4
	50		ordinal	5
	>75		ordinal	6
Rupture Resistance				
Dry	L	loose	ordinal	0
	S	soft	ordinal	1
	SH	slightly Hard	ordinal	2
	MH	moderately Hard	ordinal	3
	HA	hard	ordinal	4
	VH	very Hard	ordinal	5
	EH	extremely Hard	ordinal	6
	R	rigid	ordinal	7
Moist	L	loose	ordinal	0
	VFR	very friable	ordinal	1
	FR	friable	ordinal	2

	FI	firm	ordinal	3
	VFI	very firm	ordinal	4
	EF	extremely firm	ordinal	5
	SR	slightly rigid	ordinal	6
	R	rigid	ordinal	7
	VR	very rigid	ordinal	8
Cementation	NC	non-cemented	ordinal	0
	EW	extremely weakly cemented	ordinal	1
	VW	very weakly cemented	ordinal	2
	W	weakly cemented	ordinal	3
	M	moderately cemented	ordinal	4
	ST	strongly cemented	ordinal	5
	VS	very strongly cemented	ordinal	6
	I	indurated	ordinal	7
HCl Response				
Effervescence response (Ped face & matrix)	NE	non effervescent	ordinal	0
	VS	very slightly effervescent	ordinal	1
	SL	slightly effervescent	ordinal	2
	ST	strongly effervescent	ordinal	3
	VE	violently effervescent	ordinal	4
Ped Structure				
Unit Structure	gr	granular, small, curved, or irregular faces	nominal	n/a
	abk	angular blocky, polyhedral with faces that intersect at sharp angles	nominal	n/a
	sbk	subangular blocky, planar faces lacking sharp angles	nominal	n/a
	lp	lenticular; lens shaped peds generally parallel to soil surfaces	nominal	n/a
	pl	platy; flat and plate-like	nominal	n/a
	wg	wedge; elliptical interlocking lenses at acute angles, bounded by slickensides	nominal	n/a
	pr	prismatic, vertically elongated unites; flat tops	nominal	n/a
	cpr	columnar; vertically elongated units with rounded tops commonly bleached	nominal	n/a
	sg	no structural units; entirely noncoherent, e.g. loose sand	nominal	n/a
	m	massive; no structural units; material is a coherent mass (not necessarily cemented)	nominal	n/a
Ped Size				
Granular	vf	very fine; <1mm thick	ordinal	0
	f	fine; 1 to <2mm thick	ordinal	1
	m	medium; 2 to <5mm thick	ordinal	2

	co	coarse; 5 to <10mm thick	ordinal	3
	vc	very coarse; >/= 10mm thick	ordinal	4
Columnar/Prismatic/wedge	vf	very fine; <10mm thick	ordinal	0
	f	fine; 10 to <20 mm thick	ordinal	1
	m	20 to <50mm thick	ordinal	2
	co	50 to <100 mm thick	ordinal	3
	ec	greater than or equal to 500 mm thick	ordinal	4
angular/subangular/blocky	vf	<5mm thick	ordinal	0
	f	5 to <10mm thick	ordinal	1
	m	10 to <50mm thick	ordinal	2
	c	20 to <50mm thick	ordinal	3
	vc	>/= to 50 mm thick	ordinal	4
Grade				
	0	structureless; no discrete units observable in place or in hand samples	ordinal	0
	1	weak; units are barely observable in place or in a hand sample	ordinal	1
	2	moderate; units are well-formed and evident in place or in a hand sample	ordinal	2
	3	strong; units are distinct in place (undisturbed soil) and separate cleanly when disturbed	ordinal	3
Ped Features				
Coats & Films	CAF	carbonate coats; off-white; effervescent with HCL	nominal	n/a
	SIF	silica; off-white; non-effervescent with HCL	nominal	n/a
	CLF	clay films; waxy exterior films	nominal	n/a
	BRF	clay bridges, wax between sand grains	nominal	n/a
	GBF	gibbsite Coats; AIOH3, off white non-effervescent with HCL	nominal	n/a
	OAF	organoargillans; dark, organic stained clay films	nominal	n/a
	SNF	sand coats; separate brains visible at 10x	nominal	n/a
	SLF	silt coats; separate grains not visible	nominal	n/a
	SKF	skeletans; clean sand or silt grains as coats	nominal	n/a
	GYF	gypsum coats; CaSO4/2H2O	nominal	n/a
	OSF	organic Stains; dark organic films	nominal	n/a

Distinctness of Coats & Films	None	no coats and films	ordinal	0
	F	faint; visible only with magnification (10x hand lens) little contrast between materials	ordinal	1
	D	distinct; visible without magnification; significant contrast between materials	ordinal	2
	P	prominent; markedly visible without magnification; sharp visual contrast between materials	ordinal	3
Coat/Film % Coverage	None	no Coat or film coverage	ordinal	0
	vf	very few; <5% coverage on ped face	ordinal	1
	f	few; 5 to <25% coverage on ped faces	ordinal	2
	c	common; 25 to <50% coverage on ped faces	ordinal	3
	m	many; 50 to <90% coverage on ped faces	ordinal	4
	vm	very many; >/= to 90% coverage on ped faces	ordinal	5
Coat/Film Continuity	None	no continuity	Ordinal	0
	P	patchy; isolated surface coverage	ordinal	1
	D	discontinuous; partial surface coverage	ordinal	2
	C	continuous; entire surface coverage	ordinal	3
Stress Feature Types	PRF	pressure faces; look like clay films; sand grains uncoated	nominal	n/a
	SS	slickensides (pedogenic); shrink/swell shear features (grooves, striations, glossy surfaces) on pedostructure surfaces	nominal	n/a
	SSG	vertical/oblique, roughly planar shear faces from external stress; faults; mass movement, striations, grooves	nominal	n/a
Stress Feature Loci in Ped	PF	on all ped faces (vertical and horizontal faces)	nominal	n/a
	BF	on bottom of ped faces	nominal	n/a
	TF	on top of ped faces	nominal	n/a
	TC	on top of soil columns	nominal	n/a
	VF	on vertical faces of peds	nominal	n/a
	T	throughout center of peds	nominal	n/a
Stress Feature % Coverage	None	no stress features present	ordinal	0
	vf	very few; <5% coverage on ped face	ordinal	1

	f	few; 5 to <25% coverage on ped faces	ordinal	2
	c	common; 25 to <50% coverage on ped faces	ordinal	3
	m	many; 50 to <90% coverage on ped faces	ordinal	4
	vm	very many; >/= to 90% coverage on ped faces	ordinal	5
Distinctness of stress features	None	no stress features present	ordinal	0
	F	faint; visible only with magnification (10x hand lens) little contrast between materials	ordinal	1
	D	distinct; visible without magnification; significant contrast between materials	ordinal	2
	P	prominent; markedly visible without magnification; sharp visual contrast between materials	ordinal	3
Stress Feature Continuity	None	no continuity	ordinal	0
	P	patchy; isolated surface coverage	ordinal	1
	D	discontinuous; partial surface coverage	ordinal	2
	C	continuous; entire surface coverage	ordinal	3
Roots/pores				
Root void/Pore size	n/a	none present	ordinal	0
	VF	very fine; <1mm in diameter	ordinal	1
	F	fine; 1 to <2mm in diameter	ordinal	2
	M	medium; 2 to <5mm in diameter	ordinal	3
	C	coarse; 5 to <10mm in diameter	ordinal	4
	VC	very coarse; >/= 10mm in diameter	ordinal	5
Quantity (average count)	f	few/very few; avg. count per assessed area is <1 per area; <0.2 per area, .2 to <1 per area	ordinal	0
	c	common; 1 to <5 per area	ordinal	1
	m	many; >= 5 per area	ordinal	2
Root void/Pore Shape	DT	dendritic; cylindrical, elongated, branching voids; e.g. Empty root channels	nominal	n/a
	IG	irregular; nonconnected cavities, chambers, e.g. voids	nominal	n/a
	TU	tubular; cylindrical and elongated voids, e.g. worm tunnels	nominal	n/a

	VE	vesicular; ovoid to spherical voids; e.g. solidified pseudomorphs of entrapped gas bubbles concentrated below a crust; most common in arid and semiarid environments	nominal	n/a
	IR	interstitial; voids between sand grains or rock fragments	nominal	n/a
Vertical Continuity	none	no vertical continuity visible	ordinal	0
	L	low; <1cm	ordinal	1
	M	moderate; 1 to <10cm	ordinal	2
	H	high; >/= to 10cm	ordinal	3
Loci in Ped	PF	on all ped faces (vertical and horizontal faces)	nominal	n/a
	BF	on bottom of ped faces	nominal	n/a
	TF	on top of ped faces	nominal	n/a
	TC	on top of soil columns	nominal	n/a
	VF	on vertical faces of peds	nominal	n/a
	T	throughout center of peds	nominal	n/a
Other loci	BG	between sand grains	nominal	n/a
	BK	on bedrock	nominal	n/a
	BR	on the bottom surface of rocks	nominal	n/a
	CC	on concretions	nominal	n/a
	NO	on nodules	nominal	n/a
	RF	on rock fragments	nominal	n/a
	SS	on slickensides	nominal	n/a
	SP	on surfaces along pores	nominal	n/a
	TR	on top surface of rock fragments	nominal	n/a
Redox Features				
RMF Feature Types (Redoximorphic Features)	RMX	reduced matrix; a soil horizon that has in situ matrix chroma of less than or equal to 2 due to the presence of iron. Color becomes redder or brighter when sample is exposed to air	nominal	n/a
	CLD	clay depletions; localized zones that have either a yellow, green, or bluer hue, a higher value or a lower chroma than the matrix color. Loss of pigment results from a loss of Fe and/or Mn and Clay	nominal	n/a

	FED	iron depletions; Localized zones that have one or more the following: a yellower, greener, Value or a lower chroma than the matrix color. Loss of pigmentation results from a loss of Fe and/or Mn and clay	nominal	n/a
	FM	iron masses (non-cemented)	nominal	n/a
	MNM	manganese	nominal	n/a
	FMM	iron- Manganese masses	nominal	n/a
	FSN	ironstone	nominal	n/a
	FEF	ferriargillans (iron stained clay films)	nominal	n/a
	FMN	iron-manganese nodules	nominal	n/a
	FMC	iron manganese concretions (distinct layer)	nominal	n/a
	MNF	manganese; flack black, very thin, exterior films	nominal	n/a
RMF Shape	CU	cubic, crudely equidimensional block-like units	nominal	n/a
	C	cylindrical; tubular and elongated bodies; e.g. Filled wormholes and insect burrows	nominal	n/a
	D	dendritic; tubular, elongated, and branched bodies; e.g. Pipestems	nominal	n/a
	I	irregular; bodies of nonrepeating spacing or shape	nominal	n/a
	L	lenticular; disk-shaped forms with thicker centers and thinning towards outer edge	nominal	n/a
	PE	pendular; irregular drapes, coatings or nodules suspended from underside of frags	nominal	n/a
	P	platy; relatively thin, tabular sheets, lenses, e.g. lamellae	nominal	n/a
	R	reticulate; crudely interlocking bodies with similar spacing; e.g. plinthite	nominal	n/a
	RO	rosette-like; interlocking blades radiating from a central point- petal like	nominal	n/a
	S	spherical; well-rounded to crudely spherical bodies “shot”	nominal	n/a

	T	threadlike; thin, elongated filaments; generally, not dendritic	nominal	n/a
RMF Quantity (% covered area)	none	no RMF features observed	ordinal	0
	f	few; <2%	ordinal	1
	c	common; 2 to <20% covered	ordinal	2
	m	many greater than or equal to 20%	ordinal	3
RMF Distinctness	None	no RMF features observed	ordinal	0
	F	faint; visible only with magnification (10x hand lens) little contrast between materials	ordinal	1
	D	distinct; visible without magnification; significant contrast between materials	ordinal	2
	P	prominent; markedly visible without magnification; sharp visual contrast between materials	ordinal	3
FMN Size	None	none present	ordinal	0
(FeMn Nodules)	VF	very fine; <1mm in diameter	ordinal	1
	F	fine; 1 to <2mm in diameter	ordinal	2
	M	medium; 2 to <5mm in diameter	ordinal	3
	C	coarse; 5 to <10mm in diameter	ordinal	4
	VC	very coarse; >/= 10mm in diameter	ordinal	5
FMN Hardness	None	none present	ordinal	0
	NC	non cemented (soft)	ordinal	1
	EW	extremely weakly cemented	ordinal	2
	W	weakly cemented	ordinal	3
	M	moderately cemented	ordinal	4
	ST	strongly cemented	ordinal	5
RMF Loci in Ped	PF	on all ped faces (vertical and horizontal faces)	nominal	n/a
	BF	on bottom of ped faces	nominal	n/a
	TF	on top of ped faces	nominal	n/a
	TC	on top of soil columns	nominal	n/a
	VF	on vertical faces of peds	nominal	n/a
	T	throughout center of peds	nominal	n/a
RMF Other loci	BG	between sand grains	nominal	n/a
	BK	on bedrock	nominal	n/a
	BR	on the bottom surface of rocks	nominal	n/a
	CC	on concretions	nominal	n/a
	NO	on nodules	nominal	n/a
	RF	on rock fragments	nominal	n/a

	SS	on slickensides	nominal	n/a
	SP	on surfaces along pores	nominal	n/a
	TR	on top surface of rock fragments	nominal	n/a
CaCO3 Characteristics				
Developmental Stage	0	refer to "Pedogenic Carbonate Development Stages- Fine Earth Matrix," in the *Field Book for Describing and Sampling Soils, Version 3.0* (Soil Survey Staff 2012:2-30-2-31)	ordinal	0
	I		ordinal	1
	II		ordinal	2
	III		ordinal	3
	IV		ordinal	4
	V		ordinal	5
	VI		ordinal	6
Carbonate Location	PF	on all ped faces (vertical and horizontal faces)	nominal	n/a
	BF	on bottom of ped faces	nominal	n/a
	TF	on top of ped faces	nominal	n/a
	VF	on vertical faces of peds	nominal	n/a
	TC	on top of soil columns	nominal	n/a
	T	throughout center of peds	nominal	n/a
	BG	between sand grains	nominal	n/a
	BK	on bedrock	nominal	n/a
	BR	on the bottom surface of rocks	nominal	n/a
	CC	on concretions	nominal	n/a
	NO	on nodules	nominal	n/a
	RF	on rock fragments	nominal	n/a
	SS	on slickensides	nominal	n/a
	SP	on surfaces along pores	nominal	n/a
	TR	on top surface of rock fragments	nominal	n/a
Carbonate Nodule Shape	CU	cubic, crudely equidimensional block-like units	nominal	n/a
	C	cylindrical; tubular and elongated bodies; e.g. Filled wormholes and insect burrows	nominal	n/a
	D	dendritic; tubular, elongated, and branched bodies; e.g. Pipestems	nominal	n/a
	I	irregular; bodies of nonrepeating spacing or shape	nominal	n/a
	L	lenticular; disk-shaped forms with thicker centers and thinning towards outer edge	nominal	n/a
	PE	pendular; irregular drapes, coatings or nodules	nominal	n/a

		suspended from underside of frags		
	P	platy; relatively thin, tabular sheets, lenses, e.g. lamellae	nominal	n/a
	R	reticulate; crudely interlocking bodies with similar spacing; e.g. plinthite	nominal	n/a
	RO	rosette-like; interlocking blades radiating from a central point- petal like	nominal	n/a
	S	Spherical; well-rounded to crudely spherical bodies "shot"	nominal	n/a
	T	Threadlike; thin, elongated filaments; generally, not dendritic	nominal	n/a
	n/a	none/not applicable	nominal	n/a
CaCO3 Concentrations:				n/a
Matrix	MAT	in the matrix; not associated with peds/pores	nominal	n/a
	MAD	in the matrix surrounding redox depletions	nominal	n/a
	MAC	in the matrix surrounding redox concentrations	nominal	n/a
	TOT	Throughout the matrix; finely disseminated carbonates permeating everything	nominal	n/a
Peds	BPF	between ped faces	nominal	n/a
	MPF	infused into the matrix along faces of peds (hypocoats)	nominal	n/a
	APF	on the faces of peds (all orientations)	nominal	n/a
	HPF	on the horizontal faces of peds	nominal	n/a
	VPF	on vertical faces of peds	nominal	n/a
Pores	MPO	infused into the matrix adjacent to pores	nominal	n/a
	LPO	lining pores	nominal	n/a
	SPO	on surfaces along pores	nominal	n/a
	RPO	on surfaces along root channels	nominal	n/a
Other	CRK	in cracks	nominal	n/a
	TOH	at the top of the horizon	nominal	n/a
	ARF	around rock fragments (e.g. pendants)	nominal	n/a
	BRF	on bottom of rock fragments	nominal	n/a
	SSS	on slickensides	nominal	n/a
	ALS	along lamina or along strata surfaces	nominal	n/a

Concentrations (types & characteristics)				
Finely Disseminated Concentration types	FDC	finely disseminated carbonates	nominal	n/a
	FDS	finely disseminated salts	nominal	n/a
	FDG	finely disseminated gypsum	nominal	n/a
Masses	CAM	carbonate masses	nominal	n/a
	CBM	clay bodies	nominal	n/a
	GNM	gypsum crystal clusters	nominal	n/a
	GYM	gypsum masses	nominal	n/a
	SAM	salt masses	nominal	n/a
	SIM	silica Masses	nominal	n/a
Nodules	CAN	carbonate nodules	nominal	n/a
	OPN	opal nodules	nominal	n/a
	DNN	durinodes	nominal	n/a
	ORT	orstein Nodules	nominal	n/a
	GBN	gibbsite Nodules	nominal	n/a
CaCO3 Nodule Quantity	n/a	none present	ordinal	0
	f	few; <2% surface area	ordinal	1
	c	common; 2 to <20% surface area	ordinal	2
	m	many; greater than or equal to 20% surface area	ordinal	3
Carbonate Nodule Size	n/a	no nodules present	ordinal	0
	f	fine; < 2mm in diameter	ordinal	1
	m	medium; 2 to <5mm in diameter	ordinal	2
	c	coarse; 5 to < 20mm in diameter	ordinal	3
	vc	very coarse; 20 to <76 mm in diameter	ordinal	4
	ec	extremely coarse; > or = 76 cm in diameter	ordinal	5
Carbonate Filament quantity	n/a	none present	ordinal	0
	f	few, 2% surface area coverage	ordinal	1
	c	common, 2 to <20% surface area coverage	ordinal	2
	m	many, > or = to 20% surface area coverage	ordinal	3
Carbonate Filament Size	n/a	no filaments present	ordinal	0
	vf	very fine; <1 mm diameter	ordinal	1
	f	fine; 1 to <2 mm diameter	ordinal	2
	m	medium; 2 to <5mm in diameter	ordinal	3
	c	coarse; 5 to < 20mm in diameter	ordinal	4
	vc	very coarse; 20 to <76 mm in diameter	ordinal	5
Concretions	CAC	carbonate concretions	nominal	n/a
	GBN	gibbsite concretions	nominal	n/a

	SIC	silica concretions	nominal	n/a
	TIC	titanium oxide concretions	nominal	n/a
Finely Disseminated Carbonate Concentration (Quantity)	none	none present	ordinal	0
	f	few; <2% surface area covered	ordinal	1
	c	common; 2 to <20% surface area covered	ordinal	2
	m	many; greater than or equal to 20% surface area covered	ordinal	3
Carbonate Mass Quantity	none	none present	ordinal	0
	f	few; <2% surface area covered	ordinal	1
	c	common; 2 to <20% surface area covered	ordinal	2
	m	many; greater than or equal to 20% surface area covered	ordinal	3
Carbonate mass size	None	no nodules present	ordinal	0
	f	fine; < 2mm in diameter	ordinal	1
	m	medium; 2 to <5mm in diameter	ordinal	2
	c	coarse; 5 to < 20mm in diameter	ordinal	3
	vc	very coarse; 20 to <76 mm in diameter	ordinal	4
	ec	extremely coarse; > or = to 76 cm in diameter	ordinal	5
Crystal types	CAX	calcite crystals	nominal	n/a
	GYX	gypsum crystals	nominal	n/a
	SAX	salt crystals	nominal	n/a
	SEC	selenite crystals	nominal	n/a
Crystal Quantity	None	none present	ordinal	0
	f	few; <2% surface area covered	ordinal	1
	c	common; 2 to <20% surface area covered	ordinal	2
	m	many; greater than or equal to 20% surface area covered	ordinal	3
Crystal Size	None	no crystals present	ordinal	0
	vf	very fine; <1 mm diameter	ordinal	1
	f	fine; 1 to <2 mm diameter	ordinal	2
	m	medium; 2 to <5mm in diameter	ordinal	3
	c	coarse; 5 to < 20mm in diameter	ordinal	4
	vc	very coarse; 20 to <76 mm in diameter	ordinal	5
Biological Concentrations				
Concentration types	DIB	diatoms	nominal	n/a
	FPB	fecal pellets	nominal	n/a
	ICB	insect casts	nominal	n/a

	PPB	plant phytoliths	nominal	n/a
	WCB	worm casts	nominal	n/a
	RSB	root sheaths	nominal	n/a
	SFB	shell fragments	nominal	n/a
	SSB	sponge spicules	nominal	n/a
Quantity of biological Concentrations	None	none present	ordinal	0
	f	few; <2% surface area covered	ordinal	1
	c	common; 2 to >20% surface area covered	ordinal	2
	m	many: >/= to 20% coverage	ordinal	3
Miscellaneous				
	CBA	carbonate bands	nominal	n/a
	CBE	carbonate beds	nominal	n/a
	CAL	carbonate laminae	nominal	n/a
	CAO	carbonate ooliths	nominal	n/a
	CAP	carbonate pisoltih	nominal	n/a
	CRC	carbonate root casts (rhyzoliths)	nominal	n/a
Sedimentary Characteristics				
Sedimentary Thickness (see Goldberg & Macphail 2006)	No bedding	no bedding present	ordinal	0
	VTNL	very thin laminae <1mm in thickness	ordinal	1
	TNL	thin lamina 1-3mm	ordinal	2
	ML	medium lamina; 3-10mm	ordinal	3
	THL	thick lamina 10-30mm	ordinal	4
	VTHL	very thick lamina >30mm	ordinal	5
	VTNB	very thin bed <10mm	ordinal	6
	TNB	thin bed 10-100mm	ordinal	7
	MB	medium bed 100-300mm	ordinal	8
	THB	thick bed 300-1000mm	ordinal	9
Sorting in sediment structure	0	none	ordinal	0
	1	poorly sorted	ordinal	1
	2	moderately sorted	ordinal	2
	3	very sorted	ordinal	3
Shape of Laminae/bedding topography	EP	even/parallel	nominal	n/a
	EDP	even discontinuous parallel	nominal	n/a
	WP	wavy parallel	nominal	n/a
	WDP	wavy discontinuous parallel	nominal	n/a
	CP	curved parallel	nominal	n/a
	CDP	curved discontinuous parallel	nominal	n/a
	ENP	even non-parallel	nominal	n/a
	EDNP	even discontinuous non-parallel	nominal	n/a
	WNP	wavy non-parallel	nominal	n/a

	WDNP	wavy discontinuous non-parallel	nominal	n/a
	CNP	curvy non-parallel	nominal	n/a
	CDNP	curvy discontinuous non-parallel	nominal	n/a
Rounding of grains in bedding/laminae	A	angular	nominal	n/a
	SA	subangular	nominal	n/a
	R	round	nominal	n/a
	SR	spherical; well-rounded to crudely spherical bodies "shot"	nominal	n/a
Zone Boundaries				
Zone boundary distinctness	D	diffuse > or = to 15 cm transitional zone thickness	ordinal	0
	G	gradual 5 to <15cm transitional zone thickness	ordinal	1
	C	clear; 2 to <5cm in transitional zone thickness	ordinal	2
	A	abrupt; 0.5 to < 2cm transition	ordinal	3
	V	very Abrupt; <0.5cm transition	ordinal	4
Zone boundary topography	S	smooth; planar with few or no irregularities	nominal	n/a
	W	wavy (width of peak greater than depth of peak)	nominal	n/a
	I	irregular (depth of peak varies, generally greater than width of peak)	nominal	n/a
	B	broken; discontinuous	nominal	n/a

APPENDIX C: Degree of Development Results

Profile 1, Degree of Development Scores by Zone (DDS & DDS%).

Scored Characteristic	***Zone 1***	***Zone 2***	***Zone 3***	***Zone 4***	***Zone 5***	***Zone 6***	***Zone 7***	***Zone 8***	***Zone 9***	***Zone 10***	***Zone 11***
Plasticity	2	1	2	0	2	0	0	0	0	0	0
Percent Gravel	0	-1	0	0	0	0	0	0	0	0	-3
Rupture resistance Dry	2	1	3	3	3	1	1	1	1	1	0
Rupture resistance-Moist	1	1	3	1	2	0	0	0	0	0	0
Rupture resistance-Cemented	0	0	0	0	0	0	0	0	0	0	0
HCl Effervescence Response (Ped face)	1	1	3	1	1	0	0	0	1	1	0
HCl Effervescence Response (Matrix)	1	1	0	1	0	0	0	0	1	1	0
Ped Size	1	2	2	1	3	2	1	1	1	1	0
Grade	1	1	1	2	3	1	1	1	1	1	0
Distinctness of Coats and Films	2	2	2	3	3	3	0	0	0	0	0
Coat/Film % Coverage	1	3	2	4	3	2	0	0	0	0	0
Coat/Film Continuity	2	2	2	3	1	2	0	0	0	0	0
Distinctness of Stress Features	0	0	2	0	3	0	0	0	0	0	0
Stress Feature % Coverage	0	0	3	0	2	0	0	0	0	0	0
Stress Feature Continuity	0	0	2	0	1	0	0	0	0	0	0
RMF Quantity	0	0	1	0	3	0	2	0	0	0	0
RMF Distinctness	0	0	1	0	3	0	3	0	0	0	0
RMF Hardness	0	0	1	0	3	0	2	0	0	0	0
RMF Size	0	0	1	0	1	0	1	0	0	0	0
CaCO3 Development Stage	1	1	2	0	0	0	0	0	1	2	0
Carbonate Nodule Size	0	0	1	0	0	0	0	0	0	2	0
Carbonate Nodule Quantity	0	0	2	0	0	0	0	0	0	1	0
Carbonate Filament Size	1	1	1	1	1	1	1	0	1	1	0
Carbonate Filament Quantity	1	1	2	1	1	1	1	0	1	1	0
Quantity of Crystals	0	0	0	0	0	0	0	0	0	0	0
Size of Crystals	0	0	0	0	0	0	0	0	0	0	0
Sedimentary Bedding thickness designation	0	-1	0	0	0	0	0	0	0	-1	-2
Sorting within bedding/laminae	0	-2	0	0	0	0	0	0	0	-1	-3
Horiz. Distinctness (lower boundary)	3	4	2	3	1	2	2	2	2	4	N/A
Zone Score:	**20**	**18**	**41**	**24**	**40**	**15**	**15**	**5**	**10**	**14**	**-8**
Soil Development (%) of 113	**16.81%**	**15.13%**	**34.45%**	**20.17%**	**33.61%**	**12.61%**	**12.61%**	**4.20%**	**8.40%**	**11.76%**	**-6.72%**

Profile 2A, Degree of Development Scores by Zone (DDS & DDS%).

Scored Characteristic	*Zone 1*	*Zone 2*	*Zone 3*	*Zone 4*	*Zone 5*	*Zone 6*	*Zone 7*	*Zone 8*	*Zone 9*	*Zone 10*	*Zone 11*
Plasticity	0	1	2	2	1	2	2	3	2	1	0
Percent Gravel	0	0	0	0	-1	0	0	0	0	0	0
Rupture resistance Dry	0	1	4	3	2	2	2	1	1	2	2
Rupture resistance-Moist	0	1	3	2	2	2	2	1	1	0	2
Rupture resistance-Cemented	0	0	0	0	0	0	0	0	0	0	0
HCl Effervescence Response (Ped face)	0	0	1	2	0	1	0	2	1	0	0
HCl Effervescence Response (Matrix)	0	1	1	1	0	1	0	1	0	0	0
Ped Size (can only compare if same shape)	0	2	2	2	2	1	2	2	2	2	2
Grade	0	1	2	2	2	1	1	2	2	2	3
Distinctness of Coats and Films	0	0	0	0	3	0	0	2	0	0	0
Coat/Film % Coverage	0	0	0	0	3	0	0	2	0	0	0
Coat/Film Continuity	0	0	0	0	2	0	0	2	0	0	0
Distinctness of Stress Features	0	0	2	0	0	0	0	2	2	0	0
Stress Feature % Coverage	0	0	3	0	0	0	0	2	2	0	0
Stress Feature Continuity	0	0	2	0	0	0	0	2	2	0	0
RMF Quantity	0	0	3	2	1	2	2	2	2	2	2
RMF Distinctness	0	0	2	1	1	2	2	3	3	3	3
RMF Hardness	0	0	2	3	3	3	3	1	1	1	2
RMF Size	0	0	1	1	1	1	1	1	1	1	1
CaCO3 Development Stage	0	0	0	2	2	2	1	1	2	2	1
Carbonate Nodule Size	0	0	0	1	2	1	0	0	1	1	0
Carbonate Nodule Quantity	0	0	0	2	3	2	0	0	1	1	0
Carbonate Filament Size	0	0	0	1	1	1	1	1	1	1	1
Carbonate Filament Quantity	0	0	0	1	1	1	1	3	1	1	1
Quantity of Crystals	0	0	1	1	0	0	0	0	1	0	1
Size of Crystals	0	0	1	1	0	0	0	0	1	0	1
Sedimentary Bedding thickness designation	0	0	0	0	0	0	0	0	0	0	0
Sorting within bedding/laminae	0	0	0	0	0	0	0	0	0	0	0
Distinctness of Horizon (lower boundary)	1	3	2	1	1	1	2	3	3	2	N/A
Zone Score:	**1**	**10**	**34**	**31**	**34**	**26**	**22**	**39**	**33**	**22**	**22**
Degree of Development (%) of 113	**1%**	**8%**	**29%**	**26%**	**29%**	**22%**	**18%**	**33%**	**28%**	**18%**	**18%**

Profile 2B, Degree of Development Scores by Zone (DDS & DDS%).

Scored Characteristic	*Zone 1*	*Zone 2*	*Zone 3*	*Zone 4*	*Zone 5*	*Zone 6*	*Zone 7*	*Zone 8*	*Zone 9*	*Zone 10*
Plasticity	2	3	1	2	1	3	3	2	1	1
Percent Gravel	0	0	0	0	0	0	-1	-1	-1	-1
Rupture resistance Dry	2	1	1	4	4	4	4	3	2	2
Rupture resistance-Moist	1	1	1	3	3	2	2	2	2	0
Rupture resistance-Cemented	0	0	0	0	0	0	0	0	0	0
HCl Effervescence Response (Ped face)	3	2	1	3	4	0	4	1	3	2
HCl Effervescence Response (Matrix)	3	1	0	1	1	0	0	1	2	1
Ped Size	1	2	2	2	3	6	3	4	3	1
Grade	2	1	3	3	3	3	2	3	2	1
Distinctness of Coats and Films	1	3	2	2	3	3	3	3	2	2
Coat/Film % Coverage	1	3	1	3	3	3	3	4	3	1
Coat/Film Continuity	2	2	2	2	2	3	2	3	2	1
Distinctness of Stress Features	0	2	2	2	3	3	3	3	2	0
Stress Feature % Coverage	0	2	1	1	2	2	2	4	2	0
Stress Feature Continuity	0	1	1	2	2	2	2	3	2	0
RMF Quantity	2	1	1	3	3	3	3	3	2	1
RMF Distinctness	1	1	1	2	2	3	3	3	2	2
RMF Hardness	0	1	1	1	2	3	4	5	5	5
RMF Size	0	1	1	1	1	2	3	3	2	2
CaCO3 Development Stage	1	2	1	1	2	2	2	2	2	1
Carbonate Nodule Size	1	1	1	0	1	2	3	5	4	1
Carbonate Nodule Quantity	1	1	1	0	3	1	3	3	3	1
Carbonate Filament Size	1	1	1	1	1	1	2	0	1	1
Carbonate Filament Quantity	2	2	1	2	2	3	3	0	1	1
Quantity of Crystals	1	1	1	0	0	1	0	0	1	0
Size of Crystals	1	1	1	0	0	1	0	0	1	0
Sedimentary Bedding thickness designation	0	0	0	0	0	0	-1	-2	-2	-3
Sorting within bedding/laminae	0	0	0	0	0	0	-1	-3	-2	-3
Horiz. Distinctness (lower boundary)	3	2	3	2	1	3	2	2	3	N/A
Zone Score:	**32**	**39**	**31**	**43**	**52**	**59**	**58**	**56**	**50**	**20**
Soil Development (%) of 113	**28%**	**35%**	**27%**	**38%**	**46%**	**52%**	**51%**	**50%**	**44%**	**18%**

Profile 2C, Degree of Development Scores by Zone (DDS & DDS%).

Scored Characteristic	*Zone 1*	*Zone 2*	*Zone 3*
Plasticity	2	1	2
Percent Gravel	0	0	0
Rupture resistance Dry	2	2	3
Rupture resistance-Moist	2	1	2
Rupture resistance-Cemented	0	0	0
HCl Effervescence Response (Ped face)	1	0	0
HCl Effervescence Response (Matrix)	1	0	0
Ped Size	1	2	3
Grade	1	2	3
Distinctness of Coats and Films	1	0	2
Coat/Film % Coverage	1	0	2
Coat/Film Continuity	2	0	2
Distinctness of Stress Features	0	0	3
Stress Feature % Coverage	0	0	2
Stress Feature Continuity	0	0	2
RMF Quantity	2	2	3
RMF Distinctness	2	2	3
RMF Hardness	0	1	1
RMF Size	0	1	1
CaCO3 Development Stage	1	2	1
Carbonate Nodule Size	0	1	0
Carbonate Nodule Quantity	0	1	0
Carbonate Filament Size	1	1	1
Carbonate Filament Quantity	1	1	2
Quantity of Crystals	0	1	0
Size of Crystals	0	1	0
Sedimentary Bedding thickness designation	0	0	0
Sorting within bedding/laminae	0	0	0
Horiz. Distinctness (lower boundary)	2	3	N/A
Zone Score:	**23**	**25**	**38**
Soil Development (%) of 113	**20%**	**22%**	**34%**

Profile 5: Degree of Development Scores by Zone (DDS & DSS%).

Scored Characteristic	***Zone 1***	***Zone 2***	***Zone 3***	***Zone 4***	***Zone 5***	***Zone 6***	***Zone 7***	***Zone 8***	***Zone 9***
Plasticity	0	3	1	2	3	3	2	2	1
Percent Gravel	0	0	0	0	0	0	0	0	0
Rupture resistance Dry	1	3	3	2	3	3	2	2	2
Rupture resistance-Moist	0	2	2	2	2	2	2	2	1
Rupture resistance-Cemented	0	0	0	0	0	0	0	0	0
HCl Effervescence Response (Ped face)	1	1	2	0	1	3	1	1	1
HCl Effervescence Response (Matrix)	0	0	0	0	0	0	1	1	1
Ped Size	2	1	1	2	2	3	2	2	2
Grade	2	3	1	2	3	3	3	3	2
Distinctness of Coats and Films	0	2	0	3	3	3	0	2	2
Coat/Film % Coverage	0	2	0	3	2	2	0	2	2
Coat/Film Continuity	0	2	0	2	1	2	0	1	2
Distinctness of Stress Features	0	2	0	0	3	3	3	2	2
Stress Feature % Coverage	0	2	0	0	2	3	3	2	2
Stress Feature Continuity	0	2	0	0	2	3	2	1	1
RMF Quantity	0	0	0	1	2	3	3	2	2
RMF Distinctness	0	0	0	2	3	4	4	2	2
RMF Hardness	0	0	0	1	1	2	1	1	1
RMF Size	0	0	0	1	2	2	1	2	1
CaCO3 Development Stage	0	1	1	2	1	1	2	1	2
Carbonate Nodule Size	0	0	1	1	0	0	2	0	1
Carbonate Nodule Quantity	0	0	1	2	0	0	2	0	2
Carbonate Filament Size	0	1	1	1	1	1	1	1	1
Carbonate Filament Quantity	0	1	1	2	2	2	2	1	2
Quantity of Crystals	0	1	0	0	0	2	2	0	0
Size of Crystals	0	1	0	0	0	1	1	0	0
Sedimentary Bedding thickness designation	0	0	0	0	0	0	0	0	0
Sorting within bedding/laminae	0	0	0	0	0	0	0	0	0
Horiz. Distinctness (lower boundary)	0	0	0	3	1	2	2	1	N/A
Zone Score:	**6**	**30**	**15**	**34**	**40**	**53**	**44**	**34**	**35**
Soil Development (%) of 113	**5%**	**27%**	**13%**	**30%**	**35%**	**47%**	**39%**	**30%**	**31%**

APPENDIX D: Zone provenience data by profile.

Profile 1 zone proveniences.

Zone	Northing	Easting	Zone elev. from Dat. A (1000 m above sea level)	Depth Below Surface (Top Zone 1= 0 cmbs)	Zone Thickness (cm)
1	4896.43	4887.49	997.03	0.00	17.70
2	4896.43	4887.49	996.853	17.70	20.40
3	4896.43	4887.49	996.649	38.10	23.00
4	4896.43	4887.49	996.419	61.10	21.80
5	4896.43	4887.49	996.201	82.90	18.20
6	4896.43	4887.49	996.019	101.1	17.90
7	4896.43	4887.49	995.84	119.00	16.00
8	4896.43	4887.49	995.68	135.00	81.70
9	4896.43	4887.49	994.863	216.70	26.70
10	4896.43	4887.49	994.596	243.40	33.10
11	4896.43	4887.49	994.265	276.50	113.40
Base	4896.43	4887.49	993.13	389.9	Base

Profile 2A zone proveniences.

Zone	Northing	Easting	Zone elev. from Dat. A (1000 m above sea level)	Depth Below Surface (Top Zone 1= 0 cmbs)	Zone Thickness (cm)
1	4973.50	4864.08	999.28	0.00	8.69
2	4973.41	4864.06	999.20	8.69	12.44
3	4973.31	4864.03	999.07	21.13	26.33
4	4973.25	4864.07	998.81	47.46	39.30
5	4973.00	4864.07	998.42	86.76	21.54
6	4973.09	4864.32	998.20	108.30	62.63
7	4971.98	4864.86	997.58	170.93	24.28
8	4971.91	4864.92	997.33	195.21	49.70
9	4971.20	4865.55	996.84	244.91	21.24
10	4971.16	4865.65	996.62	266.15	47.27
11	4971.07	4865.66	996.15	313.42	25.75
Base	4971.07	4865.66	996.41	339.17	Base

Profile 2B zone proveniences.

Zone	Northing	Easting	Zone elev. from Dat. A (1000 m above sea level)	Depth Below Surface (Top 2B, Zone 1= 0 cmbs)	Depth below top of Profile 2A (cm)	Zone Thickness (cm)
1	4870.42	4864.08	997.3147	0	196.93	44.81
2	4870.62	4864.06	996.8666	44.81	241.73	32.34
3	4870.61	4864.03	996.5432	77.15	274.11	26.47
4	4870.63	4864.07	996.2785	103.62	300.58	26.26
5	4870.71	4864.07	996.0154	129.93	326.89	43.76
6	4870.68	4864.32	995.5778	173.69	370.65	32.29
7	4870.85	4864.86	995.2549	205.98	402.94	27.56
8	4870.92	4864.92	994.9793	233.54	430.5	79.97
9	4870.87	4865.55	994.1796	313.51	510.47	29.72
10	4870.85	4865.65	993.8824	343.23	540.19	6.74
Base	4870.88	4967.657	993.815	349.97	546.93	Base

Profile 2C zone proveniences.

Zone	Northing	Easting	Zone elev. From Dat. A (1000 m above sea level)	Depth below surface (Top Zone 1= 0 cmbs)	Depth below top of Profile 2A (cm)	Zone Thickness (cm)
1	4983.47	4865.70	996.72	0	256	21.68
2	4983.51	4865.73	996.50	21.68	278	20.83
3	4983.78	4865.61	996.29	42.51	299	29.9
Base	4983.78	4865.61	996.00	72.41	328	Base

Profile 5 zone proveniences.

Zone	Northing	Easting	Zone elev. from Dat. A (1000 m above sea level)	Depth below surface (Top Zone 1= 0 cmbs)	Zone Thickness (cm)
1	4892.032	3727.115	1000.287	0	13
2	4892.032	3727.115	1000.157	13	14.9
3	4892.032	3727.115	1000.008	27.9	31.2
4	4892.032	3727.115	999.696	59.1	36.7
5	4892.032	3727.115	999.329	95.8	58.4
6	4892.032	3727.115	998.745	154.2	45.9
7	4892.032	3727.115	998.286	200.1	26
8	4892.032	3727.115	998.026	226.1	44.4
9	4892.032	3727.115	997.582	270.5	20
Base	4892.032	3727.115	997.382	290.5	Base

APPENDIX E: Sample provenience data & laboratory analysis results by profile.

Profile 1 Sample Provenience & Laboratory Analysis Results

Profile 1 bulk samples		Sample provenience (m/cm)		Laser-sizer particle size results (Φ) (% per sample volume)					NRCS particle size texture designation	Mass-specific magnetic susceptibility results ($10^{-8}mm^3kg^{-1}$)			Degree of development results by zone	
Sample	*Zone*	*Sample elev. below Dat. A (1000 m above sea level)*	*Arbitrary sample depth below surface (surface= 0 cmbs)*	*Sand*	*Silt*	*Clay*	*Mean*	*Standard Deviation*	*Texture*	*Xlf*	*Xhf*	*Xfd%*	*DDS*	*DDS%*
P1-1	1	996.97	6.5	35.3	42.5	22.2	5.40	2.32	Loam	25.73	24.48	4.87	20	16.81
P1-2	2	996.67	31.2	19.3	54.4	26.3	5.89	2.20	Silty Loam	23.18	22.41	3.33	18	15.13
P1-3	3	996.30	49.6	23	56	21	5.54	2.27	Silty Loam	23.75	22.79	4.04	41	34.45
P1-4	4	995.81	69.6	41.1	38.8	20.1	4.42	3.55	Loam	25.07	24.03	4.13	24	20.17
P1-5	5	995.41	90.9	27.2	50.6	22.2	5.53	2.28	Silty Loam	23.43	22.28	4.91	40	33.61
P1-6	6	995.04	112.1	44.6	42.3	13.1	4.80	2.10	Loam	21.81	20.82	4.51	15	12.61
P1-7	7	994.68	135	35.9	45.4	18.7	5.30	2.29	Loam	24.09	23.66	1.79	15	12.61
P1-8	8	994.30	151.5	62.3	29.36	8.34	3.95	1.95	Sandy Loam	19.08	18.59	2.58	5	4.20
P1-9	9	992.76	229.2	47.2	42.8	10	4.32	2.16	Loam	28.94	28.20	2.54	10	8.40
P1-10	10	992.16	261	48	42.07	9.93	4.23	2.24	Loam	33.48	32.50	2.93	14	11.76
P1-11	11	991.53	288.74	46.8	42.2	11	4.35	2.29	Loam	32.94	32.08	2.62	-8	-6.72

Profile 2A Sample Provenience & Laboratory Analysis Results

Profile 2A high resolution samples		Sample provenience		Laser-sizer particle size results (Φ) (% per sample volume)					NRCS particle size texture designation		Mass-specific magnetic susceptibility results ($10^{-8}mm^3kg^{-1}$)			Degree of development results by zone	
Sample	*Zone*	*Sample elev. below Dat. A (1000 m above sea level)*	*Arbitrary sample depth below surface (surface= 0 cmbs)*	*Sand*	*Silt*	*Clay*	*Mean*	*Standard Deviation*	*Per sample*	*Zone Avg.*	*Xlf*	*Xhf*	*Xfd%*	*DDS*	*DDS%*
P2A-1	1	999.27	1.05	51.8	32.2	16	4.66	2.23	SL	SL	24.17	22.97	4.98	1	0.88
P2A-2	1	999.24	4.71	52.8	32.8	14.4	4.53	2.19	SL		22.23	20.92	5.90		
P2A-3	2	999.19	9.5	50.6	29.1	20.3	4.81	2.40	L	L	22.08	20.98	4.96	10	8.85

P2A-4	2	999.16	11.97	59.9	22.2	17.9	4.57	2.38	SL		21.23	20.06	5.50		
P2A-5	2	999.15	13.51	40.2	35.7	24.1	5.32	2.43	L		22.03	20.76	5.73		
P2A-6	3	999.07	21.92	23.1	58.1	18.8	5.46	2.08	SiL	SiL	24.94	23.17	7.10	34	30.09
P2A-7	3	999.01	27.39	22.5	56	21.5	5.61	2.11	SiL		25.27	23.52	6.92		
P2A-8	3	998.96	32.09	18.9	57.5	23.6	5.83	2.06	SiL		27.21	24.97	8.22		
P2A-9	3	998.91	37.37	16.6	56.4	27	6.06	2.06	L		27.62	25.59	7.37		
P2A-10	3	998.86	41.94	16.1	53.2	30.7	6.24	2.07	SiCL		27.35	25.30	7.48		
P2A-11	4	998.80	48.46	24.5	57.2	18.3	5.38	2.13	SiL	SiCL	27.13	24.95	8.03	31	27.43
P2A-12	4	998.74	54.26	16.8	60.5	22.7	5.87	2.01	SiL		27.47	25.17	8.38		
P2A-13	4	998.69	59.34	16.4	55.2	28.4	6.12	2.07	SiCL		27.65	25.18	8.92		
P2A-14	4	998.65	63.86	14.6	54.5	30.9	6.39	1.93	SiCL		28.06	26.11	6.96		
P2A-15	4	998.60	68.29	18.7	48.6	32.7	6.14	2.24	SiCL		28.36	26.47	6.67		
P2A-16	4	998.55	73.21	19.3	51.3	29.4	6.02	2.20	SiCL		27.74	25.77	7.09		
P2A-17	4	998.52	76.7	18.9	50.7	30.4	6.07	2.21	SiCL		26.96	24.92	7.55		
P2A-18	4	998.47	81.71	19.7	52.6	27.7	5.95	2.20	SiCL		26.79	25.23	5.83		
P2A-19	5	998.42	86.77	21	59.9	19.1	5.50	2.06	SiL	SiL	25.67	24.36	5.10	32	28.32
P2A-20	5	998.37	91.69	20.1	60.1	19.8	5.56	2.06	SiL		27.14	25.46	6.20		
P2A-21	5	998.32	96.04	19.6	57.4	23	5.75	2.12	SiL		26.60	24.97	6.15		
P2A-22	5	998.27	101.79	22.2	56.7	21.1	5.63	2.12	SiL		24.22	22.79	5.92		
P2A-23	5	998.23	105.88	22.7	54.1	23.2	5.72	2.18	SiL		24.37	22.90	6.00		
P2A-24	6	998.19	108.99	23.8	57.9	18.3	5.43	2.09	SiL	SiL	23.71	22.57	4.83	26	23.01
P2A-25	6	998.15	113.7	24.7	58.5	16.8	5.31	2.06	SiL		27.44	26.21	4.50		
P2A-26	6	998.11	117.81	21.8	54.6	23.6	5.78	2.16	SiL		23.86	22.78	4.51		
P2A-27	6	998.07	121.61	23.9	59.3	16.8	5.39	2.02	SiL		21.72	21.29	2.00		
P2A-28	6	998.01	127.02	28.1	53.7	18.2	5.39	2.10	SiL		22.72	22.01	3.13		
P2A-29	6	997.97	131.58	24.3	51.9	23.8	5.72	2.20	SiL		22.30	21.68	2.76		
P2A-30	6	997.92	136.36	24.8	49.9	25.3	5.78	2.24	L		21.56	20.74	3.80		
P2A-31	6	997.72	156.1	33.3	55	11.7	4.89	1.85	SiL		20.30	19.90	1.98		
P2A-32	6	997.67	161.02	30.6	56.1	13.3	5.02	1.91	SiL		20.28	19.61	3.34		
P2A-33	6	997.64	164.14	31	57.4	11.6	4.92	1.85	SiL		19.81	19.49	1.63		
P2A-34	6	997.59	169.43	31.8	56.6	11.6	4.90	1.86	SiL		20.43	19.84	2.90		
P2A-35	7	997.58	170.23	25.3	56.8	17.9	5.42	2.09	SiL	SiL	20.09	19.71	1.88	22	19.47

P2A-36	7	997.54	174.85	24.5	54.3	21.2	5.60	2.17	SiL		21.61	21.27	1.55		
P2A-37	7	997.49	179.6	26.2	56.7	17.1	5.36	2.07	SiL		18.89	18.24	3.43		
P2A-38	7	997.43	185.88	26.1	57.4	16.5	5.34	2.05	SiL		21.84	21.15	3.16		
P2A-39	8	997.36	192.68	26.7	55	18.3	5.43	2.15	SiL	SiL	20.78	19.69	5.26	39	34.51
P2A-40	8	997.28	200.37	30.3	48.9	20.8	5.52	2.23	L		20.05	19.46	2.94		
P2A-41	8	997.24	204.78	19.7	57.4	22.9	5.84	2.12	SiL		20.31	20.04	1.36		
P2A-42	8	997.05	223.31	7.82	69.78	22.4	6.19	1.74	SiL		20.06	19.21	4.26		
P2A-43	8	997.01	227.16	7.3	60.4	32.3	6.65	1.80	SiCL		20.38	20.09	1.40		
P2A-44	8	996.97	231.46	7.87	67.33	24.8	6.33	1.77	SiL		21.32	20.85	2.21		
P2A-45	8	996.93	235.28	7.84	68.66	23.5	6.27	1.76	SiL		22.21	21.59	2.80		
P2A-46	8	996.89	239.62	10.4	68.3	21.3	6.12	1.82	SiL		22.62	21.69	4.10		
P2A-47	9	996.82	246.09	12.1	60.7	27.2	6.33	1.96	SiCL	SiL	22.96	22.14	3.58	33	29.20
P2A-48	9	996.78	250.63	14.5	57.5	28	6.25	2.07	SiCL		23.21	22.21	4.33		
P2A-49	9	996.74	254.06	20.2	62.5	17.3	5.48	2.06	SiL		23.05	21.93	4.88		
P2A-50	9	996.70	258.83	24.6	56.1	19.3	5.46	2.22	SiL		23.23	22.16	4.64		
P2A-51	9	996.64	264.18	22	55.4	22.6	5.69	2.26	SiL		23.17	22.25	3.99		
P2A-52	10	996.61	267.45	24.8	45	30.2	5.87	2.55	CL	L	24.08	23.03	4.36	22	19.47
P2A-53	10	996.56	272.67	27.1	54.4	18.5	5.33	2.23	SiL		22.84	22.12	3.17		
P2A-54	10	996.52	276.01	28.7	46.7	24.6	5.64	2.38	L		22.62	21.73	3.94		
P2A-55	10	996.47	281.58	30.6	51.3	18.1	5.27	2.26	SiL		22.89	22.04	3.73		
P2A-56	10	996.42	286.29	32.2	51	16.8	5.17	2.23	SiL		23.31	22.23	4.62		
P2A-57	10	996.37	291.22	31	46.6	22.4	5.52	2.35	L		22.17	21.32	3.82		
P2A-58	10	996.33	295.49	33.1	47.1	19.8	5.33	2.33	L		21.50	20.79	3.28		
P2A-59	10	996.27	300.94	37	43.5	19.5	5.27	2.36	L		22.23	22.18	4.20		
P2A-60	10	996.23	305.71	33.3	45	21.7	5.35	2.32	L		21.77	20.79	4.48		
P2A-61	10	996.19	309.43	38.6	44.1	17.3	5.01	2.25	L		22.31	21.39	4.09		
P2A-62	11	996.14	314.14	40.1	36	23.9	5.36	2.44	L	L	21.50	20.57	4.29	22	19.47
P2A-63	11	996.11	317.56	42.3	45.1	12.6	4.71	2.00	L		22.18	20.87	5.93		
P2A-64	11	996.06	322.16	36.4	48.7	14.9	4.93	2.06	L		22.97	21.54	6.25		
P2A-65	11	996.01	327.83	32.6	54.4	13	4.93	1.97	SiL		21.62	20.53	5.02		
P2A-66	11	995.95	333.68	34.1	42.8	23.1	5.43	2.35	L		22.15	21.22	4.22		
P2A-67	11	995.89	339.17	30.5	47	22.5	5.55	2.20	L		18.11	17.28	4.61		

Profile 2B Sample Provenience & Laboratory Analysis Results

Profile 2B high resolution samples		Sample provenience		Laser-sizer particle size results (Φ) (% per sample volume)					NRCS particle size texture designation		Mass-specific magnetic susceptibility results ($10^{-8}mm^3kg^{-1}$)			Degree of development results by zone	
Sample	*Zone*	*Sample elev. below Dat. A (1000 m above sea level)*	*Arbitrary sample depth below surface (surface= 0 cmbs)*	*Sand*	*Silt*	*Clay*	*Mean*	*Standard Deviation*	*Per Sample*	*Zone Avg.*	*Xlf*	*Xhf*	*Xfd%*	*DDS*	*DDS%*
P2B-1	1	997.23	8.71	26	62.7	11.3	5.02	1.71	SiL	SiL	20.44	19.88	2.76	32	28
P2B-2	1	997.15	16.07	12.5	69.4	18.1	5.80	1.86	SiL		19.21	18.94	1.41		
P2B-3	1	997.10	21.13	22.4	64.1	13.5	5.23	1.83	SiL		18.91	18.43	2.56		
P2B-4	1	997.06	25	11	69.2	19.8	5.96	1.81	SiL		19.06	18.47	3.13		
P2B-5	1	996.91	40.71	9.76	63.84	26.4	6.40	1.85	SiL		21.89	21.26	2.90		
P2B-6	2	996.84	47.01	24.4	57.2	18.4	5.38	2.19	SiL	SiL	21.36	20.82	2.55	39	35
P2B-7	2	996.82	49.88	18.7	59.9	21.4	5.76	2.16	SiL		21.36	20.65	3.34		
P2B-8	2	996.77	54.68	22.7	59.2	18.1	5.43	2.15	SiL		21.94	21.24	3.17		
P2B-9	2	996.69	62.19	31.4	53.1	15.5	5.08	2.20	L		22.12	20.97	5.22		
P2B-10	2	996.65	66.57	29.8	55.4	14.8	5.12	2.12	SiL		22.23	21.14	4.92		
P2B-11	2	996.61	70.78	33.5	51.4	15.1	5.07	2.16	SiL		22.83	21.89	4.09		
P2B-12	3	996.56	75.42	33.1	49.4	17.5	5.19	2.28	L	L	22.73	21.94	3.47	31	27
P2B-13	3	996.49	82.2	37.4	45.4	17.2	5.09	2.27	L		22.96	21.78	5.12		
P2B-14	3	996.44	87.37	39.6	44.9	15.5	4.98	2.22	L		22.16	20.90	5.70		
P2B-15	3	996.40	91.62	52.9	36	11.1	4.32	2.02	SL		22.23	21.43	3.56		
P2B-16	3	996.33	98.3	40.1	35.2	24.7	5.40	2.43	L		21.67	20.49	5.45		
P2B-17	3	996.29	102.18	46.8	40.3	12.9	4.62	2.08	L		22.24	20.95	5.83		
P2B-18	4	996.22	109.79	50.7	39.97	9.33	4.34	1.79	L	L	21.90	20.36	7.01	43	38
P2B-19	4	996.17	114.61	27.7	55.8	16.5	5.22	2.02	SiL		20.54	19.09	7.03		
P2B-20	4	996.12	119.08	37.9	48.7	13.4	4.92	1.92	L		21.30	19.78	7.14		
P2B-21	4	996.07	124.55	31	50.7	18.3	5.30	2.13	SiL		19.15	17.95	6.28		
P2B-22	5	996.01	130.35	47.2	41.9	10.9	4.51	1.96	L	L	16.69	15.71	5.83	52	46
P2B-23	5	995.96	135.53	40.7	45.8	13.5	4.77	2.09	L		15.81	14.95	5.43		
P2B-24	5	995.93	138.92	40	47.9	12.1	4.73	1.99	L		20.00	18.94	5.28		

P2B-25	5	995.89	142.16	44.6	42.7	12.7	4.69	2.00	SiL		19.73	18.73	5.11		
P2B-26	5	995.85	146.43	26.6	52.9	20.5	5.42	2.16	SiL		19.16	17.89	6.61		
P2B-27	5	995.80	151.69	31.8	46.5	21.7	5.45	2.28	L		21.12	20.16	4.56		
P2B-28	5	995.75	156.13	48.6	37.6	13.8	4.59	2.17	L		18.40	17.86	2.96		
P2B-29	5	995.67	164.23	38.8	48.5	12.7	4.81	2.04	L		17.65	17.09	3.14		
P2B-30	5	995.61	170.16	39.2	45.7	15.1	5.01	2.06	L		20.00	19.54	2.31		
P2B-31	6	995.57	174.2	43.5	44.7	11.8	4.71	1.93	L	SiL	17.70	16.58	6.34	59	52
P2B-32	6	995.54	177.94	25.8	56.1	18.1	5.40	2.04	SiL		18.13	17.49	3.50		
P2B-33	6	995.44	187.81	29.8	53.2	17	5.28	2.05	SiL		20.39	19.54	4.14		
P2B-34	6	995.40	191.06	23.2	58.1	18.7	5.47	2.06	SiL		20.15	19.10	5.22		
P2B-35	6	995.37	194.97	20.3	58.7	21	5.65	2.07	SiL		20.87	20.12	3.62		
P2B-36	6	995.32	199.41	21.3	58.2	20.5	5.61	2.10	SiL		21.29	20.93	1.70		
P2B-37	6	995.28	203.27	18.2	56.2	25.6	5.94	2.11	SiL		21.30	20.32	4.60		
P2B-38	7	995.25	206.52	19.2	51.8	29	6.04	2.20	SiCL	SiCL	22.40	21.62	3.46	58	51
P2B-39	7	995.19	212.59	17.3	56.6	26.1	6.00	2.07	SiL		22.52	21.62	3.96		
P2B-40	7	995.13	218.81	19.2	51.9	28.9	6.02	2.20	SiCL		20.37	19.79	2.84		
P2B-41	7	995.07	224.39	12.1	51.1	36.8	6.70	1.96	SiCL		18.97	18.22	3.96		
P2B-42	7	995.02	229.34	11.9	58.6	29.5	6.43	1.88	SiCL		19.24	18.56	3.52		
P2B-43	8	995.00	231.62	14.7	55.8	29.5	6.28	2.03	SiCL	SiCL	19.56	18.78	3.98	56	50
P2B-44	8	994.96	235.8	18.9	52.8	28.3	6.03	2.18	SiCL		20.05	19.44	3.04		
P2B-45	8	994.90	241.82	19.6	51	29.4	6.04	2.21	SiCL		19.45	18.77	3.51		
P2B-46	8	994.85	246.04	19.2	49.1	31.7	6.12	2.23	SiCL		19.44	18.87	2.90		
P2B-47	8	994.82	249.59	12.5	55.8	31.7	6.45	1.96	SiCL		19.75	18.91	4.28		
P2B-48	8	994.78	253.88	11.9	53.8	34.3	6.58	1.95	SiCL		20.67	19.96	3.44		
P2B-49	8	994.72	259.34	11.1	57.1	31.8	6.48	1.99	SiCL		19.66	18.83	4.22		
P2B-50	8	994.65	266.79	13	54.9	32.1	6.43	1.99	SiCL		18.89	17.90	5.26		
P2B-51	8	994.54	277.01	12.4	55.3	32.3	6.46	1.99	SiCL		18.69	17.90	4.23		
P2B-52	8	994.45	286.21	10.4	56.5	33.1	6.54	1.92	SiCL		19.83	19.14	3.48		
P2B-53	8	994.38	293.2	9.63	59.17	31.2	6.43	1.93	SiCL		20.17	19.48	3.43		
P2B-54	8	994.31	300.38	12.1	57	30.9	6.41	1.97	SiCL		20.62	20.12	2.45		
P2B-55	8	994.26	305.32	13.1	57.4	29.5	6.29	2.01	SiCL		20.64	19.81	4.04		
P2B-56	8	994.21	310.01	21.5	50.2	28.3	5.92	2.27	CL		20.12	19.36	3.80		

P2B-57	9	994.17	314.51	8.48	56.12	35.4	6.63	1.93	SiCL	SiCL	20.31	19.38	4.57	50	44
P2B-58	9	994.13	318.51	8.78	55.62	35.6	6.60	1.97	SiCL		20.26	19.77	2.41		
P2B-59	9	994.08	327.01	1.11	62.29	36.6	6.85	1.73	SiCL		20.96	20.18	3.76		
P2B-60	9	994.00	331.59	6.81	59.99	33.2	6.60	1.84	SiCL		19.03	18.32	3.75		
P2B-61	9	993.94	337.68	11	59.3	29.7	6.33	1.95	SiCL		18.71	17.74	5.18		
P2B-62	9	993.91	340.95	0	63.1	36.9	6.93	1.76	SiCL		21.18	20.37	3.83		
P2B-63	10	993.88	343.83	31.7	43.7	24.6	5.59	2.36	L	L	20.77	20.26	2.46	20	18
P2B-64	10	993.82	349.55	24.3	47.7	28	5.80	2.36	CL		21.00	20.46	2.57		

Profile 2C Sample Provenience & Laboratory Analysis Results

Profile 2C high resolution samples		Sample provenience		Laser-sizer particle size results (Φ) (% per sample volume)					NRCS particle size texture designation		Mass-specific magnetic susceptibility results ($10^{-8}mm^3kg^{-1}$)			Degree of development results by zone	
Sample	*Zone*	*Sample elev. below Dat. A (1000 m above sea level)*	*Arbitrary sample depth below surface (surface= 0 cmbs)*	*Sand*	*Silt*	*Clay*	*Mean*	*Standard Deviation*	*Per Sample*	*Zone Avg.*	*Xlf*	*Xhf*	*Xfd%*	*DDS*	*DDS%*
P2C-1	1	996.71	1.25	16.9	52.5	30.6	6.20	2.23	SiCL	SiL	25.11	24.12	3.96	23	20
P2C-2	1	996.64	8.21	20	57.9	22.1	5.70	2.23	SiL		23.68	22.82	3.63		
P2C-3	1	996.59	12.52	24	55.2	20.8	5.54	2.24	SiL		22.62	21.71	4.03		
P2C-4	1	996.54	17.81	29.5	53.3	17.2	5.21	2.20	SiL		22.81	21.89	4.00		
P2C-5	2	996.50	21.68	37.7	49	13.3	4.84	2.11	L	L	24.06	22.99	4.46	25	22
P2C-6	2	996.49	23.47	32.9	49.9	17.2	5.15	2.26	L		23.05	21.78	5.49		
P2C-7	2	996.44	28.04	34.6	51.6	13.8	4.92	2.10	SiL		23.80	22.73	4.51		
P2C-8	2	996.38	34.04	39.6	45.2	15.2	4.96	2.22	L		23.03	21.84	5.16		
P2C-9	2	996.33	39.05	33.9	49.4	16.7	5.18	2.17	L		23.40	22.46	4.00		
P2C-10	3	996.29	42.51	36.4	50.3	13.3	4.86	1.98	SiL	SiL	23.49	22.14	5.75	38	34
P2C-11	3	996.26	45.91	27.8	57	15.2	5.18	1.94	SiL		22.77	21.22	6.80		
P2C-12	3	996.23	49.1	31	54.9	14.1	5.03	1.97	SiL		22.27	21.00	5.69		
P2C-13	3	996.19	52.69	36	52.5	11.5	4.79	1.87	SiL		20.97	19.85	5.34		
P2C-14	3	996.13	58.97	36.5	50.6	12.9	4.81	2.00	SiL		20.31	19.32	4.84		
P2C-15	3	996.06	66.08	41.1	47.8	11.1	4.61	1.91	L		18.70	17.71	5.29		
P2C-16	3	996.00	72.41	42.8	47.26	9.94	4.51	1.83	L		17.85	17.06	4.41		

Profile 5 Sample Provenience & Laboratory Analysis Results

Profile 5 bulk samples		Sample provenience (m/cm)		Laser-sizer particle size results (Φ) (% per sample volume)					NRCS particle size texture designation	Mass-specific magnetic susceptibility results ($10^{-8}mm^3kg^{-1}$)			Degree of development results by zone	
Sample	*Zone*	*Sample elev. below Dat. A (1000 m above sea level)*	*Arbitrary sample depth below surface (surface= 0 cmbs)*	*Sand*	*Silt*	*Clay*	*Mean*	*Standard Deviation*	*Texture*	*Xlf*	*Xhf*	*Xfd%*	*DDS*	*DDS%*
P5-1	1	1000.29	9.5	30.7	50.3	19	5.31	2.22	Silty loam	23.34	21.75	6.82	6	5
P5-2	2	1000.16	20.5	25.7	55.7	18.6	5.37	2.11	Silty loam	26.64	24.74	7.14	30	27
P5-3	3	1000.01	44.4	32.5	50.8	16.7	5.10	2.10	Silty loam	23.43	22.06	5.88	15	13
P5-4	4	999.70	71.1	31	49.2	19.8	5.31	2.20	Loam	21.71	20.35	6.25	34	30
P5-5	5	999.33	111.8	21.7	58.1	20.2	5.59	2.07	Silty loam	18.63	17.67	5.13	40	35
P5-6	6	998.75	174.7	11.2	66.8	22	6.01	1.90	Silty loam	19.81	19.33	2.44	53	47
P5-7	7	998.29	212.1	27.7	53.8	18.5	5.36	2.25	Silty loam	21.83	20.88	4.32	44	39
P5-8	8	998.03	244.6	49.5	42.13	8.37	4.29	1.72	Loam	18.90	16.96	10.26	34	40
P5-9	9	997.58	285.5	32.9	52.9	14.2	5.02	2.04	Silty loam	16.86	15.97	5.25	35	31

APPENDIX F: Profile descriptive narratives & field form summaries.

PROFILE 1

Zone 1, AB

Zone 1 occupies the modern service (0 cmbs) to 17.70 cm below surface and refers to an AB-horizon. The zone is characterized by fine, subangular blocky parting (breaking down into) to coarse, granular ped structures comprised of a strong brown (7.5YR 5/6 dry) to brown (7.5YR 4/4 moist) loam matrix. Matrix consistence ranges from hard when dry, to slightly friable and plastic when moistened. Ped faces and matrix, slightly effervesce when exposed to a 10% HCl solution. Ped parting planes and discrete areas of the matrix contain few, discontinuous, distinct clay bridges that connect coarse-fraction grains.

Very few carbonate filaments ranging in size from fine to very fine are observed as infillings within pores and cracks, and in a few cases, as root casts. Most of the observable carbonate filaments occur on the outside of ped faces, and less commonly, on the interior of peds. Many fine, hair-like dendritic and tubular roots penetrate peds. Grossly visible but fine, irregularly shaped pores commonly occur on ped faces as well as within the matrix. Bioturbation in the form of insect burrows containing observable amounts of fecal pellets, casts, and rodent krotovina are common features throughout the zone. The zone's lower boundary is wavy and abrupt.

Zone 2, CB

Zone 2 refers to a CB-horizon that extends from 17.70 to 38.10 cm below surface and is characterized by medium, weak subangular blocky peds discontinuously coated with distinct sandy lenses, form through a partially unaltered sedimentary unit. The

sedimentary unit is characterized by alternating strong brown (7.5YR 4/6) to brown (7.5YR 5/3) silty loam and clay laminations. Matrix consistence ranges from soft when dry, to very friable and slightly plastic when moistened.

The sedimentary unit differentiating this zone from those above and below is comprised of thin laminations ranging in width from <1 cm to 5 cm. Laminations are comprised of very fine sands, silts and moderately well-sorted pebbles separated by strong brown (7.5YR 4/6), very thin (<5mm) clay drapes. The matrix in these areas is soft when dry, and slightly plastic and very friable when moist. Clay bridges connecting the grains of larger sandy fractions occur within the laminated regions of the zone. Few, slightly malleable carbonate masses, fine in size, accumulate between laminations. The laminated sedimentary unit is bounded above and below by a very fine, discontinuous, platy, carbonate film.

Other features include few, very fine, hair-like dendritic and vertical roots which occur on ped faces, as do very fine, irregularly shaped root pores. Bioturbation in the form of insect casts, burrows, and root voids, are many and penetrate the zone throughout. Few, fine and medium vertically oriented rhyzoliths also occur near the zone's upper boundary. The lower boundary of Zone 2 is almost exclusively comprised of laminae that form a wavy, abrupt boundary with Zone 3.

Zone 3, Bkt

Zone 3 refers to an argillic Bkt-horizon. The zone extends from 38.10 to 61.1 cm below surface and is characterized by fine, moderately strong, prismatic peds comprised of a yellowish-brown (10YR 5/4 dry) to dark yellowish-brown (10YR 4/4 moist) silty loam matrix. Matrix consistence ranges from medium hard when dry, to firm and plastic

when moistened. Exterior ped faces strongly effervesce when exposed to a10% HCl solution and interior parting planes are nonreactive. Pressure features including undulating pressure faces, some of which contain well-developed argillans, are distinct, discontinuous and common on ped faces. Faces are also covered by discontinuous, distinct sand films that tend to accumulate along pressure faces and argillans. Few, soft, amorphous “flecks” of manganese also adhere to ped faces and occasionally occur within the matrix.

Very fine carbonate filaments commonly occur as infillings within cracks and pores. Also common are very fine, cubic and reticulate carbonate nodules that line pores, infill cracks and in some cases, adhere to the matrix along ped faces. Nodules are most common towards the lower boundary of the zone. Bioturbation in the form of root voids, insect burrows and cylindrical, linear worm casts are also common. Fine, vertically oriented rhyzoliths are also common, but follow suit with other carbonate features by primarily occurring towards the bottom of the zone. The lower boundary of Zone 3 is wavy and gradual.

Zone 4, Bw

Zone 4 refers to a Bw-horizon extending from 61.10 to 82.90 cm below surface and is characterized by fine, moderately strong wedge-shaped peds comprised of a strong brown (7.5YR 4/6 dry and moist) silty loam matrix. Matrix consistence ranges from moderately hard when dry, to loose and non-plastic when moistened. Ped faces and matrix slightly effervesce when exposed to 10% HCl solution. Continuous, prominent sand films occur on all ped faces. Grains match color of matrix (7.5YR 4/6). Very few, fine carbonate filaments infill cracks and pores on ped faces in localized areas at top of

zone. Very few, fine carbonate masses occur discretely on ped faces. Bioturbation in the form of worm channels, insect casts, and root voids are common. Fine roots and pores with moderate vertical continuity, dendritic and vertical in shape, commonly occur on ped faces. The lower boundary of Zone 4 is smooth and clear.

Zone 5, Btss

Zone 5 refers to a Btss-horizon and extends from 82.90 to 101.10 cm below surface. The zone is characterized by strong prismatic peds comprised of a yellowish-red (5YR 5/6 dry; 5YR 4/6 moist) silty loam matrix. Matrix consistence ranges from moderately hard when dry, to friable and plastic when moistened. Ped faces are commonly coated with patchy, discontinuous sandy films which also adhere to pressure features (slickensides). Slickensides commonly occur between horizontal ped faces and in a few places, along vertical ped faces. Many very fine dendritic and tubular pores also occur on ped faces. Bioturbation in the form of many cylindrical, linear worm channels are pervasive throughout the zone, and tend to contain a strong brown (7.5YR 5/4) matrix. Also common are insect burrows and casts, some of which contain observable amounts of fecal pellets. An active termite colony was also observed in profile.

Redox features are common in Zone 5 and are dominated by fine black Mn masses manifesting as dendritic and thread-like filaments along ped faces. Other redox features include very fine, platy Mn masses that occur on ped faces. Very fine, hard FeMn nodules are also common features found throughout the matrix and adhering to ped faces. Very few, fine, highly localized carbonate filaments occur within cracks on ped faces. The lower boundary of Zone 5 is smooth and clear.

Zone 6, Bw

Zone 6 refers to a Bw-horizon that extends from 101.10 to 119 cm below surface and is characterized by medium, weakly developed, wedge-shaped peds comprised of a yellowish-red (5YR 5/6 dry; 5YR 4/6 moist) loam matrix. Matrix consistence ranges from soft when dry to loose and non-plastic when moistened. Ped faces and the interior ped matrix are nonreactive when exposed to a 10% HCl solution. Few clay films are observed but occur in secondary contexts lining insect channels. In a few places, distinct, discontinuous clay films occur between the coarse sand fraction of the matrix within peds. Many discontinuous, distinct sand films penetrate the surface area of ped faces. Few pores, primarily vertical and dendritic in shape, are observed. Those that occur have low vertical continuity. Bioturbation in the form of linear, cylindrical worm channels containing a brown (7.5YR 5/4) matrix are very common. Other forms of bioturbation are evident due to the common occurrence of root voids and insect burrows. Very few, very fine carbonate filaments occur in cracks on ped faces. The lower boundary of Zone 6 is smooth and gradual.

Zone 7, Bw

Zone 7 refers to a Bw-horizon that extends from 119 to 135 cm below surface and is characterized by fine, weakly developed, wedge-shaped peds comprised of a strong brown (7.5YR 5/8 dry; 7.5YR 5/6 moist) loam matrix. Matrix consistence ranges from soft when dry to loose and non-plastic when moistened. Both exterior ped faces and interior parting planes/matrix are nonreactive when exposed to a 10% HCl solution. Very fine, dendritic to vertical roots with low vertical continuity are common and tend to grow

through ped structures. Common on ped faces are very fine, dendritic and vertically shaped pores.

Redox features are few and manifest as fine and very fine hard, black FeMn nodules ("shot"). Nodules accumulate along the boundaries of pores, cracks and bioturbated regions. Dark brown to black masses of Mn also develop as very fine to fine-sized, spherical and platy formations along ped faces and occasionally, lining the parting planes within ped features. Mn masses in the form of filaments (both vertical and dendritic in shape) also occur on ped faces. Very few calcium carbonate features are present. Manifestations occur as fine infillings in insect burrows and very fine filaments along ped faces, penetrating cracks and pores. Bioturbation in the form of linear, cylindrical worm channels penetrate the entire zone and contain a light yellowish-brown (10YR 6/4) matrix infilling. The lower boundary of the zone is smooth and gradual.

Zone 8, Bw

Zone 8 refers to a Bw-horizon that extends from 135 to 216.70 cm below surface. The zone is characterized by fine, weakly structured, wedge-shaped peds comprised of a strong brown (7.5YR 5/8 dry; 7.5YR 5/6 moist) sandy loam matrix. The matrix is soft when dry, turning loose and non-plastic when moistened. Very few pores with low vertical continuity (relative continuousness/length of a root penetrating the matrix) occur on ped faces. Evidence for insect bioturbation manifesting in the form of linear, tubular worm channels and insect burrows less frequently than in Zone 7. Burrows are infilled with a light, yellowish-brown (10YR 6/4) matrix containing fine to very fine sands and pebbles. The lower boundary of Zone 8 is smooth and gradual.

Zone 9, Bw

Zone 9 refers to a Bw-horizon that extends from 216.70 to 243.40 cm below surface and is characterized by fine, weakly structured subangular blocky peds comprised of a light yellowish-brown (10YR 6/4 dry; 10YR 5/4 moist) loam matrix. Matrix consistence ranges from soft when dry to loose and non-plastic when moistened. This zone, excavated along a lesser slope than above zones, is altered by many roots ranging in size from fine to very coarse. The vertical and horizontal continuity of roots are high in localized regions that have been disturbed by krotovina. Other forms of bioturbation include the presence of many linear, cylindrical worm channels and insect burrows commonly infilled with a strong brown (7.5YR 5/6) matrix. The prevalence of worm channels nearly obscures ped structure throughout the zone. Few, fine dendritic and vertical carbonate filaments form on ped faces and penetrate cracks. Few, very fine carbonate masses (flecks) also occur, accumulating on vertical ped faces. A thin, distinct, carbonate lens (approximately 2 cm in thickness) creates a clear, wavy lower boundary with Zone 10.

Zone 10, Bk/C

Zone 10 refers to a Bk/C-horizon that extends from 243.40 to 276.50 cm below surface. The zone is characterized by fine, weakly structured subangular blocky peds comprised of a pale brown (10YR 6/3) loam matrix. Matrix consistence ranges from soft when dry, to loose and non-plastic when moistened. Ped faces, including the matrix and interior parting planes, slightly effervesce when exposed to a 10% HCl solution. Fine, dendritic and vertical roots are few and tend to have low vertical continuity. Few, very fine pores occur on ped faces.

Irregular to spherical carbonate masses and concretions ranging in size from very fine to fine are common throughout the zone. Also common are very fine carbonate nodules and lenticular “flecks” of carbonate that occur throughout the zone’s matrix and along ped faces. Both upper and lower boundaries of the zone are bounded by a ~2 cm-thick, continuous carbonate lens. Between lenses, discontinuous, thin to very thin, poor and moderately sorted laminae occur. Most laminae are disrupted by bioturbation, including root penetration, insect burrows, and rodent krotovina. Dominant bioturbation features are linear, cylindrical worm channels containing a reddish-yellow (7.5YR 6/8) matrix that occasionally contain clay films along interior boundaries. Laminae contain fine and very fine sands and silts and are predominantly horizontal. In addition to bioturbation, laminae are also disrupted by pedoturbation (ped formation down profile). The lower boundary of the zone is wavy and abrupt.

Zone 11, C

Zone 11 refers to a C-horizon that extends from 276.50 to 389.90 cm below surface. The zone is characterized by loose, single-grained light yellowish-brown (10YR 6/4 dry) to yellowish-brown (10YR 5/4 moist) loam matrix. The matrix forms a massive, cross-stratified sandy bed comprised of very thin and thin well-sorted laminae. Laminae are parallel and cross-bedded in orientation and are comprised of sands, silts, and sub-rounded pebbles. Overall, the zone contains many fining upward sequences. Coarse deposits superimpose fine clay drapes consistently up profile. The base of the zone (lower 20 cm of the exposure) is primarily comprised by fine to coarse gravels and pebbles that are moderately sorted. Gravels are primarily sub-rounded and angular in shape, and are embedded in a fine, sandy matrix. Bioturbation in the form of insect burrows (live ants

observed in matrix) also penetrate this portion of the zone. Observable burrows are infilled with a strong brown (7.5YR 5/6) matrix. Though Zone 11 is bounded above by a thin carbonate lens (~2cm thick), no carbonates are observed within the matrix itself. The gravelly bedding near the base of the zone slopes downwards at 30-45º angle to the east. The lower boundary of Zone 11 was not observed and represents the base of the profile exposure.

Profile 1 Field Form Summary

Profile 1: Field Description Summary by Zone (Nominal Characteristics)

Zone Characteristics		*Zone 1*	*Zone 2*	*Zone 3*	*Zone 4*	*Zone 5*	*Zone 6*	*Zone 7*	*Zone 8*	*Zone 9*	*Zone 10*	*Zone 11*
Zone Thickness		17.7	20.4	23	21.8	18.2	17.9	16.0	81.7	26.7	33.1	113.4
Munsell Color (Dry)		7.5YR 5/6	7.5YR 4/6	10YR 5/4	7.5YR 4/6	5YR 5/6	5YR 5/8	7.5YR 5/8	7.5YR 5/8	10YR 6/4	10YR 6/3	10YR 6/4
Munsell Color (Moist)		7.5YR 4/4	7.5YR 5/4	10YR 4/4	7.5YR 4/6	5YR 4/6	5YR 4/6	7.5YR 5/6	7.5YR 5/6	10YR 5/4	10YR 5/4	10YR 5/4
Horizon Designation		AB	CB	2Bkt	2Bw	3Btss	3Bw1	3Bw2	3Bw3	3Bw4	3Bk/C	3C
Texture	Sand (S)											
	Coarse Sand (COS)											
	Fine Sand (FS)											
	Very Fine Sand (VFS)											
	Loam (L)	X					X	X		X	X	X
	Loamy Coarse Sand (LCOS)											
	Loamy Sand (LS)											
	Loamy Fine Sand (LFS)											
	Coarse Sandy Loam (COSL)								X			
	Sandy Loam (SL)											
	Fine Sandy Loam (FSL)											
	Very Fine Sandy Loam (VFSL)											
	Loamy Sand (LS)											
	Silt (SI)											
	Silty Loam (SL)		X	X	X	X						
	Sandy Clay Loam (SCL)											
	Clay Loam (CL)											
	Silty Clay Loam (SICL)											
	Sandy Clay (SC)											
	Silty Clay (SIC)											
	Clay (C)											
Unit Structure	Granular (gr)											
	Angular blocky (abk)											

	Subangular blocky (sbk)	X	X							X	X	
	Lenticular (lp)											
	Platy (pl)											
	Wedge (wg)				X		X	X	X			
	Prismatic (pr)			X		X						
	Columnar (cpr)											
	Single Grain (sg)											X
	Massive (m)											
Coats & Films	Carbonate coats (CAF)											
	Silica (SIF)											
	Clay films (CLF)											
	Clay bridges (BRF)	X	X									
	Gibbsite coats (GBF)											
	Organoargillans (OAF)											
	Sand coats (SNF)		X	X	X	X	X					
	Silt coats (SLF)											
	Skeletans (SKF)											
	Gypsum coats (GYF)											
	Organic stain (OSF)											
Stress Feature Type	Pressure faces (PRF)			X								
	Slickensides (SS)					X						
	Shear face (SSG)											
Stress feature Loci in Ped	All ped faces (PF)			X		X						
	Bottom ped faces (BPF)											
	Top of ped faces (TPF)											
	Top of soil column (TC)											
	Vertical Ped Faces (VF)											
	Throughout Ped (T)											

Root shape	Dendritic (DT)	X	X		X	X	X	X		X	X	
	Irregular (IG)											
	Tubular (TU)	X	X	X	X	X	X			X		
	Vesicular (VE)											
	Interstitial (IR)	X	X									
Root Loci in Ped	All ped faces (PF)	X	X	X	X	X	X	X				
	Bottom ped faces (BPF)		X									
	Top of ped faces (TPF)											
	Top of soil column (TC)											
	Vertical Ped Faces (VF)											
	Throughout Ped (T)	X		X	X	X	X	X		X	X	
Root- Other loci	Between sand grains (BG)											
	On bedrock (BK)											
	Bottom surfaces of rock (BR)											
	On concretions (CC)											
	On nodules (ON)											
	On rock fragments (RF)											
	On slickensides (SS)											
	On surfaces along pores (SP)											
	On top surface of rock fragments (TR)											
Pore shape	Dendritic (DT)			X	X	X	X			X	X	
	Irregular (IG)											
	Tubular (TU)			X	X							
	Vesicular (VE)				X	X	X	X	X			
	Interstitial (IR)	X	X		X			X				
Pore loci in ped	On all ped faces (PF)	X	X	X	X	X	X	X	X	X	X	
	On bottom of ped faces (BF)											

	Top of ped faces (TPF) Top of soil column (TC) Vertical Ped Faces (VF) Throughout Ped (T)	X			X							
Pore- Other loci	Between sand grains (BG) On bedrock (BK) On bottom surfaces of rocks (BR) On concretions (CC) On nodules (ON) On rock fragments (RF) On slickensides (SS) On surfaces along pores (SP) On top surface of rock fragments (TR)											
RMF Type	Reduced matrix (RMX) Clay depletions (CLD) Iron depletions (FED) Iron masses (FM) Manganese masses (MNM) Iron-manganese masses (FMM) Ironstone (FSN) Ferriargillans (FEF) Iron-manganese nodules (FMN) Iron-manganese concretions (FMC) Manganese films (MNF)			X		X X X		X X				
RMF Shape	Cubic (CU) Cylindrical (C)											

	Dendritic (DT)					X		X				
	Irregular (I)											
	Lenticular (L)											
	Pendular (PE)											
	Platy (P)					X		X				
	Reticulate (R)											
	Rosette-like (RO)											
	Spherical (S)			X		X		X				
	Thread-like (T)					X		X				
RMF Loci in Ped	All ped faces (PF)			X		X						
	On bottom of ped faces (BF)											
	On top of ped faces (TF)											
	On top of soil column (TC)											
	Vertical Ped Faces (VF)											
	Throughout center of ped (T)					X						
RMF Other loci	Between sand grains (BG)											
	On bedrock (BK)											
	Bottom surfaces of rocks (BR)											
	On concretions (CC)											
	On nodules (ON)											
	On rock fragments (RF)											
	On slickensides (SS)					X						
	On surfaces along pores (SP)											
	In cracks (CRK)							X				
	In matrix (MAT)			X		X						
	On top of rock fragments (TF)											
Carbonate Loci (General)	All ped faces (PF)			X	X					X	X	
	On bottom faces of peds (BF)			X								

	On top faces of peds (TF) On tops of soil columns (TC) On vertical ped faces (VF) Through center of peds (T) Bridging sand grains (BG) On bedrock (BK) On bottom surfaces of rocks (BR) On concretions (CC) On nodules (ON) On rock fragments (RF) On slickensides (SS) On surfaces along pores (SP) On top surfaces of rock fragments (TR)		X								X	
Carbonate shape	Cubic (CU)			X								
	Cylindrical (C)										X	
	Dendritic (DT)		X		X					X	X	
	Irregular (I)				X							
	Lenticular (L)		X									
	Pendular (PE)											
	Platy (P)		X									
	Reticulate (R)			X							X	
	Rosette-like (RO)											
	Spherical (S)									X	X	
	Thread-like (T)		X		X	X	X	X		X	X	
Carbonate Matrix Location	In matrix (MAT)		X	X						X	X	
	In matrix around redox depletions (MAD) In matrix around redox											

	concentrations (MAC) Throughout (Finely disseminated) (TOT)											
Carbonate loci in/on Ped	Between peds (BPF) Infused in matrix on faces (MPF) On faces of peds (all orientations) (APF) On horizontal ped faces (HPF) On vertical ped faces (VF)	X		X	X					X	X	
Carbonate Pore Location	Infused into matrix along faces of peds (MPF) Lining pores (LPO) On surfaces along pores (SPO) on surfaces along root channels (RPO)	X	X	X X	X						X	
Other Carbonate Locations	In cracks (CRK) At top of horizon (TOH) Around rock fragments (ARF) On bottom of rock fragments (BRF) On slickensides (SSS) Along lamina or strata surfaces (ALS)	X	X X	X	X X	X	X	X		X	X	
Types of Finely Disseminated Concentrations	Finely disseminated carbonates (FDC) Finely disseminated salts (FDS) Finely disseminated gypsum (FDG)	X	X			X					X	
Masses Types	Carbonate (CAM) Clay bodies (CBM)		X		X					X	X	

	Gypsum crystal clusters (GNM) Gypsum (GYM) Salt (SAM) Silica (SIM)											
Nodule Type	Carbonate (CAN) Opal (OPN) Durinodes (DNN) Ortstein (ORT) Gibbsite (GBN)			X							X	
Type of Concretions	Carbonate (CAC) Gibbsite (GBC) Silica (SIC) Titanium oxide (TIC)		X								X	
Crystal Type	Calcite (CAX) Gypsum (GYX) Salt (SAX) Selenite (SEC)											
Type of Biological Concretions	Diatoms (DIB)											
	Fecal pellets (FPB)	X				X						
	Insect casts (ICB)	X	X	X	X	X	X		X	X	X	X
	Plant phytoliths (PPB)		X									
	Worm casts (WCB)	X		X	X	X	X		X	X	X	
	Root sheaths (RCB)	X	X	X	X		X					
	Shell fragments (SFB)											
	Sponge spicules (SSB)											
Miscellaneous	Carbonate bands (CBA)											
	Carbonate beds (CBE)									X	X	X
	Carbonate laminae (CAL)											
	Carbonate Ooliths (CAO)											

	Carbonate pisoliths (CAP)											
	Carbonate root casts (CRC)	X	X					X				
Shape of Bedding/	Even/parallel (EP)											X
Laminae	Even discont. parallel (EDP)		X								X	X
	Wavy parallel (WP)											
	Wavy discont. parallel (WDP)		X									
	Curved parallel (CP)											
	Curved discont. parallel (CDP)										X	
	Even non-parallel (ENP)											X
	Even discon. Non-parallel (EDNP)											
	Wavy non-parallel (WNP											
	Wavy discont. Non- parallel (WDNP)											
	Curvy non-parallel (CNP)											
	Curvy discontinuous non-parallel (CDNP)											
Grain	Angular (A)										X	X
Rounding	Sub angular (SA)		X								X	X
(Bedding/	Round (R)										X	X
Laminae)	Spherical (SR)											X
Zone Topography	Smooth (S)				X	X	X	X	X	X	X	X
(Upper Bound.)	Wavy (W)	X	X	X								
	Irregular (I)											
	Broken (B)											
Zone Topography	Smooth (S)			X	X	X	X	X	X	X	X	n/a
(Lower Bound.)	Wavy (W)	X	X									
	Irregular (I)											
	Broken (B)											

Ordinal Characteristic Ratings	*Zone 1*	*Zone 2*	*Zone 3*	*Zone 4*	*Zone 5*	*Zone 6*	*Zone 7*	*Zone 8*	*Zone 9*	*Zone 10*	*Zone 11*
Plasticity	2	1	2	0	2	0	0	0	0	0	0
Percent Gravel	0	1	0	0	0	0	0	0	0	0	-3
Rupture resistance Dry	2	1	3	3	3	1	1	1	1	1	0
Rupture resistance Moist	1	1	3	0	2	0	0	0	0	0	0
Rupture resistance if cemented	0	0	0	0	0	0	0	0	0	0	0
HCl Effervescence Response (Ped face)	1	1	3	1	1	0	0	0	1	1	0
HCl Effervescence Response (Matrix)	1	1	0	1	0	0	0	0	1	1	0
Ped Size (can only compare if same shape)	2	2	2	1	3	2	1	1	1	1	0
Grade	1	1	1	2	3	1	1	1	1	1	0
Distinctness of Coats and Films	2	2	2	3	3	3	0	0	0	0	0
Coat/Film % Coverage	1	3	2	4	3	2	0	0	0	0	0
Coat/Film Continuity	2	2	2	3	1	2	0	0	0	0	0
Distinctness of Stress Features	0	0	2	0	3	0	0	0	0	0	0
Stress Feature % Coverage	0	0	3	0	2	0	0	0	0	0	0
Stress Feature Continuity	0	0	2	0	1	0	0	0	0	0	0
Root Size	2	1	1	2	1	1	1	0	3	1	0
Root Quantity	3	1	1	2	1	2	2	0	3	2	0
Vertical continuity of roots	2	1	1	2	2	2	1	0	3	2	0
Pore Size	2	1	1	1	1	1	1	1	1	1	0
Pore Quantity	2	1	3	2	3	1	2	1	1	1	0
Vertical continuity of Pores	2	1	1	2	2	1	1	1	1	1	0
RMF Quantity	0	0	1	0	3	0	2	0	0	0	0
RMF Distinctness	0	0	1	0	3	0	3	0	0	0	0
RMF Hardness	0	0	1	0	3	0	2	0	0	0	0
RMF Size	0	0	1	0	1	0	1	0	0	0	0
CaCO3 Development Stage	1	1	2	1	0	0	0	0	4	2	4
Carbonate Nodule Size	0	0	1	0	0	0	0	0	0	2	0
Carbonate Nodule Frequency	0	0	2	0	0	0	0	0	0	1	0
Carbonate Filament Size	1	1	1	1	1	1	1	0	1	1	0
Carbonate Filament Frequency	1	1	2	1	1	1	1	0	1	1	0
Quantity of Crystals	0	0	0	0	0	0	0	0	0	0	0
Size of Crystals	0	0	0	0	0	0	0	0	0	0	0
Quantity of Biological Concentrations	3	3	2	2	3	3	3	1	3	3	3
Sedimentary Bedding thickness designation	0	-1	0	0	0	0	0	0	0	-1	-2
Sorting within bedding/laminae	0	-2	0	0	0	0	0	0	0	-1	-3
Distinctness of Horizon (upper boundary)	n/a	3	4	2	3	1	2	2	2	2	4
Distinctness of Horizon (lower boundary)	3	4	2	3	1	2	2	2	2	4	n/a

PROFILE 2A

Zone 1, A

Zone 1 refers to an A-horizon that extends from the modern surface to ~8.69 cm below surface and is characterized by fine, loose, non-plastic yellowish-brown (10YR 5/4 dry; 10YR 4/6 moist) sandy loam with no structure. The matrix consistence is loose both dry and moist and is nonreactive when exposed to a 10% HCl solution. Approximately 30% of the zone is altered by dendritic and vertical roots that range in size from fine to very fine (hair-like) and exhibit moderate vertical continuity. Bioturbation in the form of rodent krotovina are common and range in diameter from ~5-8 cm. Fine and very fine insect burrows commonly penetrate the matrix. The surface of the zone comprises the modern surface and harbors drought resistant grasses and bossies. The lower boundary of the zone is smooth and gradual.

Zone 2, AC

Zone 2 is defined as an AC-horizon extends from ~8.69 to 21.13 cm below surface and is characterized by medium, weakly defined, granular peds comprised of a yellowish-brown (10YR 5/4 dry; 10YR 4/2 moist) loam matrix. Dry matrix is soft in consistence, becoming extremely friable and very slightly plastic when moistened. Ped faces and the matrix within very slightly effervesces when exposed to 10% HCl solution. Many roots, ranging in size from very fine to fine, with moderate vertical continuity alter the zone throughout. Coarse-sized roots with high vertical continuity are few. Other forms of bioturbation ranging in size from very fine to medium include insect casts, burrows and rodent krotovina. The lower boundary of the zone is smooth and abrupt.

Zone 3, ABt

Zone 3 refers to an ABt-horizon that extends from 21.13 to 47.46 cm below surface and is characterized by medium, strongly developed, angular blocky peds comprised of a brown (7.5YR 5/4 dry; 7.5YR 4/3 moist) silty loam matrix. Dry matrix is moderately hard in consistence, becoming firm and slightly plastic when moistened. Ped sizes coarsen down profile, which partly defines the zone's boundary with Zone 4. Exterior ped faces and the matrix both very slightly effervesce when exposed to a 10% HCl solution. Weakly developed, discontinuous pressure faces occur commonly along horizonal ped faces and are often speckled with very fine (sub-mm), soft, irregularly shaped FeMn masses. These redox features also occur commonly along interior ped parting planes. Other FeMn accumulations best described as "staining" occur within cracks along ped faces. Stained areas are readily visible as they are slightly darker than the surrounding matrix color. Discrete accumulations of few, very fine gypsum crystals also occur in cracks along ped faces. Many fine, hair-like, vertical and dendritic roots with moderate vertical continuity disrupt the profile, growing between ped faces, and occasionally, through peds. Bioturbation in the form of insect casts and worm channels are common, as are infillings of organic debris from the zone above. One large (~30 cm in diameter) krotovina disrupts the zone along its eastern boundary. The lower boundary of the zone is smooth and clear.

Zone 4, Btk

Zone 4 refers to a Btk horizon that extends from 47.46 to 86.76 cm below surface and is characterized by medium, moderately developed, subangular blocky peds comprised of a brown (7.5YR 5/4 dry; 7.5YR 4/4 moist) silty clay loam matrix. Dry

matrix has a hard consistence and becomes firm and plastic when moistened. Both exterior ped faces and the interior matrix slightly effervesce when exposed to a 10% HCl solution. Very fine to fine sized, vertically continuous roots are common and tend to grow along ped faces and parting planes. Areas where FeMn staining occurs are few, faint, and discontinuous (less prevalent than Zone 3), and tend to accumulate along ped faces. More common redox features include very fine, hard, spherical FeMn nodules that adhere to ped faces. Also present in this zone are fine to very fine (>2mm) carbonate nodules. These manifest in spherical and cylindrical shapes and become increasingly common down profile towards the zone's boundary with Zone 5. Few carbonate filaments also penetrate cracks and pores, and few carbonate nodules occur within the matrix itself. The lower boundary of the zone is smooth and gradual.

Zone 5, Bkt

Zone 5 refers to a Bkt-horizon that extends from 86.76 to 108.30 cm below surface. This zone is characterized by coarse, moderately defined, subangular blocky peds comprised of a brown (7.5YR 4/6 dry; 7.5YR 4/4 moist) silty loam matrix. Matrix consistency ranges from slightly hard when dry, to friable and slightly plastic when moistened. Many very fine pores occur among ped faces and separation planes. Also common on ped faces are discontinuous and distinct sandy films that are strong brown (7.5YR 5/6) in color. Bioturbation in the form of horizontal and oblique worm channels bisect the zone and are infilled with a strong brown (7.5YR 5/8) matrix. Very fine and fine vertical and dendritic roots commonly infiltrate peds, and in a few places, medium and coarse-sized roots grow between ped faces.

Carbonate nodules are common throughout the zone and manifest in spherical and reticulate shapes that range in size from 1-3 mm in diameter. Carbonates increase in frequency down profile and commonly occur within the matrix, and along ped faces. Very few, fine carbonate filaments and rhyzoliths accumulate in cracks, pores, and worm channels. Redox features are few and include fine and very fine, irregularly shaped Mn masses. Masses are soft in consistency and occur along the boundaries of cracks, among pores, and on ped faces. Few discontinuous and patchy FeMn stains also occur on ped faces. The lower boundary of the zone is smooth and clear.

Zone 6, Bk

Zone 6 refers to a Bk-horizon that extends from 108.3 to 170.93 cm below surface. This zone is characterized by a dense matrix, where ped characterization is made difficult by its consolidation. Though much of the zone is massive, fine, weakly developed, prismatic peds that part to angular blocky structures occur, and are comprised of a brown (7.5YR 5/4 dry; 7.5YR 4/4 moist) silty loam matrix. Dry matrix is medium hard in consistence, grading to friable and plastic when moistened. Both ped faces and the matrix within slightly effervesce when exposed to a 10% HCl solution. Few, fine-sized roots grow through peds both vertically and horizontally. Bioturbation in the form of worm channels alter the zone throughout. All worm channels contain a reddish-yellow (7.5YR 5/8) matrix infilling.

Both carbonates and redox features are present. Fine, sub-rounded carbonates ranging from spherical to cylindrical in shape commonly adhere to ped faces, occur in worm channels, and accumulate in the matrix. Very fine carbonate filaments with low vertical continuity are also common and occur in cracks, voids and root pores. The

presence of carbonate increases down profile towards the zone's boundary with Zone 7. Redox features also occur, but in lesser quantities. Few hard, very fine and fine (>1 mm in diameter), spherical, FeMn nodules occur infrequently on ped faces and within the matrix. The zone's lower boundary is smooth and clear.

Zone 7, Bts

Zone 7 refers to a Bts-horizon that extends from 170.93 to 195.21 cm below surface and is characterized by medium, weakly defined, subangular blocky peds that part into granular structures. Peds are comprised of a light yellowish-brown (10YR 6/4 dry) to brown (10YR 5/3 moist) silty loam matrix. Dry matrix has a slightly hard consistence that turns friable and plastic when moistened. Both exterior ped faces and interior parting planes (including the matrix) are nonreactive when exposed to a 10% HCl solution. Few very fine (sub-mm), hard FeMn nodules ranging in shape from spherical to cylindrical adhere to ped faces and occur in the matrix. Few, very fine pores, some containing fine roots, also occur on ped faces. Carbonate in the form of fine filaments are few and form in cracks, pores, and along bioturbated areas. Bioturbation in the form of worm channels are many and contain a strong brown (7.5YR 5/8) matrix containing very fine, hard FeMn nodules. The lower boundary of the zone is smooth and abrupt.

Zone 8, Bt

Zone 8 refers to a Bt-horizon that extends from 195.21 to 244.91 and is characterized by fine, weakly developed, granular peds comprised of a dark yellowish-brown (10YR 4/4) to brown (7.5YR 4/4) silty loam matrix. Matrix consistence ranges from weak when dry, to very plastic and very friable when moistened. Ped faces strongly effervesce when exposed to a 10% HCl solution, where the matrix only slightly

effervesces. Bioturbation in the form of worm channels are common and contain a matrix infilling that contains sub-mm pebbles and semi-rounded, flat inclusions of Ecca shale. Moderately developed, distinct and discontinuous pressure faces and clay films commonly occur on ped faces, as do redox features in the form of FeMn filaments and staining. Staining occurs discontinuously along worm channels and pore boundaries, while filaments accumulate along ped faces. Also common are soft, fine and very fine irregularly shaped masses of Mn that adhere to pressure faces. Very fine and fine carbonate filaments are common and infill cracks and pores along ped faces. The lower boundary of the zone is smooth and abrupt.

Zone 9, Bt

Zone 9 refers to a Bt-horizon that extends from 244.91 to 266.51cm below surface and is characterized by medium, moderately developed, prismatic peds that part to subangular blocky structures. The matrix is comprised of a yellowish-brown (10YR 5/4 dry) to brown (7.5YR 4/4 moist) silty loam. The consistence of dry matrix is slightly hard when dry, becoming friable and plastic when moistened. Moderately developed, discontinuous yet distinct pressure faces are common among vertical ped faces. FeMn staining is common and occurs on ped faces as discontinuous patches. Staining also occurs in cracks and along pores. Other redox features include ferriargillans. Very few, discontinuous, distinct ferriargillans occur discretely on ped faces. Very few Mn masses that are irregular in shape occur along vertical ped faces. Bioturbation in the form of worm channels are common and are infilled with a strong brown (7.5YR 5/8) matrix also containing coarse inclusions. Inclusions are characterized by very fine pebbles and fine, subangular flecks of Ecca shale. Few, fine and very fine gypsum crystal clusters occur

within cracks on ped faces and within pores and voids. Few very fine dendritic and vertical roots with very low vertical continuity penetrate peds and occur on ped faces. Very few carbonate nodules and “flecks’ adhere to ped faces and are primarily sub-mm in size. Very few, fine, sub-rounded, hard carbonate nodules occur between ped faces. Few carbonate filaments also line pores and cracks on ped faces. The lower boundary of the zone is smooth and gradual.

Zone 10, Bt

Zone 10 refers to a Bt-horizon that extends from 266.51 to 313.42 cm below surface. The zone is characterized by coarse, strongly defined, subangular blocky peds comprised of a brown (7.5YR 5/4 dry; 7.5YR 4/4 moist) loam matrix. Matrix consistency ranges from slightly hard when dry, to loose and slightly plastic when moistened. Features on ped faces include many, fine to very fine pores, and few, very fine to medium roots that are vertically oriented with moderate vertical continuity. Bioturbation in the form of insect burrows ranging in shape from irregular to oval are common, many of which contain visible accumulations of fecal pellets. Other forms of bioturbation include many worm channels infilled with a reddish-yellow (7.5YR 6/6) matrix. FeMn staining is common, distinct and discontinuous on ped faces, as are few, very fine to fine Mn masses. These also accumulate along the boundaries of bioturbated insect channels. Very few, very fine carbonate nodules are present, and accumulate on ped faces. Other carbonate features include very few, fine vertically oriented filaments that infill cracks and pores. The lower boundary of the zone is smooth and clear.

Zone 11, Bw

Zone 11 refers to a Bw-horizon extending 313.42 to 339.17 cm below surface and is characterized by medium, strongly developed, prismatic peds comprised of yellowish-red (5YR 4/6 dry; 5YR 5/8 moist) silty loam. Matrix consistency ranges from semi-hard when dry, to friable and non-plastic when moistened. Both exterior ped faces and interior parting planes are nonreactive when exposed to a10% HCl solution. Very distinct, discontinuous FeMn staining commonly occurs on ped faces. Redox features include few, fine Mn masses that accumulate within the matrix, particularly in pores. Few, very fine gypsum crystals also occur in discrete clusters on ped faces. Bioturbation in the form of worm channels are common and contain a brown (7.5YR 5/4) matrix infilling. Mn films lining the interiors of worm channels are also common. Very fine, few dendritic and vertical roots grow between and through peds structures. Very few, very fine vertical carbonate filaments develop in cracks along ped faces. The lower boundary of the zone is unobserved and represents the base of the profile.

Profile 2A Field Form Summary

Profile 2A: Field Description Summary by Zone (Nominal Characteristics)

Zone Characteristics		*Zone 1*	*Zone 2*	*Zone 3*	*Zone 4*	*Zone 5*	*Zone 6*	*Zone 7*	*Zone 8*	*Zone 9*	*Zone 10*	*Zone 11*
Zone Thickness		8.69	12.44	26.33	39.3	21.54	62.63	24.28	49.7	21.24	47.27	25.75
Munsell Color (Dry)		10YR 3/6	10YR 4/2	7.5YR 4/3	7.5YR 4/4	7.5YR 4/4	7.5YR 4/4	10YR 5/3	10YR 4/4	7.5YR 4/4	7.5YR 4/4	5YR 4/6
Munsell Color (Moist)		10YR 4/6	10YR 5/4	7.5YR 5/4	7.5YR 4/5	7.5YR 4/6	7.5YR 5/4	10YR 6/4	7.5YR 4/4	10YR 5/4	7.5YR 5/4	5YR 5/8
Horizon Designation		A	AC	2ABt	2Btk	2Bkt	2Bk	2Bts	2Bt1	2Bt2	2Bt3	3Bw
Texture	Sand (S)											
	Coarse Sand (COS)											
	Fine Sand (FS)											
	Very Fine Sand (VFS)											
	Loam (L)		X								X	
	Loamy Coarse Sand (LCOS)											
	Loamy Sand (LS)											
	Loamy Fine Sand (LFS)											
	Coarse Sandy Loam (COSL)											
	Sandy Loam (SL)	X										
	Fine Sandy Loam (FSL)											
	Very Fine Sandy Loam (VFSL)											
	Loamy Sand (LS)											
	Silt (SI)											
	Silty Loam (SL)			X		X	X	X	X	X		X
	Sandy Clay Loam (SCL)											
	Clay Loam (CL)											
	Silty Clay Loam (SICL)				X							
	Sandy Clay (SC)											
	Silty Clay (SIC)											
	Clay (C)											
Unit Structure	Granular (gr)		X						X			
	Angular blocky (abk)			X								

	Subangular blocky (sbk)				X	X		X			X	
	Lenticular (lp)											
	Platy (pl)											
	Wedge (wg)											
	Prismatic (pr)						X			X		X
	Columnar (cpr)											
	Single Grain (sg)	X										
	Massive (m)											
Coats & Films	Carbonate coats (CAF)											
	Silica (SIF)											
	Clay films (CLF)								X	X		
	Clay bridges (BRF)											
	Gibbsite coats (GBF)											
	Organoargillans (OAF)											
	Sand coats (SNF)					X						
	Silt coats (SLF)											
	Skeletans (SKF)											
	Gypsum coats (GYF)											
	Organic stain (OSF)											
Stress Feature Type	Pressure faces (PRF)			X					X	X		
	Slickensides (SS)											
	Shear face (SSG)											
Stress feature Loci in Ped	All ped faces (PF)								X	X	X	
	Bottom ped faces (BPF)			X	X							
	Top of ped faces (TPF)			X	X							
	Top of soil column (TC)											
	Vertical Ped Faces (VF)											
	Throughout Ped (T)											

Root shape	Dendritic (DT)	X	X	X		X				X	X	X
	Irregular (IG)											
	Tubular (TU)	X	X	X								
	Vesicular (VE)	X	X	X	X	X	X	X		X	X	X
	Interstitial (IR)							X				
Root Loci in Ped	All ped faces (PF)		X	X	X	X	X	X		X	X	X
	Bottom ped faces (BPF)											
	Top of ped faces (TPF)											
	Top of soil column (TC)											
	Vertical Ped Faces (VF)					X						
	Throughout Ped (T)	X	X	X		X	X	X		X	X	
Root- Other loci	Between sand grains (BG)											
	On bedrock (BK)											
	Bottom surfaces of rock (BR)											
	On concretions (CC)											
	On nodules (ON)											
	On rock fragments (RF)											
	On slickensides (SS)											
	On surfaces along pores (SP)											
	On top surface of rock fragments (TR)											
Pore shape	Dendritic (DT)	X	X	X		X	X	X	X			
	Irregular (IG)										X	
	Tubular (TU)											
	Vesicular (VE)											
	Interstitial (IR)									X	X	X
Pore loci in ped	On all ped faces (PF)	X	X	X	X	X	X	X	X	X	X	X
	On bottom of ped faces (BF)											

	Top of ped faces (TPF) Top of soil column (TC) Vertical Ped Faces (VF) Throughout Ped (T)	X	X	X	X	X	X	X				
Pore- Other loci	Between sand grains (BG) On bedrock (BK) On bottom surfaces of rocks (BR) On concretions (CC) On nodules (ON) On rock fragments (RF) On slickensides (SS) On surfaces along pores (SP) On top surface of rock fragments (TR)											
RMF Type	Reduced matrix (RMX) Clay depletions (CLD) Iron depletions (FED) Iron masses (FM) Manganese masses (MNM) Iron-manganese masses (FMM) Ironstone (FSN) Ferriargillans (FEF) Iron-manganese nodules (FMN) Iron-manganese concretions (FMC) Manganese films (MNF)			X X X	 X X	X X	 X 	 X 	X X 	X X X	X X 	X X

RMF Shape	Cubic (CU)											
	Cylindrical (C)						X	X				
	Dendritic (DT)											
	Irregular (I)			X	X	X			X	X	X	
	Lenticular (L)											
	Pendular (PE)											
	Platy (P)			X	X	X			X	X	X	X
	Reticulate (R)											
	Rosette-like (RO)											
	Spherical (S)			X			X	X				
	Thread-like (T)											
RMF Loci in Ped	All ped faces (PF)			X	X	X		X	X		X	X
	On bottom of ped faces (BF)											
	On top of ped faces (TF)											
	On top of soil column (TC)											
	Vertical Ped Faces (VF)									X		
	Throughout center of ped (T)			X	X	X			X			X
RMF Other loci	Between sand grains (BG)											
	On bedrock (BK)											
	Bottom surfaces of rocks (BR)											
	On concretions (CC)											
	On nodules (ON)											
	On rock fragments (RF)											
	On slickensides (SS)											
	On surfaces along pores (SP)									X		
	In cracks (CRK)			X						X		
	In matrix (MAT)			X	X	X	X	X	X			X
	On top of rock fragments (TF)											

Carbonate Loci (General)	All ped faces (PF)				X	X	X	X	X	X	X	X
	On bottom faces of peds (BF)											
	On top faces of peds (TF)											
	On tops of soil columns (TC)											
	On vertical ped faces (VF)											
	Through center of peds (T)					X						
	Bridging sand grains (BG)											
	On bedrock (BK)											
	On bottom surfaces of rocks (BR)											
	On concretions (CC)											
	On nodules (ON)											
	On rock fragments (RF)											
	On slickensides (SS)											
	On surfaces along pores (SP)									X		
	On top surfaces of rock fragments (TR)											
Carbonate shape	Cubic (CU)											
	Cylindrical (C)				X	X	X					
	Dendritic (DT)					X	X	X	X			
	Irregular (I)									X		
	Lenticular (L)											
	Pendular (PE)											
	Platy (P)											
	Reticulate (R)											
	Rosette-like (RO)											
	Spherical (S)				X	X	X			X	X	
	Thread-like (T)				X	X	X	X	X	X	X	X

Carbonate Matrix Location	In matrix (MAT) In matrix around redox depletions (MAD) In matrix around redox concentrations (MAC) Throughout (Finely disseminated) (TOT)				X	X	X					
Carbonate loci in/on Ped	Between peds (BPF) Infused in matrix on faces (MPF) On faces of peds (all orientations) (APF) On horizontal ped faces (HPF) On vertical ped faces (VF)				X	X	X	X	X	X	X X	
Carbonate Pore Location	Infused into matrix along faces of peds (MPF) Lining pores (LPO) On surfaces along pores (SPO) on surfaces along root channels (RPO)				X X	X X	X X	X X	X X	X X	X X	
Other Carbonate Locations	In cracks (CRK) At top of horizon (TOH) Around rock fragments (ARF) On bottom of rock fragments (BRF) On slickensides (SSS) Along lamina or strata surfaces (ALS)				X	X	X	X	X	X	X	X

Types of Finely Disseminated Concentrations	Finely disseminated carbonates (FDC) Finely disseminated salts (FDS) Finely disseminated gypsum (FDG)		X	X	X		X		X	X		
Masses Types	Carbonate (CAM) Clay bodies (CBM) Gypsum crystal clusters (GNM) Gypsum (GYM) Salt (SAM) Silica (SIM)											
Nodule Type	Carbonate (CAN) Opal (OPN) Durinodes (DNN) Ortstein (ORT) Gibbsite (GBN)				X	X	X			X	X	
Type of Concretions	Carbonate (CAC) Gibbsite (GBC) Silica (SIC) Titanium oxide (TIC)											
Crystal Type	Calcite (CAX) Gypsum (GYX) Salt (SAX) Selenite (SEC)			X						X		X
Type of Biological Concretions	Diatoms (DIB) Fecal pellets (FPB) Insect casts (ICB) Plant phytoliths (PPB)	X X X	X	X X	X						X	

	Worm casts (WCB) Root sheaths (RCB) Shell fragments (SFB) Sponge spicules (SSB)	X	X	X X	X X	X X	X X	X X	X	X X	X X	X
Miscellaneous	Carbonate bands (CBA) Carbonate beds (CBE) Carbonate laminae (CAL) Carbonate Ooliths (CAO) Carbonate pisoliths (CAP) Carbonate root casts (CRC)											
Shape of Bedding/ Laminae	Even/parallel (EP) Even discont. parallel (EDP) Wavy parallel (WP) Wavy discont. parallel (WDP) Curved parallel (CP) Curved discont. parallel (CDP) Even non-parallel (ENP) Even discon. Non-parallel (EDNP) Wavy non-parallel (WNP Wavy discont. Non- parallel (WDNP) Curvy non-parallel (CNP) Curvy discontinuous non-parallel (CDNP)											
Grain Rounding	Angular (A) Sub angular (SA)											

(Bedding/ Laminae)	Round (R) Spherical (SR)											
Zone Topography (Upper Bound.)	Smooth (S) Wavy (W) Irregular (I) Broken (B)	X	X	X	X	X	X	X	X	X	X	X
Zone Topography (Lower Bound.)	Smooth (S) Wavy (W) Irregular (I) Broken (B)	X	X	X	X	X	X	X	X	X	X	n/a

Ordinal Characteristic Ratings	***Zone 1***	***Zone 2***	***Zone 3***	***Zone 4***	***Zone 5***	***Zone 6***	***Zone 7***	***Zone 8***	***Zone 9***	***Zone 10***	***Zone 11***
Plasticity	0	1	2	2	1	2	2	3	2	1	0
Percent Gravel	0	0	0	0	-1	0	0	0	0	0	0
Rupture resistance Dry	0	1	4	3	2	2	2	1	1	2	2
Rupture resistance Moist	0	1	3	2	2	2	2	1	1	0	2
Rupture resistance if cemented	0	0	0	0	0	0	0	0	0	0	0
HCl Effervescence Response (Ped face)	0	0	1	2	0	1	0	2	1	0	0
HCl Effervescence Response (Matrix)	0	1	1	1	0	1	0	1	0	0	0
Ped Size (can only compare if same shape)	0	2	2	2	2	1	2	2	2	2	2
Grade	0	1	2	2	2	1	1	2	2	2	3
Distinctness of Coats and Films	0	0	0	0	3	0	0	2	0	0	0
Coat/Film % Coverage	0	0	0	0	3	0	0	2	0	0	0
Coat/Film Continuity	0	0	0	0	2	0	0	2	0	0	0
Distinctness of Stress Features	0	0	2	0	0	0	0	2	2	0	0
Stress Feature % Coverage	0	0	3	0	0	0	0	2	2	0	0
Stress Feature Continuity	0	0	2	0	0	0	0	2	2	0	0
Root Size	1	2	2	2	1	1	1	1	1	2	1
Root Quantity	3	3	2	2	2	2	1	1	1	3	1
Vertical continuity of roots	3	3	2	2	1	1	1	1	1	2	1
Pore Size	1	1	1	1	1	1	1	1	1	2	1
Pore Quantity	3	3	2	2	3	2	1	1	1	3	2
Vertical continuity of Pores	2	2	2	1	1	1	1	1	1	1	1
RMF Quantity	0	0	3	2	1	2	2	2	2	2	2

RMF Distinctness	0	0	2	1	1	2	2	3	3	3	3
RMF Hardness	0	0	2	3	3	3	3	1	1	1	2
RMF Size	0	0	1	1	1	1	1	1	1	1	1
CaCO3 Development Stage	0	0	0	2	2	2	1	1	2	2	1
Carbonate Nodule Size	0	0	0	1	2	1	0	0	1	1	0
Carbonate Nodule Frequency	0	0	0	2	3	2	0	0	1	1	0
Carbonate Filament Size	0	0	0	1	1	1	1	1	1	1	1
Carbonate Filament Frequency	0	0	0	1	1	1	1	3	1	1	1
Quantity of Crystals	0	0	1	1	0	0	0	0	1	0	1
Size of Crystals	0	0	1	1	0	0	0	0	1	0	1
Quantity of Biological Concentrations	3	3	3	2	3	3	3	3	3	3	3
Sedimentary Bedding thickness designation	0	0	0	0	0	0	0	0	0	0	0
Sorting within bedding/laminae	0	0	0	0	0	0	0	0	0	0	0
Distinctness of Horizon (upper boundary)	0	1	3	2	1	1	1	2	3	3	2
Distinctness of Horizon (lower boundary)	1	3	2	1	1	1	2	3	3	2	N/A

PROFILE 2B

Zone 1, A/Bky

Zone 1 refers to an A/Bky-horizon that extends from the exposed surface (0 cm) to 44.81 cm below surface and is characterized by coarse, moderately defined granular peds comprised of a brown (10YR5/3 dry; 10YR4/3 moist) silty loam matrix. Matrix consistence ranges from moderately hard when dry, to friable and plastic when moistened. Exterior ped faces and interior parting planes strongly effervesce when exposed to 10% HCl solution. Carbonates and gypsum represent the primary pedofeatures in this zone. Very few, fine, cylindrical and oblate, hard carbonate nodules occur within the ped matrix and adhere to ped faces. Very fine carbonate filaments are very common along ped faces and within cracks and pores. Very few, discontinuous and discrete carbonate films also form a few ped faces. Few gypsum clusters also occur along ped faces. Clusters tend to accumulate in cracks, ranging from very fine to fine in size. Bioturbation in the form of insect casts and cylindrical worm channels (1-2cm in diameter) are very common and intercept the zone vertically and horizontally. In-filled worm channels contain a yellowish-red matrix (5YR 4/6). The lower boundary of the zone is abrupt and smooth.

Zone 2, Btk

Zone 2 refers to a Btk-horizon that extends from 44.81 to 77.15 cm below surface and is characterized by fine, moderately developed, subangular blocky peds comprised of a brown (7.5YR 5/6) silty loam matrix. Dry matrix has a slightly hard consistence that becomes very friable and plastic when moistened. Redox features include FeMn staining (dark brown, 7.5YR 3/2) which occurs in discontinuous patches commonly on ped faces, as do weak, discontinuous ferriargillans. Few, distinct

ferriargillans also occur along pores and cracks. Discontinuous, distinct patchy pressure faces and clay films are also common on ped faces. Fine and very fine dendritic carbonate filaments commonly occur along ped faces and infill cracks and pores. Few, very fine, cylindrical carbonate nodules also occur on ped faces, and cover about ~5-15% of the ped face surface area. Nodules are discrete and soft. Many insect burrows and worm channels penetrate the zone vertically and horizontally. Mn concretions are few and heavily localized along worm channel boundaries. Few, very fine gypsum crystal clusters also form within bioturbated regions. The lower boundary of the zone is clear and smooth.

Zone 3, Bty

Zone 3 refers to a Bty-horizon that extends from 77.15 to 103.62 cm below surface and is characterized by fine, strong prismatic peds comprised of a reddish-brown (5YR 4/4 moist; 5YR 5/8 dry) loam. Matrix consistency ranges from soft when dry, to friable and plastic when moistened. Redox features are common. These include discontinuous FeMn staining along ped faces that cover ~5% or less of ped surface area. Few, discontinuous clay films occur on ped faces, as do distinct, patchy pressure faces that occur along bottom horizontal ped faces. Few, very fine, soft FeMn nodules also occur within the matrix. Few carbonate filaments occur on ped faces, as do very few, very fine gypsum crystals that infill exterior cracks along ped faces. Very few, fine and very fine, soft carbonate nodules occur discretely and adhere to the matrix separating ped faces. Carbonate is not a defining feature of the zone. The lower boundary of the zone is abrupt and smooth.

Zone 4, Bs

Zone 4 refers to a Bs-horizon that extends from 103.62 to 129.93 cm below surface and is characterized by medium, strongly developed, prismatic peds parting to subangular blocky and are comprised of a yellowish-red (5YR 4/6 moist & dry) silty loam. Dry peds have a moderately hard consistence and become slightly firm and plastic when moist. When exposed to 10% HCl solution, ped faces strongly effervesce while the inner matrix was nonreactive. Clay films and pressure faces are discontinuous, distinct and common on all ped faces. FeMn staining is very common and distinct on ped faces, as are Mn masses around pore openings. Few to common dendritic Mn filaments also form in fine cracks and grooves along ped faces. Few, thin, discontinuous ferriargillans are also present on ped faces. Few, vertically oriented roots ranging in size from very fine to fine and occur between ped faces. Few, very fine carbonate filaments and films also occur on ped faces. Bioturbation in the form of insect burrows and worm channels are common and intercept the zone vertically and horizontally. Tubular worm channels and insect voids tend to be infilled with a yellowish-red matrix (5YR 4/6 to 5YR 5/8) and range in diameter from 1-2 cm.Very few, very fine, soft FeMn nodules accumulate along worm channels. The lower boundary of the zone is clear and smooth.

Zone 5, Btk

Zone 5 refers to a Btk-horizon that extends from 129.93 to 173.69 cm below surface and is characterized by coarse, very strongly prismatic peds that part to angular blocky structures. The matrix is comprised of a yellowish-red (5YR 4/6 moist & dry) loam. Dry matrix demonstrates a hard consistence and becomes friable and slightly plastic when moistened. Exterior ped faces and matrix very slightly effervesce when

exposed to a 10% HCl solution. Many distinct ferriargillans occur on ped faces, covering ~75% of ped surface area. Prominent, continuous FeMn staining and fine to very fine FeMn nodules and Mn masses are common on ped faces. FeMn masses increase in frequency and firmness (turning nodular) down profile. Prominent, discontinuous clay films and pressure faces are also common and tend to occur on ped faces, though few are observed lining pores and bioturbated regions. Bioturbation in the form of ovoid insect burrows and cylindrical, linear worm channels are common. Channels are infilled with a strong brown (7.5YR 5/6), greyish-brown (10YR 5/4), to dark greyish-brown (10YR 4/2) matrix. Worm channel frequency increases from common to many down-profile. Few to common, fine and very fine carbonate nodules are also present and manifest in oblate and spherical shapes. Nodules tend to be moderately hard or rigid in consistence and are most commonly found adhering to ped faces. Carbonates increase in frequency from few to common down profile. Carbonate filaments ranging in size from fine to very fine also increase in frequency from few to common down profile. The lower boundary of the zone is gradual and smooth.

Zone 6, Btk

Zone 6 refers to a Btk-horizon that extends from 173.69 to 205.98 cm below surface and is characterized by extremely coarse, strongly developed, prismatic peds that part to coarse, angular blocky structures. Peds are comprised of a yellowish-red (5YR 5/8 dry; 5YR 4/6 moist) silty loam matrix where consistence ranges from hard when dry, to firm and plastic when moistened. Ped faces react violently when exposed to a 10% HCL solution while the matrix is non-reactive. Approximately 80% of ped faces and separation planes are covered by very distinct, continuous ferriargillans. Stress features including

distinct, discontinuous pressure faces occur commonly along ped faces and parting planes. Though few, slickenside features also occur and appear as striated and undulating features along horizontal ped faces. Dendritic Mn filaments commonly occur within cracks and pores. Redox features in the form of very fine, soft Mn nodules are very common throughout the zone's matrix. The consistence and shape of Mn nodules changes down profile, becoming harder and more rhombic in shape towards the zone's lower boundary. These primarily manifest in the matrix; few Mn nodules occur on ped faces down profile. Other features include few gypsum crystal accumulations which occur as discrete clusters along horizontal ped faces.

Zone 6 is also characterized by the frequent occurrence of calcium carbonate in a variety of forms including nodular, filamentous, and platy. Platy carbonate films create discontinuous exterior "rinds" on ped faces. Carbonate filaments are also common and accrue on vertical ped faces and infilling cracks and pores. Fine to medium, oval and spherical carbonate nodules are few to very few. Carbonates increase in frequency down zone. FeMn staining and prominent ferriargillans are many; these occur on ped faces and along separation planes. Many cylindrical, linear worm channels bisect zone and channel boundaries and tend to be coated with carbonate. The lower boundary of the zone is abrupt and smooth.

Zone 7, Bkt/C

Zone 7 refers to a Bkt/C-horizon that extends from 205.98 to 233.54 cm and is characterized by a combination of well-developed ped structure and residual, disarticulated sedimentary bedding. Peds are dominantly coarse, strongly developed, prismatic, and comprised of a strong brown (7.5YR 5/6 dry & moist) silty clay loam. Dry

matrix is hard in consistence, turning friable and very plastic when moistened. Redox features are very common, including distinct, discontinuous ferriargillans that occur on ped faces covering ~30-40% of the surface area. FeMn staining and clay films are also common and occur discontinuously along ped faces and along interior parting planes. Linear, cylindrical worm channels ranging in diameter from 1-5 cm are common and penetrate the zone horizontally. Many fine and very fine carbonate nodules ranging in shape from spherical to ovoid occur in the upper half of the horizon. Carbonates in the medium and coarse size categories are relatively few and occur lower in profile, within 5-10 cm of the boundary with Zone 8. These form concentric spheres and tend to accumulate between horizontal ped faces. The frequency of coarse carbonates increases down profile. Few, discontinuous carbonate films occur on ped faces.

The sedimentary characteristics in Zone 7 manifest as thin laminae containing sub-cm-sized pebbles, fine sands and few, fine FeMn nodules. Laminae range in thickness from ~5-7 cm and are bounded above and below by very thin clay and silt drapes, some of which are disarticulated by ped development. In general, laminae are partially to mostly obscured by pedogenesis but are distinct in localized areas. Laminae are particularly noticeable at ~215 and 225 cm below surface. The upper most laminae are dominated by horizontal bands of fine to medium carbonates and pebbles; these features characterize the zone's upper, abrupt boundary. Also observed are few, very fine gypsum crystals that occur within the laminated areas but accumulate on ped faces that disrupt laminae. The lower boundary of the zone is smooth and clear.

Zone 8, Bkss/C

Zone 8 refers to a Bkss/C-horizon that extends from 233.54 to 313.51 cm below surface and is characterized by both pedogenic development and vestigial sedimentary structures. Pedogenic development manifests as extremely coarse, strongly developed, prismatic peds that are comprised of a brown (7.5YR 5/4 dry & moist) silty clay loam matrix. Matrix consistence ranges from moderately hard when dry, to sticky, plastic and friable when moistened. Exterior ped faces and interior parting planes strongly effervesce when exposed to a 10% HCl solution. Redox features in the form of FeMn staining and FeMn nodules and masses are common. Staining occurs commonly on ped faces, altering the color to a darker brown (7.5YR 4/3). FeMn nodules ranging in size from very fine to fine are also common. These adhere to ped faces throughout the zone. Few, black Mn masses forming amorphous accumulations and dendritic filaments occur on ped faces. Stress features also alter ped faces and are dominated by well-developed, obliquely striated slickensides that tend to occur between horizontal ped faces. Also prominent are continuous ferriargillans that cover ~90% of all ped surfaces.

Other pedogenic features include carbonate development. Spherical, very fine carbonate nodules occur commonly throughout the zone. Carbonate is also observed as films coating very fine pebbles within the matrix. Coarse to very coarse spherical and irregularly shaped nodules, commonly featuring concentric formation also occur between horizontal ped faces. This type of nodule increases in frequency down profile into Zone 9. Bioturbation throughout the zone is common and manifests as linear, cylindrical worm channels that are infilled with a reddish-orange (5YR 4/6) matrix. Channels are commonly lined with discontinuous FeMn mottles and staining.

Sedimentary features manifest as thin to very thin laminae comprised of fine sands, fine to very fine carbonate nodules, fine FeMn nodules, and fine, rounded and subangular pebbles including very fine fragments of green Ecca shale. Laminae bisect the zone horizontally, starting at ~278 cm below surface, extending to ~288 cm below surface. Laminae are heavily altered and obscured by pedogenic overprinting. The lower boundary of the zone is clear and smooth.

Zone 9, Bkt/C

Zone 9 refers to a Bkt/C-horizon and extends from 313.51 to 343.23 cm below surface and is characterized by both pedogenic and sedimentary structures. Pedogenic characteristics refer to coarse, weak to moderate subangular blocky peds comprised of reddish-yellow (7.5YR 6/6 dry) to brown (7.5YR 5/4 moist) silty clay loam. Exterior ped faces and interior parting planes strongly effervesce when exposed to a 10% HCl solution.

Redox features and carbonates are common throughout the zone. FeMn staining is discontinuous and common, producing brown (7.5YR 4/4) coloration on ped faces. Hard, fine and very fine FeMn nodules also commonly adhere to ped faces. Few, distinct, patchy ferriargillans and pressure faces occur along vertical ped faces. Matrix inclusions include few, fine and very fine subangular and rounded pebbles coated in carbonate and very fine and medium dendritic root pores and voids. Pores and voids are commonly infilled with calcium carbonate. Carbonate nodules are common and manifest as coarse, concentric ovals and spheres, and occur throughout the ped matrix and between ped faces. Few, fine to medium dendritic rhyzoliths also occur.

Sedimentary features manifest as thin to very thin laminae comprised of fine to very fine angular and subangular pebbles, fine to very fine carbonate nodules, and fine sands. Thin clay and silt drapes (>1 cm in thickness) separate laminae, though pedogenic alteration is pervasive. Laminae are heavily obscured ped development which causes disarticulation of the parallel units. However, these structures are pervasive and occur throughout the zone, increasing in frequency and distinctness down profile. The lower boundary of the zone is smooth and abrupt.

Zone 10, Bw/C

Zone 10 refers to a Bw/C-horizon that extends from 343.23 to 349.97 cm below surface and is characterized by weakly developed pedogenic features and sedimentary structures. Pedogenic features consist of fine, very weak, granular to subangular blocky peds comprised of a brown (7.5YR4/4 dry & moist) silty loam and clay loam matrix. These are only slightly developed, where ped development alters thin to very thin, horizontal and obliquely bedded laminae bounded by thin to very thin clay drapes. Clay films occur discontinuously along ped faces and are few to common.

The sedimentary units in Zone 10 are only slightly altered by weathering processes. These are characterized by thin to very thin laminae consisting of fine to very fine silt and sands and that also contain fine pebbles coated in carbonate and fine to very fine carbonate nodules. Few, distinct ferriargillans and FeMn stained masses occur discontinuously between laminations. Carbonate nodules occur commonly at boundaries between laminae as well as within the laminae themselves. Sediments comprising laminae range in color, alternating between brown (10YR 4/3) clay-dominant drapes, to a

light yellowish-brown (10YR 6/4) fine silty loam. The zone's lower boundary is not characterized and represents the base of the profile exposure.

Profile 2B Field Form Summary

Profile 2B: Field Description Summary by Zone (Nominal Characteristics)											
Zone Characteristics		***Zone 1***	***Zone 2***	***Zone 3***	***Zone 4***	***Zone 5***	***Zone 6***	***Zone 7***	***Zone 8***	***Zone 9***	***Zone 10***
Zone Thickness		44.81	32.34	26.47	26.26	43.76	32.29	27.56	79.97	29.72	6.74
Munsell Color (Dry)		10YR 4/3	7.5YR 5/6	5YR 4/4	5YR 4/6	5YR 4/6	5YR 4/6	7.5YR 5/6	7.5YR5/4	7.5YR 5/4	7.5YR 4/4
Munsell Color (Moist)		10YR 5/3	7.5YR 5/6	5YR 5/8	5YR 4/6	5YR 4/6	5YR 5/8	7.5YR 5/6	7.5YR5/4	7.5YR 6/6	7.5YR 4/4
Horizon Designation		2A/Bky	2Btk	2Bty	3Bs	3Btk1	3Btk2	3Bkt/C1	3Bkss/C	3Bkt/C2	3BwC
Texture	Sand (S)										
	Coarse Sand (COS)										
	Fine Sand (FS)										
	Very Fine Sand (VFS)										
	Loam (L)			X		X					X
	Loamy Coarse Sand (LCOS)										
	Loamy Sand (LS)										
	Loamy Fine Sand (LFS)										
	Coarse Sandy Loam (COSL)										
	Sandy Loam (SL)										
	Fine Sandy Loam (FSL)										
	Very Fine Sandy Loam (VFSL)										
	Loamy Sand (LS)										
	Silt (SI)										
	Silty Loam (SL)	X	X		X		X				
	Sandy Clay Loam (SCL)										
	Clay Loam (CL)										
	Silty Clay Loam (SICL)							X	X	X	
	Sandy Clay (SC)										
	Silty Clay (SIC)										
	Clay (C)										

Unit Structure	Granular (gr) Angular blocky (abk) Subangular blocky (sbk) Lenticular (lp) Platy (pl) Wedge (wg) Prismatic (pr) Columnar (cpr) Single Grain (sg) Massive (m)	X	X	X	X	X	X	X	X	X	X
Coats & Films	Carbonate coats (CAF) Silica (SIF) Clay films (CLF) Clay bridges (BRF) Gibbsite coats (GBF) Organoargillans (OAF) Sand coats (SNF) Silt coats (SLF) Skeletans (SKF) Gypsum coats (GYF) Organic stain (OSF)	X		X	X	X	X X	X X		X	X
Stress Feature Type	Pressure faces (PRF) Slickensides (SS) Shear face (SSG)		X	X	X	X	X X	X X	X	X	
Stress feature Loci in Ped	All ped faces (PF) Bottom ped faces (BPF) Top of ped faces (TPF)		X	X X	X	X X	X	X	X	X	

	Top of soil column (TC) Vertical Ped Faces (VF) Throughout Ped (T)		X					X		X	
Root shape	Dendritic (DT) Irregular (IG) Tubular (TU) Vesicular (VE) Interstitial (IR)				X				X X 	X X 	
Root Loci in Ped	All ped faces (PF) Bottom ped faces (BPF) Top of ped faces (TPF) Top of soil column (TC) Vertical Ped Faces (VF) Throughout Ped (T)				X				X	X	
Root- Other loci	Between sand grains (BG) On bedrock (BK) Bottom surfaces of rock (BR) On concretions (CC) On nodules (ON) On rock fragments (RF) On slickensides (SS) On surfaces along pores (SP) On top surface of rock fragments (TR)										
Pore shape	Dendritic (DT) Irregular (IG)					X					

	Tubular (TU)				X	X					
	Vesicular (VE)			X			X				
	Interstitial (IR)										
Pore loci in ped	On all ped faces (PF)	X	X	X	X	X	X				
	On bottom of ped faces (BF)			X							
	Top of ped faces (TPF)										
	Top of soil column (TC)										
	Vertical Ped Faces (VF)										
	Throughout Ped (T)	X	X	X	X	X					
Pore- Other loci	Between sand grains (BG)										
	On bedrock (BK)										
	On bottom surfaces of rocks (BR)										
	On concretions (CC)										
	On nodules (ON)										
	On rock fragments (RF)										
	On slickensides (SS)						X				
	On surfaces along pores (SP)										
	On top surface of rock fragments (TR)										
RMF Type	Reduced matrix (RMX)										
	Clay depletions (CLD)										
	Iron depletions (FED)										
	Iron masses (FM)										
	Manganese masses (MNM)		X		X	X	X				X
	Iron-manganese masses (FMM)					X	X				X

	Ironstone (FSN)										
	Ferriargillans (FEF)				X	X	X	X	X	X	X
	Iron-manganese nodules (FMN)			X	X		X	X	X	X	X
	Iron-manganese concretions (FMC)		X	X	X	X		X	X		
	Manganese films (MNF)						X	X			X
RMF Shape	Cubic (CU)						X	X		X	
	Cylindrical (C)								X		
	Dendritic (DT)					X	X	X	X		
	Irregular (I)										
	Lenticular (L)										
	Pendular (PE)										
	Platy (P)		X	X	X	X	X	X	X		X
	Reticulate (R)										
	Rosette-like (RO)										
	Spherical (S)			X	X	X	X	X	X	X	X
	Thread-like (T)			X	X	X	X	X	X		
RMF Loci in Ped	All ped faces (PF)		X	X	X	X	X	X	X	X	X
	On bottom of ped faces (BF)							X			
	On top of ped faces (TF)				X						
	On top of soil column (TC)										
	Vertical Ped Faces (VF)										
	Throughout center of ped (T)		X		X	X	X	X	X	X	X
RMF Other loci	Between sand grains (BG)										
	On bedrock (BK)										
	Bottom surfaces of rocks (BR)										

	On concretions (CC)										
	On nodules (ON)										
	On rock fragments (RF)										
	On slickensides (SS)								X		
	On surfaces along pores (SP)		X	X	X		X		X		
	In cracks (CRK)		X	X	X	X	X	X	X		X
	In matrix (MAT)			X		X	X	X	X	X	X
	On top of rock fragments (TF)										
Carbonate Loci (General)	All ped faces (PF)	X	X	X	X	X	X	X	X	X	X
	On bottom faces of peds (BF)										
	On top faces of peds (TF)										
	On tops of soil columns (TC)										
	On vertical ped faces (VF)										
	Through center of peds (T)					X	X			X	
	Bridging sand grains (BG)										
	On bedrock (BK)										
	On bottom surfaces of rocks (BR)	8									
	On concretions (CC)										
	On nodules (ON)										
	On rock fragments (RF)										
	On slickensides (SS)						X				
	On surfaces along pores (SP)		X	X	X	X	X				

	On top surfaces of rock fragments (TR)										
Carbonate shape	Cubic (CU)										
	Cylindrical (C)	X	X				X	X	X	X	
	Dendritic (DT)	X	X	X		X	X	X		X	
	Irregular (I)								X	X	
	Lenticular (L)										
	Pendular (PE)										
	Platy (P)						X	X			
	Reticulate (R)										
	Rosette-like (RO)										
	Spherical (S)			X		X	X	X	X	X	X
	Thread-like (T)	X	X	X	X	X	X	X			
Carbonate Matrix Location	In matrix (MAT)						X	X	X	X	
	In matrix around redox depletions (MAD)										
	In matrix around redox concent. (MAC)										
	Throughout (Finely disseminated) (TOT)										
Carbonate loci in/on Ped	Between peds (BPF)	X		X	X	X	X	X	X		
	Infused in matrix on faces (MPF)										
	On faces of peds (all orientations) (APF)						X		X		X
	On horizontal ped faces (HPF)							X			
	On vertical ped faces (VF)			X							

Carbonate Pore Location	Infused into matrix along faces of peds (MPF) Lining pores (LPO) On surfaces along pores (SPO) On surfaces along root channels (RPO)	X	X X	X X	X X	X X X	X X				
Other Carbonate Locations	In cracks (CRK) At top of horizon (TOH) Around rock fragments (ARF) On bottom of rock fragments (BRF) On slickensides (SSS) Along lamina or strata surfaces (ALS)	X	X	X	X	X	X	X X	X		
Types of Finely Disseminated Concentrations	Finely disseminated carbonates (FDC) Finely disseminated salts (FDS) Finely disseminated gypsum (FDG)	X	X	X	X	X			X	X	X
Masses Types	Carbonate (CAM) Clay bodies (CBM) Gypsum crystal clusters (GNM) Gypsum (GYM) Salt (SAM) Silica (SIM)										
Nodule Type	Carbonate (CAN)	X	X	X		X	X	X	X	X	X

	Opal (OPN) Durinodes (DNN) Ortstein (ORT) Gibbsite (GBN)										
Type of Concretions	Carbonate (CAC) Gibbsite (GBC) Silica (SIC) Titanium oxide (TIC)								X		X
Crystal Type	Calcite (CAX) Gypsum (GYX) Salt (SAX) Selenite (SEC)	X	X	X	X		X	X			
Type of Biological Concretions	Diatoms (DIB) Fecal pellets (FPB) Insect casts (ICB) Plant phytoliths (PPB) Worm casts (WCB) Root sheaths (RCB) Shell fragments (SFB) Sponge spicules (SSB)	X X	X X	X	X	X X	X	X	X	X	X
Miscellaneous	Carbonate bands (CBA) Carbonate beds (CBE) Carbonate laminae (CAL) Carbonate Ooliths (CAO) Carbonate pisoliths (CAP) Carbonate root casts (CRC)							X	X X		X

Shape of Bedding/ Laminae	Even/parallel (EP) Even discont. parallel (EDP) Wavy parallel (WP) Wavy discont. parallel (WDP) Curved parallel (CP) Curved discont. parallel (CDP) Even non-parallel (ENP) Even discon. Non-parallel (EDNP) Wavy non-parallel (WNP Wavy discont. Non- parallel (WDNP) Curvy non-parallel (CNP) Curvy discontinuous non-parallel (CDNP)							X	X	X	X X X
Grain Rounding (Bedding/ Laminae)	Angular (A) Sub angular (SA) Round (R) Spherical (SR)							X X X	X	X X	X X
Zone Topography (Upper)	Smooth (S) Wavy (W) Irregular (I) Broken (B)		X	X	X	X	X	X X	X X	X	X
Zone Topography (Lower)	Smooth (S) Wavy (W) Irregular (I) Broken (B)	X	X	X	X	X	X	X	X	X	n/a

Ordinal Characteristic Ratings	*Zone 1*	*Zone 2*	*Zone 3*	*Zone 4*	*Zone 5*	*Zone 6*	*Zone 7*	*Zone 8*	*Zone 9*	*Zone 10*
Plasticity	2	3	1	2	1	3	3	2	1	1
Percent Gravel	0	0	0	0	0	0	-1	-1	-1	-1
Rupture resistance Dry	2	1	1	4	4	4	4	3	2	2
Rupture resistance Moist	1	1	1	3	3	2	2	2	2	0
Rupture resistance if cemented	0	0	0	0	0	0	0	0	0	0
HCl Effervescence Response (Ped face)	3	2	1	3	4	0	4	1	3	2
HCl Effervescence Response (Matrix)	3	1	0	1	1	0	0	1	2	1
Ped Size (can only compare if same shape)	1	2	2	2	3	6	3	4	3	1
Grade	2	1	3	3	3	3	2	3	2	1
Distinctness of Coats and Films	1	3	2	2	3	3	3	3	2	2
Coat/Film % Coverage	1	3	1	3	3	3	3	4	3	1
Coat/Film Continuity	2	2	2	2	2	3	2	3	2	1
Distinctness of Stress Features	0	2	2	2	3	3	3	3	2	0
Stress Feature % Coverage	0	2	1	1	2	2	2	4	2	0
Stress Feature Continuity	0	1	1	2	2	2	2	3	2	0
Root Size	0	0	1	0	0	0	0	0	1	0
Root Quantity	0	0	1	1	0	0	0	0	1	0
Vertical continuity of roots	0	0	1	1	0	0	0	0	1	0
Pore Size	1	1	1	1	1	1	0	1	0	0
Pore Quantity	1	1	1	1	1	1	0	1	0	0
Vertical continuity of Pores	1	1	1	1	1	1	0	1	0	0
RMF Quantity	2	1	1	3	3	3	3	3	2	2
RMF Distinctness	1	1	1	2	2	3	3	3	2	2
RMF Hardness	0	1	1	1	2	3	4	5	5	5
RMF Size	0	1	1	1	1	2	3	3	2	2
CaCO3 Development Stage	1	2	1	1	2	2	2	2	2	1
Carbonate Nodule Size	1	1	1	0	1	2	3	5	4	1
Carbonate Nodule Frequency	1	1	1	0	3	1	3	3	3	1
Carbonate Filament Size	1	1	1	1	1	1	2	0	1	1
Carbonate Filament Frequency	2	2	1	2	2	3	3	0	1	1
Quantity of Crystals	1	1	1	0	0	1	0	0	1	0
Size of Crystals	1	1	1	0	0	1	0	0	1	0
Quantity of Biological Concentrations	3	3	3	3	3	3	3	2	1	1
Sedimentary Bedding thickness designation	0	0	0	0	0	0	-1	-2	-2	-3
Sorting within bedding/laminae	0	0	0	0	0	0	-1	-3	-2	-3
Distinctness of Horizon (upper boundary)	N/A	3	2	3	2	1	3	2	2	3
Distinctness of Horizon (lower boundary)	3	2	3	2	1	3	2	2	3	N/A

Profile 2C

Zone 1, Bt

Zone 1 refers to a Bt-horizon that extends from the exposed surface (0 cmbs) to 21.68 cm below surface and is characterized by fine, moderately developed, subangular blocky peds. Peds are comprised of a yellowish-brown (10YR 5/4 dry) to dark yellowish-brown (10YR 4/4) silty loam matrix that ranges in consistence from semi-hard when dry, to friable and plastic when moistened. Ped faces and interior matrix slightly effervesce when exposed to a 10% HCl solution. Pedogenic features include common, discontinuous, distinct FeMn stains along ped faces and black, irregularly shaped Mn masses and dendritic filaments. Mn features commonly accumulate within cracks on ped faces. Other redox features include Mn films that line the inner boundaries of pores and worm channels. Worm channels are also common in this zone and contain a strong brown (7.5YR 5/8) matrix infilling. Carbonates are few and manifest as secondary carbonate films along the inner boundaries of worm channels. The lower boundary of the zone is smooth and clear.

Zone 2, Bt

Zone 2 refers to a Bt-horizon that extends from 21.68 to 42.51 cm below surface and is characterized by medium, moderately developed subangular blocky peds comprised of a strong brown (7.5YR 4/6 dry; 7.5YR 4/4 moist) loam matrix. Matrix consistence ranges from semi-hard when dry, to very friable and plastic when moist. Common features on ped surfaces include very fine, irregular and interstitial root pores with low vertical continuity. Fine, dendritic and tubular roots with low vertical continuity commonly occur throughout the zone.

Redox features include few to common, discontinuous, distinct FeMn staining on ped faces, and fine dendritic and vertical Mn filaments. Mn filaments primarily occur in cracks and lining pores. Soft, irregularly shaped Mn nodules are common throughout the matrix. Other pedofeatures include few, very fine gypsum crystal accumulations that occur between ped faces. Carbonate features are few and manifest as very fine carbonate filaments lining pores and worm channels. Few fine, soft, irregular carbonate nodules are also present, but primarily occupy the lower aspect of the zone and are not a defining feature of the horizon. Bioturbation in the form of worm channels are common and contain a strong brown (7.5YR 5/8) matrix infilling. The lower boundary of the zone is smooth and abrupt.

Zone 3, Bss

Zone 3 refers to a Bss-horizon that extends from 42.51 to 72.41 cm below surface and is characterized by coarse, strongly developed, prismatic peds. The ped matrix is comprised of a yellowish-red (5YR 4/6 dry; 5YR 4/4 moist) silty loam and ranges in consistence from hard when dry, to friable and plastic when moistened. The presence of stress features including slickensides, ferriargillans, and pressure faces differentiates Zone 3 from Zones 1 and 2 (Figure 6.). Slickensides are common, prominent and discontinuous along horizontal ped faces. Also common are distinct ferriargillans, developing discontinuously on most ped faces. Slickensides and argillans also coincide with the presence of irregular, black, Mn masses ranging in size from fine to very fine. Mn masses commonly adhered to slickensides and ferriargillans on ped faces. Staining caused by FeMn is pervasive and continuous along all ped surfaces. Other redox features include many dendritic filaments of Mn that infill cracks and voids on ped faces. Strong

brown (7.5YR 5/8) sand grains also coat ped faces, occurring discontinuously (18-20% coverage). Weak, Stage I carbonate formation is observed, where fine, dendritic filaments commonly infill cracks, pores, and voids, along ped faces. Absent from this zone are roots, however, bioturbation in the form of worm channels containing strong brown (7.5YR 5/6) and light yellowish-brown (10YR 6/4) infillings are common. The zone's lower boundary is uncharacterized because it terminates at the base of the exposure.

Profile 2C Field Form Summary

Profile 2C: Field Description Summary by Zone (Nominal Characteristics)				
Zone Characteristics		***Zone 1***	***Zone 2***	***Zone 3***
Zone Thickness		21.68	20.83	29.9
Munsell Color (Dry)		10YR 4/4	7.5YR 4/4	5YR 4/6
Munsell Color (Moist)		10YR 5/4	7.5YR 4/6	5YR 4/6
Horizon Designation		2Bt1	2Bt2	3Bss
Texture	Sand (S)			
	Coarse Sand (COS)			
	Fine Sand (FS)			
	Very Fine Sand (VFS)			
	Loam (L)		X	
	Loamy Coarse Sand (LCOS)			
	Loamy Sand (LS)			
	Loamy Fine Sand (LFS)			
	Coarse Sandy Loam (COSL)			
	Sandy Loam (SL)			
	Fine Sandy Loam (FSL)			
	Very Fine Sandy Loam (VFSL)			
	Loamy Sand (LS)			
	Silt (SI)			
	Silty Loam (SL)	X		X
	Sandy Clay Loam (SCL)			
	Clay Loam (CL)			
	Silty Clay Loam (SICL)			
	Sandy Clay (SC)			
	Silty Clay (SIC)			
	Clay (C)			
Unit Structure	Granular (gr)			
	Angular blocky (abk)			
	Subangular blocky (sbk)	X	X	
	Lenticular (lp)			

	Platy (pl)			
	Wedge (wg)			
	Prismatic (pr)			X
	Columnar (cpr)			
	Single Grain (sg)			
	Massive (m)			
Coats & Films	Carbonate coats (CAF)	X		
	Silica (SIF)			
	Clay films (CLF)			
	Clay bridges (BRF)			
	Gibbsite coats (GBF)			
	Organoargillans (OAF)			
	Sand coats (SNF)			
	Silt coats (SLF)			X
	Skeletans (SKF)			
	Gypsum coats (GYF)			
	Organic stain (OSF)			
Stress Feature Type	Pressure faces (PRF)			X
	Slickensides (SS)			X
	Shear face (SSG)			
Stress feature Loci in Ped	All ped faces (PF)			
	Bottom ped faces (BPF)			X
	Top of ped faces (TPF)			X
	Top of soil column (TC)			
	Vertical Ped Faces (VF)			
	Throughout Ped (T)			
Root shape	Dendritic (DT)			
	Irregular (IG)			
	Tubular (TU)			
	Vesicular (VE)			
	Interstitial (IR)			
Root Loci in Ped	All ped faces (PF)			
	Bottom ped faces (BPF)			
	Top of ped faces (TPF)			
	Top of soil column (TC)			
	Vertical Ped Faces (VF)			
	Throughout Ped (T)			
Root- Other loci	Between sand grains (BG)			
	On bedrock (BK)			
	Bottom surfaces of rock (BR)			
	On concretions (CC)			
	On nodules (ON)			
	On rock fragments (RF)			
	On slickensides (SS)			

	On surfaces along pores (SP) On top surface of rock fragments (TR)			
Pore shape	Dendritic (DT)			X
	Irregular (IG)			
	Tubular (TU)			
	Vesicular (VE)		X	
	Interstitial (IR)			X
Pore loci in ped	On all ped faces (PF)		X	X
	On bottom of ped faces (BF)			
	Top of ped faces (TPF)			
	Top of soil column (TC)			
	Vertical Ped Faces (VF)			
	Throughout Ped (T)		X	
Pore- Other loci	Between sand grains (BG)			
	On bedrock (BK)			
	On bottom surfaces of rocks (BR)			
	On concretions (CC)			
	On nodules (ON)			
	On rock fragments (RF)			
	On slickensides (SS)			
	On surfaces along pores (SP)			
	On top surface of rock fragments (TR)			
RMF Type	Reduced matrix (RMX)			
	Clay depletions (CLD)			
	Iron depletions (FED)			
	Iron masses (FM)			
	Manganese masses (MNM)	X	X	X
	Iron-manganese masses (FMM)			
	Ironstone (FSN)			
	Ferriargillans (FEF)			
	Iron-manganese nodules (FMN)		X	X
	Iron-manganese concretions (FMC)	X	X	X
	Manganese films (MNF)	X		
RMF Shape	Cubic (CU)			
	Cylindrical (C)			
	Dendritic (DT)	X	X	X
	Irregular (I)	X	X	
	Lenticular (L)			
	Pendular (PE)			
	Platy (P)	X	X	X
	Reticulate (R)			
	Rosette-like (RO)			

	Spherical (S)		X	
	Thread-like (T)	X		X
RMF Loci in Ped	All ped faces (PF)	X	X	X
	On bottom of ped faces (BF)			
	On top of ped faces (TF)			
	On top of soil column (TC)			
	Vertical Ped Faces (VF)			
	Throughout center of ped (T)	X		
RMF Other loci	Between sand grains (BG)			
	On bedrock (BK)			
	Bottom surfaces of rocks (BR)			
	On concretions (CC)			
	On nodules (ON)			
	On rock fragments (RF)			
	On slickensides (SS)			
	On surfaces along pores (SP)			
	In cracks (CRK)			
	In matrix (MAT)	X	X	
	On top of rock fragments (TF)			
Carbonate Loci (General)	All ped faces (PF)		X	X
	On bottom faces of peds (BF)			
	On top faces of peds (TF)			
	On tops of soil columns (TC)			
	On vertical ped faces (VF)			
	Through center of peds (T)			
	Bridging sand grains (BG)			
	On bedrock (BK)			
	On bottom surfaces of rocks (BR)			
	On concretions (CC)			
	On nodules (ON)			
	On rock fragments (RF)			
	On slickensides (SS)			
	On surfaces along pores (SP)			
	On top surfaces of rock fragments (TR)			
Carbonate shape	Cubic (CU)			
	Cylindrical (C)			
	Dendritic (DT)		X	X
	Irregular (I)			
	Lenticular (L)			
	Pendular (PE)			
	Platy (P)			
	Reticulate (R)			
	Rosette-like (RO)			
	Spherical (S)			

	Thread-like (T)	X	X	X
Carbonate Matrix Location	In matrix (MAT) In matrix around redox depletions (MAD) In matrix around redox concent. (MAC) Throughout (Finely disseminated) (TOT)			
Carbonate loci in/on Ped	Between peds (BPF) Infused in matrix on faces (MPF) On faces of peds (all orientations) (APF) On horizontal ped faces (HPF) On vertical ped faces (VF)			
Carbonate Pore Location	Infused into matrix along faces of peds (MPF) Lining pores (LPO) On surfaces along pores (SPO) On surfaces along root channels (RPO)		 X X	 X X
Other Carbonate Locations	In cracks (CRK) At top of horizon (TOH) Around rock fragments (ARF) On bottom of rock fragments (BRF) On slickensides (SSS) Along lamina or strata surfaces (ALS)	X	X	X
Types of Finely Disseminated Concentrations	Finely disseminated carbonates (FDC) Finely disseminated salts (FDS) Finely disseminated gypsum (FDG)	X		
Masses Types	Carbonate (CAM) Clay bodies (CBM) Gypsum crystal clusters (GNM) Gypsum (GYM) Salt (SAM) Silica (SIM)			
Nodule Type	Carbonate (CAN) Opal (OPN) Durinodes (DNN) Ortstein (ORT) Gibbsite (GBN)		X	
Type of Concretions	Carbonate (CAC) Gibbsite (GBC) Silica (SIC) Titanium oxide (TIC)			
Crystal Type	Calcite (CAX)			

	Gypsum (GYX) Salt (SAX) Selenite (SEC)			
Type of Biological Concretions	Diatoms (DIB) Fecal pellets (FPB) Insect casts (ICB) Plant phytoliths (PPB) Worm casts (WCB) Root sheaths (RCB) Shell fragments (SFB) Sponge spicules (SSB)	X	X	X
Miscellaneous	Carbonate bands (CBA) Carbonate beds (CBE) Carbonate laminae (CAL) Carbonate Ooliths (CAO) Carbonate pisoliths (CAP) Carbonate root casts (CRC)			
Shape of Bedding/ Laminae	Even/parallel (EP) Even discont. parallel (EDP) Wavy parallel (WP) Wavy discont. parallel (WDP) Curved parallel (CP) Curved discont. parallel (CDP) Even non-parallel (ENP) Even discon. Non-parallel (EDNP) Wavy non-parallel (WNP Wavy discont. Non- parallel (WDNP) Curvy non-parallel (CNP) Curvy discontinuous non-parallel (CDNP)			
Grain Rounding (Bedding/ Laminae)	Angular (A) Sub angular (SA) Round (R) Spherical (SR)			
Zone Topography (Upper)	Smooth (S) Wavy (W) Irregular (I) Broken (B)		X	X
Zone Topography (Lower)	Smooth (S) Wavy (W) Irregular (I) Broken (B)	X	X	n/a

Ordinal Characteristic Ratings	*Zone 1*	*Zone 2*	*Zone 3*
Plasticity	2	1	2
Percent Gravel	0	0	0
Rupture resistance Dry	2	2	3
Rupture resistance Moist	2	1	2
Rupture resistance if cemented	0	0	0
HCl Effervescence Response (Ped face)	1	0	0
HCl Effervescence Response (Matrix)	1	0	0
Ped Size (can only compare if same shape)	1	2	3
Grade	1	2	3
Distinctness of Coats and Films	1	0	2
Coat/Film % Coverage	1	0	2
Coat/Film Continuity	2	0	2
Distinctness of Stress Features	0	0	3
Stress Feature % Coverage	0	0	2
Stress Feature Continuity	0	0	2
Root Size	0	0	0
Root Quantity	0	0	0
Vertical continuity of roots	0	0	0
Pore Size	0	0	1
Pore Quantity	0	0	2
Vertical continuity of Pores	0	0	1
RMF Quantity	2	2	3
RMF Distinctness	2	2	3
RMF Hardness	0	1	1
RMF Size	0	1	1
CaCO3 Development Stage	1	2	1
Carbonate Nodule Size	0	1	0
Carbonate Nodule Frequency	0	1	0
Carbonate Filament Size	1	1	1
Carbonate Filament Frequency	1	1	2
Quantity of Crystals	0	1	0
Size of Crystals	0	1	0
Quantity of Biological Concentrations	2	2	2
Sedimentary Bedding thickness designation	0	0	0
Sorting within bedding/laminae	0	0	0
Distinctness of Horizon (upper boundary)	n/a	2	3
Distinctness of Horizon (lower boundary)	2	3	n/a

Profile 5

Zone 1, A/Bw

Zone 1 refers to an A/Bw-horizon that extends from the modern, eroded surface (0 cmbs) to 13 cm below surface and is characterized by medium, moderately developed, subangular blocky peds comprised of a strong brown (7.5YR 5/6 dry) to brown (7.5YR 4/4) silty loam matrix. Matrix consistence ranges from soft when dry, to loose and non-plastic when moistened. Exterior ped faces very slightly effervesce when exposed to 10% HCl solution while the matrix and interior ped parting lanes are nonreactive. Features along ped faces include many, fine and very fine dendritic, tubular and interstitial pores with high vertical continuity. These are thought to be in part, an effect of the many fine and medium-sized, dendritic and tubular roots with high vertical continuity that grow through ped structures. Another characteristic of the zone is the common presence of bioturbation in the form of root sheaths, insect casts, and worm channels. The lower boundary of the zone is smooth and gradual.

Zone 2, A/Bt

Zone 2 refers to an A/Bt-horizon that extends from 13 to 27.90 cm below surface and is characterized by fine, strongly developed, prismatic peds comprised of strong brown (7.5YR 4/6 dry; 7.5YR 4/4 moist) silty loam. Matrix consistence ranges from moderately hard when dry, to friable and very plastic when moistened. The matrix, as well as exterior ped faces, slightly effervesce when exposed to a 10% HCl solution. Visible pores are relatively few in Zone 2 and manifest as very fine, dendritic and interstitial pores with moderate vertical continuity on ped faces. Stress features area also common characteristics among peds in this zone. These include discontinuous, distinct

pressure faces with undulating “pocked” surfaces that occur along vertical ped planes. Few, waxy clay films (argillans) are also distinct, and occur discontinuously on ped faces. Roots are also noticeably fewer than in the above zone. Few, very fine, hair-like roots with moderate vertical continuity grow in discrete areas through ped structures. Other characteristics in this zone include the presence of gypsum and carbonate. Few, very fine gypsum crystal masses occur on ped faces and Stage I carbonate formation also occurs. Carbonates manifest as few, very fine, thread-like and dendritic filaments that predominantly occur in cracks and pores on vertical ped faces. Few very fine carbonate nodules and masses also occur. These are predominantly spherical in shape and occur along ped faces. Bioturbation in the form of insect casts, linear worm channels, and root sheaths are common, some of which contain observable amounts of fecal pellets. The lower boundary of the zone is smooth and gradual.

Zone 3, A/Bk

Zone 3 refers to an A/Bk-horizon that extends from 27.90 to 59.10 cm below surface and is characterized by fine, weakly developed wedge-shaped peds comprised of a strong brown (7.5YR 5/6 dry) to brown (7.5YR 4/4) silty loam matrix. Matrix consistence ranges from moderately hard when dry, to friable and slightly plastic when moistened. When exposed to a 10% HCl solution, ped faces slightly effervesce, while the matrix and interior parting planes remain nonreactive. Like the zone above, very few, fine dendritic roots grow through ped structures. Very few, fine, dendritic pores with low vertical continuity also occur on ped faces. Stage I carbonate development manifests as medium and fine, spherical and reticulate nodules that commonly adhere to ped faces. Fine, dendritic and thread-like carbonate filaments are fewer than the above zone and

occur in cracks and lining surfaces of pores in discrete areas on and between vertical ped faces. Few, fine dendritic and thread-like rhyzoliths also occur as infillings within root pores. The lower boundary of the zone is smooth and diffuse.

Zone 4, Btk

Zone 4 refers to a Btk-horizon that extends from 59.10 to 95.80 cm below surface and is characterized by medium, moderately developed, wedge-shaped peds comprised of a strong brown (7.5YR 5/6 dry) to brown (7.5YR 4/4 moist) silt. Matrix consistence ranges from slightly hard when dry, to friable and plastic when moistened. Exterior ped faces, interior parting planes, and matrix are nonreactive when exposed to a 10% HCl solution. Distinct, loose, fine sand grains (7.5YR 5/6) commonly coat ped faces and are discontinuous. Few irregular and dendritic pores occur along ped faces and exhibit low vertical continuity. Few, fine, dendritic and tubular roots with moderate vertical continuity grow between ped faces and long parting planes. Unlike the zones above, Zone 4 presents with few Mn masses that accumulate on ped faces as platy, distinct and discontinuous “patches”. Few, soft, spherical Mn nodules also adhere to vertical ped faces. Stage II carbonate development is also observed. Very fine and fine carbonate nodules ranging in shape from cubic to spherical commonly adhere to vertical ped faces. Irregular, dendritic, and thread-like carbonate filaments and soft masses are also common. Filaments manifest in cracks and pores on ped faces and accumulate around pore openings. Few, fine, dendritic rhyzoliths also form in root pores. Bioturbation in the form of root sheaths, insect burrows, and linear, cylindrical worm channels are common. The lower boundary of the zone is smooth and abrupt.

Zone 5, Btss

Zone 5 refers to a Btss-horizon that extends from 95.80 to 154.20 cm below surface and is characterized by medium, strongly developed, angular blocky peds comprised of a yellowish-brown (10YR 5/4 dry; 10YR 5/6 moist) silty loam matrix. Matrix consistence ranges from moderately hard when dry, to friable and very plastic when moistened. Exterior ped faces very slightly effervesce when exposed to a 10% HCl solution, though interior parting planes and matrix are nonreactive. Yellowish-brown (10YR 5/4) fine silt coating exterior ped faces are common, patchy, and distinct. Pressure features including pressure faces and slickensides are common and distinct, though their coverage on ped faces is discontinuous. Both features tend to form along horizontal ped faces and parting planes. Very fine and medium root pores, root casts, and very fine tubular pores with moderate vertical continuity also occur on ped faces and among ped parting planes.

Redox features are common and include soft, spherical Mn masses and thread-like filaments. These commonly accumulate in pores, along cracks on ped faces, and on the surface of slickensides. Calcium carbonate manifesting as many, very fine, soft carbonate masses and thread-like filaments line surfaces and openings of pores and cracks on ped faces. Very few, fine tubular and dendritic rhyzoliths also infill pores. Bioturbation in the form of linear, cylindrical worm channels and insect burrows are common. The lower boundary of the zone is smooth and gradual.

Zone 6, Bty

Zone 6 refers to a Bty-horizon that extends from 154.20 to 200.10 cm below surface and is characterized by coarse, strongly developed, prismatic peds comprised of a

yellowish-brown (10YR 5/4 dry) to brown (10YR 4/3) silty loam matrix. Matrix consistence ranges from moderately hard when dry, to friable and plastic when moistened. Exterior ped faces strongly effervesce when exposed to a 10% HCl solution, though interior parting planes and matrix are nonreactive. Fine, dark yellowish-brown (10YR 4/4) silty films are common, distinct and discontinuous on vertical ped faces. Strongly pressure faces commonly mottled with fine Mn masses, are also distinct and discontinuous. Few slickensides develop along horizontal ped faces. Also common are distinct, discontinuous ferriargillans on ped faces and parting planes. Few, very fine dendritic and tubular roots with moderate vertical continuity line ped faces. Ferriargillans are made more apparent by the frequent appearance of Mn masses that develop into platy structures along ped faces and into dendritic and thread-like filaments lining cracks and pores. Mn nodules, slightly hard in consistence, also occur along ped faces, commonly adhering to slickenside and pressure face features.

Carbonate filaments are common and infill cracks on ped faces and accumulate within and around pore openings. Fine, dendritic and tubular rhyzoliths also commonly accumulate along root channels and pores. Gypsum crystal accumulations occur more commonly in this zone, and manifest as fine clusters along pores, cracks and voids. Bioturbation in the form of linear, cylindrical worm channels, insect burrows, and root sheaths are also common. The lower boundary of the zone is smooth and clear.

Zone 7, Btky

Zone 7 refers to a Btky-horizon that extends 220.10 to 226.10 cm below surface and is characterized by medium, strongly developed, prismatic peds comprised of a brown (7.5YR 5/4 dry; 7.5YR 4/4 moist) silty loam matrix. Matrix consistence ranges

from slightly hard when dry, to friable and plastic when moistened. Both exterior ped faces and interior matrix and parting planes very slightly effervesce when exposed to a 10% HCl solution. Weak, discontinuous and distinct pressure faces are common features along ped faces, as are fine, dendritic and tubular pores with moderate vertical continuity. Mn masses frequently occur throughout the zone and manifest as platy masses along ped faces, and as dendritic and thread-like masses lining cracks and pores. Stage II carbonate development is also observed. Fine, platy carbonate flakes, and cubic and spherical carbonate nodules are common, as are dendritic, thread-like filaments developing along ped faces and within the matrix. Few, fine, tubular rhyzoliths also occur. Fine gypsum crystals are common and accumulate along pores and cracks on ped faces. Bioturbation in the form of insect burrows, linear, cylindrical worm channels, and very fine root sheaths are relatively few. The lower boundary of the zone is smooth and clear.

Zone 8, Bs

Zone 8 refers to a Bs-horizon that extends from 226.10 to 270.50 cm below surface and is characterized by medium, strongly developed prismatic peds comprised of yellowish-red (5YR 5/7 dry; 5YR 4/6 moist) loam. Matrix consistence ranges from slightly hard when dry, to friable and slightly plastic when moistened. Both exterior ped faces and interior matrix and parting planes very slightly effervesce when exposed to a 10% HCl solution. Silty coatings along ped faces are common features, forming discontinuously as “patches” covering ~20% o of ped surface area. Also common are strongly developed, discontinuous and distinct pressure faces along all ped faces and parting planes. Very fine dendritic and tubular pores with low vertical continuity are also common, though no roots are observed in profile. Mn masses, accumulating as medium,

platy structures on ped faces, as soft spherical nodules, and as thread-like, dendritic filaments infilling pores, cracks, and lining ped faces are common. Stage I carbonate development also occurs. Few, fine thread-like and dendritic carbonate filaments infill pores and cracks on ped faces, and occur in bioturbated areas. Bioturbation in the form of linear, cylindrical worm channels and insect burrows are many. The lower boundary of the zone is smooth and gradual.

Zone 9, Btk

Zone 9 refers to a Btk-horizon that extends from 270.50 to 290.5 cm below surface, marking the bottom of Profile 5. The zone is characterized by medium, moderately developed, subangular blocky peds comprised of strong brown (7.5YR 5/6 dry) to brown (7.5YR 4/4 moist) silty loam. Matrix consistence ranges from slightly hard when dry, to firm and slightly plastic when moistened. Both exterior ped faces and interior matrix and parting planes very slightly effervesce when exposed to a 10% HCl solution. Discontinuous, distinct, strong brown (7.5YR 5/6) sands commonly coat ped faces. Distinct yet weakly developed pressure faces also occur on ped faces, discontinuously covering ~60% of ped face surface area. Very fine tubular and irregularly shaped pores are also visible on ped faces and appear to have moderate vertical continuity, though no roots are observed in profile. Mn masses are common and occur as fine, platy rosettes and thread-like filaments on ped faces, infilling cracks, and lining pores. Stage II carbonate development also occurs. Carbonates in the form of very fine platy “flecks” and thread-like filaments commonly adhere to portions of the matrix, along ped parting planes, and along ped faces themselves. Few, very fine spherical carbonate nodules occur between ped faces. Bioturbation in the form of linear, cylindrical worm

channels and insect burrows are many. The lower boundary of the zone is uncharacterized, representing the base of the Profile 5 exposure.

Profile 5 Field Form Summary

Profile 5: Field Description Summary by Zone (Nominal Characteristics)										
Zone Characteristics		***Zone 1***	***Zone 2***	***Zone 3***	***Zone 4***	***Zone 5***	***Zone 6***	***Zone 7***	***Zone 8***	***Zone 9***
Zone Thickness		13	14.9	31.2	36.7	58.4	45.9	26	44.4	20
Munsell Color (Dry)		7.5YR 5/6	7.5YR 4/6	7.5YR 5/6	7.5YR 5/6	10YR 5/4	10YR 5/4	7.5YR 5/4	5YR 5/7	7.5YR 5/6
Munsell Color (Moist)		7.5YR 4/4	7.5YR 4/4	7.5YR 4/4	7.5YR 4/4	10YR 4/4	10YR 4/3	7.5YR 4/4	5YR 4/6	7.5YR 4/4
Horizon Designation		2A/Bw	2A/Bt	2A/Bk	2Btk	2Btss	2Bty	2Btky	3Bs	3Btk
Texture	Sand (S)									
	Coarse Sand (COS)									
	Fine Sand (FS)									
	Very Fine Sand (VFS)									
	Loam (L)								X	
	Loamy Coarse Sand (LCOS)									
	Loamy Sand (LS)									
	Loamy Fine Sand (LFS)									
	Coarse Sandy Loam (COSL)									
	Sandy Loam (SL)									
	Fine Sandy Loam (FSL)									
	Very Fine Sandy Loam (VFSL)									
	Loamy Sand (LS)									
	Silt (SI)	X	X	X		X	X	X		X
	Silty Loam (SL)				X					
	Sandy Clay Loam (SCL)									
	Clay Loam (CL)									
	Silty Clay Loam (SICL)									
	Sandy Clay (SC)									
	Silty Clay (SIC)									
	Clay (C)									
Unit Structure	Granular (gr)									
	Angular blocky (abk)					X				X

	Subangular blocky (sbk)	X								
	Lenticular (lp)									
	Platy (pl)									
	Wedge (wg)			X	X					
	Prismatic (pr)		X				X	X	X	
	Columnar (cpr)									
	Single Grain (sg)									
	Massive (m)									
Coats & Films	Carbonate coats (CAF)									
	Silica (SIF)									
	Clay films (CLF)		X			X				
	Clay bridges (BRF)									
	Gibbsite coats (GBF)									
	Organoargillans (OAF)									
	Sand coats (SNF)				X					X
	Silt coats (SLF)					X	X		X	
	Skeletans (SKF)									
	Gypsum coats (GYF)									
	Organic stain (OSF)									
Stress Feature Type	Pressure faces (PRF)		X			X	X	X	X	X
	Slickensides (SS)					X	X			
	Shear face (SSG)									
Stress feature Loci in Ped	All ped faces (PF)						X	X	X	X
	Bottom ped faces (BPF)					X				
	Top of ped faces (TPF)									
	Top of soil column (TC)									
	Vertical Ped Faces (VF)		X							
	Throughout Ped (T)					X	X			
Root shape	Dendritic (DT)	X		X	X	X	X	X		

	Irregular (IG)							X		
	Tubular (TU)	X			X	X	X	X		
	Vesicular (VE)									
	Interstitial (IR)									
Root Loci in Ped	All ped faces (PF)		X	X			X	X		
	Bottom ped faces (BPF)									
	Top of ped faces (TPF)									
	Top of soil column (TC)									
	Vertical Ped Faces (VF)				X	X				
	Throughout Ped (T)		X		X	X				
Root- Other loci	Between sand grains (BG)									
	On bedrock (BK)									
	Bottom surfaces of rock (BR)									
	On concretions (CC)									
	On nodules (ON)									
	On rock fragments (RF)									
	On slickensides (SS)									
	On surfaces along pores (SP)									
	On top surface of rock fragments (TR)									
Pore shape	Dendritic (DT)	X		X	X		X		X	X
	Irregular (IG)				X		X	X		X
	Tubular (TU)	X				X		X	X	
	Vesicular (VE)									
	Interstitial (IR)	X								
Pore loci in ped	On all ped faces (PF)	X	X		X	X	X	X	X	X
	On bottom of ped faces (BF)									
	Top of ped faces (TPF)									
	Top of soil column (TC)									

	Vertical Ped Faces (VF) Throughout Ped (T)	X								
Pore- Other loci	Between sand grains (BG) On bedrock (BK) On bottom surfaces of rocks (BR) On concretions (CC) On nodules (ON) On rock fragments (RF) On slickensides (SS) On surfaces along pores (SP) On top surface of rock fragments (TR)									
RMF Type	Reduced matrix (RMX) Clay depletions (CLD) Iron depletions (FED) Iron masses (FM) Manganese masses (MNM) Iron-manganese masses (FMM) Ironstone (FSN) Ferriargillans (FEF) Iron-manganese nodules (FMN) Iron-manganese concretions (FMC) Manganese films (MNF)				X X X	X	X X	X X	X X	X
RMF Shape	Cubic (CU) Cylindrical (C) Dendritic (DT) Irregular (I) Lenticular (L) Pendular (PE)					X	X	X		

	Platy (P)				X		X	X	X	X
	Reticulate (R)									X
	Rosette-like (RO)									
	Spherical (S)				X	X	X	X	X	
	Thread-like (T)					X	X	X	X	X
RMF Loci in Ped	All ped faces (PF)					X	X	X	X	X
	On bottom of ped faces (BF)									
	On top of ped faces (TF)									
	On top of soil column (TC)									
	Vertical Ped Faces (VF)				X					
	Throughout center of ped (T)						X			
RMF Other loci	Between sand grains (BG)									
	On bedrock (BK)									
	Bottom surfaces of rocks (BR)									
	On concretions (CC)									
	On nodules (ON)									
	On rock fragments (RF)									
	On slickensides (SS)					X				
	On surfaces along pores (SP)					X	X	X	X	X
	In cracks (CRK)				X	X			X	X
	In matrix (MAT)									
	On top of rock fragments (TF)									
Carbonate Loci (General)	All ped faces (PF)		X	X	X	X	X	X		X
	On bottom faces of peds (BF)									
	On top faces of peds (TF)									
	On tops of soil columns (TC)									
	On vertical ped faces (VF)									

	Through center of peds (T)									
	Bridging sand grains (BG)									
	On bedrock (BK)									
	On bottom surfaces of rocks (BR)									
	On concretions (CC)									
	On nodules (ON)									
	On rock fragments (RF)									
	On slickensides (SS)									X
	On surfaces along pores (SP)									
	On top surfaces of rock fragments (TR)									
Carbonate shape	Cubic (CU)				X			X		
	Cylindrical (C)									
	Dendritic (DT)		X		X	X	X		X	
	Irregular (I)		X							
	Lenticular (L)									
	Pendular (PE)									
	Platy (P)							X		X
	Reticulate (R)			X						
	Rosette-like (RO)									
	Spherical (S)		X	X	X			X		X
	Thread-like (T)		X	X	X	X	X	X	X	X
Carbonate Matrix Location	In matrix (MAT)									
	In matrix around redox depletions (MAD)									
	In matrix around redox concentrations (MAC)									
	Throughout (Finely disseminated) (TOT)									
Carbonate loci in/on Ped	Between peds (BPF)		X							
	Infused in matrix on faces (MPF)				X			X		

	On faces of peds (all orientations) (APF)			X			X	X		
	On horizontal ped faces (HPF)									
	On vertical ped faces (VF)		X		X					
Carbonate Pore Location	Infused into matrix along faces of peds (MPF)				X	X		X		X
	Lining pores (LPO)		X	X			X	X	X	X
	On surfaces along pores (SPO)		X	X			X	X	X	X
	on surfaces along root channels (RPO)		X	X			X	X		
Other Carbonate Locations	In cracks (CRK)			X	X		X	X	X	X
	At top of horizon (TOH)									
	Around rock fragments (ARF)									
	On bottom of rock fragments (BRF)									
	On slickensides (SSS)									
	Along lamina or strata surfaces (ALS)									
Types of Finely Disseminated Concentrations	Finely disseminated carbonates (FDC)							X	X	X
	Finely disseminated salts (FDS)									
	Finely disseminated gypsum (FDG)									
Masses Types	Carbonate (CAM)		X			X				
	Clay bodies (CBM)									
	Gypsum crystal clusters (GNM)						X	X		
	Gypsum (GYM)									
	Salt (SAM)									
	Silica (SIM)									
Nodule Type	Carbonate (CAN)			X	X			X		X
	Opal (OPN)									
	Durinodes (DNN)									
	Ortstein (ORT)									

	Gibbsite (GBN)									
Type of Concretions	Carbonate (CAC) Gibbsite (GBC) Silica (SIC) Titanium oxide (TIC)									
Crystal Type	Calcite (CAX) Gypsum (GYX) Salt (SAX) Selenite (SEC)		X				X	X		
Type of Biological Concretions	Diatoms (DIB) Fecal pellets (FPB) Insect casts (ICB) Plant phytoliths (PPB) Worm casts (WCB) Root sheaths (RCB) Shell fragments (SFB) Sponge spicules (SSB)	 X X X X	 X X X	 X 	 X X X	 	 X X X	 X X X	 X X 	 X X
Miscellaneous	Carbonate bands (CBA) Carbonate beds (CBE) Carbonate laminae (CAL) Carbonate Ooliths (CAO) Carbonate pisoliths (CAP) Carbonate root casts (CRC)			 X						
Shape of Bedding/ Laminae	Even/parallel (EP) Even discont. parallel (EDP) Wavy parallel (WP) Wavy discont. parallel (WDP)									

	Curved parallel (CP) Curved discont. parallel (CDP) Even non-parallel (ENP) Even discon. Non-parallel (EDNP) Wavy non-parallel (WNP Wavy discont. Non-parallel (WDNP) Curvy non-parallel (CNP) Curvy discontinuous non-parallel (CDNP)									
Grain Rounding (Bedding/ Laminae)	Angular (A) Sub angular (SA) Round (R) Spherical (SR)									
Zone Topography (Upper Bound.)	Smooth (S) Wavy (W) Irregular (I) Broken (B)	X	X	X	X	X	X	X	X	X
Zone Topography (Lower Bound.)	Smooth (S) Wavy (W) Irregular (I) Broken (B)	X	X	X	X	X	X	X	X	n/a

Ordinal Characteristic Ratings	***Zone 1***	***Zone 2***	***Zone 3***	***Zone 4***	***Zone 5***	***Zone 6***	***Zone 7***	***Zone 8***	***Zone 9***
Plasticity	0	3	1	2	3	3	2	2	1
Percent Gravel	0	0	0	0	0	0	0	0	0
Rupture resistance Dry	1	3	3	2	3	3	2	2	2
Rupture resistance Moist	0	2	2	2	2	2	2	2	1
Rupture resistance if cemented	0	0	0	0	0	0	0	0	0
HCl Effervescence Response (Ped face)	1	1	2	0	1	3	1	1	1
HCl Effervescence Response (Matrix)	0	0	0	0	0	0	1	1	1
Ped Size (can only compare if same shape)	2	1	1	2	2	3	2	2	2

Grade	2	3	1	2	3	3	3	3	2
Distinctness of Coats and Films	0	2	0	3	3	3	0	2	2
Coat/Film % Coverage	0	2	0	3	2	2	0	2	2
Coat/Film Continuity	0	2	0	2	1	2	0	1	2
Distinctness of Stress Features	0	2	0	0	3	3	2	2	2
Stress Feature % Coverage	0	2	0	0	2	3	2	2	2
Stress Feature Continuity	0	2	0	0	2	3	1	1	1
Root Size	2	1	1	1	1	1	0	0	0
Root Quantity	3	3	1	1	1	1	0	0	0
Vertical continuity of roots	3	2	1	1	1	1	0	0	0
Pore Size	1	1	1	1	1	1	2	1	1
Pore Quantity	3	1	1	1	1	1	2	1	2
Vertical continuity of Pores	3	2	1	1	1	1	2	1	2
RMF Quantity	0	0	0	1	2	3	3	2	2
RMF Distinctness	0	0	0	2	3	4	2	2	2
RMF Hardness	0	0	0	1	1	2	1	1	1
RMF Size	0	0	0	1	2	2	1	2	1
CaCO3 Development Stage	0	1	1	2	1	1	2	1	2
Carbonate Nodule Size	0	0	1	1	0	0	2	0	1
Carbonate Nodule Frequency	0	0	1	2	0	0	2	0	2
Carbonate Filament Size	0	1	1	1	1	1	1	1	1
Carbonate Filament Frequency	0	1	1	2	2	2	2	1	2
Quantity of Crystals	0	1	0	0	0	2	2	0	0
Size of Crystals	0	1	0	0	0	1	1	0	0
Quantity of Biological Concentrations	3	2	1	2	3	2	1	3	3
Sedimentary Bedding thickness designation	0	0	0	0	0	0	0	0	0
Sorting within bedding/laminae	0	0	0	0	0	0	0	0	0
Distinctness of Horizon (upper boundary)	n/a	0	0	0	3	1	2	2	1
Distinctness of Horizon (lower boundary)	0	0	0	3	1	2	2	1	n/a

APPENDIX G: Thin section provenience data.

Thin Section Provenience Data (Elevations from Datum A, 1000 m above sea level)							
Collection Year	*Thin section ID*	*Block*	*Profile*	*Zone(s)*	*Upper Elev.*	*Lower Elev.*	AU Context
2018	44MM6S9A	A	1	4	996.251	996.211	2
2018	44MM6S9C	A	1	5	996.201	996.171	3
2018	MM8P2AZ3B	B	2A	3	998.958	998.888	2
2017	38MM10S6A	C	2A	5	998.25	998.21	2
2017	38MM10S6C	C	2A	6	998.2	998.16	2
2018	MM10P2AZ9A	D	2A	10	996.805	996.715	2
2018	MM12P2AZ11B	E	2A	11	996.012	995.932	3
2018	MM7P2BZ11	F	2B	4	996.085	996.025	3
2018	MM1P2BZ12B	G	2B	5	995.948	995.858	3
2018	MM3P2BZ14B	H	2B	7	995.157	995.107	3
2018	MM4P2BZ15	I	2B	8	994.804	994.754	3
2018	MM6P2BZ16B	J	2B	9	993.896	993.846	3
2018	MM5P2BZ17B	K	2B	10	993.709	993.609	3
2018	MM14P2DZ2B	L	2C	2	996.403	996.363	2
2018	MM15P2DZ3A	M	2C	3	996.21	996.12	3
2017	40MM5S3A	N	5	3	999.746	999.686	2
2017	40MM5S3B	N	5	4	999.715	999.665	2

REFERENCES

Autin, W.J.
1992 Use of alloformations for definition of Holocene meander belts in the middle Amite River, southeastern Louisiana. *Geological Society of America Bulletin* 104:233-241.

Backwell, L., F. d'Errico, and L. Wadley
2008 Middle Stone Age bone tools from the Howiesons Poort layers, Sibudu Cave, South Africa. Journal of Archaeological Science 35:1566-1580.

Baiyegunhi, C., K. Liu, and O. Gwavava
2017 Geochemistry of sandstones and shales from the Ecca Group, Karoo Supergroup, in the Eastern Cape Province of South Africa: Implications for provenance, weathering and tectonic setting. *Open Geosciences* 9:340-360. Electronic document, https://doi.org/10.1515/geo-2017-0028, accessed May 15, 2019.

Barham, L. and P. Mitchell
2008 *The First Africans: African Archaeology from the Earliest Toolmakers to the most recent Foragers*. Cambridge World Archaeology Series, Cambridge University Press, Cambridge.

Barker, C.H.
2011 Utilizing published data for DTM construction and drainage basin delineation in the Modder River catchment, Free State, South Africa. *South African Geographical Journal* 93:89-103.

Bar-Matthews, M., C.W. Marean, Z. Jacobs, P. Karkanas, E.C. Fisher, A.I.R. Herries et al.
2010 A high resolution and continuous isotopic speleothem record of paleoclimate and paleoenvironment from 90 to 53 ka from Pinnacle Point on the south coast of South Africa. *Quaternary Science Review* 29:2131-2145.

Beaumont, P.B., and J.C. Vogel
1972 On a new radiocarbon chronology for Africa south of the Equator: Part 2. *African Studies* 31(3):155-182.

Beaumont, P.B., de Villers, H., and J.C. Vogel
1978 Modern man in sub-Saharan Africa prior to 49 000 years B.P.: a review and evaluation with particular reference to Border Cave. *South African Journal of Science* 74:409-419.

Behrensmeyer, A.K.
1987 Miocene fluvial facies and vertebrate taphonomy in northern Pakistan. *Special Publications of the Society of Economic Paleontologists and Mineralogists* SP39.

Birkeland, P.W.
1999 *Soils and Geomorphology*. 3rd ed. Oxford University Press, New York.

Born, S.M. and D.F. Ritter
1970 Modern terrace development near Pyramid lake, Nevada and its geologic implications. *Geological Society of America Bulletin* 81:1233-1242.

Bousman, C.B.
2005 Coping with risk: Later Stone Age hunter-gatherers at Blydefontein Rockshelter. *Journal of Anthropological Archaeology* 24:193-226.

Bousman, C.B. and J. Brink
2014 Excavation of Middle and Later Stone Age Sites at Erfkroon, South Africa- NSF 0918074. NSF Grant Final Report, February 19, 2014.
2017 The emergence, spread, and termination of the Early Later Stone Age event in South Africa and southern Namibia. *Quaternary International* xxx:1-20. In press.

Bousman, C.B., J.S. Brink, H. Meier, R. Mauldin, L. Scott, and L. Rossouw
In prep Late Quaternary Soil Stratigraphy and Palaeoenvironments in Modder River fluvial sediments at Erfkroon, South Africa.

Bridgeland, D.R. and R. Westaway
2008 Preservation patterns of Late Cenozoic fluvial deposits and their implications: results from IGCP 449. *Quaternary International* 189(1):5-38.

Brink, J.S.
2005 The Evolution of the Black Wildebeest, *Connochaetes gnou*, and Modern Large Mammal Faunas in Central South Africa. Ph.D. Dissertation, University of Stellenbosch, South Africa.

Brink, J.S., C.B. Bousman, and R. Grün
2015 A reconstruction of the skull of *Megalotragus priscus* (Broom, 1909), based a find from Erfkroon, Modder River, South Africa, with notes on the chronology and biogeography of the species. *Palaeoecology of Africa* 33:71-94.

Brink, J.S. and J. Lee-Thorpe
1992 The feeding niche of an extinct springbok, *Antidorcas bondi* (Antilopini, Bovidae), and its palaeoenvironmental meaning. *South African Journal of Science* 88:227-229.

Brown, T.M. and M.J. Kraus
1987 Integration of channel and floodplain suites, 1: Developmental sequence and lateral relations of alluvial paleosols. *Journal of Sedimentary Petrology* 57:578-601.

Bullock, P., N. Fedoroff, A. Jongerius, G. Stoops, and T. Tursina
1985 *Handbook for Soil Thin Section Description.* Waine Research Publications, Wolverhampton.

Buol, S.W. and M.S. Yesilsoy
1964 A genesis study of a Mohave sandy loam profile. *Proceedings of the Soil Science Society of America* 28:254-256.

Bushue, L.J., J.B. Fehrenbacher, and B.W. Ray
1974 Exhumed paleosols and associated modern till soils in western Illinois. *Proceedings of the Soil Science Society of America* 34:665-669.

Butzer, K.W.
1971 Fine alluvial fills in the Orange and Vaal basins of South Africa. *Proceedings, Association of American Geographers* 3:41-48.

Catt, J.A.
1990 Paleopedology manual. *Quaternary International* 6:1-95.
1998 Report from working group on definitions used in paleopedology. *Quaternary International* 51/52:84.

Catuneanu, O., H. Wopfner, P.G. Eriksson, B. Cairncross, B.S. Rubidge, R.M.H. Smith, and P.J. Hancox
2005 The Karoo basins of south-central Africa. *Journal of African Earth Sciences* 43:211-253.

Chadwick, O.A. and W.D. Nettleton
1994 Quantitative relationships between net volume change and fabric properties during soil evolution. In *Soil Micromorphology: Studies in Management and Genesis, Developments in Soil Science, Vol. 22*, pp. 353-360, edited by A.J. Ringrose-Voase and G.S. Humphreys. Elsevier, Amsterdam.

Chase, B.M. and M.E. Meadows
2007 Late Quaternary dynamics of southern Africa's winter rainfall zone. *Earth-Science Reviews* 84:103-138.

Churchill, S.E., J.S. Brink, L.R. Berger, R.A. Hutchinson, L. Rossouw, D. Stynder, P.J. Hancox, D. Brandt, S. Woodborne, J.C. Loock, J.C., and P. Ungar.
2000 Erfkroon: A new Florisian fossil locality from fluvial contexts in the western Free State, South Africa. *South African Journal of Science* 96:161-163.

Clark, J.D., Y. Beyene, G. Wolde, W.K. Hart, P.R. Renne, H. Gilbert, A. Defleur, G. Suwa, S. Katoh, K.R. Ludwig, J.R. Boisserie, B. Asfaw, and T.D. White
2003 Stratigraphic, chronological and behavioral contexts of Pleistocene Homo Sapiens from Middle Awash, Ethiopia. Nature 423(6941):747-752.

Coetzee, J.A.
1967 Pollen analytical studies in east and southern Africa. *Palaeoecology of Africa* 3:1-146.

Cochrane, G.W.G.
2008 The transition from Howieson's Poort to post-Howieson's Poort Industries in southern Africa. *South African Archaeological Society Goodwin Series* 10:157-167.

Courty, M.A.
1990 Pedogenesis on Holocene calcareous parent materials under semi-arid conditions (Ghaggar Plain, NW India). In *Soil Micromorphology: A Basic and Applied Science, Developments in Soil Science, Vol. 19.*, pp. 361-366, edited by L.A. Douglas. Elsevier, Amsterdam.

Crétat, J., Y. Richard, B. Pohl, M. Rouault, C. Reason, and N. Fauchereau
2012 Recurrent daily rainfall patterns over South Africa and associated dynamics during the core of the austral summer. *International Journal of Climatology* 32:261-273.

Dalal, R.C. and R.J. Henry
1986 Simultaneous determination of moisture, organic carbon and total nitrogen by near infrared reflectance spectrophotometry. *Soil Science Society of America Journal* 50:120-123.

Dalan, R.A. and S.K. Banerjee
1998 Solving Archaeological Problems Using Techniques of Soil Magnetism. *Geoarchaeology: An International* Journal 13(1):3-36.

Dart, R.
1925 Australopithecus africanus: The Man-Ape of South Africa. *Nature* 115(2884):195-199.

Deacon, H.
1976 *Where Hunters Gathered: A Study of Holocene Stone Age People in the Eastern Cape*. South African Archaeological Society Monograph Series 1, Cape Town.

Deacon, H.J. and J. Deacon
1999 *Human Beginnings in South Africa: Uncovering the Secrets of the Stone Age*. AltaMira Press, Lanham, Maryland.

Deacon, J.
1978 Changing patterns in the late Pleistocene/early Holocene prehistory of southern Africa, as seen from the Nelson Bay Cave stone artifact sequence. *Quaternary Research* 10:84-111.
1984a The Later Stone Age of southern most Africa. In *BAR International Series*, pp. 213. Oxford.
1984b Later Stone Age people and their descendants in southern Africa. In *Southern African Prehistory and Paleoenvironments* edited by R.G. Klein, pp. 221-328. Balkema, Rotterdam.
1995 Two Late Pleistocene-Holocene Archaeological Depositories from the Southern Cape, South Africa. The South African Archaeological Bulletin 50(162):121-131.

Deacon, J. and N. Lancaster
1988 *Late Quaternary Palaeoenvironments of southern Africa*. Oxford University Press, New York.
1995 An unsolved mystery at the Howiesons Poort name site. *South African Archaeological Bulletin* 50:110-120.

Deacon, H.J. and F. Thackeray
1984 Late Pleistocene environmental changes and implications for the archaeological record in southern Africa. In *Late Cenozoic palaeoclimates of the Southern Hemisphere*, pp. 375-390, edited by J.C. Vogel. Balkema, Rotterdam.

Dearing, J.A.
1994 *Environmental magnetic susceptibility: using the Bartington MS2 system*. Chi Publishing.
1999 Environmental Magnetic Susceptibility. British Library Cataloguing. Electronic document, https://www.gmw.com/magnetic_properties/pdf/Om0409%20J_Dearing_Handbook_iss7.pdf, accessed October 13, 2018.

Dearing, J.A., R.J.L. Dann, K. Hay, J.A. Lees, P.J. Loveland, B.A. Maher, and K. O'Grady
1996 Frequency-dependent susceptibility measurements of environmental materials. *Geophysical Journal International* 124:228-240.

d'Errico, F., M. Vanhearen, and L. Wadley
2008 Possible shell beads from the Middle Stone Age layers of Sibudu Cave, South Africa. *Journal of Archaeological Science* 35:2675-2685.

d'Errico, F., L. Backwell, and L. Wadley
2012 Identifying regional variability in Middle Stone Age bone technology: the case of Sibudu Cave. *Journal of Archaeological Science* 39(7):2479-2495.

Dokuchaev, V.V.
1883 *Russkii Chernozem*. Moscow. In *Soils: Genesis and Geomorphology* by R.J. Schaetzl and M.L. Thompson, pp. 284-300. Cambridge University Press, New York.

Durand, N., H.C. Monger, and M.G. Canti
2010 Calcium carbonate features. In Interpretation of Micromorphological Features of Soils and Regoliths, edited by G. Stoops, V. Marcelino, and F. Mees, pp. 149-194. Elesvier, Amsterdam.

Dusseldorp, G.L., M. Lombard, and S. Wurz
2013 Pleistocene Homo and the updated Stone Age sequence of South Africa. *South African Journal of Science* 109(5/6):1-7.

Eyre, J.K.
1997 Frequency dependence of magnetic susceptibility for populations of single-domain grains. *Geophysical Journal International* 129:209-211.

Farrell, K.M.
1987 Sedimentology and facies architecture of overbank deposits of the Mississippi River, False River region, Louisiana. In Recent Development in Fluvial Sedimentology, pp. 113-120, edited by F.G. Ethridge, R.M. Flores, and M.D. Harvey. *Special Publications for the Society of Economic Paleontologists and Mineralogists* 39:3.3.6.

Fedoroff, N., M.A. Courty, and G. Zhengtang
2010 Calcium carbonate features. In *Interpretation of Micromorphological Features of Soil sand Regoliths* edited by G. Stoops, V. Marcelino and F. Mees. Elsevier, Amsterdam, pp. 149-194.

Fisher, E.C., M. Bar-Matthews, A. Jerardino, and C.W. Marean
2010 Middle and Late Pleistocene palaeoscape modelling along the southern coast of South Africa. *Quaternary Science Reviews* 29:1382-1398.

Freeland, J.
2013 Soil Anistropy: Mechanisms and Hydrologic Consequences. Terra Central. Electronic document, https://blogs.agu.org/terracentral/2013/07/01/soil-anisotropy-mechanisms-and-hydrologic-consequences/, accessed September 30, 2019.

Gale, S.J. and P.G. Hoare
Bulk sampling of coarse clastic sediments for particle-size analysis. *Earth Surface Processes and Landforms* 17(7):729-733.

Gibson, N.E., L. Wadley, and B.S. Williamson
2004 Residue analysis of backed tools from the 60 000 to 68 000 Howiesons Poort Layers at Rose Cottage Cave, South Africa. *Southern African Humanities* 16:1-11.

Gilchrist, A.R., H. Kooi, and C. Beaumont
1994 Post-Gondwana geomorphic evolution of southwestern Africa: implications for the controls on landscape development rom observations and numerical experiments. *Journal of Geophysical Research* 99(12)12,211-12,288.

Goddard, L. and N.E. Graham
1999 Importance of the Indian Ocean for simulating rainfall anomalies of eastern and southern Africa. *Journal of Geophysical Research* 104:19099-19116.

Goldberg, P. and R.I. Macphail
2006 *Practical and Theoretical Geoarchaeology*. Blackwell Publishing, Malden, MA.

Goodwin, A.J.H.
1927 South African Archaeology. *Man* 27:29-31.
1958 Formative years of our prehistoric terminology. *South African Archaeological Bulletin* 13:25-33.

Goodwin, A.J.H. and C. van Riet Lowe
1929 The Stone Age Cultures of South Africa. *Annals of the South African Museum* 27:1-289.

Graham, R.C. and A.T. O'Green
2010 Soil mineralogy trends in California landscapes. *Geoderma* 154:418-437.

Grün, R.
1996 Direct dating of Florisbad hominid. *Nature* 382:500-501.
2006 Direct dating of human fossils. *Yearbook of Physical Anthropology* 49:2-48.

Hall, S.A. and R.J. Goble
2012 Berino Paleosol, Late Pleistocene argillic soil development on the Mescalero Sand Sheet in New Mexico. *Journal of Geology* 120:333-345.

Hawthorne, J.B.
1975 Model of a kimberlite pipe. In Physics and Chemistry of the Earth, pp. 1-15, edited by L. Ahrens et al. Proceedings of the 1st International Kimberlite Conference.

Heaton, T.H.E., A.S. Talma, and J.C. Vogel
1986 Dissolved gas palaeo-temperatures and ^{18}O variations derived from groundwater near Uitenhage, South Africa. *Quaternary Research* 25:79-88.

Heinz, V.
2002 Relict soils as paleoclimatic indicators: Examples from the Austrian Alps and the Central Andes. *Proceedings from the 17th World Congress of Soil Science* 4:1520.

Heller, F. and T.S. Liu
1984 Magnetism of Chinese loess deposits. *Geophysical Journal of the Royal Astrological Society* 77:125-141.

Hendey, Q.B.
1974 The Late Cenzoic Carnivora of the South-Western Cape Province. *Annals of the South African Museum* 63:1-369.

Henshilwood, C.S.
2012a Late Pleistocene techno-traditions in southern Africa: a review of the Still Bay and Howiesons Poort, c. 75-95 ka. *Journal of World Prehistory* 25:205-237.
2012b The Still Bay and Howiesons Poort: 'Palaeolithic' techno-traditions in southern Africa. *Journal of World Prehistory* 52:361-400.

Henshilwood, C.S., F. d'Errico, M. Vanhaeren, K.L. Van Niekerk, and Z. Jacobs
2004 Middle Stone Age Shell Beads from South Africa. *Science* 304:404.

Henshilwood, C.S. and C.W. Marean
2003 The origin of modern human behavior: a critique of the models and their test implications. *Current Anthropology* 44:627-651.

Hewitt, J.
1921 On several implements and ornaments from Strandloper sites in the Eastern Province. *South African Journal of Science* 18:454-467.

Holmes, P.J.
2017 Geomorphology and late Quaternary environmental change: An overview of central southern Africa. In *Changing Climates, Ecosystems and Environments within Arid Southern Africa and Adjoining Regions* edited by Jurgen Rünge, pp. 19-34. Palaeoecology of Africa Volume 33. Taylor & Francis Group, London.

Holmes, P.J. and C.H. Barker
2006 Geological and geomorphological controls on the physical landscape of the Free State. *South African Geographical Journal* 85:65-68.

Hseu, Z.Y. and Z.S. Chen
1999 Micromorphology of redoximorphic features of subtropical anthraquic Ultisols. *Food Science and Agricultural Chemistry* 1:194-202.

Hutson, J.M.
2018 The faunal remains from Bundu Farm and Pneil 6: Examining the problematic Middle Stone Age archaeological record within the southern African interior. *Quaternary International* 466:178-193.

Huggett, R.J.
1975 Soil Landscape Systems: A model of soil genesis. *Geoderma* 13:1-22.
1976 Conceptual models in pedogenesis: A discussion. *Geoderma* 16:261-262.

Hughes, P.D.
2010 Geomorphology and Quaternary stratigraphy: The roles of morpho-, litho-, and allostratigraphy. *Geomorphology* 123:189-199.

Humphreys, A.J.B. and A.I. Thackeray
1983 *Ghaap and Gariep: Later Stone Age studies in the Northern Cape*. South African Archaeological Society Monograph No. 2, Cape Town.

Isbell, J.L., D.I. Cole, and O. Catuneanu
2008 Carboniferous-Permian glaciation in the main Karoo Basin, South Africa: Stratigraphy, depositional controls, and glacial dynamic. *Geological Society of America* Special Paper 441:71-82.

Jacobs, Z. and R.G. Roberts
2008 Testing times: old and new chronologies for the Howieson's Poort and Still Bay industries in environmental contexts. *South African Archaeological Society Goodwin Series* 10:9-34.

Jacobs, Z., R.G. Roberts, R.F. Galbraith, H.J. Deacon, R. Grün, A. Mackay, P. Mitchell, R. Vogelsang, and L. Wadley
2008 Ages for the Middle Stone Age of southern Africa: implications for human behavior and dispersal. *Science* 322:733-735.

Janik, L.J. and J.O. Skjemstad
1995 Characterisation and analysis of soils using mid-infrared partial least squares, II. Correlations with some laboratory data. *Australian Journal of Soil Research* 33:637-650.

Jenny, H.
1941 *Factors of Soil Formation*. McGraw-Hill, New York.

Jerardino, A.
2010 Large shell middens in Lamberts Bay, South Africa: A case study of hunter-gatherer resource intensification. *Journal of Archaeological Science* 37:2291-2302.

Johnson, D.L.
1985 Soil thickness processes. *Catena Supplement* 6:29-40.
1993 Dynamic denundation evolution of tropical, subtropical, and temperate landscapes with three tiered soils: Toward a general theory of landscape evolution. *Quaternary International* 17:67-78.
2000 Soils and soil-geomorphology theories and models: The Macquarie connection. *Annals of the Association of American Geographers* 90:775-782.

Johnson, M.R.
1991 Sandstone petrography, provenance and plate tectonic setting in Gondwana context of the southeastern Cape-Karoo Basin. South African Journal of Geology 94:137-154.

Johnson, M.R., C.J. van Vuuren, J.N.J Visser, D.I. Cole, H. de V. Wickens, A.D.M Christie, D.L. Roberts, and G. Brandl
2006 Sedimentary Rocks of the Karoo Supergroup. In *The Geology of South Africa,* edited by M.R. Johnson, C.R. Anhaeusser, and R.L. Thomas. Geological Society of South Africa, Johannesburg/Council for Geoscience, Pretoria, 2006, pp. 461-499.

Johnson, D.L. and D. Watson-Stegner
1987 Evolution model of pedogenesis. *Soil Science* 143:349-366.

Kaplan, J.
1989 45,000 years of hunter-gatherer history in Natal as seen from Umhlatuzana Rock Shelter. *South African Archaeological Society Goodwin Series* 6:7-16.

King, L.C.
1963 South African Scenery: *A Textbook of Geomorphology, third ed*. Oliver and Boyd, Edinburgh, pp. 308. In *Geological controls on alluvial river behavior: a comparative study of three rivers on the South African Highveld* by S. Tooth, D. Brandt, P.J. Hancox, and T.S. McCarthy (authors). *Journal of African Earth Sciences* 38:79-97.

Kistin, E.J. and Peter J. Ashton
2008 Adapting to Change in Transboundary Rivers: An Analysis of Treaty Flexibility on the Orange-Senqu River Basin. *Water Resources Development* 24(3):385-400.

Klein, R.G.
1974 Environment and Subsistence of Prehistoric Man in the Southern Cape Province, South Africa. *World Archaeology* 5(3):249-284.
1986 The prehistory of Stone Age herders in the Cape Province of South Africa. *Prehistoric Pastoralism in Southern Africa* 5:5-12.
2008 Out of Africa and the Evolution of Human Behavior. *Evolutionary Anthropology* 17:267-281.
2009 *The Human Career: Human Biological and Cultural Origins*. University of Chicago Press, Chicago.
2011 The Earlier Stone Age of Southern Africa. *South African Archaeological Bulletin* 55:107-122.

Kovda, I. and A.R. Mermut
2010 Vertic Features. In Interpretation of Micromorphological Features of Soils and Regoliths edited by G. Stoops, V. Marcelino, and F. Mees, pp. 109-127. Elsevier, Amsterdam.

Kühn, P., J. Aguilar, and R. Miedema
2010 Textural features and related horizons. In *Interpretation of Micromorphological Features of Soils and Regoliths,* pp. 217-250, edited by G. Stoops, V. Marcelino, and F. Mees. Elsevier, Amsterdam.

Kyuma, K.
2004 *Paddy Soil Science*. Kyoto University Press and Trans Pacific Press, Melbourne, Australia.

Le Gros Clark, W.E.
1946 Significance of Australopithecinae. *Nature* 157:863-865.

Leopold, L.B., M.G. Wolman, and P. Miller
1995 Fluvial Processes in Geomorphology. Dover Publications, New York.

Lewin, J. and M.G. Macklin
2003 Preservation potential for Late Quaternary river alluvium. *Journal of Quaternary Science* 18:107-120.

Lindbo, D.L., M.H. Stolt and M.J. Vepraskas
2010 Redoximorphic Features. In Interpretation of Micromorphological Features of Soils and Regoliths edited by G. Stoops, V. Marcelino, and F. Mees, pp. 129-148. Elsevier, Amsterdam.

Liu, X., T. Rolph, J. Bloemendal, J. Shaw and T. Lieu
1995 Quantitative estimates of palaeoprecipitation at Zifeng, in the Loess Plateau of China. *Palaeoclimatology and Palaeoecology* 113:243-248.
2011 Quartz-tipped arrows older than 60 ka: further use-trace evidence from Sibudu, KwaZulu Natal, South Africa. *Journal of Archaeological Science* 38:1918-1930.
2012 Thinking through the Middle Stone Age of sub-Saharan Africa. *Quaternary International* 270:140-155.

Lombard, M.
2005 Evidence of hunting and hafting during the Middle Stone Age at Sibudu Cave, KwaZulu Natal, South Africa: a multianalytical approach.
2006 Direct evidence for the use of ochre in the hafting technology of Middle Stone Age tools from Sibudu Cave. Southern African Humanities 18(1):57-67.
2012 Thinking through the Middle Stone Age of sub-Saharan Africa. *Quaternary International* 270:140-155.

Lombard, M. and L. Phillipson
2010 Indications of bow and stone-tipped arrow use 64000 years ago in KwaZulu-Natal, South Africa. Antiquity 84(325):635-648.

Lombard, M., L. Wadley, J. Deacon, S. Wurz, I. Parsons, M. Mohapi, J. Swart, and P. Mitchell
2012 South African and Lesotho Stone Age sequence updated. *South African Archaeological Bulletin* 67(195):123-144.

Lynch, S.D. and R.E. Schulze
2007 Rainfall Database. In *South African Atlas of Climatology and Agrohydrology* by R.E. Schulz (editor). Water Research Commission, Pretoria, RSA, WRC Report, Section 2.2.

Lyons, R., Tooth, S. and G.A.T. Duller
2014 Late Quaternary climatic changes revealed by luminescence dating, mineral magnetism and diffuse reflectance spectroscopy of river terrace paleosols: a new form of geoproxy data for the southern African interior. *Quaternary Science Reviews* 95:43-59.

Mack, G.H., James, W.C., and H.C. Monger
1993 Classification of paleosols. *Geological Society of America Bulletin* 105:129-136.

Maher, B.A.
1998 Magnetic properties of modern soils and Quaternary loessic paleosols: paleoclimatic implications. *Paleogeography, Palaeoclimatology, Palaeoecology* 137:25-54.

Maher, B.A., R. Thompson and L.P. Zhou
1994 Spatial and temporal reconstructions of changes in the Asian palaeomonsoon: a new mineral magnetic approach. *Earth and Planetary Sciences* 125:462-471.

Malan, B.D.
1970 Remarks and reminiscences on the history of archaeology in South Africa. *South African Archaeological Bulletin* 25:88-92.

Marshall, T.R.
1987 The Origin of the Pans of the Western Orange Free State: A Morphotectonic Study of the Palaeo-Kimberley River. *Palaeoecology of Africa* 19.

McCave, I.N., Bryant, R.S., Cook, H.F., and C.A. Coughanowr
1986 Evaluation of a laser-diffraction-size analyser for use with natural sediments. *Journal of Sedimentary Petrology* 56:561-564.

McCave, I.N., R.J. Bryant, H.F. Cook, and C.A. Coughanowr
1986 Evaluation of a laser-diffraction-size analyzer for use with natural sediments. *Journal of Sedimentary Research* 56:561-564.

McDougall, F.H., F.H. Brown, and J.G. Fleagle
2005 Stratigraphic placement and age of modern humans from Kibish, Ethiopia. *Nature* 433(7027)733-736.

Merritts, D.J., K.R. Vincent, and E.E. Wohl
1994 Long river profiles, tectonism, and eustasy: A guide to interpreting fluvial terraces. *Journal of Geophysical Research* 99:14031-14050.

Minichillo, T.
2005 Middle Stone Age lithic study, South Africa: an examination of modern human origin. PhD dissertation, University of Washington, Seattle.

Mitchell, P.J.
1993 The archaeology of Tloutle rock-shelter, Maseru District, Lesotho. *Vavorsinge van die Nasionale Museum Bloemfontein* 9:77-132.
1997 The Holocene Later Stone Age in Africa South of the Limpopo. *Journal of World Prehistory* 11:359-424.
2002 *The archaeology of southern Africa*. Cambridge University Press, Cambridge.
2016 Discontinuities in hunter-gatherer prehistory in southern African drylands. *Journal of Anthropological Archaeology*, Electronic Document, http://dx.doi.org/10.1016/j.jaa2016.07.001, accessed February 19, 2017.

Mitchell, P.J. and Vogel, J.C.
1994 New radiocarbon dates from Sehonghong Rock Shelter, Lesotho. *South African Journal of Science* 90:284-288.

Mohapi, M.
2007 Rose Cottage Cave MSA Lithic Points: does technological change imply change in hunting techniques? *South African Archaeological Bulletin* 62(185):9-18.

Monger, H.C. and L.A. Daugherty
1991 Neoformation of palygorskite in a southern New Mexico Aridisol. *Soil Science Society of America Journal* 55:1646-1650.

Monger, H.C., L.A. Daugherty, and W.C. Lindemann
1991 Microbial precipitation of pedogenic calcite. *Geology* 19:997-1000.

Mourre, V., P. Villa, and C.S. Henshilwood
2010 Early use of pressure flaking on lithic artefacts at Blombos Cave, South Africa. *Science* 330:659-662.

Mucina, L. and M.C. Rutherford (eds)
2006 The vegetation of Southern Africa, Lesotho, and Swaziland. *Strelitzia* 19, Pretoria.

Munsell Color
2015 *Munsell Soil Color Book*. Munsell Color, Grand Rapids, MI.

Murphy, C.P.
1986 *Thin Section Preparation of Soils and Sediments*. A B Academic Press, Great Britain.

Nanson, G.S. and S. Tooth
1999 Arid-zone rivers as indicators of climate change. In *Paleoenvironmental Reconstruction in Arid Lands* edited by A.K. Singhvi and E. Derbyshire. Oxford and IBH, New Delhi and Calcutta, pp. 75-216.

Nash, David
2017 Changes in Precipitation Over Southern Africa During the Recent Centuries. Oxford Research Encyclopedia of Climate Science, DOI:10.1093/acrefore/9780190228620.013.539.

North American Commission on Stratigraphic Nomenclature (NACSN)
2005 North American Stratigraphic Code. AAPG Bulletin 89(11):1547-1591.

Olson, C.G. and W.D. Nettleton
1998 Paleosols and the effects of alteration. *Quaternary International* 51/52:184-194.

Palmison, M.
2014 Excavation, analysis, and intersite comparison of the Robberg Industry components at the open-air site of Erfkroon, South Africa. M.A. Thesis, Department of Anthropology, Texas State University. San Marcos, TX.

Parkington, J.
1984 Changing Views of the Later Stone Age of South Africa. *Advances in World Archaeology* 3:89-142.

Parkington, J., C. Poggenpoel, B. Buchanan, T. Robey, T. Manhire, and J. Sealy
1988 Holocene coastal settlement patterns in the western Cape. In *The archaeology of prehistoric coastlines* edited by G. Bailey and J.E. Parkington, pp. 22-41. Cambridge University Press, Cambridge.

Partridge, T.C. and R.R. Maud
1987 Geomorphic evolution of southern Africa since the Mesozoic. *South African Journal of Geology* 90:179-208.

Partridge, T.C., L. Scott, and J.E. Hamilton
1999 Synthetic reconstructions of southern African environments during the Last Glacial Maximum (21-18 kyr) and the Holocene Altithermal (8-6 kyr). *Quaternary Science International* 57/58:207-214.

Partridge, T.C., D.M. Avery, G.A. Botha, J.S. Brink, J. Deacon, R.S. Herbert, R.R. Maud, A. Scholtz, L. Scott, A.S. Talma, and J.C. Vogel
1990 Late Pleistocene and Holocene climatic change in Southern Africa. *South African Journal of Science* 86:302-306.

Péringuey, L.
1911 *The Stone Ages of South Africa as represented in the collection of the South African Museum.* Impr. Adlard & Son & West Newman.

Porraz, G., P.J. Texier, W. Archer, M. Piboule, J.P. Rigaud, and C. Tribolo
2013 Technological successions in the Middle Stone Age sequence at Diepkloof Rock Shelter, Western Cape, South Africa. *Journal of Archaeological Science* 40:3376-3400.

Railsback, L.B., P.L. Gibbard, M.J. Head, N.R.G. Voarintsoa, and S. Toucanne.
2015 An optimized scheme of lettered marine isotope substages for the last 1.0 million years, and the climatostratigraphic nature of isotope stages and substages. *Quaternary Science Review* 111:94-106.

Rassmussen, S.O., M. Bigler, S.P. Blockley, T. Blunier, S.L. Buchardt, H.B. Clausen, I. Cvijanovic, D. Dahl-Jensen, S.J. Johnsen, H. Fischer, V. Gkinis, M. Guillevic, W.Z. Hoek, J.J. Lowe, J.B. Pedro, T. Popp, I.K. Seierstad, J.P. Steffensen, A.M. Svensson, P. Vallelonga, B.M. Vinther, M.J. Walker, J.J. Wheatley, and M. Winstrup
2014 A stratigraphic framework for abrupt climate changes during the Last Glacial period based on three synchronized Greenland ice-core records: refining and extending the INTIMATE event stratigraphy. *Quaternary Science Reviews* xxx:1-14.

Reid, I.
2009 River Landforms and Sediments: Evidence of Climatic Change. In *Geomorphology of Desert Environments, 2nd Edition* edited by A.J. Parsons and A.D. Abrahams. Springer Science.

Retallack, G.J.
1994 The environmental factor approach to the interpretation of paleosols. In Factors of Soil Formation: A Fiftieth Anniversary Retrospective edited by R. Amundson, J.W. Harden, and M.J. Singer. *Soil Science Society of America Special Publication* 33:31-64.

Richmond, J.
2012 Discipline and Credibility in the Post-War Australopithecine Controversy: Le Gros Clark Versus Zuckerman. *History and Philosophy of the Life Sciences* 34(1/2):43-78.

Roberts, P., C.S. Henshilwood, K.L. van Niekerk, P. Keene, A. Gledhill, J. Reynard, S. Badenhorst, J. Lee-Thorpe
2016 Climate, Environment and Early Human Innovation: Stable Isotope and Faunal Proxy Evidence from Archaeological Sites (98-59ka). PLoS ONE 11(7): e0157408.doi:10.1371/journal.pone.015748.

Ruffe, S.J., J.M. Fitchett, and C.J. Curtis
2019 Classifying and mapping rainfall seasonality in South Africa: a review. *South African Geographical Journal*, 101(2):158-174.

Ruhe, R.V.
1956 Geomorphic surfaces and the nature of soils. *Soil Science* 82:223-231.
1965 Quaternary Pedology. In *Quaternary of the United States* edited by H.E. Wright and D.G. Frey. Princeton University Press, Princeton.
1970 Soils, paleosols, and environment. In *Pleistocene and Recent Environments of the Central Great Plains* edited by W. Dort and J.K. Jones. University of Kansas Press, Lawrence.

Ruhe, R.V., G.A. Miller, and W.J. Vreeken
1971 Paleosols, loess sedimentation and soil stratigraphy. In *Paleopedology* edited by D.H. Yaalon. *Origin, Nature and Dating Paleosols*, pp. 41-60. Israel University Press, Jerusalem.

Ruhe, R.V. and C.G. Olson
1980 Soil Welding. *Soil Science* 130:132-139.

Ruellan, A.
1971 The history of soils: Some problems of definition and interpretation. In *Paleopedology*, pp. 3-13 edited by D.H. Yaalon. *Origin, Nature and Dating of Paleosols*. Israel University Press, Jerusalem.

Runge, E.C.A.
1973 Soil Development Sequences and Energy Models. *Soil Science* 115:183-193.

Rutherford, M.C., L. Mucina, M.C. Lötter, G.J. Bredenkamp, J.H.L. Smit, C.R. Scott-Shaw, D.B. Hoare, P.S. Goodman, H. Bezuidonhout, L. Scott, F. Ellis, L.W. Powrie, F. Siebert, T.H. Mostert, B.J. Henning, C.E. Venter, K.G.T. Camp, S.J. Sievert, W.S. Matthews, J.E. Burrows, L. Dobson, N. van Rooyen, E. Schmidt, P.J.D. Winter, P.J. du Preez, R.A. Ward, S. Williamson, and P.J.H. Hurter
2006 Savanna Biome. In *The vegetation of South Africa, Lesotho, and Swaziland*, pp. 438-538, edited by L. Mucina and M.C. Rutherford. South African National Biodiversity Institute, Pretoria.

Sadr, K. and C.G. Sampson
2006 Through Thick and Thin: Early Pottery in Southern Africa. Journal of African Archaeology 4(2):235-252.

Sadr, K. and A. Smith
1991 On ceramic variation in the South-Western Cape, South Africa. *South African Archaeological Bulletin* 46(154):107-114.

Salvador, A.
1994 International Stratigraphic Guide: a Guide to Stratigraphic Classification, Terminology and Procedure, 2nd Edition. International Union of Geological Sciences and Geological Society of America, Boulder, CO.
2013 *International Stratigraphic Guide*. Geological Society of America, Inc. Electronic document, https://doi.org/10.1130/9780813774022, accessed June 14, 2019.

Sampson, C.G.
1974 *The Stone Age Archaeology of Southern Africa*. Academic Press, New York.
1970 The Smithfield Industrial Complex: further field results. *Memoirs of the National Museum Bloemfontein* 5:1-172.

Schaetzl, R.
1991 A lithosequence of soils in extremely gravelly, dolomitic parent materials, Bois Blanc Island, Lake Huron. *Geoderma* 48:305-320.

Schaetzl, R.J. and M.L. Thompson
2015 *Soils: Genesis and Geomorphology*. University of Cambridge Press, New York.

Schmidt, V.C., N.J. Conrad, J.E. Parkington, P.J. Texier, and G. Porraz
2013 The 'MSA 1' of Elands Bay Cave (South Africa) in the context of the southern African Early MSA Technologies. *Southern African Humanities* 29:153-201.

Schoeneberger, P.J., D.A. Wysocki, E.C. Benham, and W.D. Broderson
2001 *Field Book for Describing and Sampling Soils*. USDA-NRCS, National Soil Survey Center, Lincoln, NE.

Schoeneberger, P.J., D.A. Wysocki, E.C. Benham, and Soil Survey Staff
2012 *Field Book for Describing and Sampling Soils, Version 3.0*. Natural Resources Conservation Service, National Soil Survey Center, Lincoln, NE.

Schwertmann, U. and D.S. Fanning
1976 Iron-manganese concretions in hydrosequences of soils in loess in Bavaria. *Soil Science Society of America* 40:731-738.

Scott, L.
1999 Palynological analysis of the Pretoria Saltpan (Tswaing Crater) sediments and vegetation history in the bushveld savanna biome, South Africa. In *Tswaing: Investigations into the Origin, Age and Palaeoenvironments of the Pretoria Saltpan*, pp. 143-166, edited by T.C. Partridge. South African Council for Geoscience, Mem. 85.
2016 Fluctuations of vegetation and climate over the last 75,000 years in the Savanna Biome, South Africa: Tswaing Crater and Wonderkrater pollen sequences reviewed. *Quaternary Science Reviews* 145:117-133.

Scott, L., F.H. Neumann, G.A. Brook, C.B. Bousman, E. Norström, and A.A. Metwally
2012 Terrestrial fossil-pollen evidence of climate change during the last 26 thousand years in Southern Africa. *Quaternary Science Reviews* 32:100-118.

Scott, L. and F.H. Neumann
2018 Pollen-interpreted paleoenvironments associated with the Middle and Late Pleistocene peopling of Southern Africa. *Quaternary International* xxx:1-16 (in press).

Scott, L., M. Steenkamp and P.B. Beaumont
1995 Palaeoenvironmental conditions in South Africa at the Pleistocene-Holocene transition. *Quaternary Science Review* 14:937-947.

Sealy, J.
2016 Culture Change, Demography, and the Archaeology of the Last 100 kyr in Southern Africa. In *Africa from MIS6-2: Population Dynamics and Paleoenvironments* edited by S.C. Jones and B. A. Stewart, pp. 65-75. Vertebrate Paleobiology and Paleoanthropology, DOI 10.1007/978-94-017-7520-5_4.

Sealy, J. and R. Yates
1994 The chronology of the introduction of pastoralism to the Cape, South Africa. *Antiquity* 68(258):58-67.

Seghal, J.L. and G. Stoops
1972 Pedogenic calcite accumulation in arid and semi-arid regions of the Indo-Gangetic alluvial plain of erstwhile Punjab (India)- Their morphology and origin. *Geoderma* 8:59-72.

Shepherd, N.
2002 Disciplining archaeology; the invention of South African prehistory, 1923-1953. *Kronos* 28:127-145.

Simonson, R.W.
1978 A multiple proxy model of soil genesis. In *Quaternary Soils* edited by W.C. Mahaney, pp. 1-25. Geological Abstracts, Norwich.

Sinha, R. and P.F. Friend
1999 Pedogenic alteration in the Overbank sediments, North Bihar Plains, India. *Journal of the Geological Society of India* 53:163-171.

Smith, R.M.H.
1990 A review of stratigraphy and sedimentary environments of the Karoo Basin of South Africa. *Journal of African Earth Sciences* 10:117-137.

Soil Science Division Staff
2017 *Soil Survey Manual*. United State Department of Agriculture Handbook No. 18. U.S. Department of Agriculture, Washington.

Steele, T.E. and R.G. Klein
2009 Late Pleistocene subsistence strategies and resource intensification in Africa. In *The evolution of hominin diets: integrating approaches to the study of Palaeolithic subsistence*, pp. 113-126, edited by J.J. Hublin and M.P. Richards. Springer, New York.

Steele, T.E., A. Mackay, J. Orton, and S. Schwortz
2012 Varsche River 003, a new Middle Stone Age site in southern Namaqualand South Africa. *South African Archaeological Bulletin* 67(195):108-119.

Stokes, S., G. Haynes, D.S.G. Thomas, M. Higginson, and M. Malifa
1998 Punctuated aridity in Southern Africa during the last glacial cycle: the chronology of linear dune construction in the Northeastern Kalahari. *Palaeogeography, Palaeoclimatology, Palaeoecology* 137:305-322.

Stoops, G.
2003 *Guidelines for Analysis and Description of Soil and Regolith Thin Sections*. Soil Science Society of America, Madison.

Stoops, G., V. Marcelino, and F. Mees (eds)
2010a *Interpretations of Micromorphological Features of Soils and Regoliths*. Elsevier, Amsterdam.
2010b *Micromorphological Features and their Relation to Processes and Classifications: General Guidelines and Keys.* In *Interpretations of Micromorphological Features of Soils and Regoliths* by G. Stoops, V. Marcelino, and F. Mees, pp. 15-35. Elsevier, Amsterdam.

Stuart, D.M. and R.M. Dixon
1973 Water movement and caliche formation in layered arid and semiarid soils. *Proceedings of the Soil Science Society of America* 37:323-324.

Talma, A.S. and J.C. Vogel
1992 Late Quaternary paleotemperatures derived from a speleothem from Cango caves, Cape province, South Africa. *Quaternary Research* 37:203-213.

Thackeray, J.F.
2009 Chronology, Climate, and technological innovation associated with the Howiesons Poort and Still Bay industries in South Africa. *South African Journal of Science* 105:90.

Todd, D.K.
1980 *Groundwater Hydrology*. John Wiley & Sons, New York.

Tooth, S.
2007 Arid geomorphology: investigating past, present and future changes. *Progress in Physical Geography* 31:319-335.

Tooth, S., D. Brandt, P.J. Hancox, and T.S. McCarthy
2004 Geological controls on alluvial river behavior: a comparative study of three rivers on the South African Highveld. *Journal of African Earth Sciences* 38:79-97.

Tooth, S., P.J. Hancox, D. Brandt, T.S. McCarthy, Z. Jacobs, and S.M. Woodborne
2013 Controls on the genesis, sedimentary architecture, and preservation potential of dryland alluvial successions in stable continental interiors: insights from the incising Modder River, South Africa. *Journal of Sedimentary Research* 83:541-561.

Underhill, David
2011 A History of Stone Age Archaeological Study in South Africa. *South African Archaeological Bulletin* 66(193):3-14.

Van Aardt, A., C.B. Bousman, J.S. Brink, G.A. Brook, Z. Jacobs, P.J. du Preez, L. Rossouw, and L. Scott
2015 First chronological, Palaeoenvironmental, and archaeological data from the Baden-Baden fossil spring complex in the western Free State, South Africa. In *Changing Climates, Ecosystems, and Environments within Arid Southern Africa and Adjoining Regions, Palaeoecology of Africa Vol. 33*, pp. 117-152, edited by J. Runge. CRC Press/Balkema, Leiden, The Netherlands.

Van Hoepen, E.C.N.
1928 Die Koningse Kultuur. I. Die Doningse Industrie. *Argeologiese Navorsinge van die Nasionale Museum* 1(1).
1932 Die Doningse Kultuur. II. Die verspreiding van die Koningse Industrie. *Argeologiese Navorsinge van die Nasionale Museum* 1(2).

Vepraskas, M.J.
2015 Redoximorphic Features for Identifying Aquic Conditions. *Technical Bulletin 301,* North Carolina Agricultural Research Service, Raleigh, NC.

Verster, E. and T.H. van Rooyen
1999 Palaeosols on a fluvial terrace at Driekop, Northern Province, South Africa as indicators of climate changes during the Late Quaternary. *Quaternary International* 57-58:229-235.

Villa, P., M. Soressi, C.S. Henshilwood, and V. Mourre
2009. The Still Bay points of Blombos Cave (South Africa). *Journal of Archaeological Science* 36(2):441-460.

Villa, P. and S. Soriano
2010 Hunting weapons of Neanderthals and early modern humans in South Africa. *Journal of Anthropological Research* 66:5-38.

Villa, P., S. Soriano, T. Tsanova, I. Degano, T.F.G. Higham, F. d'Errico, L. Backwell, J.J. Lucejko, M.P. Colombini, and P.B. Beaumont
2012 Border Cave and the beginning of the Later Stone Age in South Africa. *Proceedings of the National Academy of Sciences of the USA* 109(33):13208-13213.

Viscarra Rossel, R.A., Y.S. Jeon, I.O.A. Odeh, and A.B. McBratney
2006 Visible, near infrared, mid infrared or combined diffuse reflectance spectroscopy for simultaneous assessment of various soil properties. *Geoderma* 131:59-75.

Wadley, L.
1986 Segments of time: a mid-Holocene Wilton site in the Transvaal. *South African Archaeological Bulletin* 41:54-62.
1997 Rose Cottage Cave: Archaeological work 1987-1997. *South African Journal of Science* 93:439-444.
2013 Recognizing complex cognition through innovative technology in Stone Age and Palaeolithic sites. Cambridge Archaeological Journal 23(2):163-183.
2015 Those marvelous millennia: the Middle Stone Age of Southern Africa. *Azania: Archaeological Research in Africa* 50(2):155-126.

Wadley, L., T. Hodgkiss, and M. Grant
2007 Announcing a Still Bay Industry at Sibudu Cave, South Africa. *Journal of Human Evolution* 52:681-689.
2009 Implications for complex cognition from the hafting of tools with compound adhesives in the Middle Stone Age, South Africa. *Proceedings of the National Academy of Sciences* 106:9590-9594.
2013 MIS 4 and MIS 3 Occupations in Sibudu, Kwazulu-Natal, South Africa. *South African Archaeological Bulletin* 68(197):41-51.

Wadley, L., B.S. Williamson, and M. Lombard
2004 Ochre in hafting in Middle Stone Age southern Africa: a practical role. Antiquity 78:661-675.

Weerts, H.J.T. and W.E. Westerhoff
2007 Lithostratigraphy. In *Quaternary Stratigraphy* edited by S. Elias, pp. 2826-2840. Encyclopedia of Quaternary Sciences Section 3. Elsevier, Amsterdam.

Weider, M. and D.H. Yaalon
1982 Micromorphological fabrics and developmental stages of carbonate nodular forms related to soil characteristics. *Geoderma* 28:203-220.

Wellington, J.H.
1944 The boundaries of the Highveld. *South African Geographical Journal* 26:44-47.
1955 Physical Geography. In *Southern Africa: A Geographical Study, vol. 1*. pp. 528. Cambridge University Press, Cambridge.

Werts, S.P. and M. Milligan
2012 Controls on soil organic matter content and stable isotope signatures in a New Mexico lithosequence. *Soil Science* 177:599-606.

Wilkins, J. and M. Chazan
2012 Blade production ~500 thousand years ago at Kathu Pan 1, South Africa: support for the multiple origins hypothesis for Early Middle Pleistocene blade technologies. *Journal of Archaeological Science* 39:1883-1900.

Wilkins, J., B.J. Schoville, K.S. Brown, and M. Chazan
2012 Evidence for early hafted hunting technology. *Science* 338:942-946.

Wilkins, J. and B.J. Schoville
2016 Edge damage on 500-thousand-year-old spear tips from Kathu Pan 1, South Africa: The combined effects of spear use and taphonomic processes. *Multidisciplinary approaches to the study of Stone Age Weaponry*. Pp. 101-117. Springer, Dordrecht.

Wurz, S.
2001 Variability in the Middle Stone Age Lithic Sequence, 115,000-60,000 Years Ago at Klasies River, South Africa. *Journal of Archaeological Science* 29:1001-1015.
2013 Technological Trends in the Middle Stone Age of South Africa between MIS 7 and MIS 3. *Current Anthropology* 54(8):305-319.

Ziegler, M., M.H. Simon, I.R. Hall, S. Barker, C. Stringer, and R. Zahn
2013 Development of Middle Stone Age innovation linked to rapid climate change. *Nature Communications* 4:1905, doi:10.1038/ncomms2897.